ProQuest LLC.
789 East Eisenhower Parkway
P.O. Box 1346
Ann Arbor, MI 48106 – 1346

Distribution of Anti-Cancer Drugs in Solid Tumours Studied by MALDI-MSI

Afnan Batubara

A thesis submitted in partial fulfilment of the requirements of Sheffield Hallam University for the degree of Doctor of Philosophy

April 2015

Acknowledgments

First and above all, I praise God, the almighty for providing me this opportunity and granting me the capability to proceed successfully.

Second, I warmly thank and appreciate my **mother** and **father for** their material and spiritual support in all aspects of my life.

I also would like to thank my **brothers and sister** for they have provided assistance in numerous ways.

Also, my sincere appreciation goes to my supervisor Professor Malcolm Clench whose guidance, careful reading and constructive comments was valuable. His timely and efficient contribution helped me shape this into its final form and I express my sincerest appreciation for his assistance in any way that I may have asked. I am also deeply thanks my second supervisor from the University of Bradford, Professor Paul Loadman for his invaluable advice and supervision at the initial stages of this study. Professor Chris Sutton also encouraged me in this topic.

Finally, I would like to thanks member of the mass spectrometry group at Sheffield Hallam University, Many thanks to Dr. Laura Cole, Dr. Leesa Ferguson, Dr. Bryn Finders, Dr. Jill Newton, Dr. Philippa Hart, Dr. Robert Bradshaw, Christopher Mitchell and Ekta Patel for their help and support.

Abstract

Vascular disrupting agents (VDAs) have been used in treatment of many cancers. 5, 6 - dimethylxanthenone-4-acetic acid (DMXAA) is a low molecular weight drug of the flavonoid group which has an anti-vascular effect in tumours causing endothelial cell apoptosis and activation of cytokines.

A study employing matrix assisted laser desorption ionisation-mass spectrometry (MALDI-MS) imaging to examine LS174T colorectal adenocarcinoma xenografts following administration of DMXAA has been conducted to study the distribution of anti-cancer drugs and to explore markers of efficacy and resistance. Initial work established the limit of detection /quantitation of DMXAA in tissue. The drug limit of detection (LoD) is determined as 10 ng/ml and the drug lower limit of quantitation (LLoQ) is 45 ng/ml. MALDI images were recorded from LS174T colorectal adenocarcinoma xenografts removed from immunodeficient mice following treatment with with 27.5 mg/kg DMXAA. These indicated that the drug was distributed mainly in the centre of tumour 4h post-treatment, whilst it was distributed around the periphery 24h post-treatment.

A study of lipid expression in treated tumors demonstrated that washing tissue sections with 150 mM ammonium acetate solution (NH_4Ac) improved the intensity of lipids signals in both negative and positive ion mode. These images also indicated that sphingomyelins (SM) and phosphatidylcholines (PC) lipid species were highly expressed in cancerous tissue.

A thin layer chromatography-matrix assisted laser desorption ionisation-mass spectrometry (TLC-MALDI-MS) experiment has been carried out for the analysis of phospholipids extracted from the treated xenograft tumours. The lipid extracts were separated into 6 spots on the TLC plate. These were identified as lysophosphatidylcholines (LPC), sphingomyelins (SM), phosphatidylcholines (PC) and phosphatidylethanolamines (PE). The TLC-MALDI-MS data indicated that LPC were highly expressed in the 4h and 24h post-treated tumour samples compared to the control. An increase in expression of LPC lipids in solid tumours treated with DMXAA has been demonstrated and shown to be localised in the central area of the tumour.

Mass spectrometry imaging was also used to characterise proteins and peptide signal in tumours after treatment with DMXAA. Histone H2A peaks at 944 m/z were highly expressed in the region of the tumours. In addition, a characteristic increase in the Hb β chain at 1274.74 m/z in the 24h post-treated tumour has been seen. The data obtained from PCA has shown that the levels of certain proteins changed over the different tumour time point.

Table of Contents

General introduction

List of figures

1. General Introduction

List of tables

1. General Introduction

Abbreviations and units

eV	electron volt
kg	kilogram
kHz	kilohertz
mg	milligrams
ml	millilitre
mm^3	cubic millimeter
µm	micrometer
ng	nanogram
Rf	retention factor
SD	standard deviation
Th	Thomson
µJ	Micro Joule
µL	microliter
(3-HPA)	3-Hydroxypicolinic acid
(5-HIAA)	5-hydroxyindoleacetic acid
(5-HT)	5-hydroxyltryptamine
(CA4P)	combretastatin A4 phosphate
(CEA)	carcino-embryonic-antigen
(CHCA)	α-cyano-4-hydroxycinnamicacid
(CRC)	colorectal cancer
(dc)	direct-current
(DESI)	desorption electrospray ionization
(DHAP)	2,6 - dihydroxyacetophenone
(DHB)	2,5 -dihydroxybenzoic acid

(DMXAA)	5, 6 -Dimethylxanthenone-4-acetic acid
(ECM)	extracellular matrix
(ESI)	electrospray Ionization
(FAB)	fast-atom bombardment
(FASN)	fatty acid synthase
(GC)	gas chromatography
(GC/MS)	gas chromatography MS
(H&E)	haematoxylin and Eosin
(Hbβ)	haemoglobin β chain
(HPTLC)	high performance thin layer chromatography
(ICP-MS)	inductively plasma mass spectrometry
(IM)	ion mobility
(ITO)	indium-tin-oxide
(LA)	laser ablation
(LC/MS)	liquid chromatography
(LDI)	direct laser desorption ionization
(LoD)	limit of detection
(LLoQ)	lower limit of quantitation
(LPC)	lysophosphatidylcholine
(LV)	latent variables
(m/z)	mass-to-charge
(MALDI)	matrix-assisted-laser-desorption/ionization
(MALDI-MS)	matrix-assisted laser desorption/ionization mass spectrometry
(MeOH)	methanol
(MRS)	magnetic resonance spectroscopy

(MRSI)	magnetic resonance spectroscopic imaging
(MS)	mass spectrometry
(MSI)	mass spectrometry imaging
(Nd:YVO4)	neodymium-doped Yttrium Vanadate
(NfkB)	nuclear transcription factor
(NH_4Ac)	ammonium acetate
(NO)	nitric oxide
(NSCLC)	non-small cell lung cancer
(OCT)	optimal cutting temperature
(PC)	phosphatidylcholine
(PCA)	principle component analysis
(PCA-DA)	principal components analysis - discriminate analysis
(PDE)	phosphodiesters
(PE)	phosphatidylethanolamine
(PEG)	polyethylene glycol
(PI)	phosphatidylinositol
(PIP)	phosphatidylinositol phosphate
(PLSDA)	partial least squares discriminant analysis
(PS)	phosphotidylserine
(Q)	quadrupole
(QIT)	quadrupole ion trap
(QTOF)	quadrupole/time of flight mass spectrometer
(ROI)	region of interest
(ROS)	reactive oxygen species
(SA)	3, 5-Dimethoxy-4-hydroxycinnamic acid

(SEM)	secondary electron multiplier
(SIMS)	secondary ion mass spectrometry
(SM)	sphingomyelin
(SMase)	sphingomyelin phosphodiesterase
(TFA)	trifluoroacetic acid
(THAP)	4,6 trihydroxyacetophenone
(TLC)	thin-layer chromatography
(TME)	tumour-microenvironment
(TNF-α)	tumour necrosis factor
(TOF)	time-Of-Flight
(UTLC)	ultra-Thin-Layer Chromatography
(VDAs)	vascular disrupting agents

Chapter 1

General Introduction

1 Introduction

1.1 Microenvironment of a solid tumour

Normally solid tumours consist of three specific regions; cancer cells, non-transformed stromal cells, blood vessels and the interstitium. Cancerous and stromal cells form the major parts of solid tumours and cover more than 50% of the tumour volume; whereas, blood vessels which nourish both the stromal and cancer cells in tumours cover up to 10% of the tumour volume. The remaining tumour volume is covered by the interstitium which provides the nutritional and structural framework for the tumour to grow (Jain, 1994). The blood vessels of a tumour mainly consist of veins/venules in the inner part of tumour and a few arteries /arterioles in the peripheral part of tumour. Therefore, the difference in artery / vein pressure is low in the central region of a tumour but it is high in the peripheral region. This might be expected to lead to a lower blood flow in the centre and a higher blood flow in the periphery of the tumour. In fact, the distribution of blood vessels within a tumour depends on the tumour size and location. Small tumours are usually spread by surrounding vessels and further growth is initiated by formation of new micro-vessels. In terms of their blood supply solid tumours can be thought of as containing three regions: a vascular necrotic region with no vasculature, a semi-necrotic region (which contains capillaries and pre and post capillaries) and a stable perfuse region containing many venous vessels and a few arteriolar vessels (Danquah *et al.*, 2011).

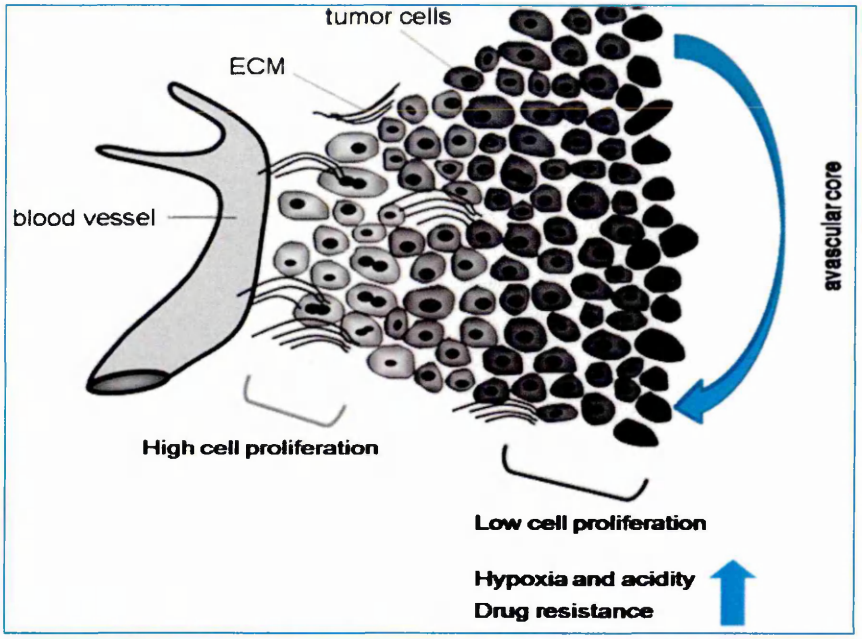

Figure 1.1 *Schematic of the tumour microenvironment showing tumour cells and the extracellular matrix (ECM) surrounding a capillary. Hypoxia and acidity increase with distance from blood vessels resulting in increasing drug resistance from the tumour periphery to the vascular core (Image Adapted and reproduced from Danquah et al., 2011).*

The heterogeneity in the intramural vascular structure leads to uneven drug distribution within solid tumours. In addition tumour blood vessels are generally leaky due to the discontinuity of the endothelium (Danquah *et al.*, 2011).When tumours grow the need for an oxygen supply is increased. This is due to increased cell proliferation and growth within the tumour which require high amounts of oxygen. Hypoxia is defined as an area of low oxygen levels. It is a characteristic hallmark of solid tumours because of the imbalance between oxygen supply and consumption (Brown & Wilson, 2004). About 50–60% of solid tumours display a heterogeneous distribution of hypoxic regions within the tumour. Such characteristic hypoxic regions in tumours are generated because of the abnormal tumour vasculature structure, previously described. This reduces the blood flow and limits the delivery of oxygen within the tumour (Danquah *et al.*, 2011). Therefore, increased resistance to radiation therapy and chemotherapy in solid tumours arise due to the presence of these hypoxic regions (Rapisarda and Melillo., 2009).

1.2 Tumour vs. Normal tissues

Tumour tissue is characterized by the uncontrolled proliferation of cells. In the early stages of tumour growth, the blood supply to the tumour tissue area mainly comes from the vessels which surround the normal tissue. When a tumour exceeds a critical mass, it develops its own blood supply. Studying tumour vascular structure is of great interest in cancer treatment and targeted drug delivery to tumour sites. Tumour vasculature differs from normal tissue vasculature in many aspects (Narang and Varia., 2011).

- Tumour vasculature is mainly characterized by the lack of smooth muscle cells and pericytes in vessel walls, no lymphatic drainage, an irregular basement membrane, discontinuous endothelial lining. Also, tumour vessels have complex branching patterns compared to normal blood vessels. Furthermore, the growth of tumour vasculature is poorly regulated. Nevertheless; the factors controlling tumour vascular growth are similar to that of normal tissue.

- The border of tumour-normal tissue is usually highly vascularised while the interior parts of the tumour could be avascular.

- The vessel diameter and the branching structure in tumour vasculature are different from the normal vasculature for e.g. tumour shows abnormal structure and function, twisted and poorly organized blood vessels which make the vessels "leaky" and it has hence been identified as a good target for cancer therapy.

As shown in Fig. 1.2 A and Fig. 1.2 B, the arteries, veins and capillaries in normal tissue are uniformly arranged forming an evenly distributed compact network. This distribution of vessels in normal tissue is important for normal blood flow without any obstruction. On the other hand, Fig. 1.2 C shows that the vascular network in tumour appears haphazard with high vascular density in certain regions and a complete lack of vasculature in others. This irregular structure in tumour vasculature causes a resistance to blood flow (Narang and Varia., 2011).

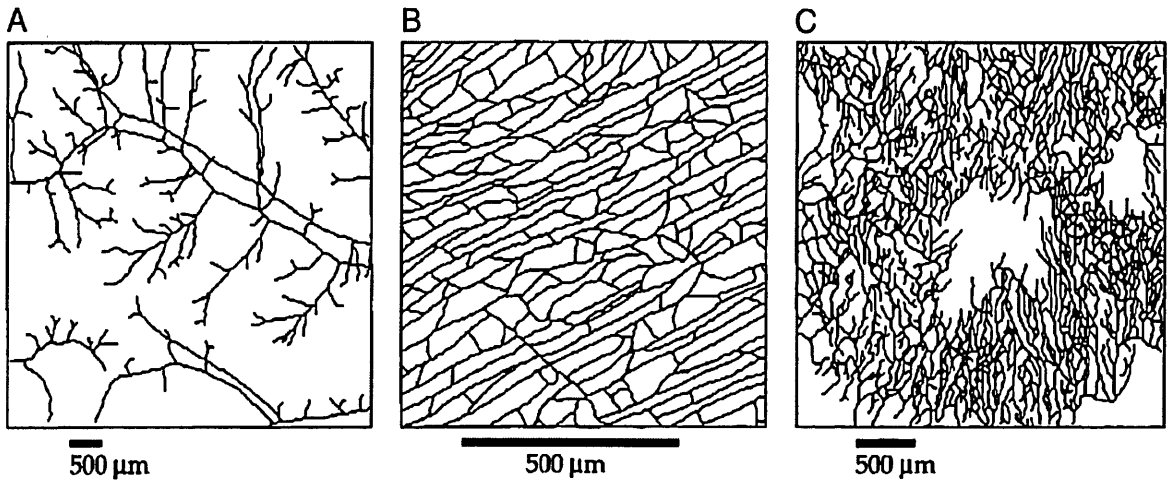

Figure 1.2 *2D images of (A) normal subcutaneous arteries and veins follow a sub-divisional tree-model, (B) normal capillaries are uniformly arranged forming a compact network, and (C) The tumor vascular network is irregular with high tortuosity (Image adapted from Gazit et al., 1995).*

Since vascularisation in tumour tissue tends to be heterogeneous and it shows some regions with high blood flow while others are avascular when a drug is administrated it can be distributed mainly around the outer well perfused regions of solid tumours and less distributed in central avascular tumour regions (Narang and Varia 2011).

Therefore, developing methods for assessing tumour blood flow or perfusion characteristics such as markers of hypoxia can help clinicians to predict the response or select a more aggressive alternative therapeutic approach (Serkova *et al.*, 2011)

1.3 Vascular targeted therapies

The process of new blood vessel formation is known as angiogenesis. It is an essential process for the spreading and growth of solid tumours. Numerous cancer treatments are focused on the dependency of tumour cells on new blood vessels for growth and metastatic spread. Currently the widespread interest in targeting tumour vasculature represents a new era in the treatment of cancer. Varieties of novel vascular targeted agents have been developed and are currently under clinical consideration. These novel agents differ from the cytotoxic drugs that normally used in the treatment of solid tumours.

Vascular targeted therapies are divided into two distinct types of agent: Firstly, the anti-angiogenic agents and secondly, the vascular-disrupting agents (Fig.1.3). Anti-angiogenic agents work by mainly inhibiting the formation of new blood vessels. Therefore they have a defensive action which require chronic administration and are of particular benefit in early stage or asymptomatic metastatic disease (Siemann *et al.*, 2005). In contrast vascular-disrupting agents mainly target the endothelial cells and pericytes of the already established tumour blood vessels causing ischemia and necrosis of tumour blood vessels (Girdlelli *et al.*, 2009). Therefore, these agents are given acutely and they show more immediate effects against advanced disease (Siemann *et al.*, 2005).

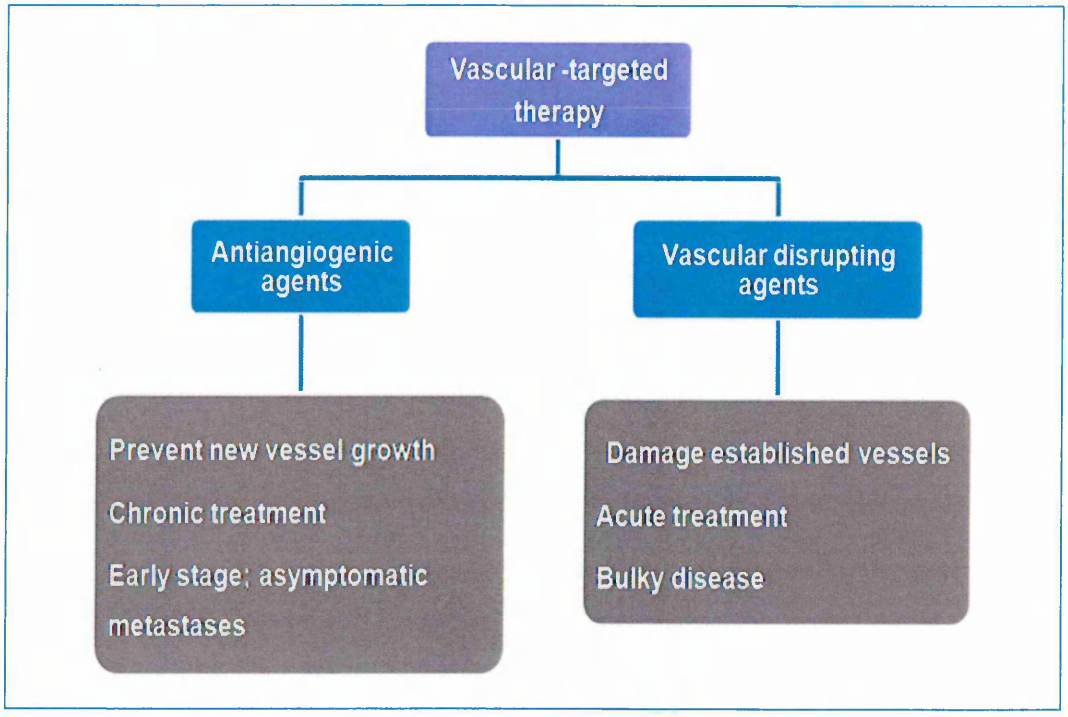

Figure 1.3 *Classification of vascular targeted therapies (Image adapted and reproduced from Siemann et al., 2005).*

Vascular disrupting agents (VDAs) are divided into two types: ligand-directed VDAs and small molecules. Ligand-directed VDAs contain targeting and effector moieties which are linked together, but their clinical effects are limited because of their cost and the lack of specificity and toxicity. Usually targeting moieties involve antibody, peptide or growth factors directed against a marker that is specifically up-regulated in tumour endothelial cells (such as antigens involved in angiogenesis, thrombosis, and vascular remodelling processes). The effector moiety, however, directly induces thrombosis by killing endothelial cells or causes thrombosis indirectly, by attacking tumour vessels, or by causing shape changes in endothelial cells and hence causing a blockage of tumour blood vessels (Thorpe 2004).

Small molecule VDAs are in a more advanced stage of clinical development in comparison to the ligand directed VDAs. They can again be divided into two groups; the tubulin-binding agents and the flavonoids. The synthetic flavonoids work through induction of local cytokine production (Danquah *et al.*, 2011), while tubulin binding agents work at the colchicine binding site of the β-subunit of endothelial tubulin (Hinnen & Eskens., 2007). This binding results in depolymerisation of microtubules and disorganisation of actin and tubulin (Hinnen & Eskens., 2007). The resulting disruption of the endothelial cytoskeleton causes a conformational change which leads to a loss of blood flow. Combretastatin A4 phosphate (CA4P) is an example of typical tubulin binding agent (Fig 1.4) (Vincent *et al.*, 2005).

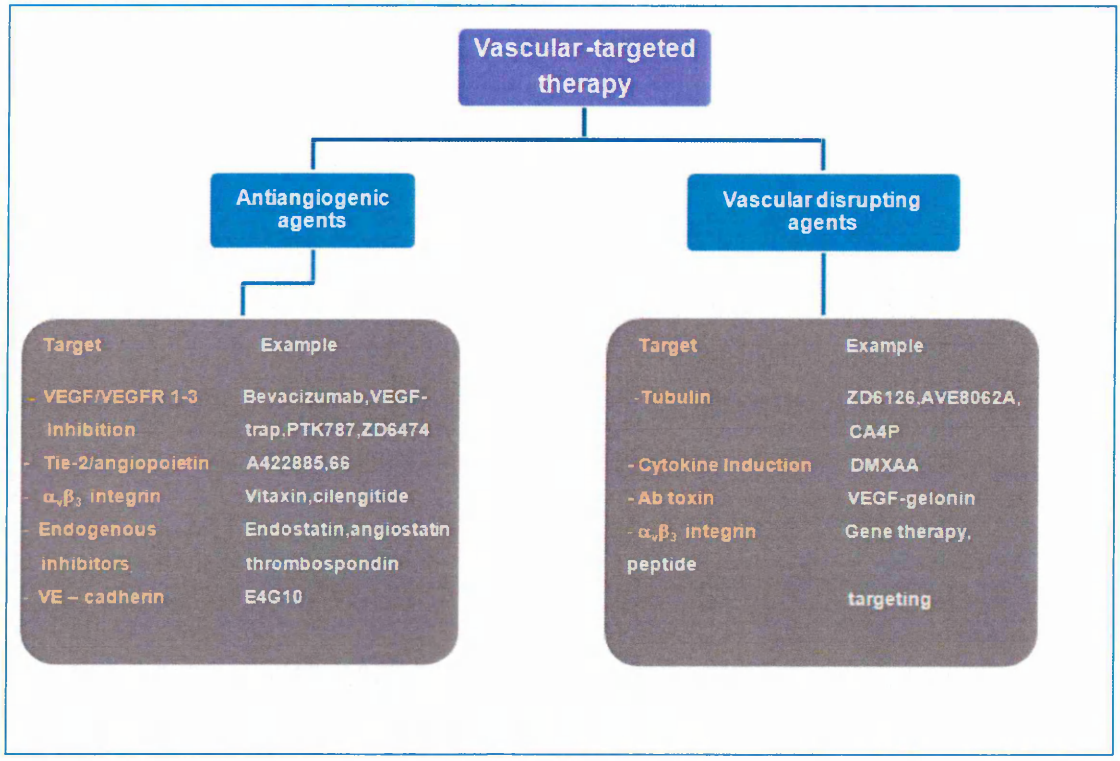

Figure 1.4 *Example of the target and drug of the vascular targeted therapies (Image adapted and reproduced from Siemann et al., 2005).*

Preliminary results have reported that these agents are active and safe for the treatment of advanced solid tumours, however, the responses of tumours to VDAs delivered as a single agent was poor (Gridelli *et al.*, 2009). The combination of VDAs with cytotoxic chemotherapy, external-beam radiotherapy and radio-immunotherapy has, in contrast, given an excellent response in animal models (Gridelli *et al.*, 2009). This is believed to be because the co-administered agent targets peripheral tumour cells, in the so called "viable rim".

1.4 Mechanism of action of vascular disrupting agent (VDAs)

In contrast to anti-angiogenic drugs anti-vascular drugs mainly target tumour blood vessels that have already formed. VDAs can however act not only on tumour vessels but also on normal vessels, with a risk for subsequent ischemic complications. This effect is in fact minimal since the structural difference in the endothelium of tumour vessels compared with that of normal vessels allows a selective vascular shutdown. Normally, in tumour vasculature there is a high rate of endothelial cell proliferation, absence of pericytes, abnormalities of the basement membrane and increased vascular permeability (Gridelli *et al.*, 2009). Also, tumour vessels are structurally disorganized, thin-walled with obstructed blood flow (Gridelli *et al.*, 2009). In addition, the irregular vessel diameters in a tumour lead to high resistance to blood flow. Therefore, tumours can be affected by small decreases in perfusion pressure which might not affect normal tissue (Kakolyris *et al.*, 2000, Tozer *et al.*, 1990).

VDAs consist of a large group of compounds which mainly target endothelial cells and act on several pathways. Endothelial cells depend mainly on a tubulin cytoskeleton for their motility, invasion, attachment, alignment, and proliferation (Denekamp., 1982). VDAs change the endothelial cell shape by causing a disruption of the cytoskeleton and cell-to-cell junctions of the cells. They also induce necrosis of tumour cells by inhibiting blood flow and reduce the amount of oxygen and nutrient supply to the tumour (Gridelli *et al.*, 2009).

These effects increase the permeability to proteins and increase the interstitial fluid pressure, which reduce the vessel diameter and leads to plasma leakage as a result of increased blood viscosity and decreased blood flow (Gridelli *et al.*, 2009). Furthermore, the basement membrane components are exposed and become activated through contact with platelets which trigger a vascular shutdown. All these events selectively occur in tumour endothelial cells only. Therefore, VDA activity is considered as being cytotoxic rather than cytostatic (Hinnen & Eskens., 2007).

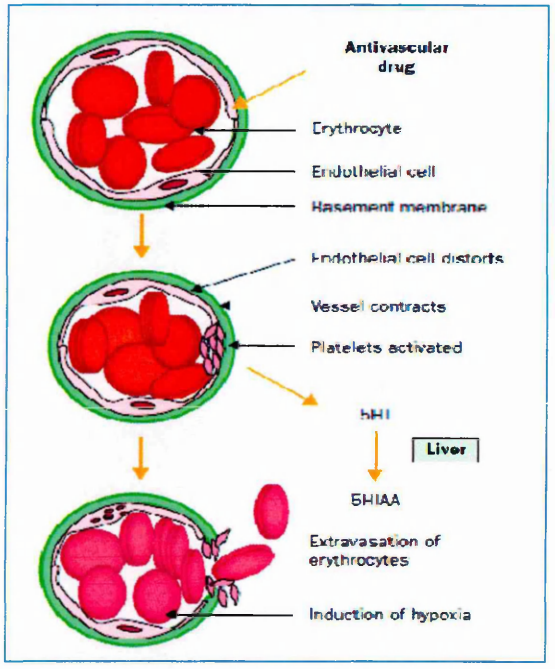

Figure 1.5 *The main principle of anti-vascular therapy (Image adapted and reproduced from (Baguley., 2003).*

Whilst VDAs are new and promising targeted agents, it has been reported in preclinical models that although the centre of the tumour becomes necrotic, a characteristic rim around the periphery of tumour remains (Fig.1.6). This rim of tumour cells is less responsive to VDAs and it survives because it derives nutritional support from nearby normal blood vessels.

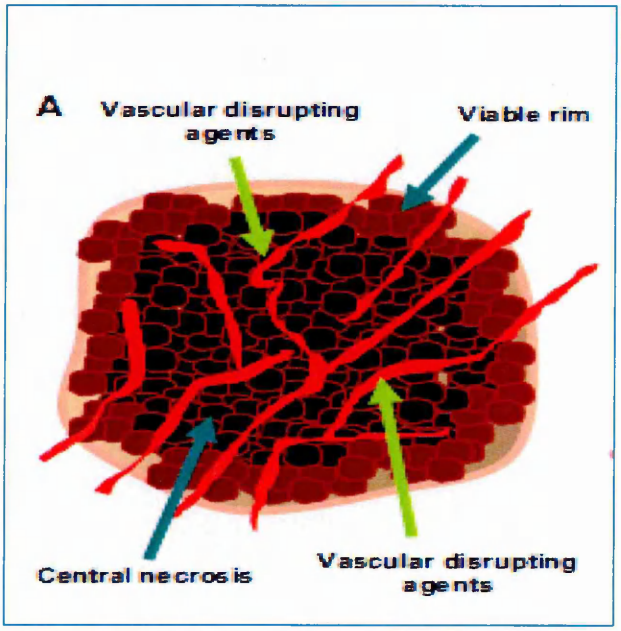

Figure 1.6 *The mechanisms of action of vascular disrupting agents (A): Vascular disrupting agents are mainly targets established tumour blood vessels of large solid tumours causing vessel occlusion and necrosis in the central part of the tumour and a viable rim around the periphery of tumour (Image adapted from Gridelli et al .,2009).*

1.5 Types of Vascular disrupting agents (VDAs)

VDAs have been divided into two types: small molecule and ligand directed VDAs. In this project the focus will be on small molecule VDAs which are currently in preclinical and clinical development (Hinnen & Eskens 2007).

1.5.1 Ligand-Directed VDAs

The mode of action of this type of VDA involves the use of ligands that bind selectively to components of tumour blood vessels and which occlude those vessels. Ligand-directed VDAs are composed of targeting and effector moieties that are linked together. The targeting moieties include antibodies, peptides or growth factors against a marker that is selectively up regulated in tumour tissue endothelial cells (O'Hanlon 2005 and Siemann *et al* 2004).

The antigens involved in angiogenesis, thrombosis, and vascular remodelling and cell adhesion molecules are usually up-regulated in tumour compared to normal tissue vessels (Thorpe., 2004). The effector molecule can directly induce thrombosis, kill endothelial cells or cause shape changes in endothelial cells that then physically block tumour vessels (Thorpe ., 2004). Research is trying to identify these receptors to target them with drugs, monoclonal antibodies, or gene therapy but the clinical development of these agents is limited due to the cost, toxicity, and a lack of specificity (Gridelli *et al.*, 2009).

1.5.2 Small Molecule VDAs

Small molecule VDAs are mainly divided into two groups; The first type is known as tubulin-binding agents which work by induction of local cytokine production and the second type is synthetic flavonoids (Hinnen & Eskens 2007).

1.5.2.1 Tubulin-Binding Agents

Tubulin binding agents mainly work at the colchicine-binding site of the β-subunit of endothelial tubulin. They cause depolymerisation of microtubules and disorganisation of actin and tubulin. As a result, disruption of the endothelial cytoskeleton occurs which leads to conformational changes and loss of blood flow. CA4P is a typical microtubule-destabilising agent and it selectively disrupts the VE-cadherin/b-catenin complex which interferes with cell-cell contact (Vincent *et al.*, 2005). The loss of cell-cell contact leads to increased vascular permeability and increased interstitial pressure as well as loss of blood flow.

Additionally, losses of cell–cell contact may results in the exposure of abnormal basement membrane which causes an induction of the coagulation cascade with subsequent thrombus formation. Indeed, tumour endothelial cells are more susceptible to the activity of tubulin-binding agents than endothelial cells of normal tissue (Chaplin and Dougherty., 1999).

1.5.2.2 Synthetic flavonoids (DMXAA)

5, 6-Dimethylxanthenone-4-acetic acid (DMXAA) is an active analogue of flavone acetic acid which causes DNA damage to endothelial cells and induces apoptosis in preclinical models (Corbett *et al.*, 1986). Flavone acetic acid was found to induce haemorrhagic necrosis of murine tumours but it was inactive in clinical trials (Smith *et al.*, 1987, Kerr and Kaye., 1989). There was an attempt to develop more active analogues of flavone acetic acid through testing their ability to induce haemorrhagic necrosis after 24 h in murine colon tumour cells (Dvorak and Gresser., 1989). Xanthenone-4-acetic acid was the initial compound to be tested along with a series of derivatives which were synthesised and evaluated (Fig. 1.7). The most active of these was DMXAA which showed an excellent experimental anti-tumour activity (Rewcastle *et al.*, 1991). DMXAA had a well tolerated anti-tumour action in phase I clinical trials, and it was therefore combined with conventional therapies in a number of successful phase II clinical trials (Gabra., 2006). However when it moved to phase III clinical trials, the same responses were not observed and the clinical development of DMXAA has been halted (Buchanan *et al.*, 2012).

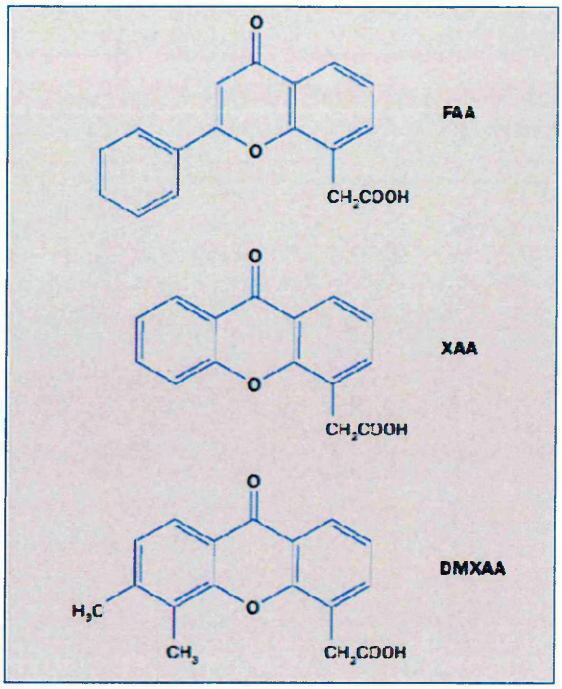

Figure 1.7 *Structure of DMXAA and its synthesized compounds (Image adapted from Baguley., 2003).*

1.6 Mechanism of action of DMXAA

5, 6-Dimethylxanthenone-4-acetic acid (DMXAA) is a low molecular weight drug which has a striking anti-vascular effect in experimental tumours (Baguley., 2003). It is mainly acts on vascular endothelial cells through a cascade of events causes induction of tumour haemorrhagic necrosis. These events include both direct and indirect effects. The indirect effect involves the release of vasoactive agents, such as serotonin, tumour necrosis factor (TNF-α), cytokines and nitric oxide (NO) from host cells (Baguley., 2003). In addition, 5-hydroxyltryptamine (5-HT) is released by platelets as a response to vascular damage (Baguley *et al* ., 1997).Therefore, tumour blood flow decreases and 5-HT levels increase. Indeed, the exact mechanism of action of DMXAA is unknown but its activity involves pathways which lead to up regulation of the nuclear transcription factor (NfκB) as well as production of TNF-α and other cytokines (Ching *et al.*, 2002).

Furthermore, NO is produced in response to DMXAA resulting in increase blood flow and vascular permeability as well as increasing the effects of TNF-α and 5-HT. The way in which these forces oppose each other is still unknown (Thomsen *et al.*, 1991).

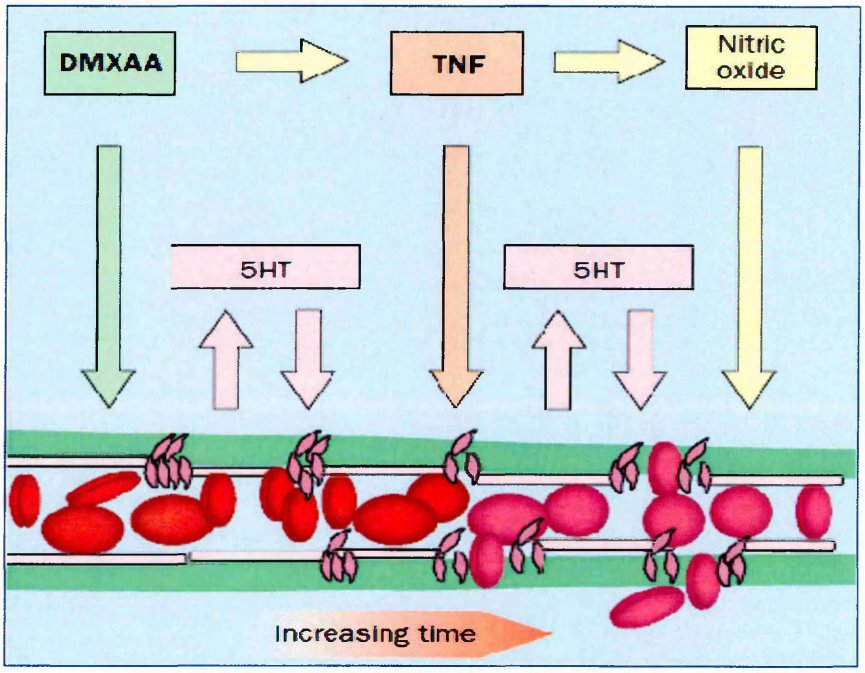

Figure 1.8 *The vasoactive event of DMXAA. The drug has a direct effect causing a release of 5-hydroxyltryptamine (5HT) by platelets and indirect effect by production of TNF-α and other cytokine in tumour tissue. 2-3h after drug administration a release of 5HT occurs and after 6h a release of nitric oxide occur (Image adapted from Baguley., 2003).*

The molecular mechanism of action of DMXAA includes activation of NFκB in monocytes, vascular endothelial cells, and other tumour cells. This activation can mediate the direct effects of DMXAA on vascular endothelial cells and also lead to cytokine synthesis in host and tumour cells. NFκB is known to be the main transcription factor which causes production of TNF and is involved in the synthesis of interferons and other cytokines (Karin & Benneriah., 2000). The range of cytokines and chemokines produced in response to DMXAA is consistent with the

involvement of NFκB (Cao *et al.*, 2001). Also DMXAA can stimulates the enzyme that phosphorylates the inhibitor of NFκB (IκB kinase) in a pathway linked to NFκB activation (Philpott *et al* ., 2001). This enzyme complex, include α subunit, αβ subunit, and aγ subunit in which it catalyses phosphorylation of the inhibitory IκB protein causing an enzyme degradation. The active NFκB are then translocated to the nucleus (Karin & Benneriah., 2000).

DMXAA induce the stimulation of TNF synthesis through various agents, such as endotoxin, interleukin 1, okadaic acid, and phorbol myristate acetate which involved in activation of IκB kinase by a different pathway. Therefore, β subunit is considered as a possible target for DMXAA (Philpott *et al.*, 2001).

Earlier studies have stated that DMXAA can reduce tumour growth in several mouse tumour models by two phases. The first phase effect was initiated by macrophages which release significant amounts of TNF-α and NO (Ching *et al.*, 1992). The release of cytokines results in hemorrhagic necrosis in tumours. The second phase response were initiated by migration of activated tumour-specific CD8+ T-cells due to secretion of chemokines, such as CCL2 (MCP-1), CXCL10 (IP-10) and CCL5 (RANTES) induced by DMXAA in mouse macrophages and dendritic cells (Ching *et al.*, 1999). Phase I and phase II clinical trials have proven the clinical benefits of DMXAA in humans. In fact, the exact mechanism in which DMXAA exerts its anti-tumour action has been attracting researcher attention. It has been demonstrated that DMXAA can act on both endothelial cells and leukocytes particularly macrophages and dendritic cells in murine systems. DMXAA induces the secretion of large amounts of pro-inflammatory cytokines and chemokines such as TNF-a, IL-6, IP-10, and interferon-b) from macrophages (Sun *et al.*, 2011).

1.7 MALDI imaging in drug distribution

In the early stage of drug development, drug and metabolite distribution studies have traditionally been carried out in animal tissues using a range of techniques. MALDI-MSI is a technique that has been used for imaging the distribution of a range of drugs and metabolites in whole body sections and in a variety of applications since its development as a protein imaging technique by Caprioli *et al.* in 1997. The first study using MALDI that was performed to directly study a pharmaceutical compound in animal tissue was published by Troendle *et al.*, 1999. MALDI quadrupole ion trap mass spectrometry was used to detect the anticancer drug paclitaxel in a human ovarian tumour and the antipsychotic drug spiperone in spiked sections of rat liver tissue (Troendle *et al.*, 1999). The Caprioli group reported a study of the distribution of anti-tumour drugs in mouse tumour tissue and rat brain sections (Reyzner *et al.*, 2003). This paper is generally regarded as the first MALDI-MSI paper to study drug distribution. A study of the distribution of the bio-reductive anticancer drug AQ4N in H460 lung tumour xenografts showing imaging of the prodrug and its reduced active form in one experiment along with imaging the distribution of ATP and showing the inverse correlation with the active reduced form of the drug in regions of hypoxia was reported by Atkinson *et al.*, 2007.

Stockli *et al.*, 2007 described some of the practical aspects of obtaining MALDI-MSI data for drug and metabolite distributions in whole body sections and have reported on some of the limitations of the technique (Stockli *et al.*, 2007). In addition, the Caprioli group extended this approach by combining their own work on protein imaging to produce whole body images which shown the location of drug, drug metabolites and endogenous markers for various organs of the body (Shahidi *et al.*,2006).

1.8 Lipids and Colon cancer

Currently, colon cancer has become a major cause of mortality and morbidity. Aging is one of the factors that increases the incidence of colorectal cancer. Environmental factors such as diet, high intake of animal protein and fat with a low intake of fibre are also thought to increase the risk of colon cancer (Shimma *et al.*, 2007). Many studies have also focused on identifying bio-molecules differentially expressed in cancerous and normal tissues as biomarkers (Alessandro *et al.*, 2005, Westra *et al.*, 2004). Others concentrate on phospholipids, which are an important constituent of cell membranes and are important molecules to be investigated especially in colon cancer. It is suggested that the characteristics of cell membranes can be determined by analyzing phospholipids (Cullis *et al.*, 1991). Previous studies have demonstrated that cancerous tissue contains high levels of total amounts of all phospholipids with altered phospholipids composition of the membrane (Dueck *et al.*, 1996, Dobrzynska *et al.*, 2005). All these studies indicated that phospholipids can be used, as a useful marker for the detection of colon cancer.

Profiling biological molecules on tissues using matrix-assisted laser desorption/ionization mass spectrometry (MALDI-MS) can identify subtypes of phospholipids. Furthermore, accurate mass MS can profile fatty acids which can be considered as a part of phospholipids. This area of study has been extended to visualize the distribution of individual biomolecules in a tissue section using mass spectrometry imaging (MSI).

In the study of Shimma *et al*, the distribution of two types of phospholipids was visualized to be differentially expressed between the cancerous and normal areas (Shimma *et al.*, 2007).

Gao *et al*, reported that Lysophosphatidylcholine (LPC) level can be considered as a clinical diagnostic indicator of pathophysiological changes which occurred by anti-tumour action of flavonoid derivate, 1-(3-chloro-4-(6-ethyl-4-oxo-4H-chromen-2-yl) phenyl)-3-(4-chlorophenyl) urea (3D). In this study, three LPCs including Lyso PC (18:1), Lyso PC (20:3) and Lyso PC (20:4) were increased by 1:40 times in cells treated with potent anti-tumour agent (3D). This increase of LPC level is due to increase oxidative stress caused by (3D) anti-tumour agent which lead to lipid peroxidation and formation of LPC (Gao *et al., 2014).* In contrast, levels of three PCs were significantly decreased ($p<0.05$) in 3d treated HepG2 cells, including PC (14:0/0:0) and PC (20:0/4:0)] and one phosphatidylcholine (PC) (15:0/20:5). The decrease in PC level indicated the lesions of cell membrane occurred by potent anti-tumour agent (3D) (Gao *et al., 2014).*

1.8.1 The effect of antibody directed and anti-vascular combination therapies on LS174T colorectal xenografts tumour

Solid tumours have an extremely heterogeneous pathophysiology; therefore, for successful treatment a combination of therapeutic strategies may be required. In order to optimize combination therapies detailed information on how tumours respond to the individual treatments are required. The use of antibody-directed therapy such as carcino-embryonic-antigen (CEA) in colorectal carcinomas is the most selective strategy for anti-cancer treatment and targets a therapeutic moiety of the tumour (Jain., 1998, Pedley., 1996). Targeting the tumour vasculature is however, also seen as a promising option. Anti-vascular therapy in fact has many advantages over direct tumour cell targeting therapy: it is easily accessible; resistance issues are rare and it is applicable to all types of solid tumour.

A range of tumour parameters has been studied which either influence or can be influenced by anti-vascular therapy. These parameters include blood vessel distribution, perfusion status, hypoxia and apoptosis (Pedely *et al.*, 2002). Fluorescence images of tumours have shown that the viable regions of the tumour contain an abundant supply of blood vessels that were mainly perfused whereas hypoxia was found in the more central regions of the tumour which contain less or no perfused blood vessels (Fig. 1.9) (Pedely *et al* ., 2002).

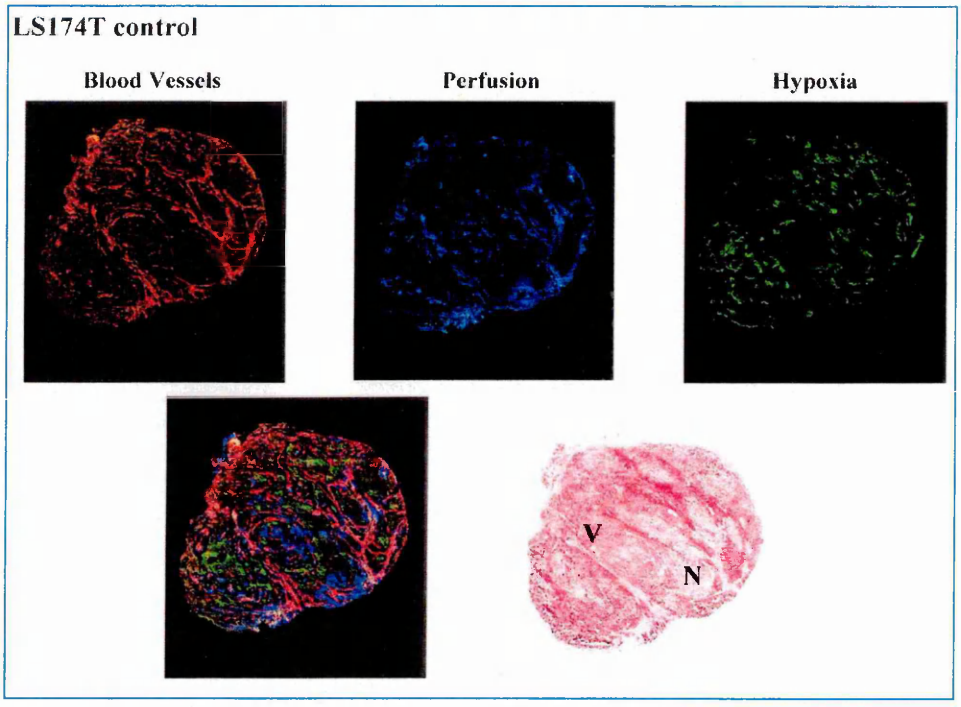

Figure 1.9 *Fluorescence images for a typical untreated (control) colorectal xenograft tumour (LS174T) Stained for the following (left to right): blood vessels (anti-CD31, red), perfusion (Hoechst 33342, blue), and hypoxia (pimonidazole, green).The relative distributions of three biologic parameters shows that most of the remaining viable regions contain well-perfused blood vessels (red & blue) with hypoxia (green) developing away from the vessels and adjacent to necrosis. H&E stained section for morphology, showing viable (V) and necrotic (N) tissue (Image adapted from Pedely et al., 2002).*

Pedley *et al* demonstrated that the addition of an anti-vascular agent to antibody-directed therapy can be a curative treatment because the two therapies treat specific regions of the tumour with different patho-physiologies (Pedley *et al.*, 2002). In this study the antibody targeted therapy was targeted at the viable tumour tissue in the well oxygenated "viable rim" of the tumour with the poorly vascularised central tumour region receiving less antibody (Fig 1.10). Therefore, the combination of antibody-directed therapy with a treatment that attacks the tumour centre is extremely essential.

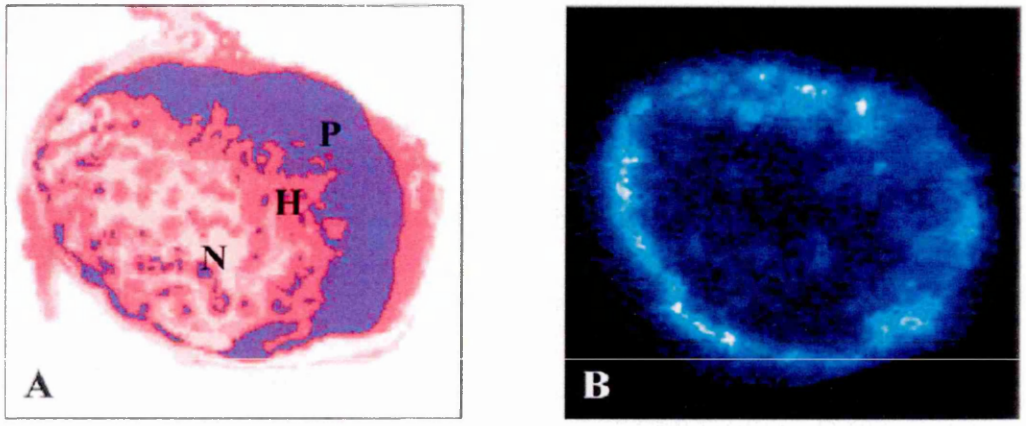

Figure 1.10 *Antibody-directed therapy demonstrated in the section of a colorectal xenograft tumour (A) H&E section of untreated tumour showing well-perfused region (P), poorly perfused (H), and necrotic (N).(B) Radioluminograph of labelled anti-CEA antibody (blue colour) showing how radioimmunotherapy effectively treated the outer, well-oxygenated tumour periphery only (Image adapted from Pedely et al., 2002)*

It has been demonstrated that the addition of anti-vascular drugs such as DMXAA and CA4 to antibody-directed therapy had a greater effect than any other combination therapy (Lash *et al.*, 1998, Chaplin *et al.*, 1999). In addition, a study of LS174T colorectal adenocarcinoma xenografts showed that there are still some fairly large areas of viable tumour remaining at the periphery of such a tumour after treatment with anti-vascular drug, while, the central tissue exhibited extensive regions of dead or dying tumour (Pedley *et al* ., 2002).

1.8.2 Exploring phospholipids distribution in tissue using MALDI imaging mass spectrometry

Profiling of lipids species represents an attractive field especially for novel cancer biomarker discovery. There is growing evidence suggesting that membrane lipids play a vital role in the carcinogenesis process (Sparvero *et al.*, 2012, Meriaux *et al.*, 2010). Lipids are important cell membrane molecules and have critical physiological roles in: regulation of energy metabolism, cellular signalling and the trafficking of immune cells (Quehenberger *et al.*, 2011, Fernandis *et al.*, 2007). In fact, disordered lipid metabolism at the cellular level is now recognised as a hallmark feature across a variety of cancer subtypes (Smith *et al.*, 2008).

MALDI mass spectrometry imaging (MALDI-MSI) is considered to be a rapidly advancing technique for intact tissue analysis. It allows simultaneous localization and quantification of biomolecules in different histological regions of interest which can offer a novel insight into the biochemistry of the tumour-microenvironment (TME) (Mirnezami *et al.*, 2014). Initially, MALDI-MSI studies focussed on the localization of proteins which have higher mass-to-charge (m/z) ratio. The application of MALDI-MSI for the study of biomolecules at the lower m/z range such as metabolites and lipids is more challenging due to the matrix-analyte cluster peaks which can interfere with the detection of low molecular weight compounds (Inoue *et al.*, 2011).

The current staining methods for lipid detection and localisation including Nile Red, Oil Red O or osmium tetroxide can be applied to frozen sections to reveal the distribution of a specific lipid classes. However, they do not provide any information about the distribution of individual lipids in the way that MALDI – MSI is able to (Goor *et al.*, 1986).

So far a limited number of studies have applied MALDI - MSI technique to identify specific lipid signatures with respect to colorectal cancer (CRC). Shimma *et al*, identified region specific lipid profiles in CRC liver metastasis samples obtained from a single patient (Shimma *et al.*, 2007). Also, Thomas *et al,* 2013 found a panel of lipid-based biomarkers to be up- and down regulated in CRC liver metastases. These preliminary studies have highlighted the potential of lipid profiling in the identification of disease relevant lipid signaures for biomarker discovery (Mirnezami *et al.*, 2014).

1.9 Introduction To Mass Spectrometry Imaging (MSI)

Mass Spectrometry Imaging (MSI) is a technique which displays the 2D structures of chemical abundance and it has been used in biological and non-biological analyses of surfaces since the 60s (Cameron *et al.*, 2012). It also allows the spatial distribution of the specific molecule to be determined. Conventional imaging techniques such as optical imaging, positron tomography, electron microscopy; atomic force microscopy and scanning tunnel microscopy are able to generate multidimensional pictures with a spatial resolution that can approach the atomic scale or femto-second temporal resolution. However, most of these techniques are unable to identify the presence of specific analytes in the images without labelling; therefore, they only provide partial chemical information. In contrast, the various MSI techniques can satisfy many of these challenges. This is due to the fact that in MSI the molecular mass of analyte, depending only on the atomic composition of the molecule, is used as the bases of detection.

This allows the detection and imaging of known and unknown analytes without need to develop a specialized label which sometimes can be difficult to produce. Also, MSI uses the analytical power of mass spectrometry (MS) to produce chemical images illustrating the distribution of both known and unknown molecules in a sample (Rubakhin *et al.*, 2005).MSI is able to measure the composition and abundance of molecules within an area of fixed dimension in a region specific manner. In MSI, data is represented as an x/y coordinate set for a given mass-to-charge (m/z) signal. The full imaging MS data set presents information in a 2^{+}n dimension space ($x/y/i_n$), where n is the number of m/z signals detected during the course of MS data acquisition and i represent the intensity of the signal which is proportional to the abundance of the corresponding molecule and can be visualized as shades of grey or with different coloured schemes. An intensity plot or image can be constructed of each m/z value (Chaurand 2012).

1.9.1 Basic Principles of Mass Spectrometry Imaging (MSI)

A mass spectrometer measures the mass-to-charge ratio (m/z) of an ionised atom or molecule and it is mainly composed of three major parts: an ion source, a mass analyzer and an ion detector (Fig .1.11). The major concept of mass spectrometric analysis is that the analyte must be transferred from the condensed phase to the gas phase and then ionized, separated in a vacuum and detected. The analyte desorption and ionization mainly occurs in the ion source. Then the generated ions are separated according to their mass to-charge ratio in the mass analyzer and are finally detected by the ion detector (Rubakhin *et al.*, 2005).

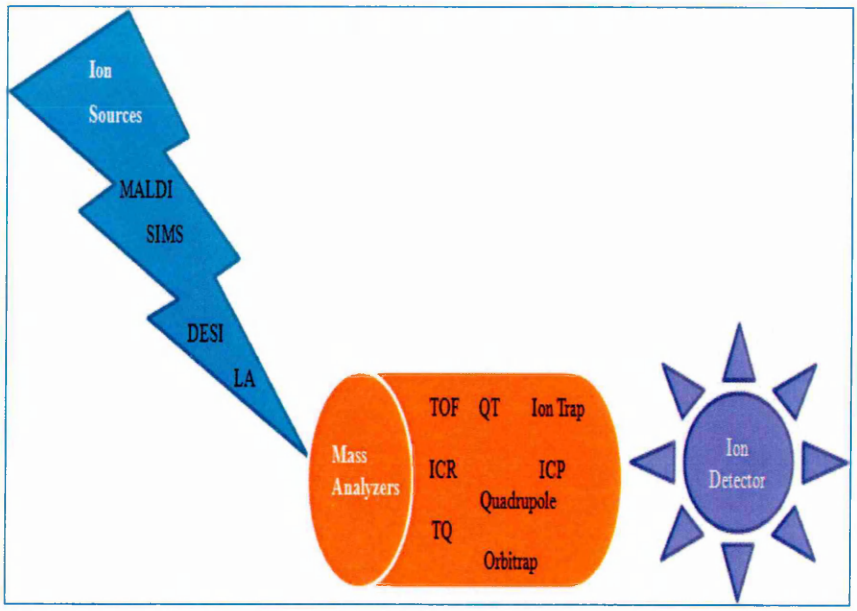

Figure 1.11: *Three Basic Components of mass spectrometer (Image adapted and reproduced from Cameron et al., 2012).*

1.9.1.1 The Ion Source

The ion source is mainly responsible for applying a charge to the molecules to produce ionization. The most common ion sources used in biological mass spectrometry are Electrospray Ionization (ESI) and Matrix-Assisted-Laser-Desorption/Ionization (MALDI) (Cameron *et al.*, 2012). In MALDI laser irradiation is used to desorb analyte ions from the sample surface. In ESI the analyte is introduced into the gas phase and ionized during the evaporation of a highly charged aerosol of a volatile solvent containing the analytes (Rubakhin *et al.*, 2005). Other desorption/ionization methods are also currently used for MSI such as secondary ion mass spectrometry (SIMS), desorption electrospray ionization (DESI), and laser ablation (LA) with post-ionization (Cameron *et al.*, 2012) (See Table 1.1).

1.9.1.2 The mass analyser

Once ionization process occurs, the ions are transferred into the mass analyser. The mass analyser is primarily responsible for separating the ions generated from the ion source. Ions are mainly selected according to their mass, charge and shape. The commonly used mass analyzers in MSI are the Time-of-Flight (TOF), ion trap and Orbitrap (Cameron *et al.*, 2012).

1.9.1.3 The detector

The detector is the last part of a mass spectrometer and it is responsible for generating signals from ions separated by the mass analyzer. These signals reach the data processing computer where they are processed to mass spectra, chromatograms or images.

1.10 Ionization approaches for imaging

Currently three desorption/ionization techniques are routinely used in MSI: SIMS, MALDI and desorption electrospray ionization (DESI). Other MS techniques such as laser ablation coupled to inductively plasma mass spectrometry (ICP-MS) are increasingly gaining popularity (Chaurand., 2012).

Types of MSI	Ionization source	Mass analyzer	Optimal analytes	Mass range (Da)	Spatial resolution (μm)
MALDI	UV/IR laser Soft ionization	TOF	Lipids, peptides, proteins, small molecules	0-50,000	5
SIMS	Ion gun Hard ionization	TOF Magnetic sector Orbitrap	Lipids, small peptides, small molecules	0-2000	0.5-1
DESI	Solvent spray Soft ionization	Orbitrap	Lipids, peptides, small molecules	0-2000	100

Table 1:1 *Comparison of different ionization approaches in MSI (Weaver and Hummon et al, 2013).*

1.10.1 MALDI

The MALDI technique was introduced in the second half of 1980s by Karas and Hillenkamp (Karas and Hillenkamp 1988) and Tanaka and co-workers (Tanaka *et al.*, 1988). It is one of the most powerful methods that are used to ionize intact biological molecules and is classified as a soft desorption/ionization method. After the development of MALDI, it was adapted to imaging. This MSI technique was first used for biological tissue imaging by the Caprioli group (Caprioli *et al.*, 1997) and this is generally held to be a major advance in the field of biological MS (Rubakhin *et al.*, 2005). To date MALDI MSI is the most widely used of the MSI techniques.

MALDI itself is performed by mixing the analyte molecule of interest with a matrix solution (Hillenkamp *et al.*, 1991). Matrices are usually small organic acids with conjugated double bond systems.

The role of the matrix is to facilitate the absorption of the ionizing laser. Once the mixture is added onto the target plate and the solvent is evaporated, matrix: analyte co-crystals are formed. The irradiation of these crystals with a pulse of, generally UV but sometimes IR, laser light generates the desorption/ionization event (Fig. 1.12). Then, the resulting ions are analyzed by MS (Chaurand., 2012). MALDI can be performed in a vacuum or at atmospheric pressure. The UV or IR laser pulses excite the matrix, causing a rapid and localized heating and the subsequent ejection of neutral and charged molecules.

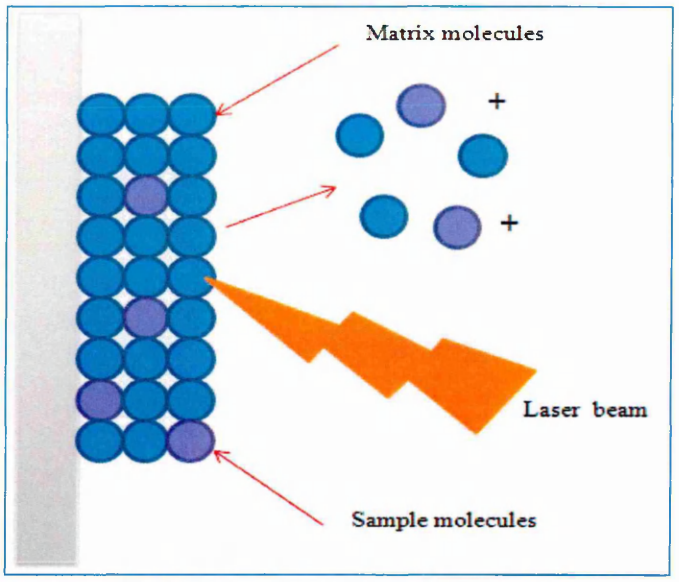

Figure 1.12 *Schematic representation of MALDI ionization process, showing the analyte molecule (purple dot) Co-crystallized with matrix molecules (blue color), the laser beam fire at the mixture causing the desorption and ionization process of both analyte and matrix molecule (Dass., 2007).*

MALDI can be used to generate both; positive and negative ions. In positive ionisation mode, the sample is kept on a positively charged metal substrate and the mono-protonated $[M + H]^+$ species are mainly generated.

However, in negative ionisation mode the deprotonated $[M - H]^-$ ions are mostly generated. Little fragmentation of analyte molecules occurs during the MALDI desorption process (Stoeckli *et al.* 2001, Garden and Sweedler .,2000). The MALDI technique allows the ionisation of several types of molecules including lipids, peptides and proteins. In 1995 by Gusev and co-workers (Gusev *et al.,* 1995) demonstrated that it was possible to analyse samples directly from thin layer chromatography (TLC) plates by MALDI and hence it could be argued provided the inspiration for much subsequent work.

1.10.1.1 Sample preparation and matrix selection for MALDI analysis

Sample preparation is usually a critical part in any experiment. Protocols for the examination of tissue by MSI require the tissue samples to be sliced into very thin sections. In the MALDI technique, the tissue samples are subject to sectioning on a cryostat with a temperature below -20°C (Amstalden *et al.*, 2010). Sample thickness is an important factor in MSI because the amount of material available for ionization depends on tissue thickness. Also, sometimes the media used in the cryo-sectioning process such as Optimal Cutting Temperature (OCT) are not suitable for MSI samples, because background interferences with MALDI MSI image are produced. Following tissue sectioning, the samples are mounted onto an appropriate MALDI target, depending on the instrument type these might be conductive plates or indium-tin-oxide (ITO) coated slides.

Additional sample preparation issues need to be considered before running the MSI experiment; washing procedures which can remove any artifacts and salts from the tissue section and enhance the matrix crystallization (Amstalden *et al.*, 2010), might be required. Choosing the washing procedures depends mainly on the analyte of interest and therefore, it is important to choose a washing procedure that is able to enhances the analyte signal and remove the suppressing interference species.

In MALDI-MSI the matrix is applied in such a way as to allow the matrix/solvent mixture to extract a sufficient amount of analyte for ionization. Enough matrix is required for optimal ionization. The acidic matrix chemicals are used with solvents such as methanol, ethanol, isopropanol or acetonitrile.

Different types of matrix are available and some of them are more compatible with certain classes of molecule than others. For example, 2,5-dihydroxybenzoic acid (DHB) is recommended for the analysis of lipids sample and small peptides while sinapinic acid (SA) is commonly used for analysis of large proteins sample (Kaletas *et al.*, 2009). In addition, α-cyano-4-hydroxycinnamicacid (α-CHCA) can cause some interference in the lower mass regions due to the fragmentation of the matrix material itself and hence is often mixed with additives such as ammonium salts, citrates or phosphates to remove the interference signals and to improve sensitivity (Smirnov *et al.*, 2004). After being coated with layers of the MALDI matrix, mass spectra are acquired by firing the laser across the sample in a raster pattern. The chemical images of the distribution of one or more analytes according to m/z values can then be produced using appropriate software (Rubakhin *et al.*, 2005).

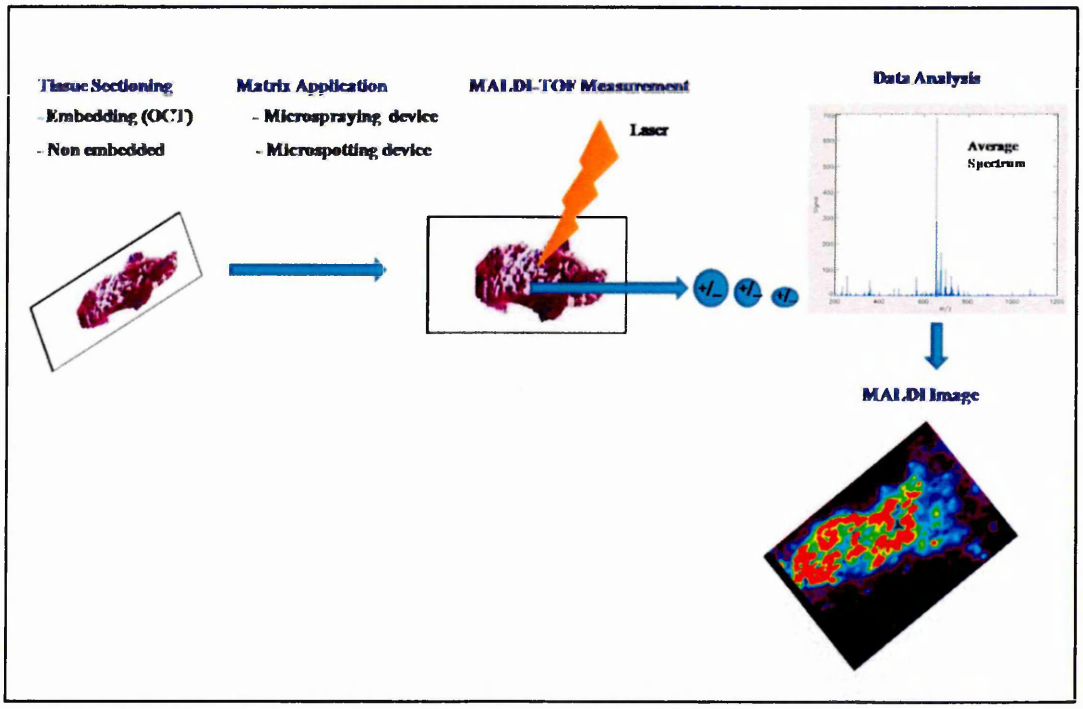

Figure 1.13 *A schematic diagram outlining the general steps in the MSI sample preparation workflow (Image adapted and reproduced from Kaspar et al., 2011).*

Matrix	Mass (Da)	Applications
2,5-Dihydroxybenzoic acid **(DHB)**	154	Lipids, small peptides ,carbohydrates and nucleotides
α-cyano-4-hydroxycinnamic acid **(HCCA)**	189	Peptides, small proteins,lipids,glycoprotein's and nucleotides
3,5-Dimethoxy-4-hydroxycinnamic acid **(SA)**	224	Large proteins, glycoprotein's and hydrophobic proteins
4,6 Trihydroxyacetophenone **(THAP)**	186	Oligo-nucleotides
3-Hydroxypicolinic acid **(3-HPA)**	139	Oligo-nucleotides
Picolinic acid	123	Oligo-nucleotides
2,6- Dihydroxyacetophenone **(DHAP)**	152	Phospholipids and large proteins
Nicotinic acid	123	Protein and oligo-nucleotides

Table 1:2 *Types of MALDI matrices and their applications (Weaver and Hummon et al., 2013).*

1.10.1.2 Matrix application for MALDI analysis

Matrix application is the most critical step in MALDI-MSI (Weaver and Hummon *et al.*, 2013). Matrix application procedures are divided into manual methods such as spraying with an airbrush, TLC sprayer or dipping the tissue sections into matrix containing solutions and automated methods. Automated devices can fall into two classes: spotting devices and spraying devices. Higher reproducibility can be achieved by using automated sprayer methods (Schwartz *et al.*, 2003 and (Kaletas *et al.*, 2009). There are many commercial devices developed for matrix application both matrix spotters (e.g. the Labcyte Portrait 630, 1190 Borregas Avenue Sunnyvale, CA, USA) which can apply small droplets of matrix solution in a controlled array onto the tissue and matrix sprayers such as the ImagePrep device (Bruker Daltonics) which utilizes vibrational vaporization of the matrix with a piezo-electric spray head to spray a fine coating of matrix onto the tissue.

Spraying allows a high spatial resolution of up to 25 μm with a good spectra quality to be obtained. Another robotic matrix sprayer is the TM-sprayer (Leaptec) in a heated capillary is used with a pneumatic spray that moves in defined patterns over the tissue section. Automatic sprayers are more reproducible than manual pneumatic sprayers (Walch *et al.*, 2008). The size of the matrix crystals deposited on the tissue is a significant factor especially in determining the spatial resolution and avoiding large volumes of matrix solvent is critical to maintain optimal spatial resolution particularly when performing MSI on small samples (Weaver and Hummon *et al.*, 2013).

1.10.1.3 MALDI imaging modes

There are several modes of imaging acquisition that can be used in MALDI- MSI. The first mode is a laser or ion microprobe imaging mode. The ion microprobe mode works by sequentially analysing an array of discrete points as the microprobe beam is scanned across the sample surface in a raster pattern typically with micron or submicron dimensions.

Then, the individual mass spectra are acquired for each point and stored digitally. By using specially designed software which enables the selection of an analyte signal from the array of mass spectra and plots the intensity of the signal for each individual point in a 2D array. The signal intensity is presented as a colour scale which creates an ion image of analyte distribution. This method is imaging in a point-by-point manner. The second mode is the ion microscope mode (e.g. the camera mode) in which a chemical images are created in manner similar to optical imaging. In this mode MSI uses desorbed (sputtered) ions from the sample to generate an image. Then the ions are separated by the specialized ion optics which preserves the relative position of these ions in the plane of the sample surface. Finally, the ions are detected in a spatially resolved manner and a chemical image is generated. Each of these two MSI methods is produces different types of data (Rubakhin *et al.*, 2005).

1.10.2 Secondary ion mass spectrometry (SIMS)

MALDI MSI has been widely used to obtain information about the distribution of large proteins and peptides at limited spatial resolution. Secondary ion mass spectrometry (SIMS) imaging has to date been mainly concerned with the imaging of much smaller analytes such as lipids, metabolites and pharmaceuticals at high spatial resolution compared to MALDI or (desorption electrospray ionisation (DESI) (Weaver and Hummon *et al.*, 2013).

Historically SIMS was used to study solid surfaces and thin films by sputtering the surface of the specimen with a focused primary ion beam and collecting and analyzing the ejected secondary ions by MS (Pacholski and Winograd., 1999). In conventional SIMS the primary ion source requires high vacuum conditions ($<10^{-6}$ torr) and uses monatomic, polyatomic, or cluster ion beams (Tempez *et al.,* 2004-Hand *et al.,* 1990). These primary ions are accelerated and focused by an electric field to form a continuous ion beam that is normally pulsed to produce an ionization event. The diameter of the ion beam can vary from a few hundred micrometers to tens of nanometers according to the application used.

The primary ions induce a chain of binary collisions on the sample surface in which the analyte atoms and molecules located within a few nano-meters of the impact point are affected (Postawa., 2004). As a result, some of the analyte atoms and molecules are ejected from the surface of the sample into the gas phase in the form of charged and neutral particles (Fig. 1.14).

There are two modes of operation in SIMS. The first mode called static SIMS and the second mode is called dynamic SIMS. In static SIMS analysis, the primary ion beam is pulsed and kept at very low energy level. However, this type of ion beam allows for detection of larger species but at lower sensitivity (Lanni *et al.*, 2012).

In order to be sure that each spectrum is acquired from undamaged sample, a very low primary ion doses are used that damage less than 1% of the sample surface area. This dose of primary ions is known as "the static SIMS limit" and this differentiates static SIMS from dynamic SIMS (McDonnell *et al.*, 2007, Lanni *et al.*, 2012). In contrast, dynamic SIMS is used to create a 3D images and it use ion dosages beyond the static limit. Dynamic SIMS tends to yield only atomic and small fragment ions; therefore, during imaging of the distributions of large molecules in biological specimens the static mode is mainly used (Rubakhin *et al.*, 2005).

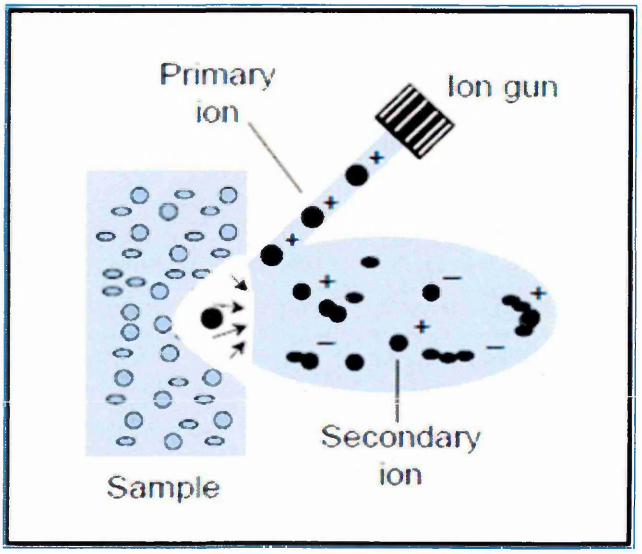

Figure 1.14 *Schematic representation of secondary ion mass spectrometry (SIMS), showing the primary ion beam hitting the sample causing the production of secondary ion (Image adapted from Rubakhin et al., 2005).*

1.10.3 Electrospray Ionization (ESI)

The electrospray ionization technique (ESI) was first successfully applied in the mid 1980s by Fenn and co-workers (Fenn *et al.*,1989) to study large organic molecules. The first demonstration of two-dimensional ESI-MSI was presented by Ford and VanBerkel in 2004 by using a surface sampling probe. This work was continued with several investigations and enhancement to produce a true MSI (Modestov *et al.*, 2001, Wachs and Henion., 2001) technique. In ESI, an aerosol of highly charged droplets containing volatile solvents and analytes is formed in an electric field (Fig. 1.15). These formed droplets are then reduced as a result of solvent evaporation and explosions until the charged and neutral analyte molecules are introduce into the gas phase. Basically, the first step in the ESI process is the formation of a Taylor cone in which the ESI droplets are emitted. The ESI ionization source is operated at atmospheric pressure and it used to ionize proteins and large peptides to produce multiply protonated or deprotonated ions as well as ions with sodium and potassium adducts.

Analytes with multiple charges can complicate the spectral interpretation because the single analyte might be represented as multiple charge states. The currently available mass analysers can analyse multiply charged ions as the distribution of m/z often exceeds 2500 - 3000. ESI is considered as a soft ionization technique which is used to characterise little or no analyte fragmentation (Rubakhin *et al.*, 2005).

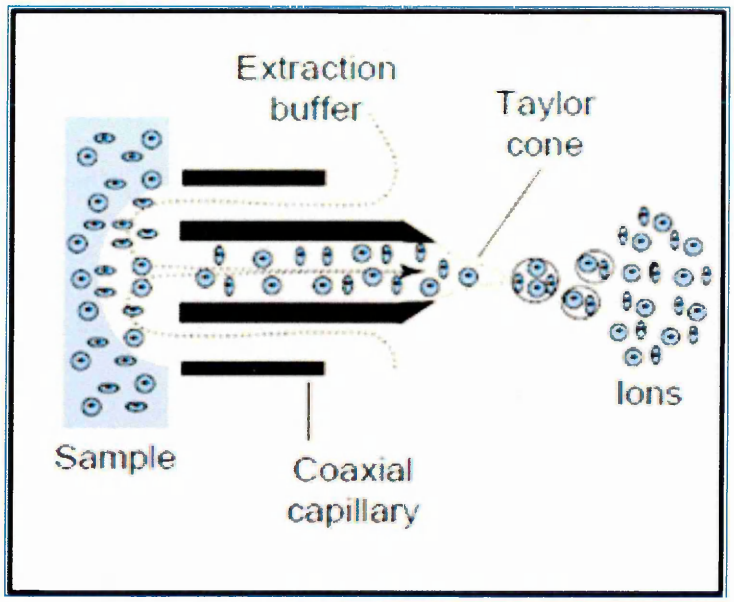

Figure 1.15 *Schematic representation of an electro-spray ionization source (ESI), showing the formation of taylor cone and the production of charged droplets, (Image adapted from Rubakhin et al., 2005).*

1.10.4 Desorption Electrospray Ionisation (DESI)

Recently, Cooks and his team have introduced a new method called desorption electrospray ionization (DESI) (Cooks., 2006). This method enables the acquisition of chemical images of untreated surfaces (Takats *et al.,* 2004). MALDI and SIMS imaging techniques require the sample to be in a vacuum chamber, while DESI is performed in ambient conditions and doesn't require the addition of matrix solution. In, DESI the ion is directly produced from the sample surface by a small jet of electrostatically charged solvent located at the angle to the sample surface. Then, the second collection tube is used to collect the ions produced after the jet of solvent extracts them from the sample surface (Vickerman., 2011).

DESI is a soft ionization technique; therefore a little fragmentation of the analytes occurs.

In DESI the ionization reactions occurring in the gas phase are similar to the ones that occur in conventional ESI. Therefore, the spectra obtained by DESI are multiply charged and similar to those obtained in an ESI experiment (Vickerman., 2011, Cooks., 2006). It has been shown that DESI isable to ionise a wide range of analytes ranging from drugs, polymers, proteins and lipids (Vismeh *et al.*, 2012). In addition, VanBerkel *et al.*, has applied DESI for line scanning of thin-layer chromatography plates in which the spatial localization of several drugs such as acetaminophen and aspirin separated on a normal-phase silica gel TLC plate was demonstrated (VanBerkel *et al* ., 2005). Finally, the rapid analysis time and the ability to couple various types of mass analysers to DESI ionization source make it an attractive technique for tissue imaging of all kinds (Weaver and Hummon *et al.*, 2013).

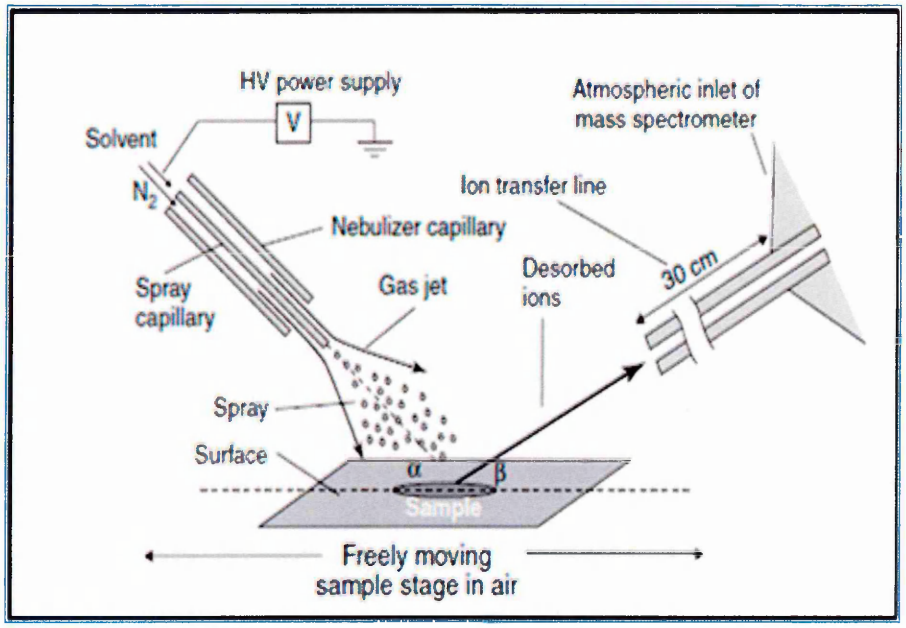

Figure 1.16 *Schematic representation of the principle of desorption electrospray ionization technique (DESI), showing the spray of charged droplets which is directed to the sample causing the production of gaseous ions of analytes (Image adapted from Dass., 2007).*

1.11 Mass Analysers

The mass analyser is the most important part of the mass spectrometer. The performance of the mass spectrometer is dependent mainly on the design of the mass analyser. The mass analyser has two basic functions: Firstly; it separates all ions according to their mass-to-charge (m/z) ratio and secondly; it focuses the resolved mass ions at a single focal point. Also, the mass analyser has the ability to maximize the transmission of all ions that come from the ion source. Basically, a mass analyser can distinguish the movement of the charged particle from another ion according to the differences in their momentum, kinetic energy, and velocity (Dass., 2007). They can be divided into two groups: The beam analysers and the trapping analysers. In the beam analysers, the ions leave the ion source in a beam and pass through the analyzing field to the detector.

While, in trapping analysers the ions are trapped in the analyzing field after being formed in the analyser itself or being injected from an external ion source (Glish and Vachet., 2003). There have been different types of mass analysers developed and the most popular designs include time-of-flight (TOF), quadrupole (Q), quadrupole ion trap (QIT), and ion mobility (Dass., 2007).

1.11.1 Time-of -Flight mass spectrometer

1.11.1.1 Linear Time-of-flight

Practically, the time-of-flight (TOF) mass spectrometer is considered as the simplest mass analyser. The TOF mass analyser mainly separates ions based on their velocity. All ions are formed at the same time and placed in the ion source and then accelerated through a fixed potential into the TOF drift tube. The ions with the same charge obtain the same kinetic energy after acceleration and the ion with lower m/z achieves higher velocities than the ion with higher m/z ions. Ion velocities are inversely linked to the square root of m/z.

After the acceleration of ions, they travel through a fixed distance typically 0.5–2.0 metres before reaching the detector. The m/z of the ion can be determined by measuring the time it takes to reach the detector after the ion formation.

Early TOF mass spectrometer were rarely used for routine MS experiments, however, the development of new pulsed-ionization techniques such as MALDI lead to a revival in TOF in the 1990s. Modern TOF mass analysers can offers mass resolution in thousands and it mass accuracies in the tens of parts per million (ppm) (Glish and Vachet., 2003).

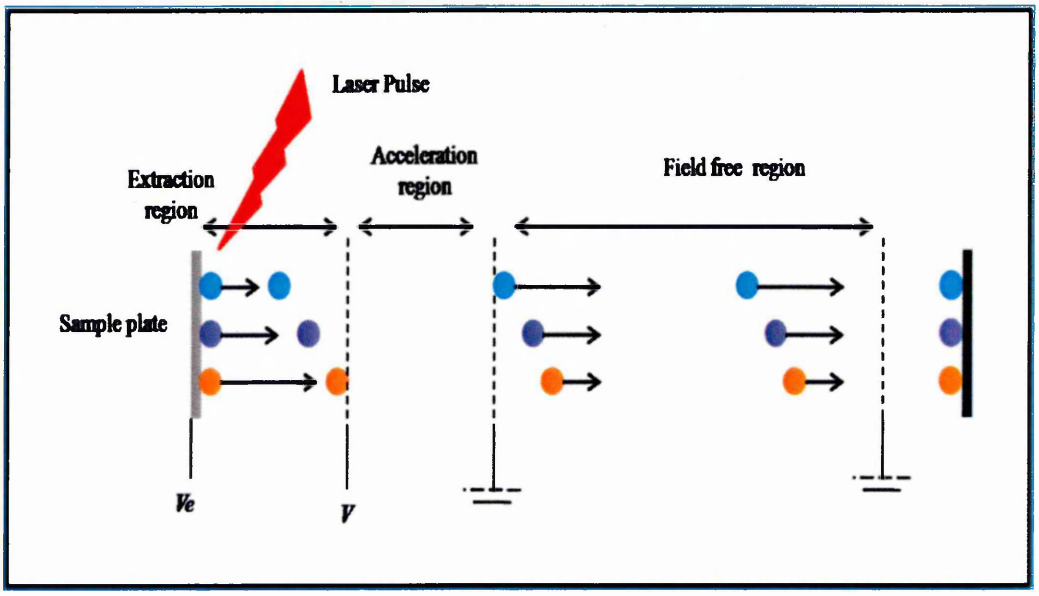

Figure 1.17 *Schematic of linear time-of-flight mass analyser, ions with initial velocity spreading to a different extent in the field-free environment of the extraction region; the slower-moving ions appear behind the faster moving ions. After the ions are produced, it accelerated in acceleration region by applying pulse into the field-free flight tube in which the ions are separated according to their velocity. In the field free region, the lighter ions (orange dots) travel faster than the larger ions (blue dots) and therefore it reach the detector first (Image adapted and reproduced from Dass., 2007).*

1.11.1.2 Reflectron Time-of-flight

In the reflectron TOF mass analysers, the ion travels through one flight distance and it then enters an electrostatic mirror (reflectron) which causes the ion to turns around and sends it down a second flight distance to the detector. The main function of the reflectron is to adjust the small differences in the velocities of ions with the same m/z. Therefore, the reflectron increases the resolution of TOF mass spectrometry (Fig. 1.18). The combination of high m/z range and compatibility with pulsed-ionization methods has made TOF the most commonly used mass analyser for MALDI experiments (Glish and Vachet., 2003).

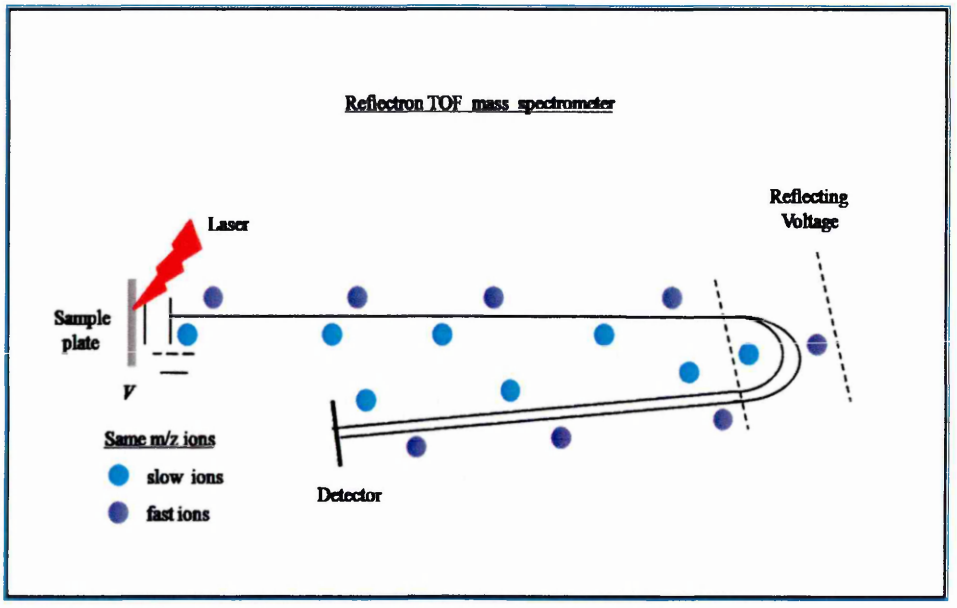

Figure 1.18 *Schematic of Reflectron time-of-flight mass analyser, ions (purple dots) of the same mass but with more kinetic energy will enter the reflectron more deeply compared to the ions (blue dots) with lower kinetic energy which result in reaching the second detector at the same time (Image adapted and reproduced from* **http://msr.dom.wustl.edu/mass-analyzers**).

1.11.2 Quadrupole Mass Filter

The quadrupole mass analyser was used as the mass analyser of choice especially for gas chromatography MS (GC/MS) and liquid chromatography MS (LC/MS) in the 1980s and 1990s. In quadrupoles, much lower voltages are used to accelerate the ions from the source to the analyser (2–50 V versus kV) compared to sector and TOF analysers (Glish and Vachet., 2003). Basically, the quadrupole consists of four parallel metal rods. The mass separation occurs by the constant movement of ions through a high-frequency oscillating electric field that is formed by applying direct-current (dc) and radio-frequency (rf) potentials to these electrodes. Ions of a specific *m/z* value pass through the geometry of quadrupole rods and reach a detector (Dass., 2007). The size of the quadrupole and the rf frequency are usually kept constant so the ions of different m/z can be consecutively allowed to reach the detector by increasing the magnitude of the rf and dc voltages. The quadrupole is in fact still considered as the instrument of choice for the combination of mass spectrometry with a range of separation techniques (Glish and Vachet., 2003). The basic principles of the quadrupole mass analyser are shown in the schematic below (Fig. 1.19).

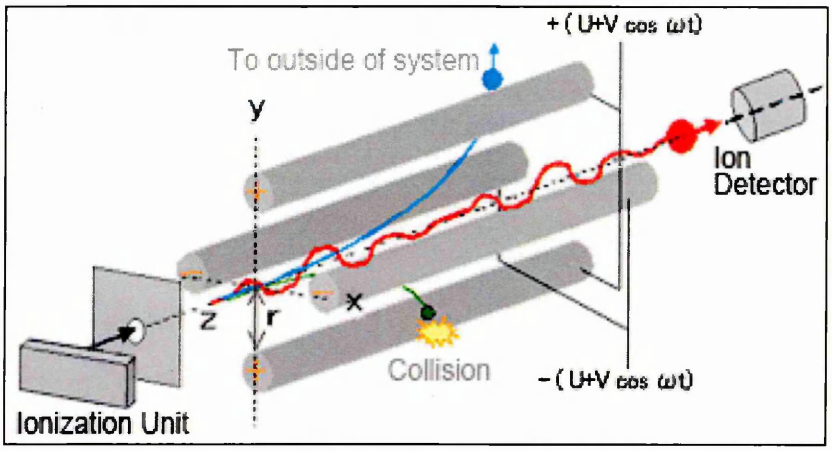

Figure 1.19 *Schematic representation of quadrupole mass analyser, the systems contain four parallel cylindrical metal rods. The ions generated in the ionization source are accelerated in the Z-direction by a low voltage and enter the quadrupole area. Voltage of the same polarity is applied to diagonally-opposite poles and opposite voltage polarity is applied to adjacent poles. When a combination of direct current voltage U and high-frequency current voltage V is applied to each pole (where, ω is frequency and t is time), ions (red dots) with a specific mass-to-charge ratio (m/z) maintain a stable oscillation and pass through the quadrupole to the detector. While, the oscillations of ions with other m/z values (blue dot) become unstable causing them to collide with the poles and removed from the system (Image adapted from www.shimadzu.co.uk).*

1.11.3 Quadrupole Ion-Trap mass spectrometer

The quadrupole ion trap (QIT) mass analyser consist of an electric field that is mainly formed in three dimensions in which ions are trapped (Glish & Vachet., 2003). The mass separation in a QIT is brought about by initially trapping all ions in the trapping space in which an oscillating electric field is formed within the boundaries of a three-electrode structure. The mass spectrum is acquired (and mass separation produced) by changing the applied rf field in order to eject ions sequentially from the trapping field.

The three-electrode structure of a QIT consists of a doughnut-shaped central ring electrode and two identical end-cap electrodes, each with a hyperbolic geometry (Fig. 1.20).

One of the end-cap electrodes contains a small gap in which an externally formed ion beam can enter the trap. Whereas, the other end-cap electrode contain several gaps used for the ejection of ions into a detector (Dass., 2007). The three-dimensional quadrupole field is formed by applying a potential to the ring electrode and maintain the end-cap electrodes at ground potential. This created quadrupole field forces the ions with a broad *m/z* range to be trapped within the boundaries of the electrodes. Then, helium is introduced into the trap to cool the ions collisionally and to confine them in the centre of the trap. By increasing the magnitudes of the dc and rf voltages and the frequency of the rf signal ions with higher *m/z* values become sequentially unstable in the axial direction and ejected out of the trap for external detection. The mass spectrum of the trapped ions is obtained by using this mass-selective instability (also known as mass-selective axial ejection) mode of mass analysis (Dass., 2007).

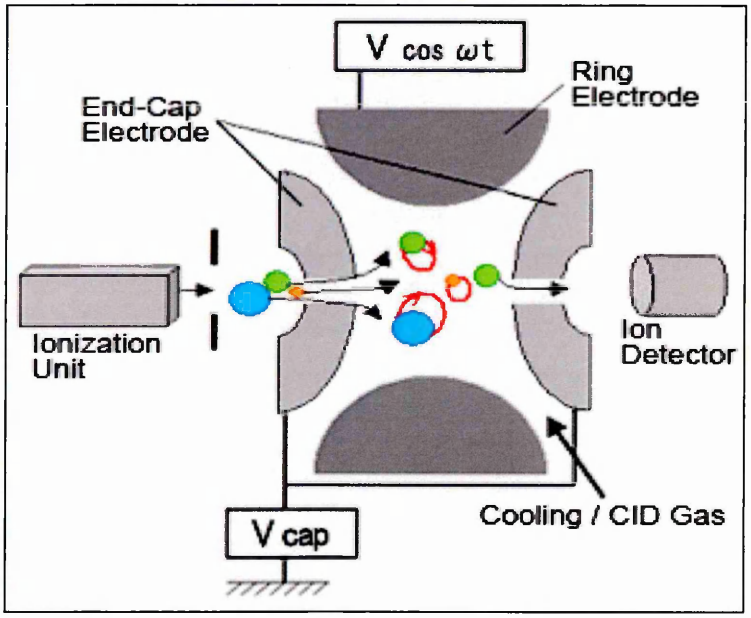

Figure1.20 *Schematic of quadrupole Ion trap mass analyser, shown a donut shaped ring electrode sandwiched between two end-cap electrodes. An ionization unit is located at the entrance and a detector at the exit (Image adapted from www.shimadzu.co.uk).*

1.11.4 Ion Mobility Spectrometry and Ion Mobility Mass Spectrometry

The ion mobility (IM) spectrometer is considered as a hybrid instrument which combines IM separation with a conventional mass spectrometry system. An IM spectrometer uses gas-phase mobility rather than *m/z* ratio to separate ions (Wu *et al.*, 1998, Clemmer and Jarrold., 1997). The mobility of ions can be measured under the influence of a gradient electrical field and depends mainly on an ion's collision cross section and net charge. The IM spectrometer consists of two regions: a reaction region and a drift region. Both regions contain a series of uniformly spaced electrodes connected through a series of high resistors to provide uniform electric field strength. The two regions are separated by an electrical shutter. The buffer gas is circulated into the drift tube. The ions are generated in the reaction chamber and then enter the drift region by opening the electrical shutter for a short period. With the influence of an electrical field, the ions drift into the drift tube in which separation occurs according to size-to-charge ratio. The mobility of ions is as a result of combined effect of ion accelerated by the electric field and the retardation occurs by collisions with the buffer gas. A detector is placed at the end of the drift region for the detection of the separated ions (Eiceman and Stone., 2004).

Ion mobility separation can be coupled with a quadrupole or TOF mass analyser in which the IM is used purely as an ion pre-separation device and the quadrupole or TOF mass analyser is used for separation by m/z and as the detection device (Laboda., 2006 , Srebalus and Clemmer., 2001). The MALDI ion source has been coupled to IM-MS type instruments for the analysis of proteins and tryptic peptides (Laboda., 2006, Ruotolo *et al.*, 2002). IMS has also been applied for the detection of drugs, chemical reagents, and environmental pollutants; size distribution of aerosol particles; structure information of gas-phase clusters; and conformational studies of proteins and oligonucleotides (Srebalus *et al.*, 2001, Clemmer et *al.*, 1997).

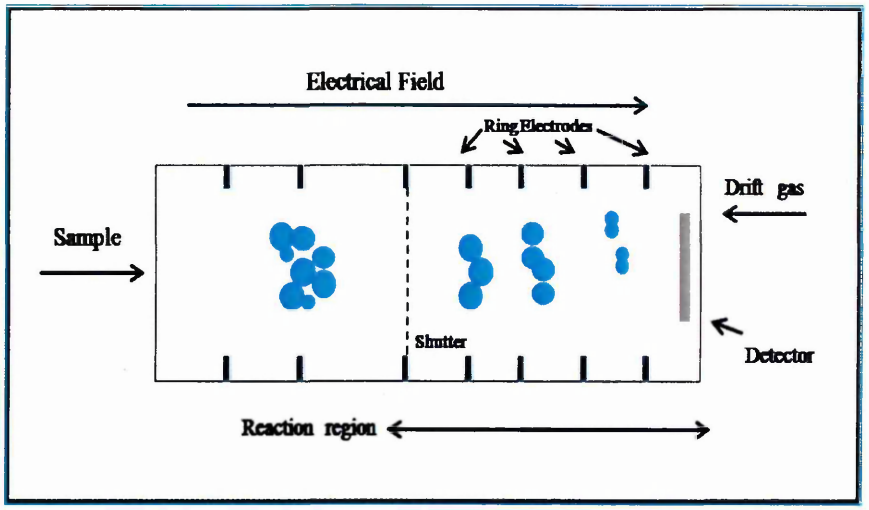

Figure 1.21 *Schematic representation of ion mobility spectrometry (Image adapted and reproduced from Dass., 2007).*

1.12 Mass detector

1.12.1 Electron multiplier

The electron multiplier or secondary electron multiplier (SEM) is the most commonly used ion detector in mass spectrometry. It works via secondary electron emission and consist of a series of dynodes (16 or 20) that are connected together through a chain of resistors of equal value. About (−3000 V) voltage is applied between the first dynode (the conversion dynode) and the last dynode (the anode) and each dynode is maintained at a higher positive potential than the previous one. So when a beam of fast moving ions hits the conversion dynode, several secondary electrons are emitted. Then the emitted electron hits the second dynode in which several more secondary electrons are emitted for each electron. This process is repeated in subsequent dynodes causing an amplification of secondary electrons at each successive stage. Finally, amplification of the cascade electron current that arrives at the anode is used to provide an excess of 10^7 electrons for each incident ion. This detector can be used in an analog or pulse counting mode. Also, this detector is characterised by fast response time, high sensitivity, and high gains (Dass., 2007).

1.13 The Major Methodologies Used for the Separation of Lipids

1.13.1 Overview

Currently mass spectrometry is one of the key methods that are successfully used for lipid analysis (Lin *et al.*, 2014). However, NMR spectroscopic methods are considered to be powerful tools in lipid research regardless of their relatively low sensitivity. NMR has many advantages such as it doesn't require a previous extraction when it used under *in vivo* conditions. Also, it is able to locate the position of double bonds within a given lipid which can help in the differentiation between cis and trans isomers (Gunstone, 1993).

Another particular powerful method is 31P NMR in which it can be exclusively used in the analysis of phosphorous containing compounds (Spyros *et al.*, 2000). This method allows the differentiation and quantification of all phospholipids (PL) classes within a single spectrum based on the differences in their head group (Schiller *et al.*, 2007). The main advantage of 31P NMR is that it doesn't require an extraction of the sample of interest with organic solvents but that the sample can be directly solubilised in the detergent and this prevents losses of phospholipids (PL). A limitation of the technique is however that the spectra of 31P NMR are normally recorded in the presence of a suitable detergent (e.g. sodium cholate) in which it suppress the aggregation of PL resulting in severe line-broadening and loss of resolution (NouriSorkhabi., 1996). Many different methods of lipid analysis based on chromatographic and spectroscopic methods have been established e.g. high performance liquid chromatography (HPLC). These are summarised in Table 2:1.

High performance thin layer chromatography (HPTLC) is generally considered to be a versatile and reliable technique for lipid analysis. It is known as an extremely powerful tool and can be applied to all relevant lipid classes of physiological and diagnostic interest including apolar cholesteryl esters, triacylglycerols to highly polar poly-phosphoinositides. Furthermore, HPTLC can speed analysis in comparison to other chromatographic techniques (Fuchs *et al.*, 2011).

Method	Principles	Advantages	Disadvantages
Thin-layer chromatography (TLC)	Separation is achieved on stationary phase normally silica gel due to the polarity differences of the analytes	TLC is quite inexpensive and fast. Variations of the mobile phase enable separation of even complex mixtures. Different staining can beeasily performed	Oxidation of unsaturated Lipids occur if the TLC plate is stored for a while since a large (lipid) surface is exposed to atmospheric oxygen. Preparativ applications are limited
High-performance liquid chromatography (HPLC)	Separation on stationary Phase under high pressure by elution with different solvents	High quality separations are achievable. Also applicable on a preparative scale. Coupling with MS is well established.	More time-consuming and expensive than TLC. Detection of saturated lipids (lack of UV absorptions) is difficult. Post-column derivatisation is challenging
Gas chromatography (GC)/GC/MS	Separation of volatile compounds on a carrier gas. Detection often performed by means of mass spectrometry	Highly established in fatty acid analysis. Automated devices are commercially available	Only volatile compounds can be analyzed. Thus, derivatisation of the analyte is required
Soft ionization mass spectrometry	MALDI and ESI MS enable the characterization of lipids without major analyte fragmentation	Both techniques are highly sensitive and enable direct analyte detection. Handling is normally quite simple	Ion suppression may occur; different lipid classes are detectable with strongly different sensitivities. Impurities affect spectral quality significantly
1H/13C NMR	Differences in electron densities lead to different chemical shifts of the observed nucleus within a given compound	Basically all lipids are detectable. Correlation (2D) experiments can be performed to obtain further information, for instance to differentiate isomers. Interaction studies (e.g. with proteins) can be easily performed	Complex spectra are obtained if mixtures are analyzed. Very limited sensitivity (13C) and need of deuterated solvents. Expensive equipment
31P NMR	Differences in electron densities lead to different chemical shifts of the observed nucleus within a given compound	Direct absolute quantitation is possible. Isomeric lipids can be differentiated.	Only lipids containing phosphorous are detectable. Limited sensitivity. Expensive equipment

Table 1:3 *Important techniques for lipid analysis and their advantages and disadvantages (Fuchs et al., 2011).*

1.14 Introduction to TLC-MALDI Coupling

Thin layer chromatography (TLC) was known since about 1938. In 1975, one major progress was achieved when HPTLC was introduced to allow separations with much higher quality and higher sensitivity. Then in 2001, an additional improvement was also achieved by the introduction of Ultra-Thin-Layer Chromatography (UTLC) which allows even more efficient separations. Currently, a wide range of pre-coated TLC plates are commercially available to allow reproducible, time-saving separations. In the past, there were considerable attempts to combine TLC with mass spectrometry (MS). However, TLC coupling with MS became first really successful with the invention of the soft ionization and desorption MS techniques such as MALDI and DESI as previously described (Fuchs *et al.*, 2011). TLC–MALDI MS has been applied for the analysis of different kinds of polymers, including peptides and proteins (Gusev *et al.*, 1995), nucleotides (Isbell *et al.*, 1999), glycol sphingolipids (Guittard *et al.*, 1999), lipopolysaccharides (Therisod *et al.*, 2001) and styrene oligomers (Matsumoto *et al.*, 1999, Matsumoto *et al* ., 2001). Low-molecular- weight compounds such as dyes (Mehl *et al.*, 1997, Mehl and Hercules., 2000, Bristow and Creaser., 1995), drugs (Nicola *et al.*, 1996) and pesticides (Vermillion-Salsburg *et al.*, 1999). TLC-MALDI-MS has many advantages over other methods of analysis:

(a) There is no need to extract the sample from the TLC plate before analysis which helps to avoid the risk of losing some material upon the extraction process.

(b) The analysis can be performed very fast, therefore the risks of sample alteration by oxidation, can be reduced.

(c) A higher resolution is achieved compared to the visual inspection of the TLC plate. The achievable MS resolution is determined mainly by the laser spot size that is normally about 50μm which means that 20 individual MALDI mass spectra can be recorded from a TLC spot of a diameter of 1mm and this could resolve different components that could never be resolved by common staining protocols (Fuchs *et al.*, 2011).

Mass spectrometric detection can bring additional information complementary to the chromatographic process, in which it improves the certainty of identification and the specificity of detection. The evolution of TLC–MS has been slow compared with LC-MS *(Poole., 2003).* Coupling TLC with MS greatly increases the information content and effective separation capabilities of TLC because chromatographically overlapping analytes can be resolved using MS detection. Also, TLC-MALDI takes the advantage of the high sensitivity (femtomole-attomole range) of MALDI which can ionize both low and high molecular weight compounds without significant fragmentation. It has been shown that a better spatial resolution and sensitivity is achieved when directly coupling TLC with MALDI in comparison to secondary ion mass spectrometry (SIMS) (Busch *et al.*, 1992, Doherty and Busch., 1989) and fast-atom bombardment (FAB) (Monaghan *et al.,* 1992, Oka *et al.*, 1993). MALDI is more applicable than direct laser desorption ionization (LDI) (Fanibanda *et al.*, 1994 , Kubis *et al.*, 1989) because the fragmentation of larger analytes is reduced in MALDI in comparison to these other techniques.

1.15 MALDI and proteomic biomarker studies

Proteomic experiments involve several well established methods which work to resolve and analyse complex mixtures of proteins derived from cells and tissues. However, the resolving power of these methods can be affected by the diversity and dynamic nature of the proteome (Westont *et al.*, 2004).

The proteome is defined as the sum of all proteins in an organism, a cell, organelle or a body fluid. Since the proteome is a highly dynamic system it includes much more information than the genome. The major application of proteomics is to study disease related biomarkers which are over or under expressed. These will help to differentiate between healthy and diseased samples for earlier diagnosis and can give an insight to the advancement of the case (Rifai *et al.*, 2006). The understanding of cancer process relies mainly on the identification of diagnostic biomarkers such as proteins which are correlated to disease states or represent a potential therapeutic targets. In fact, stress protein i.e. heat shock proteins families and some membrane proteins were found to be involved in tumour progression and considered as potential novel chemotherapeutic targets (Scriven *et al.*, 2007, Matsumoto *et al.*, 2000). Therefore, studying the distribution of protein biomarkers and monitoring the changes occur in their expression during tumour development has attracted much attention.

The MALDI-MSI technique allows direct screening of proteomic information from a tissue section without need of a specific target. This can help to identify target proteins that related to tumour progression. Many papers have reported on the usefulness of the MALDI technique for the direct analysis of proteins in biological tissue sections by plotting their spatial distribution within different regions of tissue section (Chaurand *et al.*, 2001, Lemaire *et al.*, 2007). In addition, MALDI-MSI has been used to explore the changes in protein profiles within tumour tissue sections and also the changes occur in response to therapeutic agents (Stoeckli *et al.*, 2001, Reyzer *et al.*, 2004). Such studies prove that MALDI-MSI can be used to distinguish between cancerous and normal tissues highlighting the benefit of the technique for rapid characterisation of a disease at the protein level.

Protein sample pre-treatment in direct MALDI-MSI is often carried out by the use of *in situ* digestion to increase the amount of protein information and improve the detection of some proteins (Djidja *et al.*, 2009).

Lemaire *et al.*, 2007 have been reported a strategy which facilitates and improves the identification and localisation of proteins within samples by combining *in situ* micro-digestion and *in situ* extraction of proteins in formalin-fixed paraffin embedded (FFPE) tissue sections (Lemaire *et al.*, 2007, Stauber *et al.*, 2008). Another study has reported the use of *in situ* digestion on frozen tissue sections which allowed the identification of many signals within rat brain tissue sections (Shimma *et al*, 2006, Groseclose *et al*, 2007). Djidja *et al.* reported that protein signals show different profiles in tumour and necrotic regions in terms of signal intensities and that the necrotic area was found to be rich in the m/z range between 4000 and 10,000 compared with the tumour region. In addition, some signals were mostly detected in the tumour area such as m/z 6904.6 and 7673.4 which correspond to haemoglobin alpha (Djidja *et al.*, 2009). Furthermore, histones have been reported as good targets for MALDI-MSI in tumour tissue sections (Reyzer *et al.*, 2004, Chaurand *et al.*, 2004).

A study of Cole *et al*, 2011 reported the use of MALDI-MSI to study the effect of treatment with CA-4-P vascular disrupting agent on mouse VEGF120 tumours. In this work the suspected pharmacological response of haemorrhaging to treatment with CA-4-P has been investigated. Also, the MALDI-MS image shows an increase in haemoglobin (Hb) signal along with other peptides such as actin at m/z 1198 and histone 2A at 944 m/z after treatment with CA-4-P. This increase in tissue haemoglobin is due to the vascular damaging properties of CA-4-P which cause a disruption of the capillary, endothelial cell necrosis and leakage of blood cells into tumour tissues.

Examples of protein biomarkers observed by MALDI-MSI along with the m/z of the peptides used for their identification in *in-situ* digestion experiments are listed in Table 1.4.

Protein assignment	Observed m/z with MALDI - MSI	Molecular function
Actin, aortic smooth muscle	1198.7	Cell mobility
Actin, cytoplasmic1	1790.9 1954.1	Cell mobility
Albumin	1467.8	
Estrogens receptor beta	837.4	Nuclear hormone
Fibroblast growth factor 13	844.5	Nervous system development
Haemoglobin subunit alpha	958.6 1361.7 1529.7	Gene regulation
Histone H2A	944.5 2104.2 2915.6	Gene regulation
Histone H2B	901.5 1743.8	Gene regulation
Histone H3	788.5 831.5 1032.6 1489.9	
Histone H4	1325.7 1466.8	Gene regulation
High mobility group protein β1	1944.9	DNA binding
Metastasis associated protein 2	2428.2	Regulation of gene expression as repressor and activator

Table 1:4 *List of some observed peptides by direct MALDI-MSI analysis following in situ digestion (Djidja et al., 2009).*

1.16 Scope of this thesis

1.16.1 Aims of the study

The main aim of the study reported in this thesis was to use Matrix Assisted Laser Desorption Ionisation - Mass Spectrometry Imaging (MALDI-MSI) to study the distribution, effect and fate of anti-cancer drugs, in particular DMXAA in xenograft tumours. A xenograft model of an LS 174T human colorectal adenocarcinoma cell line was used in this study and the tissue samples were analysed for markers of efficacy/resistance using both MALDI-MSI and conventional TLC and proteomic techniques. The project was a collaborative one between the Biomedical Research Centre at Sheffield Hallam University and The Institute of Cancer Therapeutics, The University of Bradford.

Chapter 2 describes the use of MALDI-MSI to study the distribution of anti-cancer drugs, DMXAA, in LS1 74T xenograft tumours. The mass spectrometry imaging experiment of drug distribution was carried out along with drug limit of detection /quantitation study on tissue. The interpretation of histological and imaging data is also presented.

Chapter 3 presents data on MALDI-MSI analyses of phospholipids induced by DMXAA treatment in dosed and control LS 174T xenograft tumours. In addition, the application of a tissue washing technique using NH_4Ac to improve the analysis of phospholipids in both positive and negative ions modes is described in this chapter.

Chapter 4 introduces the method of direct TLC coupling with MALDI mass spectrometry for the analysis of extracted phospholipids from xenograft tumours treated with the vascular disrupting agent, DMXAA. MALDI MS/MS analysis was used to confirm and identify the structure of the phospholipids. PCA and PCA-DA statistical analysis of these data is also described in this chapter.

Chapter 5 characterisation of the proteins induced by DMXAA treatment in LS1 74T xenograft tumours using MALDI-MSI was carried out to determine the treatment response. The method of *in situ* tissue tryptic digestion is described in this chapter. Further data analysis using bioinformatics software (MASCOT) and the statistical software MarkerView to identify differences in the expression of protein between different time courses is also presented.

Chapter 6 presents a summary of the whole work performed in this thesis, along with concluding remarks and recommendations for future studies.

1.17 References

AERNI, H., CORNETT, D.S. and CAPRIOLI, R.M., 2006. Automated acoustic matrix deposition for MALDI sample preparation. *Analytical Chemistry,* **78**(3), pp. 827-834.

ALESSANDRO, R., BELLUCO, C. and KOHN, E.C., 2005. Proteomic approaches in colon cancer: promising tools for new cancer markers and drug target discovery. *Clinical colorectal cancer,* **4**(6), pp. 396-402.

AMSTALDEN VAN HOVE, ERIKA R, SMITH, D.F. and HEEREN, R., 2010. A concise review of mass spectrometry imaging. *Journal of chromatography A,* **1217**(25), pp. 3946-3954.

ATKINSON, S.J., LOADMAN, P.M., SUTTON, C., PATTERSON, L.H. and CLENCH, M.R., 2007. Examination of the distribution of the bioreductive drug AQ4N and its active metabolite AQ4 in solid tumours by imaging matrix-assisted laser desorption/ionisation mass spectrometry. *Rapid communications in mass spectrometry,* **21**(7), pp. 1271-1276.

BAGULEY, B.C., 2003. Antivascular therapy of cancer: DMXAA. *The lancet oncology,* **4**(3), pp. 141-148.

BAGULEY, B.C., ZHUANG, L. and KESTELL, P., 1997. Increased plasma serotonin following treatment with flavone-8-acetic acid, 5,6-dimethylxanthenone-4-acetic acid, vinblastine, and colchicine: relation to vascular effects. *Oncology research,* **9**(2), pp. 55-60.

BRISTOW, A.W. and CREASER, C.S., 1995. Matrix-assisted laser desorption/ionization combined with quadrupole ion-trap mass spectrometry for the direct analysis of colour couplers adsorbed on solid substrates. *Rapid communications in mass spectrometry,* **9**(14), pp. 1465-1469.

BROWN, J.M. and WILSON, W.R., 2004. Exploiting tumour hypoxia in cancer treatment. *Nature Reviews Cancer,* **4**(6), pp. 437-447.

BUCHANAN, C.M., SHIH, J., ASTIN, J.W., REWCASTLE, G.W., FLANAGAN, J.U., CROSIER, P.S. and SHEPHERD, P.R., 2012. DMXAA (Vadimezan, ASA404) is a multi-kinase inhibitor targeting VEGFR2 in particular. *Clinical science,* **122**(10), pp. 449-457.

BUSCH, K., MULLIS, J. and CHAKEL, J., 1992. High resolution imaging of samples in thin layer chromatograms using a time-of-flight secondary ion mass spectrometer. *JPC.Journal of planar chromatography, modern TLC,* **5**(1), pp. 9-15.

CAO, Z., BAGULEY, B.C. and CHING, L.M., 2001. Interferon-inducible protein 10 induction and inhibition of angiogenesis in vivo by the antitumor agent 5,6-dimethylxanthenone-4-acetic acid (DMXAA). *Cancer research,* **61**(4), pp. 1517-1521.

CAMERON, L., 2012. Mass spectrometry imaging: facts and perspectives from a non-mass spectrometrist point of view. *Methods,* **57**(4), pp. 417-422.

CAPRIOLI, R.M., FARMER, T.B. and GILE, J., 1997. Molecular imaging of biological samples: localization of peptides and proteins using MALDI-TOF MS. *Analytical Chemistry,* **69**(23), pp. 4751-4760.

CHAPLIN, D.J. and DOUGHERTY, G.J., 1999. Tumour vasculature as a target for cancer therapy. *British journal of cancer,* **80 Suppl 1**, pp. 57-64.

CHAPLIN, D.J., PETTIT, G.R. and HILL, S.A., 1999. Anti-vascular approaches to solid tumour therapy: evaluation of combretastatin A4 phosphate. *Anticancer Research,* **19**(1A), pp. 189-195.

CHAURAND, P., 2012. Imaging mass spectrometry of thin tissue sections: a decade of collective efforts. *Journal of proteomics,* **75**(16), pp. 4883-4892.

CHAURAND, P., DAGUE, B.B., PEARSALL, R.S., THREADGILL, D.W. and CAPRIOLI, R.M., 2001. Profiling proteins from azoxymethane-induced colon tumors at the molecular level by matrix-assisted laser desorption/ionization mass spectrometry. *Proteomics,* **1**(10), pp. 1320-1326.

CHAURAND, P., SCHWARTZ, S.A. and CAPRIOLI, R.M., 2004. Assessing protein patterns in disease using imaging mass spectrometry. *Journal of proteome research,* **3**(2), pp. 245-252.

CHING, L., CAO, Z., KIEDA, C., ZWAIN, S., JAMESON, M. and BAGULEY, B., 2002. Induction of endothelial cell apoptosis by the antivascular agent 5, 6-dimethylxanthenone-4-acetic acid. *British journal of cancer,* **86**(12), pp. 1937-1942.

CHING, L.M., GOLDSMITH, D., JOSEPH, W.R., KORNER, H., SEDGWICK, J.D. and BAGULEY, B.C., 1999. Induction of intratumoral tumor necrosis factor (TNF) synthesis and hemorrhagic necrosis by 5,6-dimethylxanthenone-4-acetic acid (DMXAA) in TNF knockout mice. *Cancer research*, **59**(14), pp. 3304-3307.

CHING, L.M., JOSEPH, W.R. and BAGULEY, B.C., 1992. Antitumour responses to flavone-8-acetic acid and 5,6-dimethylxanthenone-4-acetic acid in immune deficient mice. *British journal of cancer*, **66**(1), pp. 128-130.

CHRISTIE, W.W., 1993. Preparation of lipid extracts from tissues. *Advances in lipid methodology,* **2**, pp. 195-213.

CLEMMER, D.E. and JARROLD, M.F., 1997. Ion mobility measurements and their applications to clusters and biomolecules. *Journal of Mass Spectrometry,* **32**(6), pp. 577-592.

COOKS, R.G., OUYANG, Z., TAKATS, Z. and WISEMAN, J.M., 2006. Detection Technologies. Ambient mass spectrometry. *Science (New York, N.Y.),* **311**(5767), pp. 1566-1570.

COLE, L., DJIDJA, M., BLUFF, J., CLAUDE, E., CAROLAN, V., PALEY, M., TOZER, G. and CLENCH, M., 2011. Investigation of protein induction in tumour vascular targeted strategies by MALDI MSI. *Methods,* **54**(4), pp. 442-453.

CULLIS, P.R., FENSKE, D.B. and HOPE, M.J., 1996. Physical properties and functional roles of lipids in membranes. *New comprehensive biochemistry,* **31**, pp. 1-33.

DANQUAH, M.K., ZHANG, X.A. and MAHATO, R.I., 2011. Extravasation of polymeric nanomedicines across tumor vasculature. *Advanced Drug Delivery Reviews,* **63**(8), pp. 623-639.

DASS, C., 2007. Fundamentals of contemporary mass spectrometry. John Wiley & Sons.

DJIDJA, M., FRANCESE, S., LOADMAN, P.M., SUTTON, C.W., SCRIVEN, P., CLAUDE, E., SNEL, M.F., FRANCK, J., SALZET, M. and CLENCH, M.R., 2009. Detergent addition to tryptic digests and ion mobility separation prior to MS/MS improves peptide yield and protein identification for *in situ* proteomic investigation of frozen and formalin-fixed paraffin-embedded adenocarcinoma tissue sections. *Proteomics,* **9**(10), pp. 2750-2763.

DOBRZYŃSKA, I., SZACHOWICZ-PETELSKA, B., SULKOWSKI, S. and FIGASZEWSKI, Z., 2005. Changes in electric charge and phospholipids composition in human colorectal cancer cells. *Molecular and cellular biochemistry,* **276**(1-2), pp. 113-119.

DOHERTY, S.J. and BUSCH, K.L., 1989. Preservation of spatial resolution with use of a phase-transition extraction matrix in chromatography/secondary ion mass spectrometry. *Analytica Chimica Acta,* **218**, pp. 217-229.

DUECK, D., CHAN, M., TRAN, K., WONG, J.T., JAY, F.T., LITTMAN, C., STIMPSON, R. and CHOY, P.C., 1996. The modulation of choline phosphoglyceride metabolism in human colon cancer. *Molecular and cellular biochemistry,* **162**(2), pp. 97-103.

DVORAK, H.F. and GRESSER, I., 1989. Microvascular injury in pathogenesis of interferon-induced necrosis of subcutaneous tumors in mice. *Journal of the National Cancer Institute,* **81**(7), pp. 497-502.

EICEMAN, G. and STONE, J., 2004. Peer reviewed: Ion mobility spectrometers in national defense. *Analytical Chemistry,* **76**(21), pp. 390 A-397 A.

FANIBANDA, T., MILNES, J. and GORMALLY, J., 1994. Thin layer chromatography—mass spectrometry using infrared lase desorption. *International Journal of Mass Spectrometry and Ion Processes,* **140**(1), pp. 127-132.

FENN, J.B., MANN, M., MENG, C.K., WONG, S.F. and WHITEHOUSE, C.M., 1989. Electrospray ionization for mass spectrometry of large biomolecules. *Science (New York, N.Y.),* **246**(4926), pp. 64-71.

FERNANDIS, A.Z. and WENK, M.R., 2007. Membrane lipids as signaling molecules. *Current opinion in lipidology,* **18**(2), pp. 121-128.

FORD, M.J. and VAN BERKEL, G.J., 2004. An improved thin-layer chromatography/mass spectrometry coupling using a surface sampling probe electrospray ion trap system. *Rapid communications in mass spectrometry,* **18**(12), pp. 1303-1309.

FUCHS, B., SÜß, R., TEUBER, K., EIBISCH, M. and SCHILLER, J., 2011. Lipid analysis by thin-layer chromatography—a review of the current state. *Journal of Chromatography A,* **1218**(19), pp. 2754-2774.

GABRA, H. and AS1404-202 STUDY GROUP INVESTIGATORS, 2006. Phase II study of DMXAA combined with carboplatin and paclitaxel in recurrent ovarian cancer, *ASCO Annual Meeting Proceedings 2006*, pp. 5032.

GARDEN, R.W. and SWEEDLER, J.V., 2000. Heterogeneity within MALDI samples as revealed by mass spectrometric imaging. *Analytical Chemistry,* **72**(1), pp. 30-36.

GLISH, G.L. and VACHET, R.W., 2003. The basics of mass spectrometry in the twenty-first century. *Nature Reviews Drug Discovery,* **2**(2), pp. 140-150.

GOTO-INOUE, N., HAYASAKA, T., ZAIMA, N. and SETOU, M., 2011. Imaging mass spectrometry for lipidomics. *Biochimica et Biophysica Acta (BBA)-Molecular and Cell Biology of Lipids,* **1811**(11), pp. 961-969.

GRIDELLI, C., ROSSI, A., MAIONE, P., ROSSI, E., CASTALDO, V., SACCO, P.C. and COLANTUONI, G., 2009. Vascular disrupting agents: a novel mechanism of action in the battle against non-small cell lung cancer. *The oncologist,* **14**(6), pp. 612-620.

GROSECLOSE, M.R., ANDERSSON, M., HARDESTY, W.M. and CAPRIOLI, R.M., 2007. Identification of proteins directly from tissue: in situ tryptic digestions coupled with imaging mass spectrometry. *Journal of Mass Spectrometry,* **42**(2), pp. 254-262.

GUITTARD, J., HRONOWSKI, X.L. and COSTELLO, C.E., 1999. Direct matrix-assisted laser desorption/ionization mass spectrometric analysis of glycosphingolipids on thin layer chromatographic plates and transfer membranes. *Rapid communications in mass spectrometry,* **13**(18), pp. 1838-1849.

GUSEV, A.I., PROCTOR, A., RABINOVICH, Y.I. and HERCULES, D.M., 1995. Thin-layer chromatography combined with matrix-assisted laser desorption/ionization mass spectrometry. *Analytical Chemistry,* **67**(11), pp. 1805-1814.

GUSEV, A.I., VASSEUR, O.J., PROCTOR, A., SHARKEY, A.G. and HERCULES, D.M., 1995. Imaging of thin-layer chromatograms using matrix-assisted laser desorption/ionization mass spectrometry. *Analytical Chemistry,* **67**(24), pp. 4565-4570.

HAND, O.W., MAJUMDAR, T.K. and GRAHAM COOKS, R., 1990. Effects of primary ion polyatomicity and kinetic energy on secondary ion yield and internal energy in SIMS. *International journal of mass spectrometry and ion processes,* **97**(1), pp. 35-45.

HILLENKAMP, F., KARAS, M., BEAVIS, R.C. and CHAIT, B.T., 1991. Matrix-assisted laser desorption/ionization mass spectrometry of biopolymers. *Analytical Chemistry,* **63**(24), pp. 1193A-1203A.

HINNEN, P. and ESKENS, F., 2007. Vascular disrupting agents in clinical development. *British journal of cancer,* **96**(8), pp. 1159-1165.

ISBELL, D.T., GUSEV, A.I., TARANENKO, N.I., CHEN, C. and HERCULES, D.M., 1999. Analysis of nucleotides directly from TLC plates using MALDI-MS detection. *Fresenius' journal of analytical chemistry,* **365**(7), pp. 625-630.

JAIN, R.K., 1994. Barriers to drug delivery in solid tumors. *Scientific American,* **271**(1), pp. 58-65.

KAKOLYRIS, S., FOX, S.B., KOUKOURAKIS, M., GIATROMANOLAKI, A., BROWN, N., LEEK, R.D., TAYLOR, M., LEIGH, I.M., GATTER, K.C. and HARRIS, A.L., 2000. Relationship of vascular maturation in breast cancer blood vessels to vascular density and metastasis, assessed by expression of a novel basement membrane component, LH39. *British journal of cancer,* **82**(4), pp. 844-851.

KALETAŞ, B.K., VAN DER WIEL, INGRID M, STAUBER, J., DEKKER, L.J., GÜZEL, C., KROS, J.M., LUIDER, T.M. and HEEREN, R., 2009. Sample preparation issues for tissue imaging by imaging MS. *Proteomics,* **9**(10), pp. 2622-2633.

KARAS, M. and HILLENKAMP, F., 1988. Laser desorption ionization of proteins with molecular masses exceeding 10,000 daltons. *Analytical Chemistry,* **60**(20), pp. 2299-2301.

KARIN, M. and BEN-NERIAH, Y., 2000. Phosphorylation meets ubiquitination: the control of NF-κB activity. *Annual Review of Immunology,* **18**(1), pp. 621-663.

KASPAR, S., PEUKERT, M., SVATOS, A., MATROS, A. and MOCK, H., 2011. MALDI-imaging mass spectrometry–An emerging technique in plant biology. *Proteomics,* **11**(9), pp. 1840-1850.

KERR, D. and KAYE, S., 1989. Flavone acetic acid—preclinical and clinical activity. *European Journal of Cancer and Clinical Oncology,* **25**(9), pp. 1271-1272.

KHATIB-SHAHIDI, S., ANDERSSON, M., HERMAN, J.L., GILLESPIE, T.A. and CAPRIOLI, R.M., 2006. Direct molecular analysis of whole-body animal tissue sections by imaging MALDI mass spectrometry. *Analytical Chemistry,* **78**(18), pp. 6448-6456.

KUBIS, A.J., SOMAYAJULA, K.V., SHARKEY, A.G. and HERCULES, D.M., 1989. Laser mass spectrometric analysis of compounds separated by thin-layer chromatography. *Analytical Chemistry,* **61**(22), pp. 2516-2523.

LANNI, E.J., RUBAKHIN, S.S. and SWEEDLER, J.V., 2012. Mass spectrometry imaging and profiling of single cells. *Journal of proteomics,* **75**(16), pp. 5036-5051.

LASH, C.J., LI, A.E., RUTLAND, M., BAGULEY, B.C., ZWI, L.J. and WILSON, W.R., 1998. Enhancement of the anti-tumour effects of the antivascular agent 5,6-dimethylxanthenone-4-acetic acid (DMXAA) by combination with 5-hydroxytryptamine and bioreductive drugs. *British journal of cancer,* **78**(4), pp. 439-445.

LEMAIRE, R., DESMONS, A., TABET, J., DAY, R., SALZET, M. and FOURNIER, I., 2007. Direct analysis and MALDI imaging of formalin-fixed, paraffin-embedded tissue sections. *Journal of proteome research,* **6**(4), pp. 1295-1305.

LEMAIRE, R., AIT MENGUELLET, S., STAUBER, J., MARCHAUDON, V., LUCOT, J., COLLINET, P., FARINE, M., VINATIER, D., DAY, R. and DUCOROY, P., 2007. Specific MALDI imaging and profiling for biomarker hunting and validation: fragment of the 11S proteasome activator complex, Reg alpha fragment, is a new potential ovary cancer biomarker. *Journal of proteome research,* **6**(11), pp. 4127-4134.

LEVITZKI, A. and GAZIT, A., 1995. Tyrosine kinase inhibition: an approach to drug development. *Science (New York, N.Y.),* **267**(5205), pp. 1782-1788.

LI, L., HAN, J., WANG, Z., LIU, J., WEI, J., XIONG, S. and ZHAO, Z., 2014. Mass spectrometry methodology in lipid analysis. *International journal of molecular sciences*, **15**(6), pp. 10492-10507.

LOBODA, A., 2006. Novel ion mobility setup combined with collision cell and time-of-flight mass spectrometer. *Journal of the American Society for Mass Spectrometry,* **17**(5), pp. 691-699.

MATSUMOTO, K., AJIRO, H., HABAUE, S. and OKAMOTO, Y., 2001. Modifications of TLC-MALDI-TOFMS for Lower Detection Limits Comparable with Conventional MALDI-TOFMS. *Journal of the Mass Spectrometry Society of Japan,* **49**(3), pp. 127-132.

MATSUMOTO, K., HABAUE, S., AJIRO, H. and OKAMOTO, Y., 1999. Application of TLC-MALDI/TOFMS to Identification of Unknown Mixtures Produced in an Organic Synthetic Process. *Journal of the Mass Spectrometry Society of Japan,* **47**(4), pp. 274-280.

MATSUMOTO, A. and HANAWALT, P.C., 2000. Histone H3 and heat shock protein GRP78 are selectively cross-linked to DNA by photoactivated gilvocarcin V in human fibroblasts. *Cancer research,* **60**(14), pp. 3921-3926.

MCDONNELL, L.A. and HEEREN, R., 2007. Imaging mass spectrometry. *Mass spectrometry reviews,* **26**(4), pp. 606-643.

MEHL, J.T. and HERCULES, D.M., 2000. Direct TLC-MALDI coupling using a hybrid plate. *Analytical Chemistry,* **72**(1), pp. 68-73.

MEHL, J., GUSEV, A. and HERCULES, D., 1997. Coupling protocol for thin layer chromatography/matrix-assisted laser desorption ionization. *Chromatographia,* **46**(7-8), pp. 358-364.

MERIAUX, C., FRANCK, J., WISZTORSKI, M., SALZET, M. and FOURNIER, I., 2010. Liquid ionic matrixes for MALDI mass spectrometry imaging of lipids. *Journal of proteomics,* **73**(6), pp. 1204-1218.

MIRNEZAMI, R., SPAGOU, K., VORKAS, P., LEWIS, M., KINROSS, J., WANT, E., SHION, H., GOLDIN, R., DARZI, A. and TAKATS, Z., 2014. Chemical mapping of the colorectal cancer microenvironment via MALDI imaging mass spectrometry (MALDI-MSI) reveals novel cancer-associated field effects. *Molecular oncology,* **8**(1), pp. 39-49.

MODESTOV, A.D., SREBNIK, S., LEV, O. and GUN, J., 2001. Scanning capillary microscopy/mass spectrometry for mapping spatial electrochemical activity of electrodes. *Analytical Chemistry,* **73**(17), pp. 4229-4240.

MONAGHAN, J., MORDEN, W., JOHNSON, T., WILSON, I. and MARTIN, P., 1992. Thin layer chromatography/mass spectrometry: the advantages of tandem mass spectrometry. *Rapid communications in mass spectrometry,* **6**(10), pp. 608-615.

NARANG, A.S. and VARIA, S., 2011. Role of tumor vascular architecture in drug delivery. *Advanced Drug Delivery Reviews,* **63**(8), pp. 640-658.

NICOLA, A.J., GUSEV, A.I. and HERCULES, D.M., 1996. Direct quantitative analysis from thin-layer chromatography plates using matrix-assisted laser desorption/ionization mass spectrometry. *Applied Spectroscopy,* **50**(12), pp. 1479-1482.

NOURI-SORKHABI, M.H., WRIGHT, L.C., SULLIVAN, D.R. and KUCHEL, P.W., 1996. Quantitative31P nuclear magnetic resonance analysis of the phospholipids of erythrocyte membranes using detergent. *Lipids,* **31**(7), pp. 765-770.

O'HANLON, L.H., 2005. Taking down tumors: vascular disrupting agents entering clinical trials. *Journal of the National Cancer Institute,* **97**(17), pp. 1244-1245.

OKA, H., IKAI, Y., HAYAKAWA, J., MASUDA, K., HARADA, K., SUZUKI, M., MARTZ, V. and MACNEIL, J.D., 1993. Improvement of chemical analysis of antibiotics. 18. Identification of residual tetracyclines in bovine tissues by TLC/FABMS with a sample condensation technique. *Journal of Agricultural and Food Chemistry,* **41**(3), pp. 410-415.

PACHOLSKI, M. and WINOGRAD, N., 1999. Imaging with mass spectrometry. *Chemical reviews,* **99**(10), pp. 2977-3006.

PEDLEY, R.B., 1996. Pharmacokinetics of monoclonal antibodies. *Clinical Immunotherapeutics,* **6**(1), pp. 54-67.

PEDLEY, R.B., EL-EMIR, E., FLYNN, A.A., BOXER, G.M., DEARLING, J., RALEIGH, J.A., HILL, S.A., STUART, S., MOTHA, R. and BEGENT, R.H., 2002. Synergy between vascular targeting agents and antibody-directed therapy. *International Journal of Radiation Oncology Biology Physics,* **54**(5), pp. 1524-1531.

PHILPOTT, M., CHING, L. and BAGULEY, B., 2001. The antitumour agent 5, 6-dimethylxanthenone-4-acetic acid acts in vitro on human mononuclear cells as a co-stimulator with other inducers of tumour necrosis factor. *European journal of cancer,* **37**(15), pp. 1930-1937.

POOLE, C.F., 2003. Thin-layer chromatography: challenges and opportunities. *Journal of Chromatography A,* **1000**(1), pp. 963-984.

POSTAWA, Z., 2004. Sputtering simulations of organic overlayers on metal substrates by monoatomic and clusters projectiles. *Applied Surface Science,* **231**, pp. 22-28.

QUEHENBERGER, O. and DENNIS, E.A., 2011. The human plasma lipidome. *New England Journal of Medicine,* **365**(19), pp. 1812-1823.

REWCASTLE, G.W., ATWELL, G.J., ZHUANG, L., BAGULEY, B.C. and DENNY, W.A., 1991. Potential antitumor agents. 61. Structure-activity relationships for in vivo colon 38 activity among disubstituted 9-oxo-9H-xanthene-4-acetic acids. *Journal of medicinal chemistry,* **34**(1), pp. 217-222.

REYZER, M.L., HSIEH, Y., NG, K., KORFMACHER, W.A. and CAPRIOLI, R.M., 2003. Direct analysis of drug candidates in tissue by matrix-assisted laser desorption/ionization mass spectrometry. *Journal of Mass Spectrometry,* **38**(10), pp. 1081-1092.

REYZER, M.L., CALDWELL, R.L., DUGGER, T.C., FORBES, J.T., RITTER, C.A., GUIX, M., ARTEAGA, C.L. and CAPRIOLI, R.M., 2004. Early changes in protein expression detected by mass spectrometry predict tumor response to molecular therapeutics. *Cancer research,* **64**(24), pp. 9093-9100.

RIFAI, N., GILLETTE, M.A. and CARR, S.A., 2006. Protein biomarker discovery and validation: the long and uncertain path to clinical utility. *Nature biotechnology,* **24**(8), pp. 971-983.

RUBAKHIN, S.S., JURCHEN, J.C., MONROE, E.B. and SWEEDLER, J.V., 2005. Imaging mass spectrometry: fundamentals and applications to drug discovery. *Drug discovery today,* **10**(12), pp. 823-837.

RUOTOLO, B.T., GILLIG, K.J., STONE, E.G., RUSSELL, D.H., FUHRER, K., GONIN, M. and SCHULTZ, J.A., 2002. Analysis of protein mixtures by matrix-assisted laser desorption ionization-ion mobility-orthogonal-time-of-flight mass spectrometry. *International Journal of Mass Spectrometry,* **219**(1), pp. 253-267.

RUOTOLO, B.T., MCLEAN, J.A., GILLIG, K.J. and RUSSELL, D.H., 2005. The influence and utility of varying field strength for the separation of tryptic peptides by ion mobility-mass spectrometry. *Journal of the American Society for Mass Spectrometry,* **16**(2), pp. 158-165.

SCHWARTZ, S.A., REYZER, M.L. and CAPRIOLI, R.M., 2003. Direct tissue analysis using matrix-assisted laser desorption/ionization mass spectrometry: practical aspects of sample preparation. *Journal of Mass Spectrometry,* **38**(7), pp. 699-708.

SCRIVEN, P., BROWN, N.J., POCKLEY, A.G. and WYLD, L., 2007. The unfolded protein response and cancer: a brighter future unfolding? *Journal of Molecular Medicine,* **85**(4), pp. 331-341.

SERKOVA, N.J., STANDIFORD, T.J. and STRINGER, K.A., 2011. The emerging field of quantitative blood metabolomics for biomarker discovery in critical illnesses. *American journal of respiratory and critical care medicine,* **184**(6), pp. 647-655.

SHIMMA, S., FURUTA, M., ICHIMURA, K., YOSHIDA, Y. and SETOU, M., 2006. A novel approach to in situ proteome analysis using chemical inkjet printing technology and MALDI-QIT-TOF tandem mass spectrometer. *Journal of the Mass Spectrometry Society of Japan,* **54**(4), pp. 133-140.

SHIMMA, S., SUGIURA, Y., HAYASAKA, T., HOSHIKAWA, Y., NODA, T. and SETOU, M., 2007. MALDI-based imaging mass spectrometry revealed abnormal distribution of phospholipids in colon cancer liver metastasis. *Journal of Chromatography B,* **855**(1), pp. 98-103.

SIEMANN, D.W., CHAPLIN, D.J. and HORSMAN, M.R., 2004. Vascular-targeting therapies for treatment of malignant disease. *Cancer,* **100**(12), pp. 2491-2499.

SIEMANN, D.W., BIBBY, M.C., DARK, G.G., DICKER, A.P., ESKENS, F.A., HORSMAN, M.R., MARME, D. and LORUSSO, P.M., 2005. Differentiation and definition of vascular-targeted therapies. *Clinical cancer research : an official journal of the American Association for Cancer Research,* **11**(2 Pt 1), pp. 416-420.

SMIRNOV, I., ZHU, X., TAYLOR, T., HUANG, Y., ROSS, P., PAPAYANOPOULOS, I., MARTIN, S. and PAPPIN, D., 2004. Suppression of α-cyano-4-hydroxycinnamic acid matrix clusters and reduction of chemical noise in MALDI-TOF mass spectrometry. *Analytical Chemistry,* **76**(10), pp. 2958-2965.

SMITH, G.P., CALVELEY, S.B., SMITH, M.J. and BAGULEY, B.C., 1987. Flavone acetic acid (NSC 347512) induces haemorrhagic necrosis of mouse colon 26 and 38 tumours. *European Journal of Cancer and Clinical Oncology,* **23**(8), pp. 1209-1211.

SMITH, R.E., LESPI, P., DI LUCA, M., BUSTOS, C., MARRA, F.A., DE ALANIZ, M.J. and MARRA, C.A., 2008. A reliable biomarker derived from plasmalogens to evaluate malignancy and metastatic capacity of human cancers. *Lipids,* **43**(1), pp. 79-89.

SPARVERO, L.J., AMOSCATO, A.A., DIXON, C.E., LONG, J.B., KOCHANEK, P.M., PITT, B.R., BAYIR, H. and KAGAN, V.E., 2012. Mapping of phospholipids by MALDI imaging (MALDI-MSI): realities and expectations. *Chemistry and physics of lipids,* **165**(5), pp. 545-562.

SPYROS, A. and DAIS, P., 2000. Application of 31P NMR spectroscopy in food analysis. 1. Quantitative determination of the mono-and diglyceride composition of olive oils. *Journal of Agricultural and Food Chemistry,* **48**(3), pp. 802-805.

SREBALUS BARNES, C.A. and CLEMMER, D.E., 2001. Assessment of purity and screening of peptide libraries by nested ion mobility-TOFMS: identification of RNase S-protein binders. *Analytical Chemistry,* **73**(3), pp. 424-433.

ST. HILAIRE, P.M., LOWARY, T.L., MELDAL, M. and BOCK, K., 1998. Oligosaccharide mimetics obtained by novel, rapid screening of carboxylic acid encoded glycopeptide libraries. *Journal of the American Chemical Society,* **120**(51), pp. 13312-13320.

STAUBER, J., LEMAIRE, R., FRANCK, J., BONNEL, D., CROIX, D., DAY, R., WISZTORSKI, M., FOURNIER, I. and SALZET, M., 2008. MALDI imaging of formalin-fixed paraffin-embedded tissues: application to model animals of Parkinson disease for biomarker hunting. *Journal of proteome research,* **7**(3), pp. 969-978.

STOECKLI, M., CHAURAND, P., HALLAHAN, D.E. and CAPRIOLI, R.M., 2001. Imaging mass spectrometry: a new technology for the analysis of protein expression in mammalian tissues. *Nature medicine,* **7**(4), pp. 493-496.

STOECKLI, M., CHAURAND, P., HALLAHAN, D.E. and CAPRIOLI, R.M., 2001. Imaging mass spectrometry: a new technology for the analysis of protein expression in mammalian tissues. *Nature medicine,* **7**(4), pp. 493-496.

STOECKLI, M., STAAB, D. and SCHWEITZER, A., 2007. Compound and metabolite distribution measured by MALDI mass spectrometric imaging in whole-body tissue sections. *International Journal of Mass Spectrometry,* **260**(2), pp. 195-202.

SUN, J., WANG, L.S., FRIDLENDER, Z.G., KAPOOR, V., CHENG, G., CHING, L. and ALBELDA, S.M., 2011. Activation of mitogen-activated protein kinases by 5, 6-dimethylxanthenone-4-acetic acid (DMXAA) plays an important role in macrophage stimulation. *Biochemical pharmacology,* **82**(9), pp. 1175-1185.

TAKATS, Z., WISEMAN, J.M., GOLOGAN, B. and COOKS, R.G., 2004. Mass spectrometry sampling under ambient conditions with desorption electrospray ionization. *Science (New York, N.Y.),* **306**(5695), pp. 471-473.

TANAKA, K., WAKI, H., IDO, Y., AKITA, S., YOSHIDA, Y., YOSHIDA, T. and MATSUO, T., 1988. Protein and polymer analyses up to m/z 100 000 by laser ionization time of flight mass spectrometry. *Rapid communications in mass spectrometry,* **2**(8), pp. 151-153.

TEMPEZ, A., SCHULTZ, J., DELLA-NEGRA, S., DEPAUW, J., JACQUET, D., NOVIKOV, A., LEBEYEC, Y., PAUTRAT, M., CAROFF, M. and UGAROV, M., 2004. Orthogonal time-of-flight secondary ion mass spectrometric analysis of peptides using large gold clusters as primary ions. *Rapid communications in mass spectrometry,* **18** (4), pp. 371-376.

THERISOD, H., LABAS, V. and CAROFF, M., 2001. Direct microextraction and analysis of rough-type lipopolysaccharides by combined thin-layer chromatography and MALDI mass spectrometry. *Analytical Chemistry,* **73**(16), pp. 3804-3807.

THOMAS, A., PATTERSON, N.H., MARCINKIEWICZ, M.M., LAZARIS, A., METRAKOS, P. and CHAURAND, P., 2013. Histology-driven data mining of lipid signatures from multiple imaging mass spectrometry analyses: application to human colorectal cancer liver metastasis biopsies. *Analytical Chemistry,* **85**(5), pp. 2860-2866.

THOMSEN, L.L., CHING, L.M., ZHUANG, L., GAVIN, J.B. and BAGULEY, B.C., 1991. Tumor-dependent increased plasma nitrate concentrations as an indication of the antitumor effect of flavone-8-acetic acid and analogues in mice. *Cancer research,* **51**(1), pp. 77-81.

THORPE, P.E., 2004. Vascular targeting agents as cancer therapeutics. Clinical cancer research : an official journal of the American Association for Cancer Research, **10**(2), pp. 415-427.

TROENDLE, F.J., REDDICK, C.D. and YOST, R.A., 1999. Detection of pharmaceutical compounds in tissue by matrix-assisted laser desorption/ionization and laser desorption/chemical ionization tandem mass spectrometry with a quadrupole ion trap. *Journal of the American Society for Mass Spectrometry,* **10**(12), pp. 1315-1321.

VAN BERKEL, G.J., FORD, M.J. and DEIBEL, M.A., 2005. Thin-layer chromatography and mass spectrometry coupled using desorption electrospray ionization. *Analytical Chemistry,* **77**(5), pp. 1207-1215.

VAN GOOR, H., GERRITS, P. and GROND, J., 1986. The application of lipid-soluble stains in plastic-embedded sections. *Histochemistry,* **85**(3), pp. 251-253.

VERMILLION-SALSBURY, R.L., HOOPS, A.A., GUSEV, A.I. and HERCULES, D.M., 1999. Analysis of Cationic Pesticides by Thin Layer Chromatography/Matrix—Assisted Laser Desorption Ionization Mass Spectrometry. *International journal of environmental analytical chemistry,* **73**(3), pp. 179-190.

VICKERMAN, J.C., 2011. Molecular imaging and depth profiling by mass spectrometry—SIMS, MALDI or DESI? *Analyst,* **136**(11), pp. 2199-2217.

VINCENT, L., KERMANI, P., YOUNG, L.M., CHENG, J., ZHANG, F., SHIDO, K., LAM, G., BOMPAIS-VINCENT, H., ZHU, Z., HICKLIN, D.J., BOHLEN, P., CHAPLIN, D.J., MAY, C. and RAFII, S., 2005. Combretastatin A4 phosphate induces rapid regression of tumor neovessels and growth through interference with vascular endothelial-cadherin signaling. *The Journal of clinical investigation,* **115**(11), pp. 2992-3006.

VISMEH, R., WALDON, D.J., TEFFERA, Y. and ZHAO, Z., 2012. Localization and quantification of drugs in animal tissues by use of desorption electrospray ionization mass spectrometry imaging. *Analytical Chemistry,* **84**(12), pp. 5439-5445.

WACHS, T. and HENION, J., 2001. Electrospray device for coupling microscale separations and other miniaturized devices with electrospray mass spectrometry. *Analytical Chemistry,* **73**(3), pp. 632-638.

WEAVER, E.M. and HUMMON, A.B., 2013. Imaging mass spectrometry: from tissue sections to cell cultures. *Advanced Drug Delivery Reviews,* **65**(8), pp. 1039-1055.

WESTON, A.D. and HOOD, L., 2004. Systems biology, proteomics, and the future of health care: toward predictive, preventative, and personalized medicine. *Journal of proteome research,* **3**(2), pp. 179-196.

WESTRA, J.L., PLUKKER, J.T., BUYS, C.H. and HOFSTRA, R.M., 2004. Genetic alterations in locally advanced stage II/III colon cancer: a search for prognostic markers. *Clinical colorectal cancer,* **4**(4), pp. 252-259.

WU, C., SIEMS, W.F., ASBURY, G.R. and HILL, H.H., 1998. Electrospray ionization high-resolution ion mobility spectrometry-mass spectrometry. *Analytical Chemistry,* **70**(23), pp. 4929-4938.

Chapter 2

Analysis of DMXAA in Dosed Xenograft Tumours

Over the past 20 years the concept of targeting tumour vasculature, especially in cancer therapy, has been rapidly developed. The endothelial cells lining tumour blood vessels are the main target for anti-vascular agents and they respond in less than 1 hour by increasing their permeability; this results in a subsequent decrease in blood flow (Jain., 1988, Milosevic *et al.*, 1999). The induction of apoptosis is initiated after between 12 and 24 h. The continuous cessation of tumour blood flow leads to the development of haemorrhagic necrosis in the tumour which is a critical step in the action mechanisms of anti-vascular drugs. To increase the efficacy of anti-vascular therapy, it must be selective for tumour vascular endothelium. Tumours show extensive heterogeneity in blood flow and those vessels with low rates of flow are particularly sensitive to the effects of anti-vascular agents (Baguley & Bruce., 2003).

DMXAA (5,6-dimethylxanthenone-4-acetic acid) is a low molecular weight drug which selectively destroys established tumour blood vessels. As mentioned earlier in the introductory chapter, DMXAA acts on vascular endothelial cells through a cascade of direct and indirect events which lead to the induction of tumour haemorrhagic necrosis. DMXAA selectively arrests blood flow in murine tumours within 30 minutes after its administration (Zwi *et al.*, 1994, Lash *et al.*, 1998). Images of hypoxic tumour tissue from mice treated with DMXAA show the onset of hypoxia as a result of inhibiting the blood flow (Siim *et al.*, 2000).

Preclinical studies have reported that vascular disrupting agents (VDAs) can cause rapid and significant effects which lead to dose-dependent tumour necrosis in a matter of hours or days. To date, phase I clinical trials have reported interesting results. However, only a few VDAs have entered phase II and III trials, either as a single drug or used in combination with other forms of chemotherapy.

VDAs readily induce central tumour necrosis but leave a viable rim at the periphery; the reasons for this are still being investigated. Perhaps for this reason, the responses of tumours to VDAs delivered as single agents are poor; however, combination therapies which also targets peripheral tumour cells can give better results (Gridelli *et al.*, 2009).

DMXAA is unable to induce delay in the growth of some human xenograft tumours because of the rapid repopulation of cells from a viable rim of tumour cells nourished by intact blood vessels (Baguley *et al.*, 2002). However, several murine tumours have shown no evidence of viable cells in tumour sections taken 24 h after treatment; this reveals that DMXAA can, in favourable situations, induce complete responses (Philpott *et al.*, 1995). This may reflect differences in host responses; or simply indicate that anti-vascular agents which penetrate the tumour tissue may also diffuse to blood vessels on a tumour's periphery (Baguley & Bruce, 2003).

A variety of analytical methods have been used for DMXAA quantification, such as reversed-phase HPLC with fluorescence detection (Zhou *et al.*, 1999). Each of these methods has some advantages and disadvantages. A rapid and sensitive analytical method for the determination of DMXAA concentrations in mouse plasma, based on LC/MS/MS, and with electrospray positive ionization has been developed. The method is quantitatively accurate over concentrations ranging from 5 to 3000 ng/mL which is sufficient for measuring plasma pharmacokinetics in mice after a single intra-peritoneal administration of DMXAA (Zhang *et al.*, 2007).

The use of MALDI-MSI to study two separate classes of anti-cancer agent has been previously reported. A study of the bio-reductive drug, AQ4N, in solid tumours was carried out using MALDI-MSI (Atkinson *et al.*, 2007) and a study of Vinblastine in whole animal sections was carried out using MALDI-MSI in combination with ion mobility separation (Trim *et al.*, 2008).

These experiments have shown the power of MALDI-MSI in such studies. The lower limit of quantitation (LLoQ) is known as the minimum concentration which determined with acceptable accuracy and precision. However, the limit of detection (LoD) can be defined as the amount which could be detected with a signal-to- noise ratio of 3 (Zhou *et al.*, 1999).

In this Chapter determination of the lower limit of detection /quantitation study of DMXAA drug on tissue is performed and an investigation of the use of MALDI-MSI to study the distribution of DMXAA, in LS 174T xenograft tumours at different time points are reported.

2.1 Materials and methods

2.1.1 Chemicals

α-Cyano-4-hydroxycinnamic acid (CHCA) matrix, ethanol (EtOH), methanol (MeOH) trifluoroacetic acid (TFA) and the drug (5,6-dimethylxanthenone-4-acetic acid, DMXAA) were purchased from Sigma-Aldrich (Gillingham, Dorset, UK).

2.1.2 Preparation of DMXAA dosed Xenograft tumours

Male, immune-deficient, nude mice, between the ages of 8 and 10 weeks, were used (n = 9) that is (n = 3) for each time point. Mice received a Harlan 2018 diet (Harlan, Blackthorn, UK) and water *ad libitum*, and were kept in cages in an air-conditioned room with regular alternating cycles of light and darkness. This work has been done in the Institute of cancer therapeutic, university of Bradford under a United Kingdom Home Office Project License, following the UK National Cancer Research Institute Guidelines for the Welfare of Animals guidelines (Workman *et al.*, 2010).

Under brief general inhalation anesthesia, 2-3 mm^3 fragments of LS174T colorectal adenocarcinoma were implanted subcutaneously in the right abdominal flank. Once the tumour volumes reached approximately 500 mm^3, the mice (n = 6) were treated with a 27.5 mg/kg concentration of DMXAA via intra-peritoneal (i.p.) administration. At both 4 hours and 24 hours post-treatment, three mice were euthanised and tumours were excised, snap frozen and stored at -80°C until use. Tumours were also taken from an untreated control group (n=3).

2.1.3 Tissue preparation

Frozen xenograft tumours (n=1) from each time point were sliced into (12 μm) thickness using a Lecia CM 1850 cryostat (Leica Microsystems, Milton Keynes, UK) set at -20 °C. Then, tissue sections (n=1) from each time point were mounted on to conventional microscopic glass slides for analysis by mass spectrometry; these were stored at -80°C in a freezer prior to analysis. The glass slide was then optically scanned in a Nikon Super Cool scan 500ED scanner (Nikon Corporation, Tokyo, Japan) to produce an optical image.

Figure 2.1: *Image of the Cryostat machine used in the experiment*

2.1.4 Modification of matrix solvent

In order to optimise the extraction of the drug from the tumour tissue sections, different concentrations of matrix solvent were tested. About 5 mg/ml of α-CHCA matrix was dissolved in different concentrations ranging from 50% to 80% of solvent (MeOH / water) with 0.1% TFA and 50% to 80% of solvent (EtOH / water) with 0.1% TFA. Solutions were then vortexed until the matrix dissolved. Matrix solutions had to be used within one day of preparation.

2.1.5 Drug limit of detection / quantitation study on tissue

Drug limit of detection / quantitation studies on tissue were performed by preparing a dilution series of the drug from a 1mg/ml stock solution of DMXAA. The concentrations prepared ranged from 10, 50, 100 and 150 to 250 ng/ml of DMXAA. About 0.5 µL of each concentration was spotted on a section of control tissue and spray-coated with 5mg/ml alpha-cyano-4-hydroxycinnamic acid (α-CHCA) matrix dissolved in 70:30% ethanol: water with 0.1% TFA.

2.1.6 Matrix deposition and analysis of DMXAA from a dosed xenograft tumour

2.1.6.1 Matrix application

The tissue sections were spotted with 5 mg/ml (αCHCA) matrix dissolved in 70:30 % ethanol: water with 0.1% TFA using the Portrait™ 630 Multi-spotter (Labcyte, Sunnyville, CA) automated pneumatic sprayer.

2.1.6.2 Instrumentation

The glass slides were cut to (12 µm) thickness and mounted into a MALDI target plate holder (Applied Biosystems / MDS Sciex, Concord, Ontario, Canada) using double-sided tape. The analyses were performed using a hypbrid quadrupole-time of flight mass spectrometer with an orthogonal MALDI ion source, a "Q-Star Pulsar-*i*" instrument (Applied Biosystems, Foster City, California, USA).

A high repetition Neodymium-doped Yttrium Vanadate (Nd: YVO4) laser with a laser repetition rate of 5 KHz (Elforlight Ltd, Daventry, Northamptonshire, UK) was used (Trim *et al.*, 2010). Mass spectra and images were acquired in a positive ion mode at a spatial resolution of 200 µm x 200 µm in full scan MS mode and MS/MS mode. Then, images were generated using Biomap 3.7.5.5 imaging software (www.maldi-msi.org).

2.1.6.3 Haematoxylin and Eosin staining

After imaging, the tissue sections were retained for Haematoxylin and Eosin (H&E) staining to be compared with the MALDI image. Each section of tissue was washed with 5ml of 100% ethanol to remove the matrix from the tissue. Then, the tissue section was rehydrated using a series of graded alcohols. Each section was immersed in 100% ethanol for 5 minutes, followed by a further 5 minutes in 95%, 80% and 70% ethanol. The rehydrated tissue section was then washed with tap water for 5 minutes to remove the ethanol. Afterwards, the tissue section was deposited in a rack filled with haematoxylin for 5 minutes to stain the nucleus with a blue-purple colour. Then, the tissue section was rinsed with tap water for 10 minutes to remove the Haematoxylin. The section was then dipped 3 times in a jar containing 0.1% HCl and then into tap water 3 to 4 times. Before staining with Eosin, the tissue section was dipped 3 times in a jar containing 0.1% NaOH and then into tap water 3 to 4 times. Eosin stains the eosinophilic structure pink. The tissue section was immersed in Eosin for 3 minutes and then dehydrated in 100% ethanol with 0.1% acetic acid 5 times. This was followed by 2 washes in 100% ethanol 5 times each and another 2 washes in acetone 5 times each. Finally, the dehydrated section was then placed in xylene until it mounted with DPX and cover slipped.

2.2 Results and discussion

2.2.1 Modification of matrix solvents for method optimisation

The matrix chosen for the MALDI-MSI analysis plays a vital role in the desorption and ionization of analyte from tissue. Therefore, different concentrations of matrix solvent were used. Varying the concentrations of the matrix solvents added during matrix deposition might affect drug detection. In this study, two types of matrix solvent were used at varying concentration ranges with α-CHCA matrix.

A 0.5 µl of DMXAA drug was spotted onto the tissue and then spiked with 0.5 µl of α-CHCA matrix dissolved in varied concentrations of matrix solvent ranging from 50% to 80% of solvent (MeOH / Water) + 0.1% TFA and 50% to 80% of solvent (EtOH / Water) + 0.1% TFA. Fig. 2.2 shows that a strong spot of the DMXAA drug on the tissue was observed when 70% EtOH / H_2O + 0.1 TFA was used as a matrix solvent (Fig. 2.2). However, no drug spot was detected when concentrations of 50%, 60% and 80% Et/H_2O and 50%, 60%, 70% and 80% Me / H_2O were used as matrix solvents. Therefore, the 70% EtOH / H_2O + 0.1 TFA was chosen as the matrix solvent for future experimentation.

The formation of clear concise spot could be explained by the fact that matrix solution contains a polar solvent, such as EtOH which will cause droplet of matrix solution to be spread on the surface of the tissue reflecting low surface tension and lead to the formation of matrix crystals from the outer rim of the deposited solution.

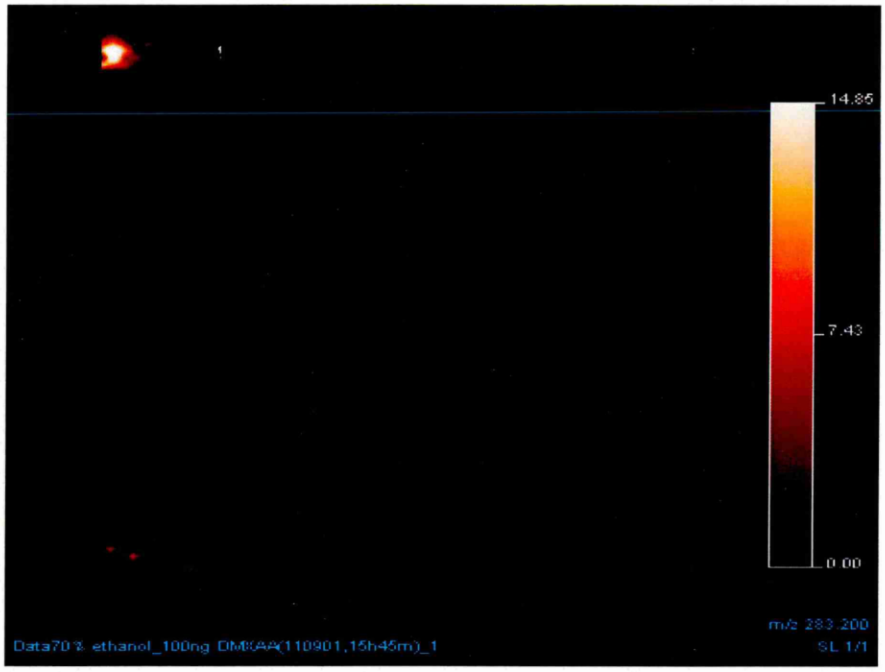

Figure 2.2: *MALDI image showing 0.5 µl of DMXAA spot (red) on tissue spiked with 0.5 µl of α-CHCA matrix in 70% Et/H2O + 0.1 TFA. The intensity of signal increase from red colour to white.*

2.2.2 Drug limit of detection / quantitation study on tissue

To determine accurately the limit of detection / quantitation of the drug on tissue, the following concentrations of the drug (250, 100, 150, 50 and 10 ng/ml) were applied on different areas of tissue sections against a blank (matrix). Then the matrix solution (∝CHCA 5mg/ml dissolved in 70% EtOH / H_2O + 0.1 TFA) was applied to each spot. Fig. 2.3 shows that the DMXAA was clearly observable at a concentration of 250 ng/ml right down to the lowest concentration of 10 ng/ml. Also, the image shows that visually the limit of detection (LoD) of DMXAA is approximately 10 ng/ml.

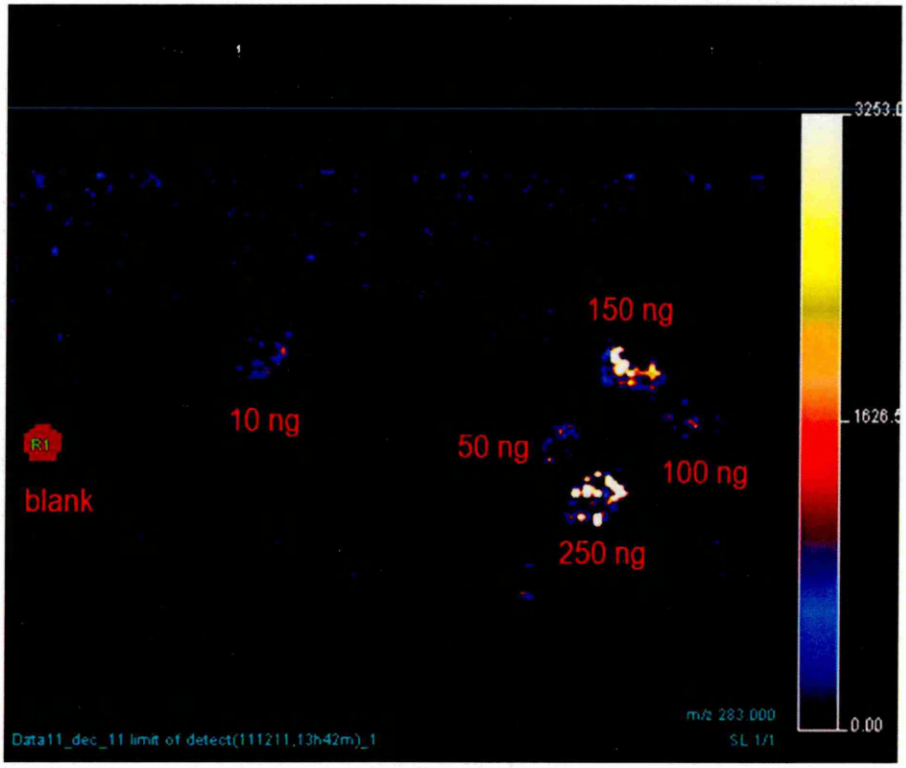

Figure 2.3: *MALDI-MSI image shows a blank spot (matrix) and different spots of DMXAA on tissue at concentrations ranging from 10-250 ng/ml. The intensity of signal increase from blue colour (low signal) to white colour (high signal) as shown in scalebar.*

Fig. 2.4 shows the MALDI - Mass spectra constructed from each spot of drug at concentration ranges from 250, 150, 100 and 50 ng/ml, as shown in Fig. 2.3. It was observed that the intensity of the peaks increased as the concentration increased. Intense signals of the drug were observed at concentrations of 250, 150 and 100 ng/ml (see Fig. 2.4 c, d and e) while Fig 2.4 a displays the spectrum with the lowest intensity peak at a concentration of 10 ng/ml.

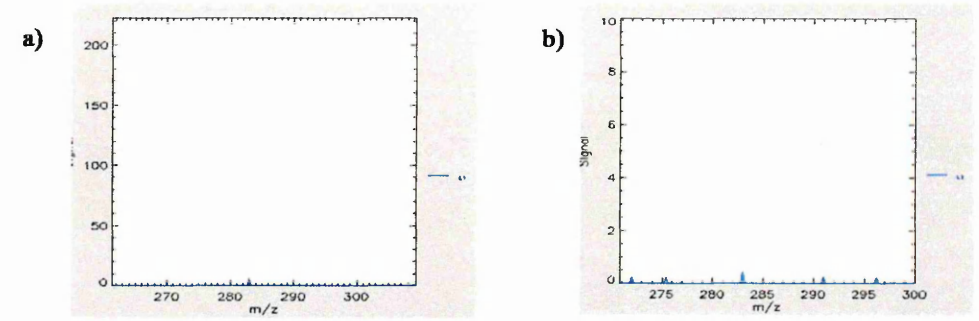

Mass spectra of 10 ng /ml conc, peak are shown at 283 m/z. Mass spectra of 50 ng /ml conc, peak are shown at 283 m/z.

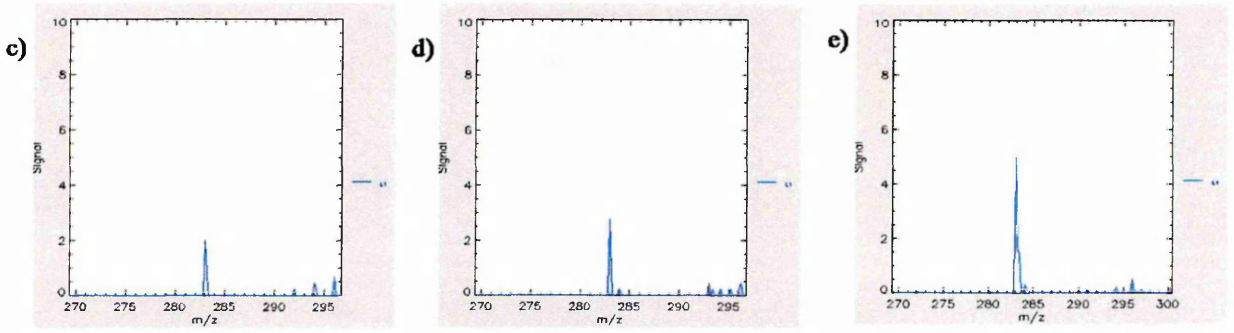

Mass spectra of 100 ng /ml conc, peak are shown at 283 m/z. Mass spectra of 150 ng /ml conc, peak are shown at 283 m/z. Mass spectra of 250 ng /ml conc, peak are shown at 283 m/z.

Figure 2.4: *MALDI/TOF MS spectra acquired directly from different concentration of drug spotted on tissue section: (a) peak of 10 ng/ml concentration of drug, (b) peak of 50 ng/ml concentration of drug, (c) peak of 100 ng/ml concentration of drug, (d) peak of 150 ng/ml concentration of drug and (e) peak of 250 ng/ml concentration of drug at 283 m/z.*

Fig. 2.5 below shows the calibration curve constructed from region of interest (ROI) of each spot of drug at concentration ranges from 250, 150, 100, 50 and 10 ng/ml, as shown in Fig. 2.3. The intensity of each concentration was determined and plotted against the concentration range from 10 to 250 ng. The calibration curve shows a linear response (R^2=0.564) from 10 to 100 ng/ml. The result from 150 - 250 ng/ml was excluded since they caused the graph to plateau. The intensity of matrix peak at 175 m/z is used as a blank. From the calibration curve we can say that the limit of detection (LoD) is approximately 10 ng/ml and lower limit of quantitation (LLoQ) is 45 ng/ml.

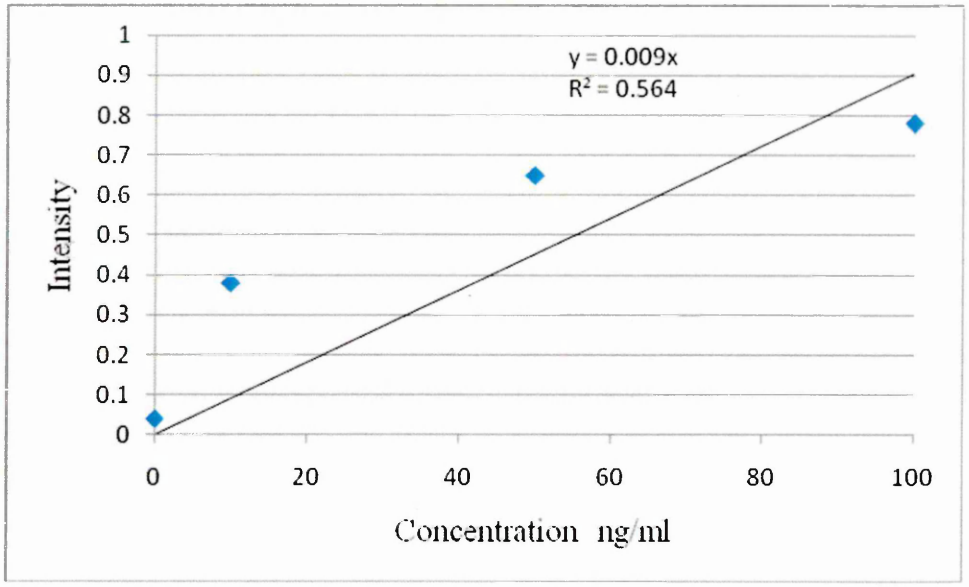

Figure 2.5: *Calibration curve produced from the exported region of interest (ROI) of different concentration of DMXAA on tissue. The intensity of signal is plotted against different concentration of DMXAA. The calibration curve shows a linear response (R^2=0.564) from 10 to 100 ng/ml. The result from 150 - 250 ng/ml was excluded since they caused the graph to plateau.*

2.2.3 Analysis of DMXAA from a dosed xenograft tumour using MALDI-MSI

Before imaging, MALDI spectra were acquired in full-scan MS mode (Fig. 2.6) and MS/MS mode (Fig. 2.7). The MALDI-MS spectrum shows an intense peak for the protonated molecule $[M+H]^+$ of the DMXAA drug at 283 m/z.

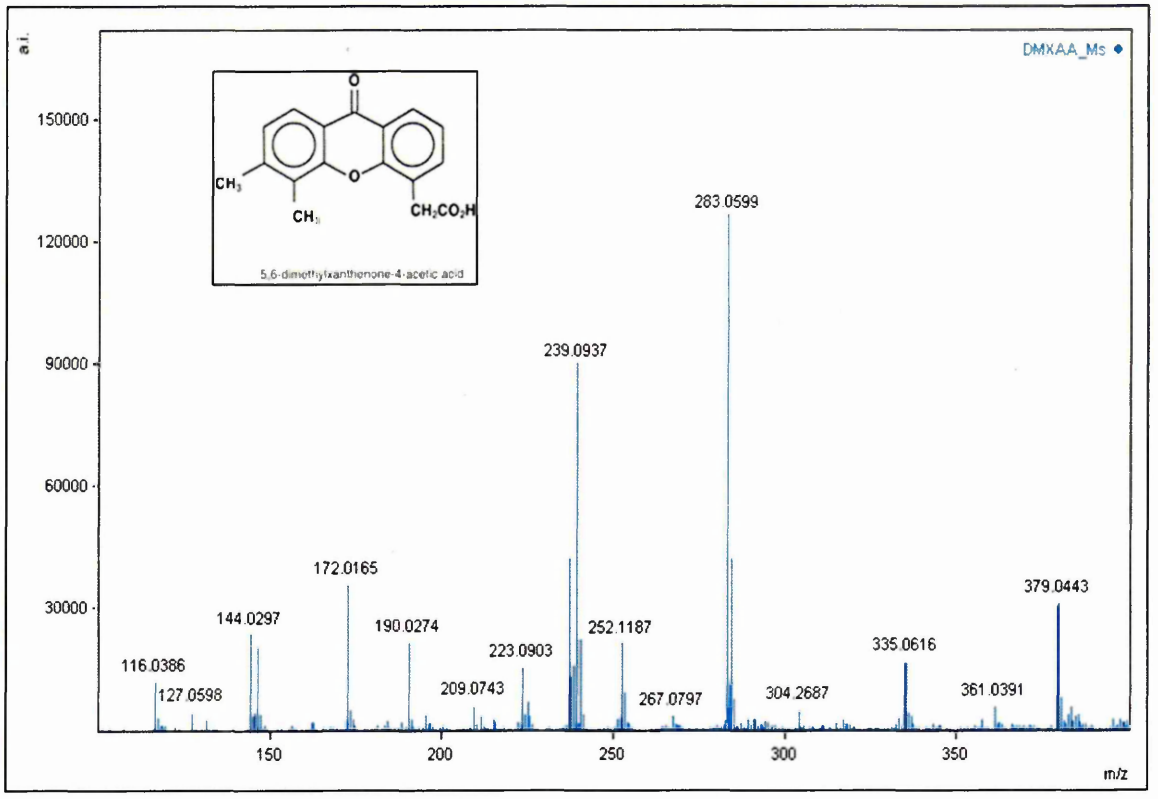

Figure 2.6: *MALDI-MS spectrum of DMXAA showing the [M+H]* $^{+}$ *peak at 283 m/z and the corresponding α CHCA matrix peaks.*

The MALDI-MS/MS spectrum below shows the precursor ion at 283 m/z and major product ions at 237 m/z and 209 m/z (Fig. 2.7).

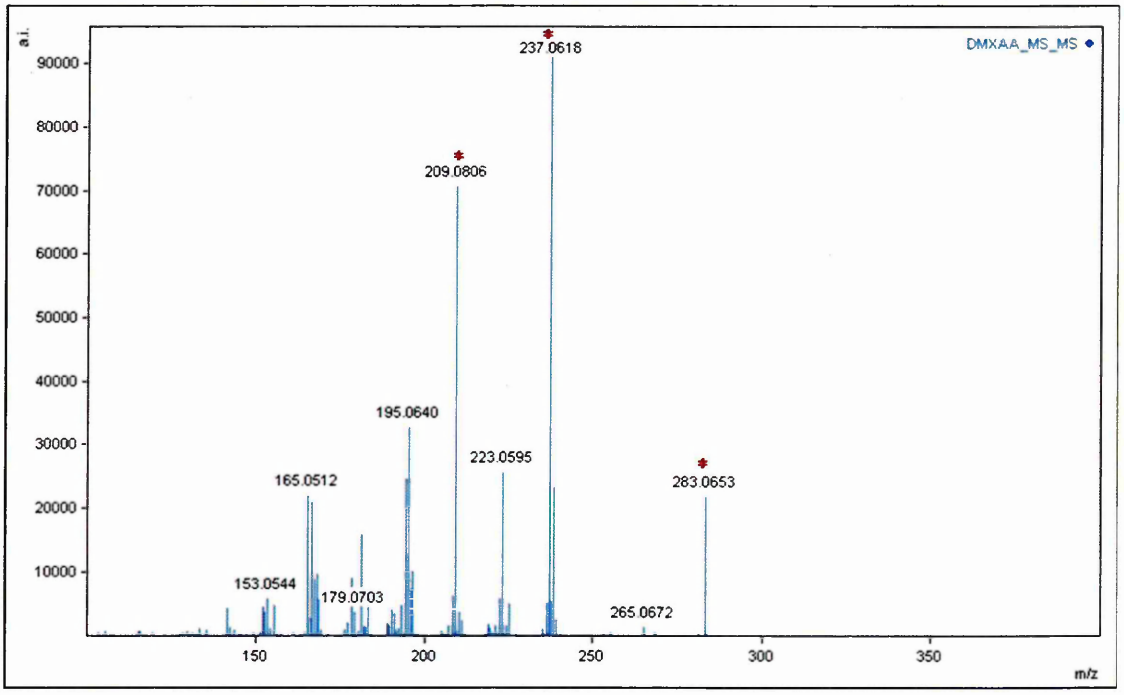

Figure 2.7: *MALDI-MS/MS spectrum of DMXAA showing the product ions at 237 m/z , 209 m/z and the corresponding precursor ion at 283 m/z.*

The MALDI-MS images of the distribution of the matrix and the drug from the DMXAA treated xenograft tumours, following a 4h treatment performed on the Q-star mass spectrometer, are shown below in Fig. 2.8.

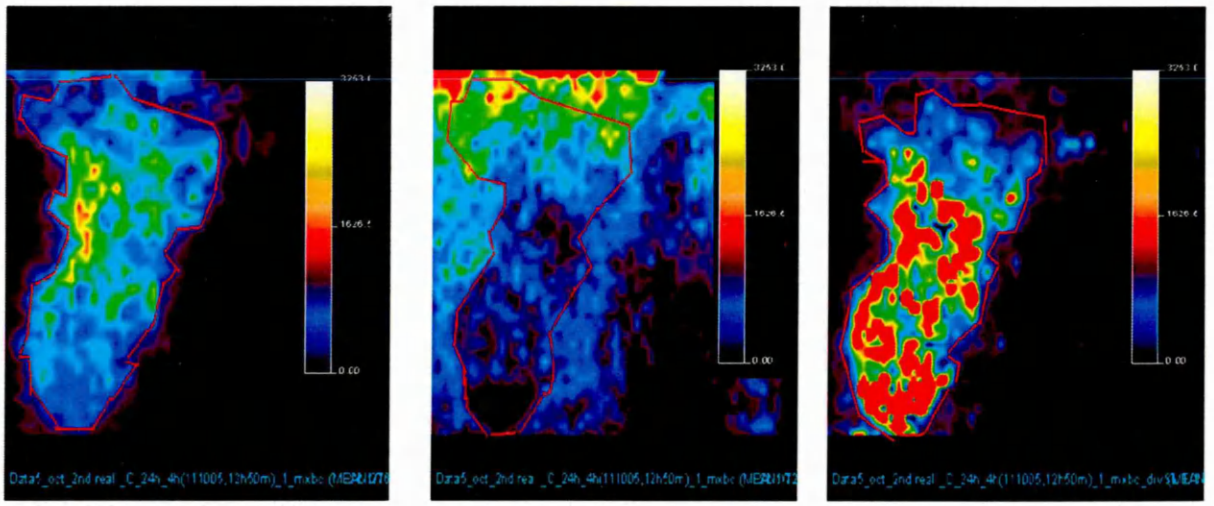

drug layer at 283 .2 m/z after 4h treatment

matrix layer at 173 m/z

image of division of matrix layer at 173 m/z over drug layer at 283.22 m/z

Figure 2.8: *The MALDI-MS images of the drug at 283.2 m/z after 4h treatment, matrix layer at 173 m/z and the overlaid image of matrix peaks at 173 m/z divided by drug peaks at 283.2 m/z . The outline of the tumour is shown in red. Blue colour gives low intensity of signal while orange white colours indicates high intensity of signal as shown in scalebar.*

The MALDI-MS images, performed on the Q-star mass spectrometer, of the distribution of the matrix and the drug from xenograft tumours following a 24h DMXAA treatment are shown below in Fig.2.9.

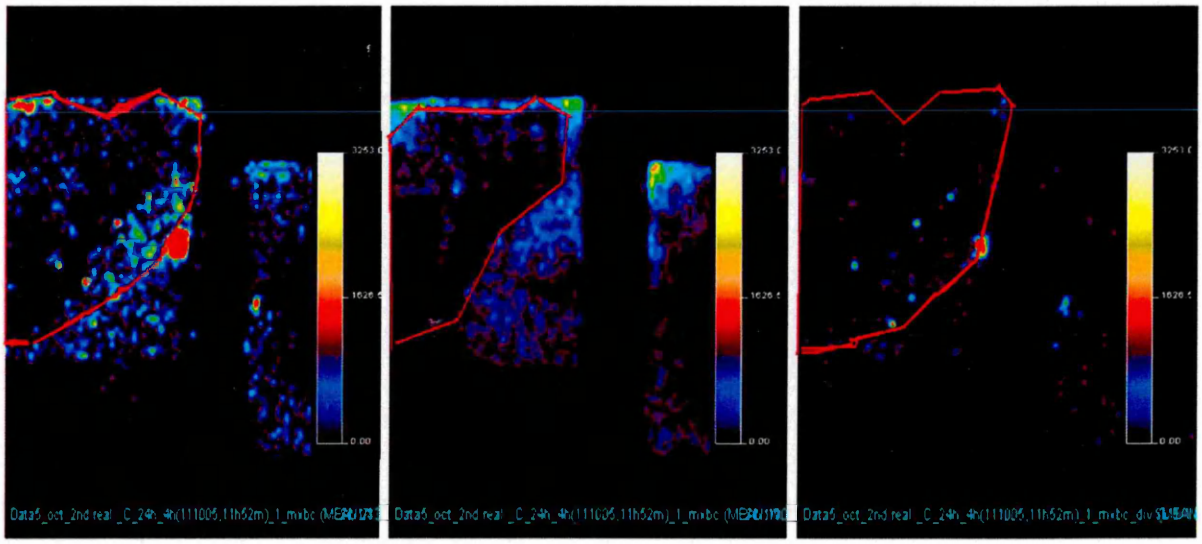

drug layer at 283 .2 m/z after 24h treatment

matrix layer at 191m/z

image of division of matrix layer at 191 m/z over drug layer at 283 m/z

Figure 2.9: *The MALDI- MS images of the drug at 283.2 m/z after 24h treatment, matrix layer at 191 m/z and the overlaid image of matrix peaks at 191 m/z divided by drug peaks at 283.2 m/z. The outline of the tumour is shown in red. Blue colour gives low intensity of signal while orange white colours indicates high intensity of signal as shown in scalebar.*

Fig. 2.10 below shows the MALDI-MS image of the DMXAA drug distributed within the tissue after 4 hours of treatment.

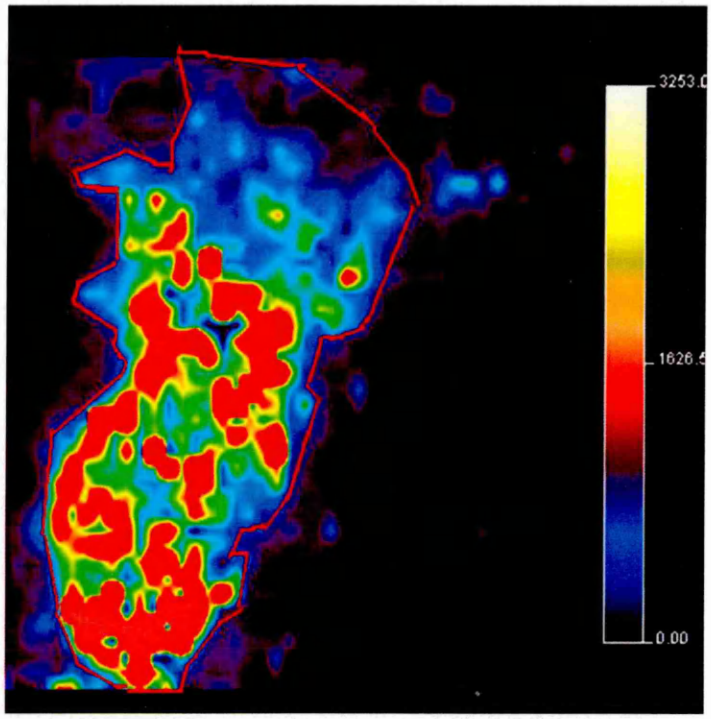

Figure 2.10: *MALDI-MS image showing the distribution of the drug (red area) in the middle of the tumour at 283.2 m/z after 4h treatment. The outline of the tumour is shown in the mass spectral image in red. Blue colour gives low intensity of signal while orange white colours indicate high intensity of signal as shown in scalebar.*

The MALDI image (shown in Fig. 2.10) of the 4-hour, post-treated xenograft tumour at 283 m/z shows that the drug was located mainly in the central region of the tumour.

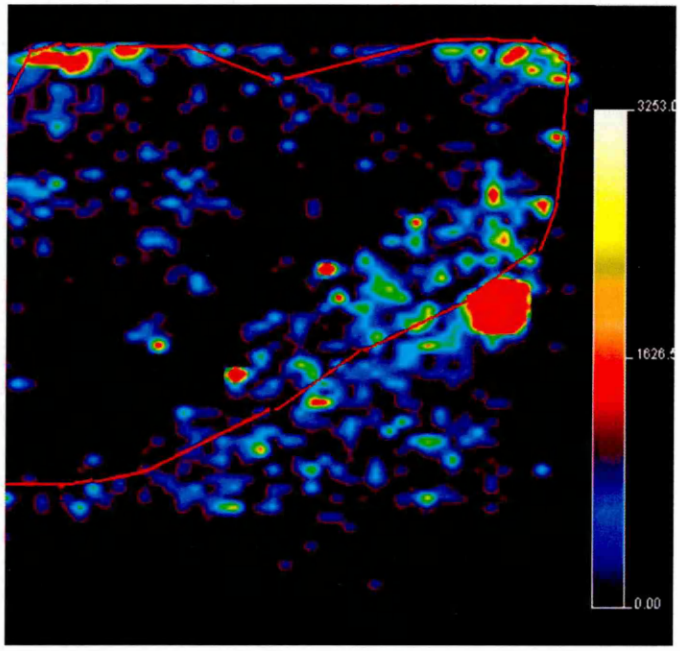

Figure 2.11: *MALDI-MS image showing the distribution of the drug (red area) in the periphery of the tumour at 283.2 m/z after 24h treatment. Blue colour gives low intensity of signal while orange white colours indicates high intensity of signal as shown in scalebar.*

The MALDI image of a 24h post-treated xenograft tumour (Fig. 2.11) shows that the drug was primarily distributed in the periphery of the tumour. Hence, as part of its mechanism of action, the drug tends to migrate to the periphery of the cancerous tissue following vascular damage.

2.2.4 Haematoxylin and Eosin staining

Haematoxylin and Eosin (H&E) staining of 4h and 24h DMXAA-treated xenograft tumour tissues was carried out after MS analysis in order to find a correlation between the MALDI image and the H&E stained section. As initial observation made (Fig 2.12-2.13) was that, the overall tissue structure is partly destroyed and quite damaged. This is probably due to the snap freeze process of the tissue and the damage occurred after MS analysis which makes it difficult to identify specific features from the H&E stained section.

However the Haematoxylin and Eosin stained sections of the 4h post-treated xenograft tumour, shown in Fig 2.12, do present an area of necrotic tissue (blue colour cells) in the centre of the tumour, reflecting the effect of the vascular disrupting agent and a viable rim on the periphery of the tumour can be seen.

These observations are similar to those observed in the study of (Gridelli *et al.,* 2009). These workers found that treatment with VDAs causes a necrosis in the centre of a tumour with a characteristic rim around its periphery. This could be explained by the fact that blood vessel occlusion, which progressed to complete vessel breakdown with haemorrhaging into the tumour and induced blood vessel destruction, lay between 4h and 5h post DMXAA for an LS174T xenograft tumour. Also, around 70 –75% inhibition of blood flow was observed in a 4h post DMXAA administration in colorectal xenograft tumour (Pedley *et al.,* 1999).

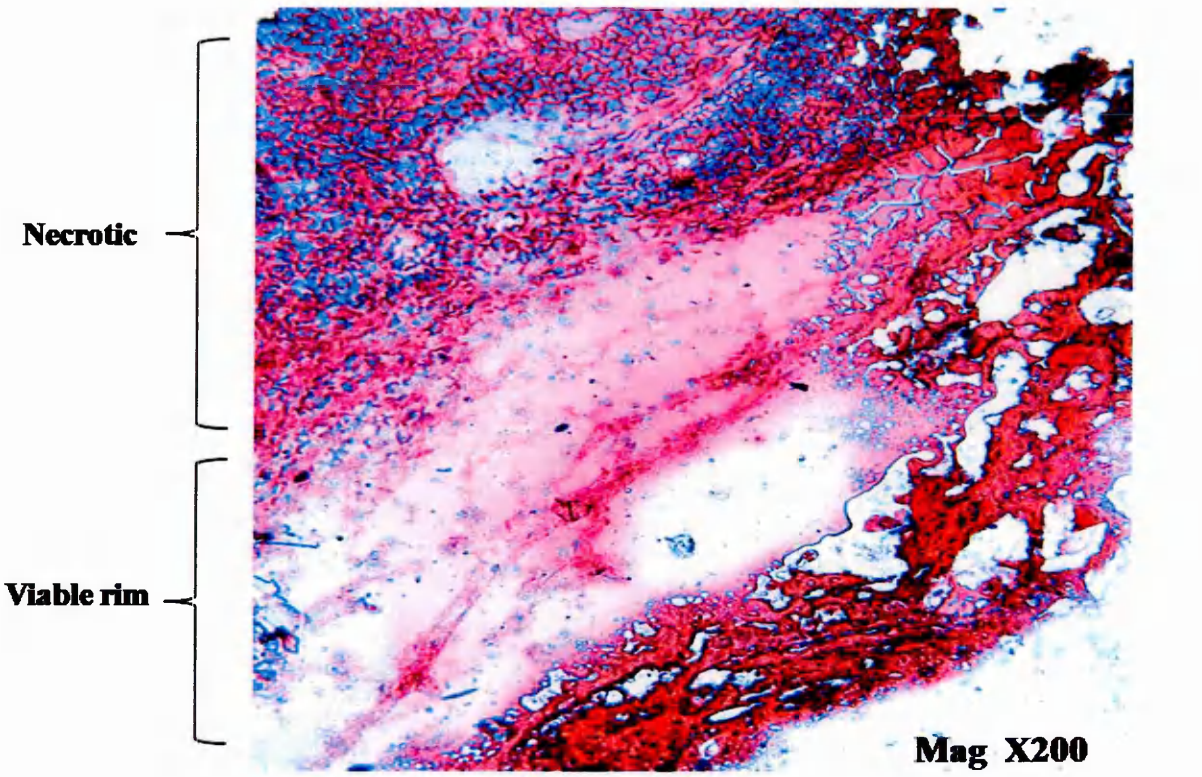

Figure 2.12: *Haematoxylin and Eosin (H&E) stained sections of a 4h post- treated xenograft tumour at Mag X200, showing a viable tissue rim on the edge and necrotic cells (blue colour).*

Fig. 2.13 below shows an H&E stained section of a xenograft tumour following 24h DMXAA treatment: areas of haemorrhaging, which gives a pink colour to the tissue, along with necrotic cells (nuclei stained blue) can be observed.

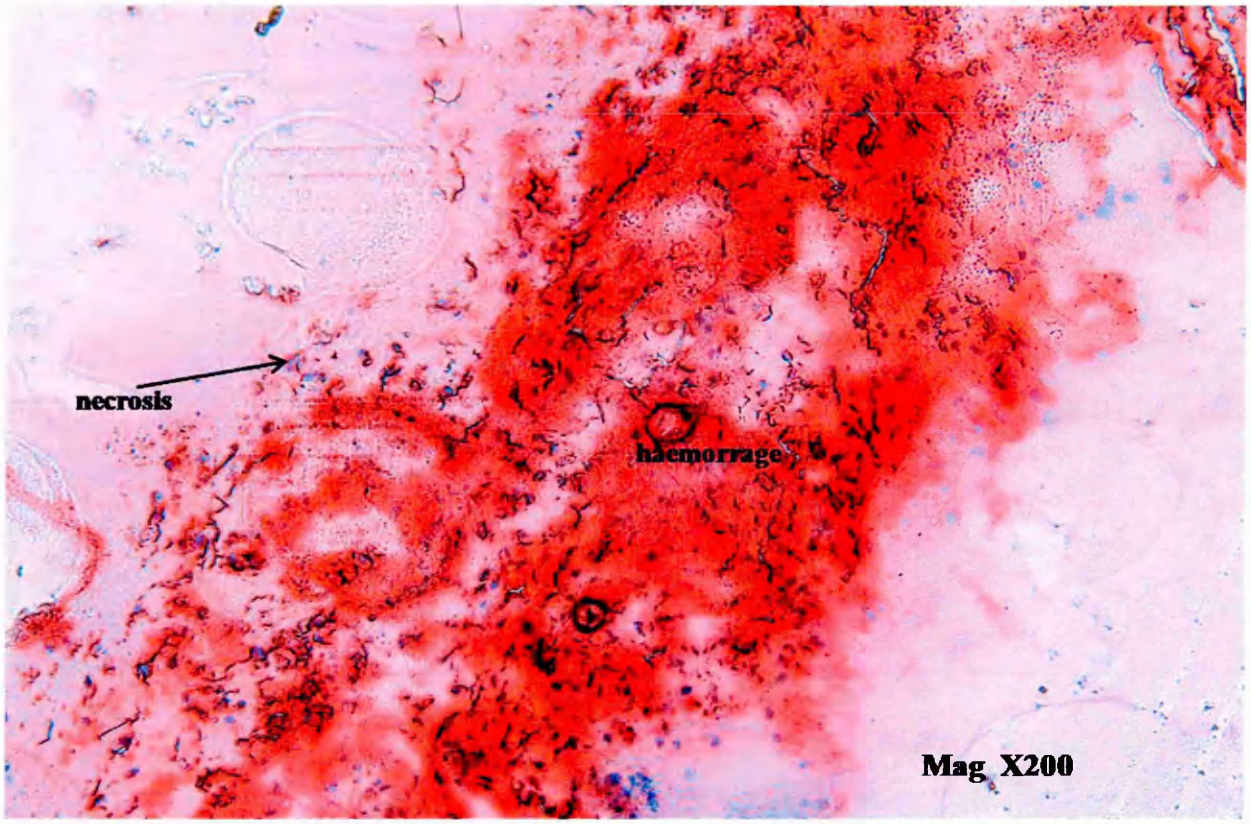

Figure 2.13: *Haematoxylin and Eosin (H&E) stained section of 24h post DMXAA at Mag X200, showing haemorrhagic area (pink colour) with presence of necrotic cells (nuclei stained blue).*

The development of tumour haemorrhagic necrosis following 24h treatment with DMXAA could be as a result of damage of blood vessels occurred drug which leads to rupture of the vessel and extravasation of erythrocytes into the surrounding tissue (Baguley & Bruce., 2003).

2.3 Conclusion

In the study of optimal conditions for the MALDI-MSI of DMXAA in tissue a matrix comprising ∝CHCA 5mg/ml dissolve in 70% EtOH / H_2O + 0.1 TFA matrix solvent gave better results compared to the other matrix solvents tested and was therefore considered as the matrix of choice for this study's experiment. The limit of detection /quantitation study showed that the anti-cancer agent, DMXAA, could be detected in a range of 10 ng/ml to 250 ng/ml on tissue. From the calibration curve the drug limit of detection (LoD) is determined as 10 ng/ml and the drug lower limit of quantitation (LLoQ) is 45 ng/ml. The MALDI image of the 4h post-treated xenograft tumour at 283 m/z showed that the drug was located mainly in the central region of the tumour, while the MALDI image of the 24h post- treated xenograft tumour showed that the drug was primarily distributed in the periphery of the tumour. Hence, as part of the mechanism of action, the drug tends to migrate to the periphery of the cancerous tissue following vascular damage.

An H&E stained section of a 4h post-treated xenograft tumour showed a necrotic area with a viable rim in the tumour's periphery; this is a characteristic feature of VDA treatment. Also, the H & E stained section of the 24h post-treated xenograft tumour showed some areas area of haemorrhage (pink colour) with some necrotic cells (nuclei stained blue).

2.4 References

ATKINSON, S.J., LOADMAN, P.M., SUTTON, C., PATTERSON, L.H. and CLENCH, M.R., 2007. Examination of the distribution of the bioreductive drug AQ4N and its active metabolite AQ4 in solid tumours by imaging matrix-assisted laser desorption/ionisation mass spectrometry. *Rapid communications in mass spectrometry,* **21**(7), pp. 1271-1276.

BAGULEY, B.C., 2003. Antivascular therapy of cancer: DMXAA. *The lancet oncology,* **4**(3), pp. 141-148.

BAGULEY, B.C. and WILSON, W.R., 2002. Potential of DMXAA combination therapy for solid tumors. *Expert Review Anticancer Therapy,* **2**(5):PP.593-603.

CHAPLIN, D.J., ACKER, B.D. and HORSMAN, M.R., 1989. Reduction of tumour blood flow by vasoactive drugs: a role in cancer therapy. *Biomedica biochimica acta,* **48**(2-3), pp. S264-8.

GRIDELLI, C., ROSSI, A., MAIONE, P., ROSSI, E., CASTALDO, V., SACCO, P.C. and COLANTUONI, G., 2009. Vascular disrupting agents: a novel mechanism of action in the battle against non-small cell lung cancer. *The oncologist,* **14**(6), pp. 612-620.

JAIN, R.K., 1988. Determinants of tumor blood flow: a review. *Cancer research,* **48**(10), pp. 2641-2658.

LASH, C.J., LI, A.E., RUTLAND, M., BAGULEY, B.C., ZWI, L.J. and WILSON, W.R., 1998. Enhancement of the anti-tumour effects of the antivascular agent 5,6-dimethylxanthenone-4-acetic acid (DMXAA) by combination with 5-hydroxytryptamine and bioreductive drugs. *British journal of cancer,* **78**(4), pp. 439-445.

MILOSEVIC, M.F., FYLES, A.W. and HILL, R.P., 1999. The relationship between elevated interstitial fluid pressure and blood flow in tumors: a bioengineering analysis. *International Journal of Radiation Oncology* Biology* Physics,* **43**(5), pp. 1111-1123.

PEDLEY, R.B., 1996. Pharmacokinetics of monoclonal antibodies. *Clinical Immunotherapeutics,* **6**(1), pp. 54-67.

PHILPOTT, M., BAGULEY, B.C. and CHING, L., 1995. Induction of tumour necrosis factor-α by single and repeated doses of the antitumour agent 5, 6-dimethylxanthenone-4-acetic acid. *Cancer chemotherapy and pharmacology,* **36**(2), pp. 143-148.

SIIM, B.G., LAUX, W.T., RUTLAND, M.D., PALMER, B.N. and WILSON, W.R., 2000. Scintigraphic imaging of the hypoxia marker (99m)technetium-labeled 2,2'-(1,4-diaminobutane)bis(2-methyl-3-butanone) dioxime (99mTc-labeled HL-91; prognox): noninvasive detection of tumor response to the antivascular agent 5,6-dimethylxanthenone-4-acetic acid. *Cancer research,* **60**(16), pp. 4582-4588.

TRIM, P.J., DJIDJA, M., ATKINSON, S.J., OAKES, K., COLE, L.M., ANDERSON, D.M., HART, P.J., FRANCESE, S. and CLENCH, M.R., 2010. Introduction of a 20 kHz Nd: YVO4 laser into a hybrid quadrupole time-of-flight mass spectrometer for MALDI-MS imaging. *Analytical and bioanalytical chemistry,* **397**(8), pp. 3409-3419.

TRIM, P.J., HENSON, C.M., AVERY, J.L., MCEWEN, A., SNEL, M.F., CLAUDE, E., MARSHALL, P.S., WEST, A., PRINCIVALLE, A.P. and CLENCH, M.R., 2008. Matrix-assisted laser desorption/ionization-ion mobility separation-mass spectrometry imaging of vinblastine in whole body tissue sections. *Analytical Chemistry,* **80**(22), pp. 8628-8634.

WORKMAN, P., ABOAGYE, E.O., BALKWILL, F., BALMAIN, A., BRUDER, G., CHAPLIN, D.J., DOUBLE, J.A., EVERITT, J., FARNINGHAM, D.A.H., GLENNIE, M.J., KELLAND, L.R., ROBINSON, V., STRATFORD, I.J., TOZER, G.M., WATSON, S., WEDGE, S.R. and ECCLES, S.A., 2010. Guidelines for the welfare and use of animals in cancer research. *British journal of cancer,* **102**(11), pp. 1555-1577.

www.maldi-msi.org.uk

ZHANG, X., ZHAO, M., RUDEK, M.A., HE, P. and VOGELSTEIN, B., 2007. Development and validation of a liquid chromatography/tandem mass spectrometry method for the determination of DMXAA in human and mouse plasma. *Journal of Chromatography B,* **852**(1), pp. 217-222.

ZHOU, S., PAXTON, J.W., TINGLE, M.D., MCCALL, J. and KESTELL, P., 1999. Determination of two major metabolites of the novel anti-tumour agent 5, 6-dimethylxanthenone-4-acetic acid in hepatic microsomal incubations by high-performance liquid chromatography with fluorescence detection. *Journal of Chromatography B: Biomedical Sciences and Applications,* **734**(1), pp. 129-136.

ZWI, L.J., BAGULEY, B.C., GAVIN, J.B. and WILSON, W.R., 1994. Correlation between immune and vascular activities of xanthenone acetic acid antitumor agents. *Oncology research,***6**(2),pp.79-85.

Chapter 3

Analysis of Lipids in DMXAA treated LS 174T Xenograft Tumours using MALDI-MSI

Lipids consist of different groups of molecules such as triacylglycerides, phosphoglycerides, sterols and sphingolipids that play important roles in cellular processes including membrane synthesis, metabolic regulation and immunity (Gschwind et al., 2002, Coussens et al., 2002). Phosphoglycerides, sterols and sphingolipids are the major structural components of biological membranes. Lipids also play a vital role in signalling processes and can work as second messengers and as hormones (Santos & Schulze, 2012). There is increasing evidence that cancer cells show some alterations in lipid metabolism which in turn affects the synthesis of membranes, the synthesis and degradation of lipids involved in energy homeostasis, and the signalling functions of lipids. These changes in lipid metabolism may affect different cellular processes, such as the growth, proliferation, differentiation and motility of cells (Santos & Schulze, 2012).

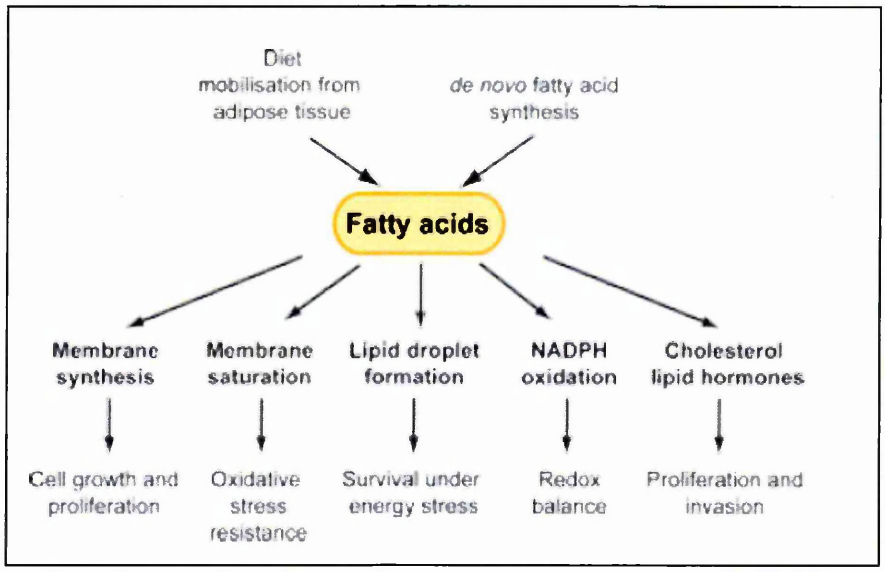

Figure 3.1: *Lipids are involved in many aspects of cancer development. Fatty-acid synthesis is stimulated by oncogenic signals and increased mobilisation from adipose tissue, resulting in an increased availability of lipids in cancer cells. Some of the potential functions of an altered lipid metabolism in cancer cells include: growth and proliferation, survival under oxidative and energy stress, support of a high-glycolytic rate by promoting redox balance, and the stimulation of signalling pathways which lead to proliferation and invasion (image adapted from Santos & Schulze, 2012).*

Examination of the lipid composition of tissue has been proposed as a method to determine response to chemotherapy (Todor *et al.*, 2012). In addition, the characterisation of lipidomic profiles in cancerous tissue can offer a new area of discovery for markers of diagnosis, prognosis and therapeutic efficacy (Mirnezami *et al.*, 2014).

3.1 Phospholipids and Cancer

Phospholipids are an important part of the cell membrane; they determine the membrane's structure. Data in the literature demonstrate that human colon cancer shows an increased amount of phospholipids (Dueck *et al.*, 1996). This increased amount of phospholipids results from the enhanced cell membrane synthesis associated with accelerated neoplastic cell replication (Ruiz-Cabello & Cohen, 1992). Over 50 years ago, it was noted that neoplastic tissues are able to synthesise lipids in a manner similar to embryonic tissues (Medes *et al.*, 1953). Since then, several studies have shown that tumour cells can reactivate *de novo* lipid synthesis (Menendez & Lupu, 2007). Some cancers, such as breast and prostate, show increased expressions of fatty acid synthase (FASN), suggesting that fatty-acid synthesis has a vital role in cancer pathogenesis (Li et al., 2000,Yoon et al., 2007). The mechanisms which are responsible for increases in phospholipids may vary depending on the nature of the cell, the cell's growth phase and its malignancy. The greatest changes in the content of phosphatidylcholine (PC) and phosphatidylethanolamine (PE) were seen in the first phase G1, of the cell cycle (Jackowski, 1996, Jackowski, 1994). Earlier reports were confirmed by the observations of Dueck *et al.*, 1996; these show that the content of PC in normal mucosa or lesions of colorectal cancer cells is higher than other phospholipids while the PC content is still higher in cancer cells compared to the normal mucosal cells.

The presence of an altered PC metabolism in cancerous tissue is well known and this has in fact been used to develop *in vivo* magnetic resonance spectroscopy (MRS) for tumour localisation across a variety of cancer subtypes (Klomp *et al.*, 2011, Wilson *et al.*, 2009, Venkatesh *et al.*, 2012).The anionic phospholipids in tumour vessels can be considered as markers for tumour vessel targeting and imaging (Ran *et al.*, 2002).

Sphingomyelin (SM) is an important content of plasma membranes and it is the main source of the free ceramide and sphingosine found in membranes which have powerful second messenger properties (Hannun, 1997, Chao, 1995).

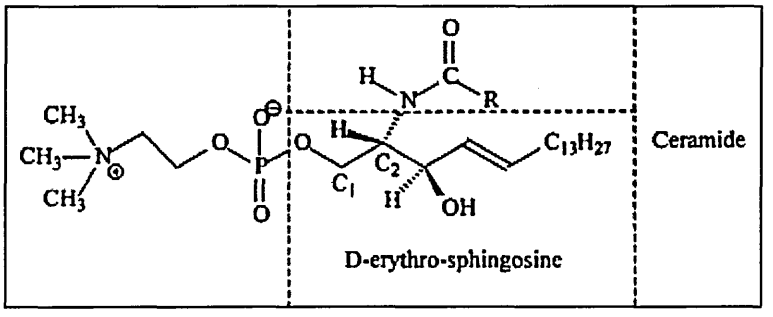

Figure 3.2: *Structures of sphingomyelin (Image adapted and reproduced from Hsu and Turk, 2000)*

Since ceramide and sphingosine are known as regulators of cell growth, differentiation and apoptosis (Duan & Nilsson, 2009), one current research question is whether the metabolites from dietary or membrane SM affect the cell cycle of the gut epithelium under normal and tumorigenic conditions, and whether sphingolipid metabolites regulate normal proliferation and differentiation in cell progenitor compartments and cells' fate (Duan & Nilsson, 2009). More than two decades ago, analytical studies identified differences in sphingolipid composition between tumour tissue and normal tissue in the gastrointestinal tract.

For example, in the study by Dudeja *et al.* (1986), an injection of dimethylhydrazine (a colonic chemical carcinogen) into an animal resulted in an increased amount of SM in colonic tissues, together with a reduction of Sphingomyelin phosphodiesterase (SMase). This indicated a decrease in SM hydrolysis prior to malignant transformation (Dudeja *et al.*, 1986). Multiple factors may account for the changes of SM and ceramide in colonic tissues, including the *de novo* biosynthesis of sphingolipids, the hydrolysis of SM by different sphingomyelinases, and the glycosylation of ceramide. Furthermore, SM was able to enhance the chemotherapeutic effects of anti-cancer drugs both *in vivo* and *in vitro* (Modrak *et al.*, 2000). However, the hydrolysis of sphingolipid to ceramide is a key procedure for such anticancer effects (Duan & Nilsson, 2009).

The aim of the work presented in this chapter is to identify changes in phospholipids in response to DXMAA treatment in LS 174T xenogaft tumours in mice using MALDI-MSI and MALDI-MS profiling.

3.2 Materials and methods

3.2.1 Chemicals

α-Cyano-4-hydroxycinnamic acid (CHCA) matrix, ethanol (EtOH), trifluoroacetic acid (TFA) and ammonium acetate (NH_4Ac) were purchased from Sigma-Aldrich (Gillingham, Dorset,UK).

3.2.2 Tissue preparation

LS174T colorectal adenocarcinoma xenografts grown in male immune-deficient mice were treated with 27.5 mg/kg DMXAA. The control (before treatment) and 4 h and 24 h post-treatment tumours were excised. The full detail of xenograft preparation was explained in more detail in Chapter 2, section 2.1.2. MALDI-MS imaging experiments were carried out on 12 µm cryosections sections using a Lecia CM 1850 cryostat (Leica Microsystems, Milton Keynes, UK) set at - 20°C. Then, tissue sections (n=1) from each time point were mounted on to conventional

microscopic glass slides; these were stored at - 80°C in a freezer prior to lipid analysis by MALDI.

3.2.3 Lipid washing with ammonium acetate (NH_4Ac)

For washing studies, serial tissue sections were obtained. Tissue sections were then washed with 150 mM ammonium acetate solution (NH_4Ac). The sections were either completely immersed in a coplin jar containing cold (4°C) NH_4Ac for 30 seconds, or they were gently dipped three times (dips of 10 seconds each) in the cold NH_4Ac. Then, the sections were dried in a vacuum for 20 minutes before running in MALDI-MS for profiling of phosphocholine (PC) and sphingomyelin (SM) species in the tissue samples.

3.2.4 Matrix Coating

After drying, tissue sections were spray-coated with 5 mg/ml ∝-CHCA matrix dissolved in 70% ethanol/H_2O + 0.1 TFA using a Suncollect automated pneumatic sprayer (Sun Chrom, Friedrichsdorf, Germany) in a series of layers; approximately 5 coats were applied.

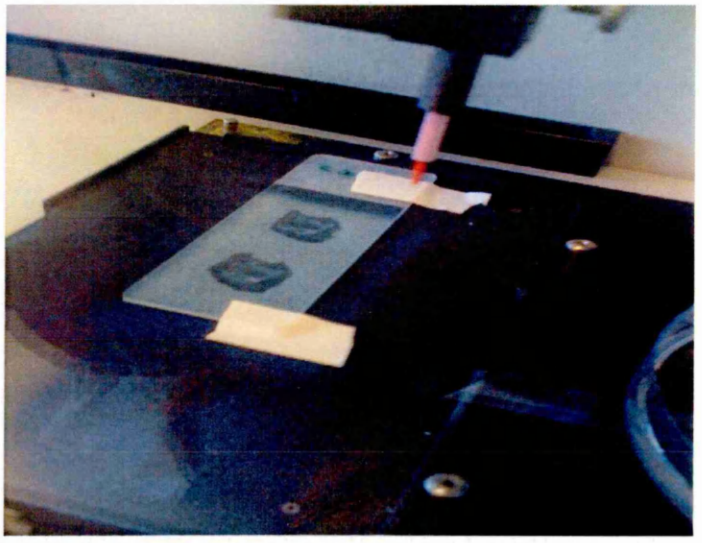

Figure 3.1: *Image of tissue coated with matrix in the Suncollect automated pneumatic sprayer (Sun Chrom, Friedrichsdorf, Germany).*

3.2.5 Mass spectrometry imaging of phospholipids and data analysis

The tissues glass slides were cut to size and mounted onto a glass slide MALDI target holder (Applied Biosystems / MDS Sciex, Concord, Ontario, Canada) using double-sided carbon tape. For lipid analysis, imaging experiments were performed in positive and negative ion modes using a Q Star Pulsar I Quadrupole/Time of Flight Mass (QTOF) Spectrometer (Applied Biosystems / MDS Sciex) with an orthogonal MALDI ion source (Applied Biosystems, Foster City, California, USA). MALDI images and spectra were acquired in the range of 200 to 1200 m/z at 200 µm x 200 µm spatial resolution and with laser frequency of 5KHz. The images were then converted into Analyst 7.5 file format using oMALDI server 5.1 software. These were then analysed using Biomap 3.7.5.5 imaging software (www.maldi-msi.org).

3.2.6 Haematoxylin and Eosin staining

After imaging, the tissue sections were retained for Haematoxylin and Eosin (H&E) staining so that they could be compared with the MALDI image. Each section of tissue was washed with 5ml of 100% ethanol to remove the matrix from the tissue. Then, the tissue section was rehydrated using a series of graded alcohols. Each section was immersed in 100% ethanol for 5 minutes, followed by a further 5 minutes in 95%, 80% and 70% ethanol. The rehydrated tissue section was then washed with tap water for 5 minutes to remove the ethanol. Afterwards, the tissue section was deposited in a rack filled with Haematoxylin for 5 minutes to stain the nucleus a blue-purple colour. Then, the tissue section was rinsed with tap water for 10 minutes to remove the Haematoxylin. The section was then dipped 3 times in a jar containing 0.1% HCl and then into tap water 3 to 4 times. Before staining with eosin, the tissue section was dipped 3 times in a jar containing 0.1% NaOH and then in tap water 3 to 4 times. Eosin stains the eosinophilic structure pink.

The tissue section was immersed in eosin for 3 minutes and then dehydrated 5 times in 100% ethanol with 0.1% acetic acid. This was followed by 2 washes of 5 times each in 100% ethanol and another 2 washes of 5 times each in acetone. Finally, the dehydrated section was then placed in xylene until cover slipped.

3.3 Results and discussion

3.3.1 Lipid washing with ammonium acetate (NH_4Ac)

Spectra were acquired in both positive and negative ion modes for lipid analysis before and after washing the tissue with 150 Mm NH_4AC. Fig.3.3 shows a representative mass spectrum image of phospholipids analysed in positive ion mode at a range of 700 to 750 m/z before and after the tissue had been washed with 150mMNH_4AC. Fig.3.4 shows a mass spectrum image of phospholipids analysed in negative ion mode at a range of 800 to 900 m/z before and after washing the tissue with 150mM NH_4AC.

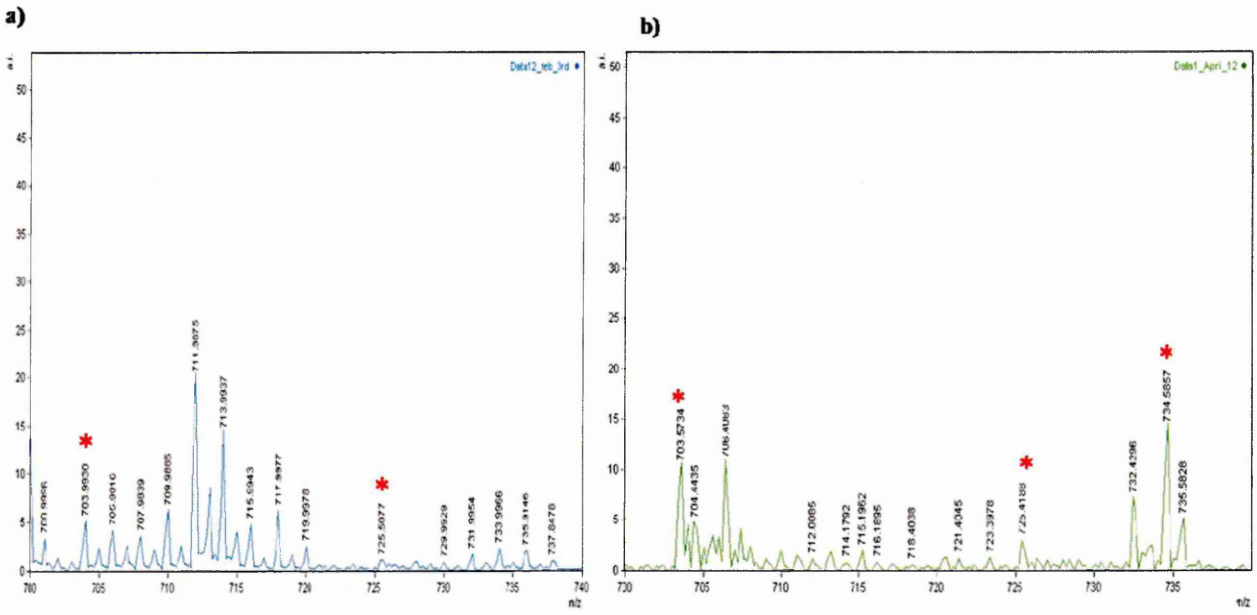

Figure 3.3: *Positive ion MALDI-MS spectrum a) without washing and b) after washing the tissue with 150 mM NH_4AC.The spectrum shows phospholipid peaks in a range of 700-750 m/z. The red marks shows lipid peaks which enhanced by 150 mM NH_4AC washing.*

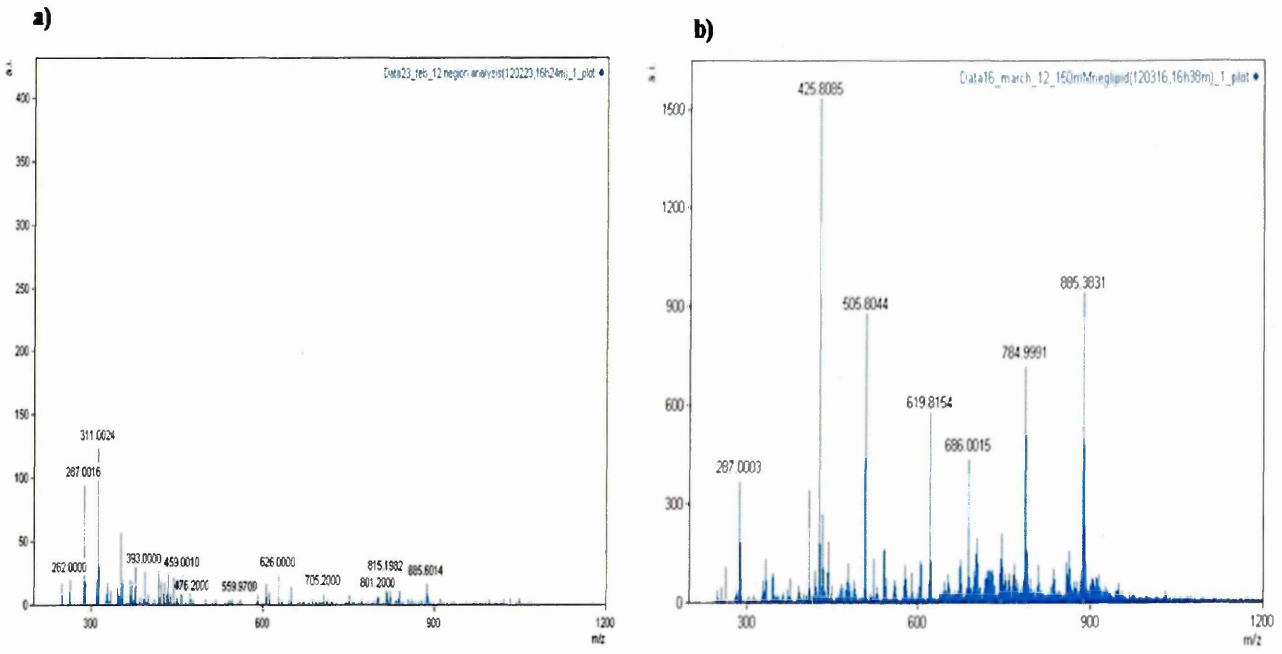

Figure 3.4: *Negative ion MALDI-MS spectrum a) without washing and b) after washing the tissue with 150 mM NH_4AC. The spectrum shows phospholipid peaks in a range of 800-900 m/z; the peak at 885 m/z is identified as PI.*

This study's data from the direct profiling of tissue lipids of sections washed with 150 mM ammonium acetate (NH_4AC) in both positive and negative ion modes revealed that incorporating an ammonium acetate wash into the sample processing improved and enhanced the S/N ratio in the subsequent mass spectrometry analysis. Also, more phospholipids species were detected, which could be as a result of desalting and removing contamination from the tissue which occurred after washing the tissue with 150 mM NH_4AC (Wang *et al.*, 2011). In addition, data from the negative ion mode analysis revealed that the peak at m/z 885 and other peaks showed a 5-fold increase in intensity after washing with NH_4AC. This allowed for a better identification of lipids in negative ion mode compared to spectra obtained before washing.

This result is in agreement with the study of Angel *et al.* (2012) in which they found that washing the tissue with ammonium acetate significantly improved sensitivity for negative ion mode lipid imaging. It also produced a nearly 5-fold increase in the total ion current which allowed the imaging and identification of glycerophospholipids, as well as sulfatides and gangliosides; in the negative ion mode (Angel *et al.*, 2012). This proves that NH_4Ac washing was successful in this study.

3.4 Mass spectrometry imaging of lipids

3.4.1 Analysis of phospholipids in positive ion mode

For lipid analysis, images were obtained in both positive and negative ion modes in the m/z range of 200-1200. Fig.3.5 shows a typical positive ion mode full scan spectrum and image of 24h, 4h post-treated xenograft tumours, as well as control tissue in a range of 700 -800 m/z. The peak at 703.38 m/z $[M+H]^+$ was identified as SM (16:0) and was highly expressed in the 4h compared to 24h tumour tissues and control tissue.

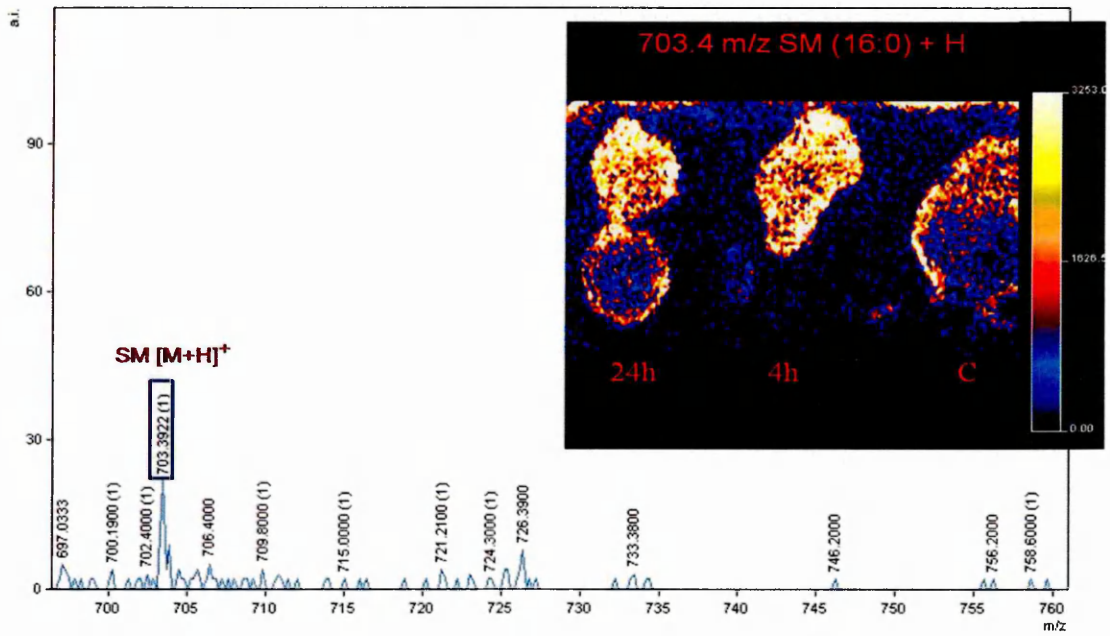

***Figure 3.5**: MALDI-MS spectrum and image showing the distribution of sphingomyelin $[M+H]^+$ at 703.38 m/z in positive ion mode. Blue colour gives low intensity of signal while orange white colours indicates high intensity of signal as shown in scalebar.*

Figure 3.6 shows a positive ion mass spectrum and image of sodiated sphingomyelin at 725.30 m/z $[M+Na]^+$ identified as SM (16:0) + Na. It is also highly expressed in 4h compared to 24h tumour tissues and the control tissue.

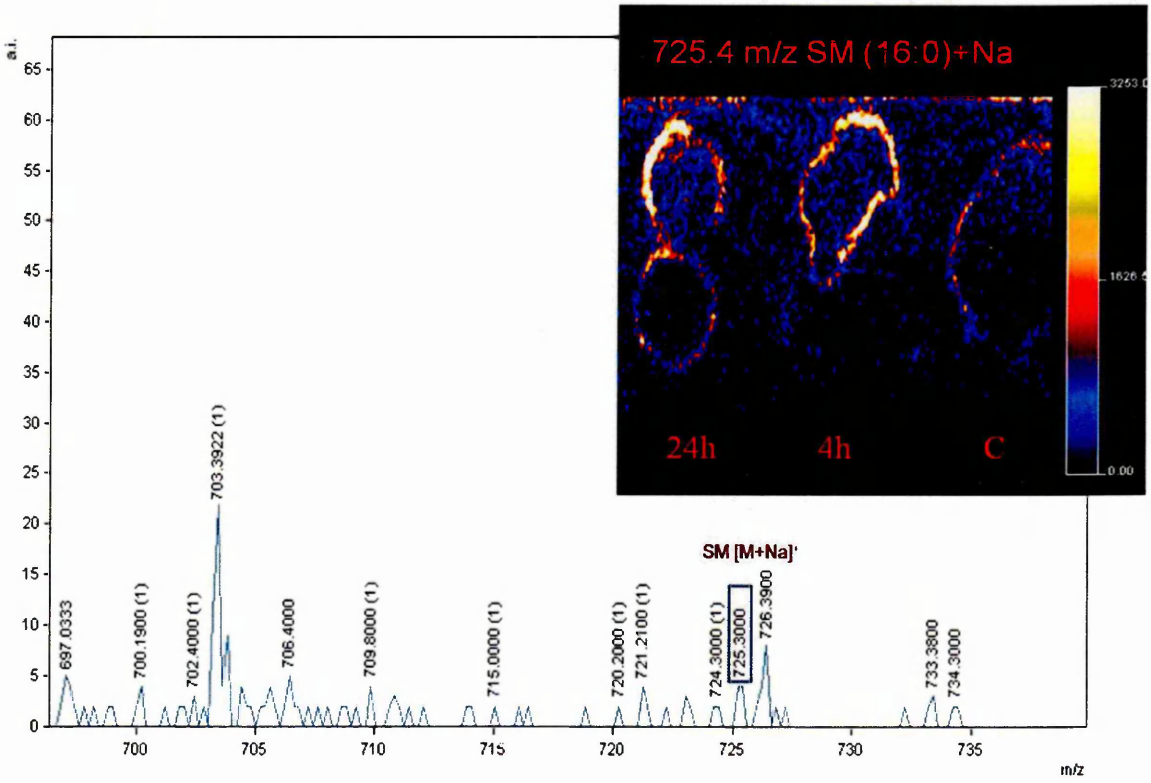

Figure 3.6: *MALDI-MS spectrum and image showing the distribution of sodiated sphingomyelin* $[M+Na]^+$ *at 725.30 m/z in positive ion mode. Blue colour gives low intensity of signal while orange white colours indicates high intensity of signal as shown in scalebar.*

Fig. 3.7 below shows a positive ion mass spectrum and image of Phosphocholine at 734.30 m/z $[M+H]^+$ identified as PC (32:0). This is also highly expressed in the 4h and 24h tumour tissues compared to the control tissue.

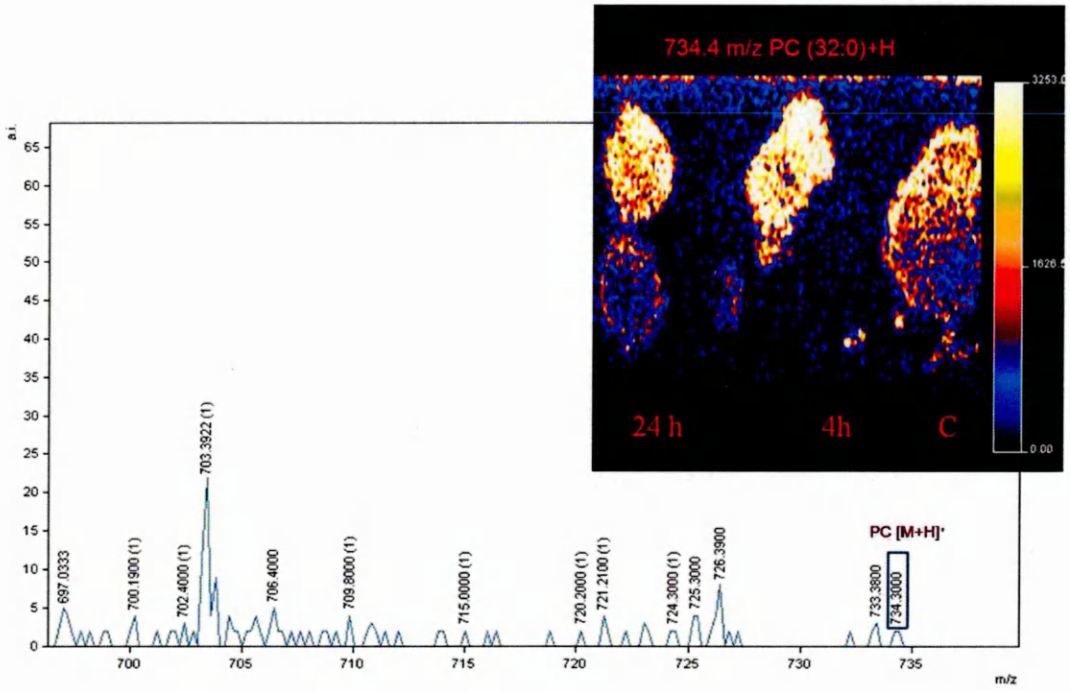

***Figure 3.7**: MALDI-MS spectrum and image showing the distribution of phosphocholine [M+H]$^+$ at 734.30 m/z in positive ion mode. Blue colour gives low intensity of signal while orange white colours indicates high intensity of signal as shown in scalebar.*

Based on the obtained data which is presented above, it appears that tumour tissue exhibits increased absolute intensities for the signals of SM (16:0) at m/z 703 and 725 when compared with normal tissue. This observation is in agreement with the study of Shimma *et al.* (2007) which showed that MALDI-MS/MS analysis of human colon cancer liver metastasis in normal and cancerous areas suggested that SM (16:0) accumulated in cancer cells.

This could be explained by the fact that an inflammatory response is linked to the production of cytokines such as TNF-alpha which affects the metabolism of phospholipids. TNF-alpha and IL-1alpha/beta can induce phospholipases and sphingomyelinases; this leads to the hydrolysis of phosphatidylcholine and sphingomyelin-synthesising enzymes (Meriaux *et al.*, 2010). Therefore, in serous cancer, the over production of ascites can be related to the overproduction of phosphatidylcholine and sphingomyelin caused by stimulating TNF alpha (Meriaux *et al.*, 2010).

3.4.2 Analysis of phospholipids in negative ion mode

Images and spectra were also obtained in negative ion mode in the range of approximately 200 to 1100 m/z for lipid analysis. Fig. 3.8 shows a single negative ion MALDI-MS spectrum taken from control tissue. Prominent phospholipid peaks were assigned, according to the lipid map database, to the following: phosphatidylcholine (PC) (P-39:0) $[M-H]^-$ at 814.80 m/z, PC (O-40:0) $[M-H]^-$ at 830.80 m/z; phosphatidylinositol phosphate (PIP) (33:9) $[M-H]^-$ at 885.38 m/z; phosphatidylinositol (PI)(O-48:0) $[M-H]^-$ at 1019.82 m/z and PI (P-50:2) $[M-H]^-$ at 1041.81 m/z.

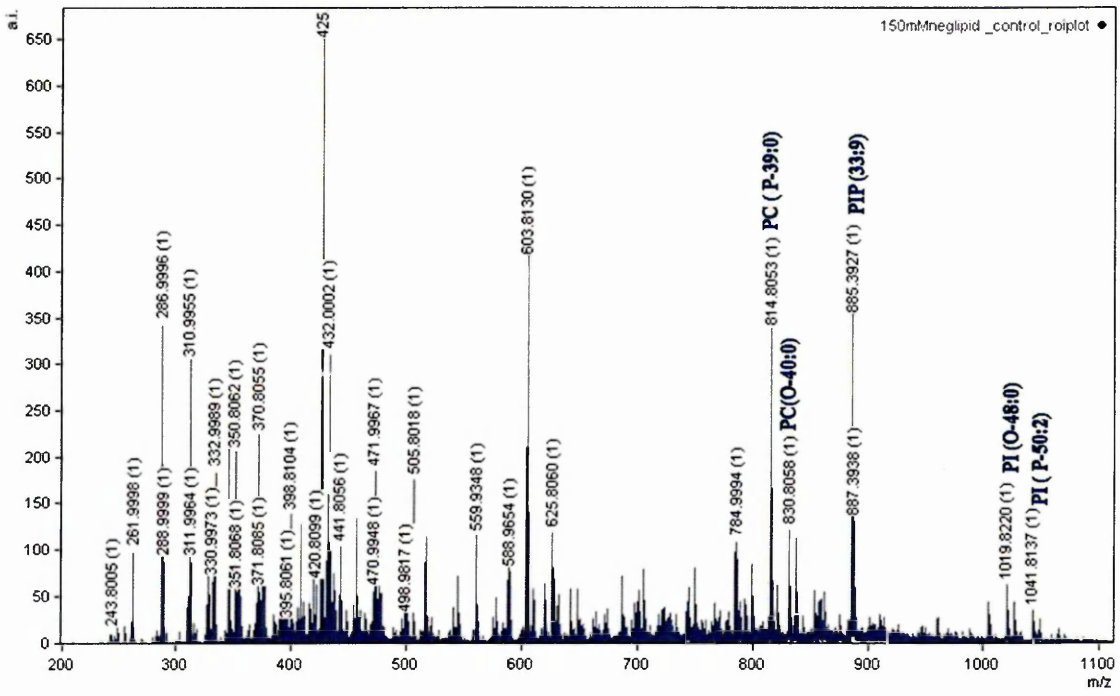

Figure 3.8: *Single negative ion MALDI-MS spectrum of control tissue showing phospholipid peaks in a range of 800 to 900 m/z.*

Fig 3.9 shows a single negative ion MALDI-MS spectrum taken from a 4h post-treated xenograft tumour. Prominent phospholipid peaks were assigned, according to the lipid map database, to the following: phosphatidylinositol phosphate (PIP) (22:0) $[M-H]^-$ at 748.99 m/z; phosphatidylcholine (PC) (P-39:0) $[M-H]^-$ at 814.80 m/z, PC (O-40:0)$[M-H]^-$ at 830.80 m/z, (PIP) (33:9)$[M-H]^-$ at 885.38 m/z ; phosphatidylinositol(PI) (O-48:0) $[M-H]^-$ at 1019.82 m/z and PI (P-50:2) $[M-H]^-$at 1041.81 m/z.

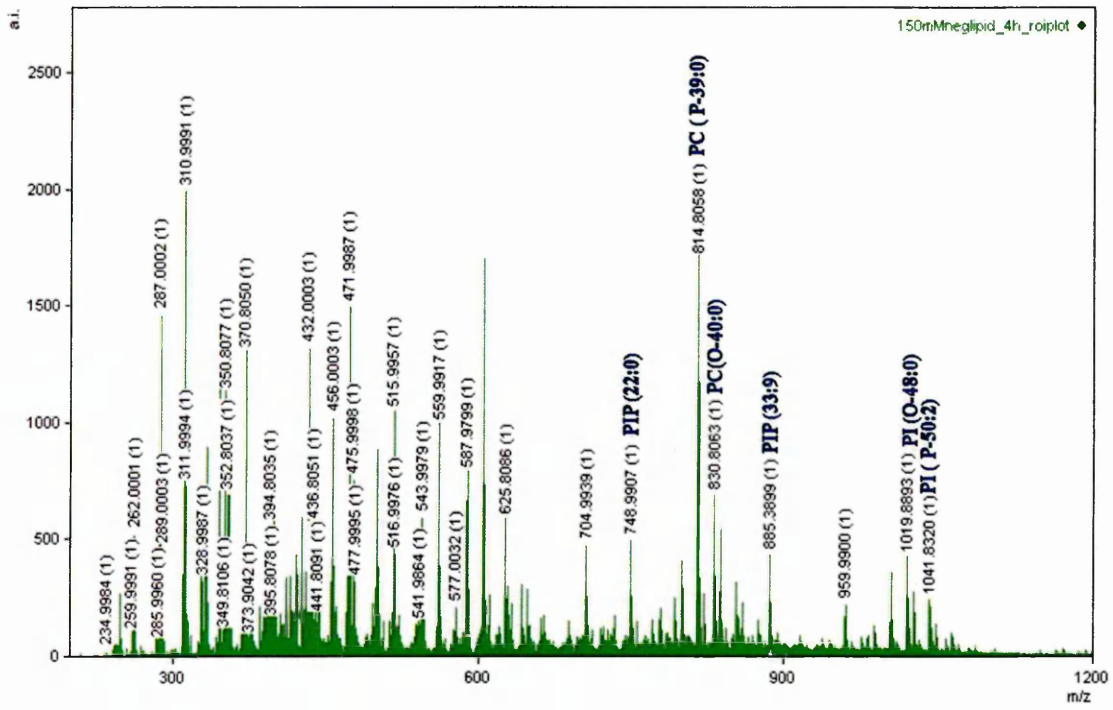

Figure 3.9: *Single negative ion MALDI-MS spectrum of 4h post-treated tumour tissue showing phospholipid peaks in a range of 800 to 900 m/z.*

Fig.3.10 shows a single negative ion MALDI-MS spectrum taken from a 24h post-treated xenograft tumour. Prominent phospholipid peaks were assigned, according to the lipid map database, to the following: phosphatidylcholine (PC) (P-39:0) $[M-H]^-$ at 814.80 m/z and (PIP) (33:9) $[M-H]^-$ at 885.38 m/z.

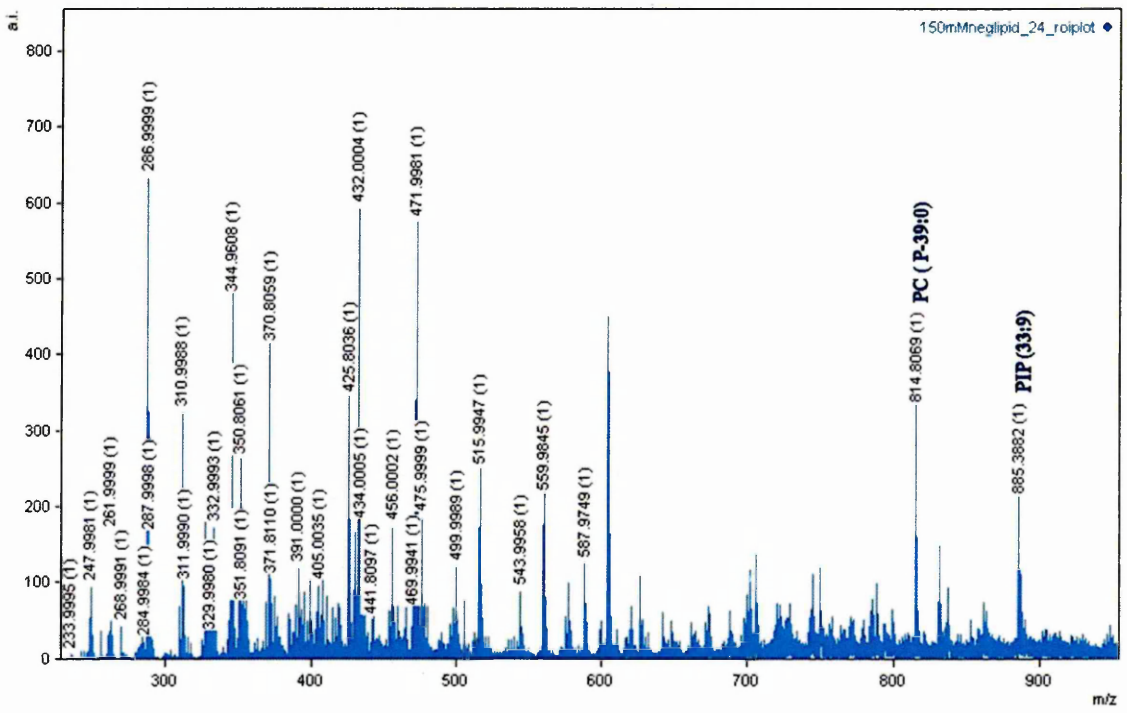

Figure 3.10: *Single negative ion MALDI-MS spectrum of 24h post-treated tumour tissue showing phospholipid peaks in a range of 800 to 900 m/z.*

In order to allow direct comparison, Fig. 3.11 show the overlaid negative ion MALDI-MS spectra of control, 4h and 24h post-treated xenograft tumours, in a range of 800 to 900 m/z. The spectrum taken from the 4h post-treated xenograft tumour shows the highest signal of phospholipids species compared to the 24h post-treated and control spectra.

In contrast, the spectrum taken from the 24h post-treated xenograft tumour showed a lower signal of phospholipid species compared to the 4h post-treated tumour. This finding is similar to results in the study of McPhai *et al.* (2015) which found a significant decrease in total choline *in vivo* following 24-hour post-treatment with 21mg/kg DMXAA (McPhai *et al.*, 2015). The reduction in PC in the 24h post-treated tumour could be a result of the vascular-disrupting activity of DMXAA.

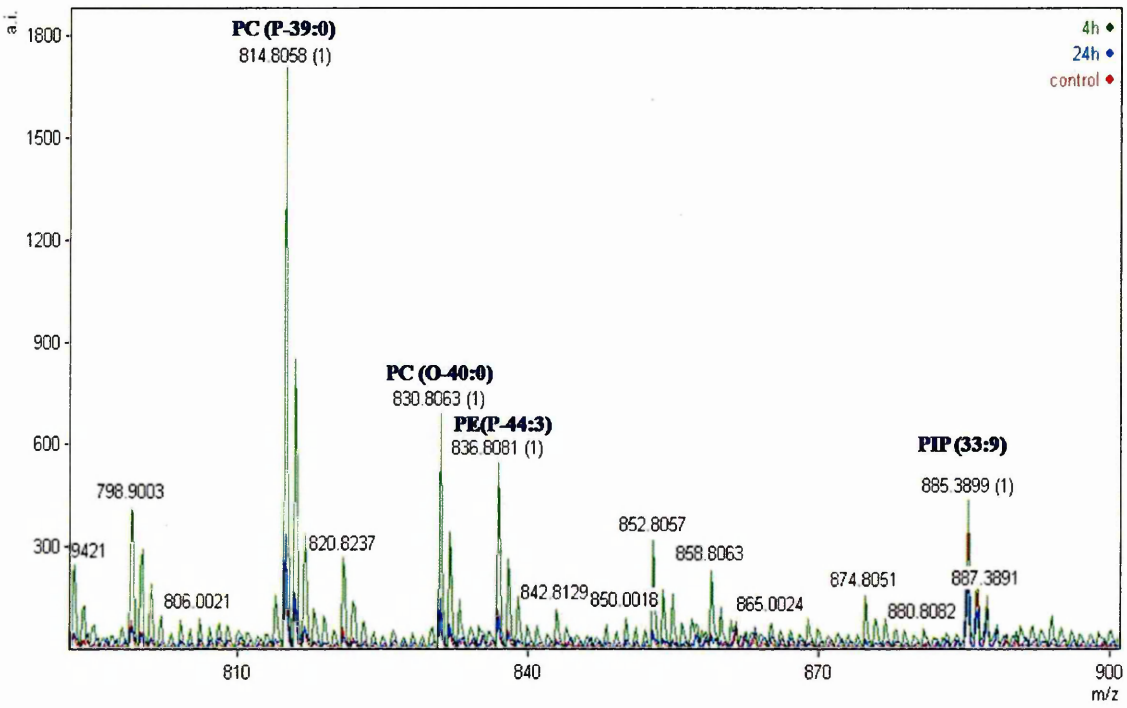

Figure 3.11: *Overall negative ion MALDI-MS spectra of control (red colour), 4h (green colour) and 24h (Blue colour) post-treated xenograft tumours showing phospholipid peaks in a range of 800 to 900 m/z. Peaks were assigned according to their masses to the following: phosphatidylcholine, PC (P-39:0) [M-H]$^-$ at 814.80 m/z; PC (O-40:0)[M-H]$^-$ at 830.80 m/z; PE (P-44:3)[M-H]$^-$ at 836.80 m/z; and PIP (33:9)[M-H]$^-$ at 885.38 m/z.*

Fig. 3.12 presents MALDI-MSI images showing the distribution of a number of different phospholipids in control, 4h and 24h post-treated xenograft tumours. The image at 748.9 m/z was assigned to (PIP) (22:0) $[M-H]^-$; the image at 788.4 m/z was assigned to PS (37:8) [M-H]. The image at 814.6 m/z was assigned to PC (P-39:0) $[M-H]^-$ and it showed a reduced intensity in the 24h post-treated xenograft tumour compared to the control and 4h post-treated xenograft tumours. Also, the image at 830.9 m/z, which was assigned to PC (O-40:0)$[M-H]^-$, showed a reduced intensity in the 24h post-treated xenograft tumour compared to the control and 4h post-treated xenograft tumours. This observation confirms the results obtained from the spectra presented in Fig. 3.11 which show that PC was decreased in the 24h post-treated tumour compared to the 4h post-treated tumours. This suggests that this decrease is a result of the vascular-disrupting activity of DMXAA.

The image at 836.9 m/z was assigned to PE (P-44:3) $[M-H]^-$. This also shows a decrease in intensity in the 24h post-treated xenograft tumour. The image at 885.4 m/z was assigned to (PIP) (33:9) $[M-H]^-$ while the image at 1019.9 m/z corresponded to PI (O-48:0) $[M-H]^-$ and the image at 1041.9 m/z was assigned to PI (P-50:2) $[M-H]^-$.

Overall the image data in this study show a decrease of PC and PE in the 24h post-treated xenograft tumour compared to the 4h post-treated tumour. This finding is in agreement with the study of McPhai *et al.* (2015) which found that the membrane associated phosphodiesters (PDE) consisted of glycerophosphoethanolamine and glycerophosphocholine, which are products of membrane degradation; was significantly depleted within tumour tissue 6 and 24 hours post-treatment with 21 mg/kg DMXAA (McPhai *et al.*, 2015).

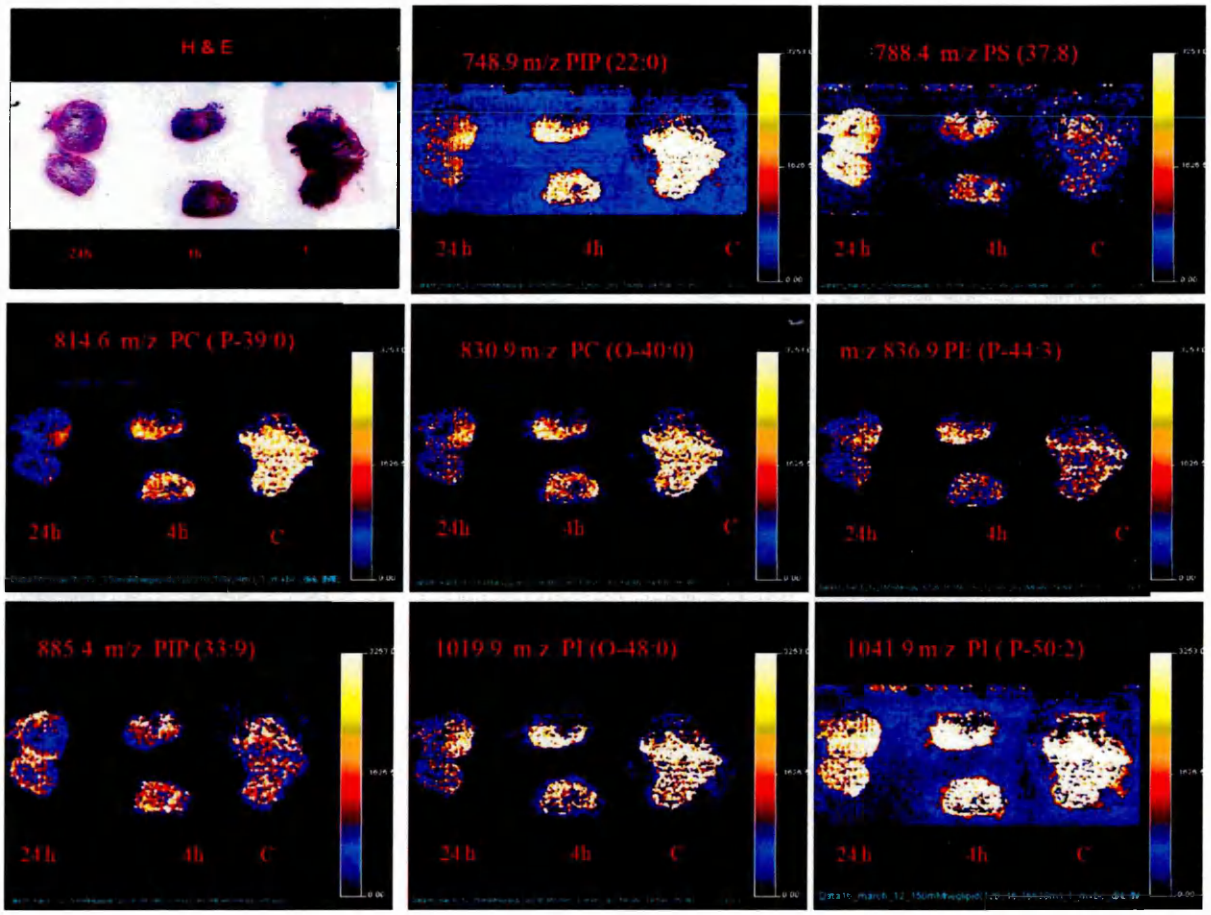

Figure 3.12: *Negative ion MALDI-MSI images with the corresponding H&E stained tissue sections showing the up and down regulation of phospholipids of interest: (PIP) phosphatidylinositol phosphate, (PS) phosphotidylserine, (PC) phosphatidylcholine, (PE) phosphatidylethanolamine and (PI) phosphatidylinositol in control, 4h and 24h xenograft tumours after treatment with DMXAA.The principal lipid class called PIP3 was identified at 885.4 m/z and it present at much higher abundance in cancerous tissue. The 748.9 m/z was assigned to (PIP) (22:0) [M-H]⁻ ; the 788.4 m/z was assigned to PS (37:8) [M-H]. The 814.6 m/z was assigned to PC (P-39:0) [M-H]⁻ and the 830.9 m/z was assigned to PC (O-40:0)[M-H]⁻ which shows a down-regulation in the 24h post-treated xenograft tumour compared to the control and 4h post-treated xenograft tumours. Blue colour gives low intensity of signal while orange white colours indicate high intensity of signal as shown in scalebar.*

Table 3.1 below shows a comparision of the calculated mass and the experimentally observed mass for each of the lipids based on the lipidmap database.

Observed Mass Units	Accurate Mass Units	Delta Units	Abbreviation	Formula	Ion
885.3898	885.3597	.0301	PIP(33:9)	$C_{42}H_{63}O_{16}P$	$[M-H]^-$
887.3891	887.3753	.0138	PIP(33:8)	$C_{42}H_{65}O_{16}P$	$[M-H]^-$
1019.8220	1019.7897	.0323	PI(O-48:0)	$C_{57}H_{112}O_{12}P$	$[M-H]^-$
1041.8320	1041.7740	.0580	PI(P-50:2)	$C_{59}H_{110}O_{12}P$	$[M-H]^-$

*Table 3.1: Comparison of observed mass and measured mass taken from the spectra shown in Figure 3.11.This shows the possible lipid species identified using (**http://www.lipidmaps.org**) by comparing the mass of observed ions to the matched mass within a mass error of +/- 0.05 Dalton. The difference between observed mass and accurate mass is known as delta units.*

3.4.3 Haematoxylin and Eosin Staining

Haematoxylin and Eosin (H&E) staining of control, 4h and 24h post-treated xenograft tumor tissues was carried out after phospholipids were imaged using MALDI-MSI to find a correlation between the MALDI image and the H&E stained sections.

Fig 3.13 shows the H&E stained section of the control untreated xenograft tumour. Due to the snap freeze process, the tissue shows its structure has been damaged or even destroyed; making it difficult to identify a specific feature from the H&E stained section.

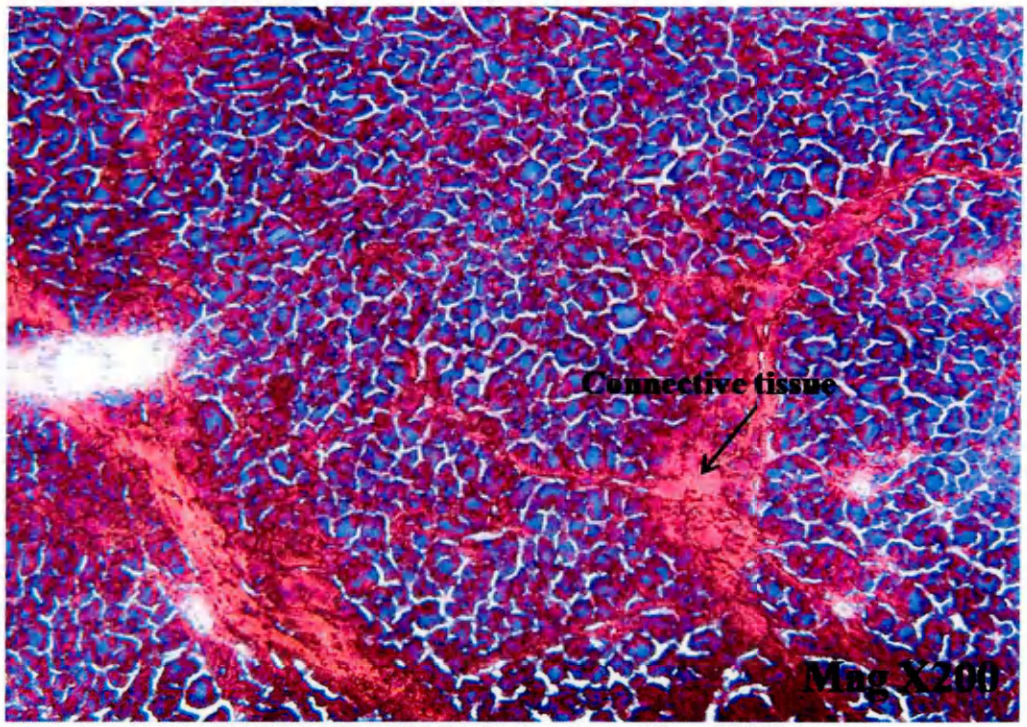

Figure 3.13: *H&E stained section of the control untreated xenograft tumour at Mag X200, tissue shows uniformed appearance of cells (blue) with connective tissue (red).*

Fig. 3.14 shows the Haematoxylin and Eosin stained sections of the 4h post-treated xenograft tumor. An area of both necrotic and viable cells is located in the core of the tumour tissue, while a characteristic viable rim can be located on the tumour's periphery.

The observation above is similar to that of McPhai *et al.* (2015) which showed that HT29 tumours presented a viable rim and a large central area of necrosis 6 hours after treatment with 21 mg/kg DMXAA (McPhai *et al.*, 2015).

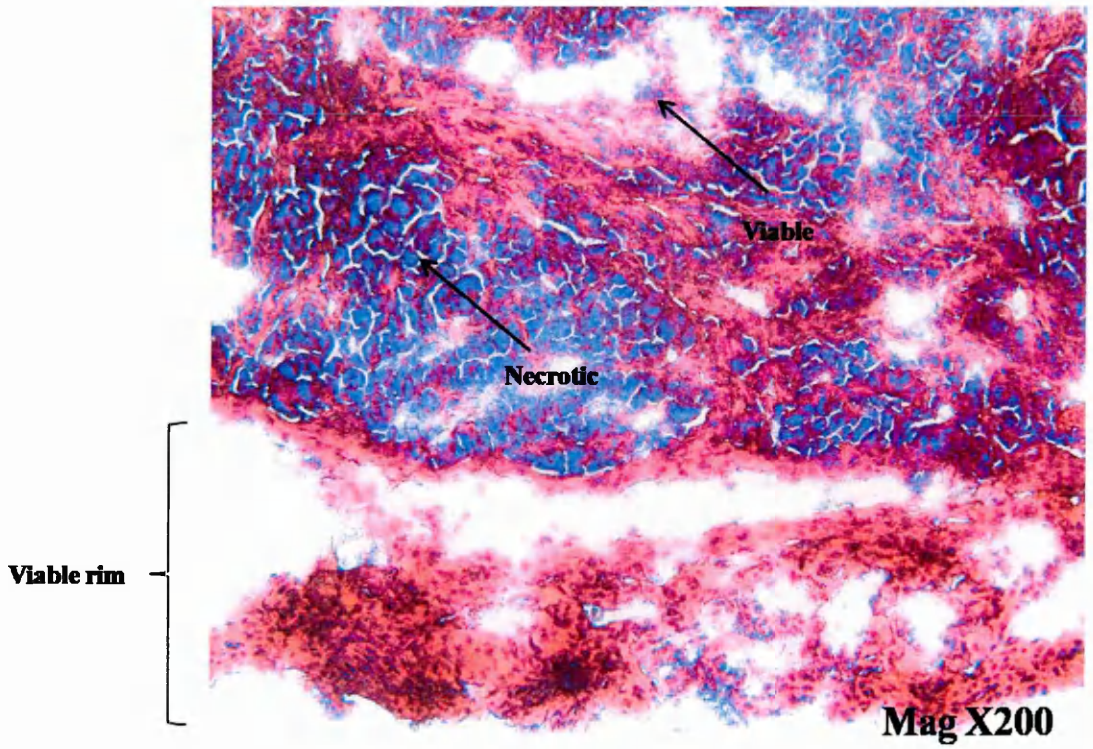

Figure 3.14: *H&E stained section of the 4h post-treated xenograft tumour at Mag X200 and showing an area of necrotic and viable cells in the centre of the tumor and a viable rim in the tumour's periphery.*

Fig. 3.15 shows an H&E stained section of the 24h post-treated xenograft tumours with widespread necrosis on the tumour's periphery. This is known as a disorganised region since it has less blue staining.

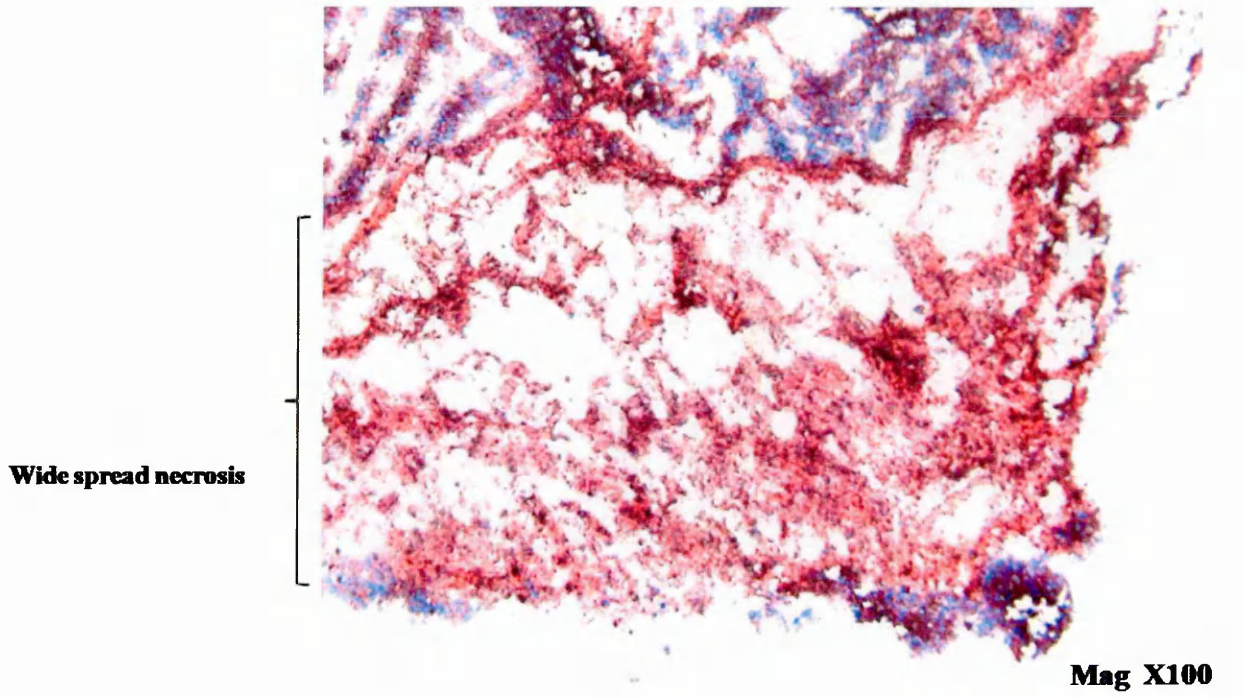

Figure 3.15: *H&E stained section of the 24h post-treated xenograft tumour at Mag X100. It shows an extensive area of widespread necrosis in the tumour's periphery.*

3.5 Conclusion

The addition of NH_4AC washing results in better images of lipids in positive and negative ion modes; it also enhances the signal's abundance. For lipid analysis, images were obtained in both positive and negative ion modes at a range of 200-1200 m/z. In positive ion mode, two classes of sphingomyelin SM (16:0) at 703.38 m/z, 725.30 and PC (32:0) at 734.30 m/z, were highly expressed in tumours tissue compared to the normal tissue. Spectra and images in negative ion mode showed a decrease in PC and PE in the 24h post-treated xenograft tumour compared to the 4h post-treated.

3.6 References

ANGEL, P.M., SPRAGGINS, J.M., BALDWIN, H.S. and CAPRIOLI, R., 2012. Enhanced sensitivity for high spatial resolution lipid analysis by negative ion mode matrix assisted laser desorption ionization imaging mass spectrometry. *Analytical Chemistry,* **84**(3), pp. 1557-1564.

CHAO, M.V., 1995. Ceramide: a potential second messenger in the nervous system. *Molecular and Cellular Neuroscience,* **6**(2), pp. 91-96.

COUSSENS, L.M. and WERB, Z., 2002. Inflammation and cancer. *Nature,* **420**(6917), pp. 860-867.

DUAN, R. and NILSSON, A., 2009. Metabolism of sphingolipids in the gut and its relation to inflammation and cancer development. *Progress in lipid research,* **48**(1), pp. 62-72.

DUDEJA, P.K., DAHIYA, R. and BRASITUS, T.A., 1986. The role of sphingomyelin synthetase and sphingomyelinase in 1, 2-dimethylhydrazine-induced lipid alterations of rat colonic plasma membranes. *Biochimica et Biophysica Acta (BBA)-Biomembranes,* **863**(2), pp. 309-312.

DUECK, D., CHAN, M., TRAN, K., WONG, J.T., JAY, F.T., LITTMAN, C., STIMPSON, R. and CHOY, P.C., 1996. The modulation of choline phosphoglyceride metabolism in human colon cancer. *Molecular and cellular biochemistry,* **162**(2), pp. 97-103.

GSCHWIND, A., PRENZEL, N. and ULLRICH, A., 2002. Lysophosphatidic acid-induced squamous cell carcinoma cell proliferation and motility involves epidermal growth factor receptor signal transactivation. *Cancer research,* **62**(21), pp. 6329-6336.

HANNUN, Y.A., 1997. Sphingolipid second messengers: tumor suppressor lipids. *Eicosanoids and Other Bioactive Lipids in Cancer, Inflammation, and Radiation Injury 2.* Springer, pp. 305-312.

HSU, F. and TURK, J., 2000. Structural determination of sphingomyelin by tandem mass spectrometry with electrospray ionization. *Journal of the American Society for Mass Spectrometry,* **11**(5), pp. 437-449.

http://www.lipidmaps.org.uk

JACKOWSKI, S., 1994. Coordination of membrane phospholipid synthesis with the cell cycle. *The Journal of biological chemistry,* **269**(5), pp. 3858-3867.

JACKOWSKI, S., 1996. Cell cycle regulation of membrane phospholipid metabolism. *The Journal of biological chemistry,* **271**(34), pp. 20219-20222.

KLOMP, D.W., VAN DE BANK, BART L, RAAIJMAKERS, A., KORTEWEG, M.A., POSSANZINI, C., BOER, V.O., VAN DE BERG, CORNELIUS AT, VAN DE BOSCH, MAURICE AAJ and LUIJTEN, P.R., 2011. 31P MRSI and 1H MRS at 7 T: initial results in human breast cancer. *NMR in biomedicine,* **24** (10), pp. 1337-1342.

LI, J.N., MAHMOUD, M.A., HAN, W.F., RIPPLE, M. and PIZER, E.S., 2000. Sterol regulatory element-binding protein-1 participates in the regulation of fatty acid synthase expression in colorectal neoplasia. *Experimental cell research,* **261**(1), pp. 159-165.

MCPHAIL, L.D., CHUNG, Y.L., MADHU, B., CLARK, S., GRIFFITHS, J.R., KELLAND, L.R. and ROBINSON, S.P., 2005. Tumor dose response to the vascular disrupting agent, 5,6-dimethylxanthenone-4-acetic acid, using in vivo magnetic resonance spectroscopy. *Clinical cancer research : an official journal of the American Association for Cancer Research,* **11**(10), pp. 3705-3713.

MEDES, G., THOMAS, A. and WEINHOUSE, S., 1953. Metabolism of neoplastic tissue. IV. A study of lipid synthesis in neoplastic tissue slices in vitro. *Cancer research,* **13**(1), pp. 27-29.

MENENDEZ, J.A. and LUPU, R., 2007. Fatty acid synthase and the lipogenic phenotype in cancer pathogenesis. *Nature Reviews Cancer,* **7**(10), pp. 763-777.

MERIAUX, C., FRANCK, J., WISZTORSKI, M., SALZET, M. and FOURNIER, I., 2010. Liquid ionic matrixes for MALDI mass spectrometry imaging of lipids. *Journal of proteomics,* **73**(6), pp. 1204-1218.

MIRNEZAMI, R., SPAGOU, K., VORKAS, P., LEWIS, M., KINROSS, J., WANT, E., SHION, H., GOLDIN, R., DARZI, A. and TAKATS, Z., 2014. Chemical mapping of the colorectal cancer microenvironment via MALDI imaging mass spectrometry (MALDI-MSI) reveals novel cancer-associated field effects. *Molecular oncology,* **8**(1), pp. 39-49.

MODRAK, D.E., LEW, W., GOLDENBERG, D.M. and BLUMENTHAL, R., 2000. Sphingomyelin potentiates chemotherapy of human cancer xenografts. *Biochemical and biophysical research communications,* **268**(2), pp. 603-606.

RAN, S., DOWNES, A. and THORPE, P.E., 2002. Increased exposure of anionic phospholipids on the surface of tumor blood vessels. *Cancer research,* **62**(21), pp. 6132-6140.

RUIZ-CABELLO, J. and COHEN, J.S., 1992. Phospholipid metabolites as indicators of cancer cell function. *NMR in biomedicine,* **5**(5), pp. 226-233.

SANTOS, C.R. and SCHULZE, A., 2012. Lipid metabolism in cancer. *FEBS Journal,* **279**(15), pp. 2610-2623.

SHIMMA, S., SUGIURA, Y., HAYASAKA, T., HOSHIKAWA, Y., NODA, T. and SETOU, M., 2007. MALDI-based imaging mass spectrometry revealed abnormal distribution of phospholipids in colon cancer liver metastasis. *Journal of Chromatography B,* **855**(1), pp. 98-103.

TODOR, I., LUKYANOVA, N.Y. and CHEKHUN, V., 2012. The lipid content of cisplatin-and doxorubicin-resistant MCF-7 human breast cancer cells. *Exp.Oncol,* **34**(2), pp. 97-100.

VENKATESH, H.S., CHAUMEIL, M.M., WARD, C.S., HAAS-KOGAN, D.A., JAMES, C.D. and RONEN, S.M., 2012. Reduced phosphocholine and hyperpolarized lactate provide magnetic resonance biomarkers of PI3K/Akt/mTOR inhibition in glioblastoma. *Neuro-oncology,* **14**(3), pp. 315-325.

WANG, H.Y., LIU, C.B. and WU, H.W., 2011. A simple desalting method for direct MALDI mass spectrometry profiling of tissue lipids. *Journal of lipid research,* **52**(4), pp. 840-849.

WILSON, M., DAVIES, N.P., GRUNDY, R.G. and PEET, A.C., 2009. A quantitative comparison of metabolite signals as detected by in vivo MRS with ex vivo1H HR-MAS for childhood brain tumours. *NMR in biomedicine,* **22**(2), pp. 213-219.

www.maldi-msi.org.uk

YOON, S., LEE, M.Y., PARK, S.W., MOON, J.S., KOH, Y.K., AHN, Y.H., PARK, B.W. and KIM, K.S., 2007. Up-regulation of acetyl-CoA carboxylase alpha and fatty acid synthase by human epidermal growth factor receptor 2 at the translational level in breast cancer cells. *The Journal of biological chemistry,* **282**(36), pp. 26122-26131.

Chapter 4

Analysis of Lipids in Dosed Tumours by TLC-MALDI-MS

5,6-dimethylxanthenone-4-acetic acid (DMXAA) is a flavonoid type drug which has an antivascular effect on tumours causing endothelial cell apoptosis and activation of cytokines resulting in necrosis at the tumour core and is classed as a vascular disrupting agent (VDA) (Rustin *et al.*, 2003). The degree of DMXAA-induced tumuor haemorrhagic necrosis is significantly correlated with increased tumuor vascular permeability, decreased functioning tumour blood vessels and increased plasma 5-hydroxyindoleacetic acid (5-HIAA) concentrations (McKeage *et al.*, 2006). DMXAA has been evaluated as monotherapy in phase I trials and was assessed in a number of successful phase II trials, where it was used in combination with paclitaxel/carboplatin for the treatment of non-small cell lung cancer (NSCLC). Whilst subsequent phase III trials were unsuccessful, DMXAA remains an interesting compound for the study of the biochemical effects of VDA.

Gao *et al.* have recently demonstrated that one pharmacodynamic response to treatment with flavonoid agents is an increase in the amount of lysophosphatidylcholine (LPC) type lipids. In their study, conducted using HepG2 cells and a novel flavonoid compound synthesised in their own laboratory, LPC levels were increased 40 fold in treated cells compared to the control group (Gao *et al.*, 2014). LPC are a class of cellular metabolite comprising a phosphocholine head group and one fatty acyl side chain. The fatty acyl side chain can be of differing chain lengths. LPC levels can be considered as a clinical diagnostic indicator of pathio-physiological changes (Gao *et al.*, 2014). They can be formed during oxidation at the sn-2 fatty acid of PCs by reactive oxygen species (ROS) (Catala., 2009). The increase in oxidative stress caused by flavonoid type molecules has been reported to lead to lipid peroxidation which causes an increase in LPC expression. Since the mitochondria are one of the most important organelles for energy transduction within the cell which support cellular survival they are a vulnerable intercellular target to ROS.

Thus, Gao *et al (2014)* proposed that the effect they observed indicated mitochondrial dysfunction and increased oxidative stress which would affect cellular metabolism and finally lead to cellular anti-proliferation *i.e.* an anti-cancer effect.

In this follow up study, here we are interested in developing methodology to study changes in lipid expression in treated xenografts by MALDI-MSI. The aim was to use this as means of correlating the distribution of DMXAA to its pharmacodynamic response. This is of particular interest since changes in phosphocholine containing lipids are also observable *in vivo* using 31P magnetic resonance spectroscopic imaging (MRSI) (Glunde *et al.*, 2011). However concerns arose that without some additional analysis of the lipid composition of the xenografts, the data set obtained from the MALDI-MSI experiments would be too complex to allow biological meaning to be extracted.

A number of methods for the analysis of lipids exist. TLC was one of the earliest forms of chromatography used for lipid analysis and is still widely used today. It is often used as a sample preparation step to separate lipids by class prior to subsequent analysis using HPLC or mass spectrometry (Fuchs *et al.*, 2011). TLC-MALDI-MS coupling combines the simplicity of TLC analysis with the detection capabilities of MS and allows scanning of a TLC plate within a few minutes (Busch., 1996). This combined method has been applied for analysis of complex lipid mixtures such as extracts from stem cells (Fuchs *et al.*, 2008). Unlike other techniques, the sample can be stored within the TLC plate and chromatograms can be obtained anytime. Whilst the literature contains some reports on the direct coupling of TLC with MALDI-TOF-MS for the analysis of polar molecules (Crecelius *et al.*, 2004) and glycolipids (Ivleva *et al.*, 2005-Nakamura *et al.*, 2006) there is so far only one paper describing the direct mass spectrometric analysis of phospholipids on a TLC sample plate (Rohlfing *et al.*, 2007) and no reports of its combination with MALDI-MSI.

In this paper, we describe the use of TLC-MALDI-MS for the analysis of phospholipids extracted from DMXAA treated xenograft tumors. Lipid class separation is performed by TLC-MALDI-MS to reduce the complexity of the data set to be studied, to aid identification of specific lipids and to indicate to us target lipid signals for study by MALDI-MS imaging. Subsequent to the TLC-MALDI-MS experiments MALDI-MS imaging was carried out on xenograft sections and images showing changes in distribution of LPC identified from the TLC-MALDI-MS experiments produced.

4.1 Experimental

4.1.1 Materials

Chloroform ($CHCl_3$), ethanol (EtOH), methanol (CH_3OH), acetonitrile (ACN) and acetone ($(CH_3)_2CO$) were all HPLC grade and obtained from Sigma-Aldrich (Gillingham, Dorset, UK). Acetic acid (CH_3COOH), α-cyano-4-hydroxycinnamic acid (CHCA) matrix, amido black stain, sodium chloride (NaCl), lithium chloride (LiCl) and trifluoroacetic acid (TFA), were all obtained from Sigma-Aldrich (United Kingdom). The water used was deionized water which was generated in house. TLC was performed on 20 x 20 cm aluminum backed plates coated with 0.2 mm layer of silica gel 60 F254 (Merck, Germany).

4.1.2 Tissue Sample Preparation

A detailed description of the preparation of the tissue samples can be found in Chapter 2, Section 2.1.2).

4.1.3 Lipid extraction

Lipids were extracted from tissue according to the Folch extraction method (Folch *et al.*, 1957) by initially homogenizing the weighed xenografts with an appropriate volume of, $CHCl_3$ / CH_3OH, (2:1, v/v) to yield a solvent: tissue ratio of 20:1 v/w. After dispersion, the whole mixture was agitated for 20 min in an orbital shaker at room temperature. Phase separation was induced by adding deionized water (1.5 ml).

Afterward, the homogenized mixtures were centrifuged at low speed (2000 rpm) to separate the two phases. The upper phase was removed and the entire lower chloroform phase (along with washings) which contained the lipids was collected into a glass tube and evaporated to dryness under a nitrogen stream and weighed.

The weights of the dried extracts were: 109.0 mg control (n=1), 108.3 mg 4h sample (n=1) and 226.0 mg 24h sample (n=1). The final extracts were then dissolved in an appropriate volume of $CHCl_3$ / CH_3OH, (2:1, v/v) to yield a 1mg/ml solution.

4.1.4 TLC Separation

Lipid extracts (1 µl) were applied onto an aluminum backed TLC plate (20 x 20 cm) coated with a 0.2 mm layer of silica gel as stationary phase. Then TLC plate was developed in a TLC chamber using $CHCl_3$, methanol, water, and acetic acid (30:15:2:4, v/v/v/v) as mobile phase one. When the solvent front had reached half the way up the plate, the plate was removed and air dried. After that, a second mobile phase was employed (acetone, acetonitrile, $CHCl_3$, 5:4:2 v/v/v) and the plate developed to the top. Following this the plate was removed from the TLC chamber and air dried. The lipid spots were visualized using 0.5% amido black 10 B stain in 1M NaCl.

4.1.5 Coupling TLC with MALDI- MS

α-CHCA matrix (5 mg/mL) was dissolved in 70% ethanol /water (v/v). 0.2% TFA (v/v) was then added. The developed TLC plate was cut in two parts to fit onto the MALDI target plate and adhered to a MALDI target using double sided tape. The TLC plates were spray coated with αCHCA matrix using a ''Suncollect'' (SunChrom, Friedrichsdorf, Germany) automatic pneumatic sprayer. Four layers of the 5 mg/mL α-CHCA matrix were applied at a flow rate of 5 µl/min using the "slow" spray pass setting of the instrument.

4.1.6 TLC-MALDI-MS

Mass spectra together with the high resolution images were recorded directly from the TLC plate using a Waters MALDI high-definition MS (HDMS) SYNAPT G2 mass spectrometer (Waters Corporation, Manchester, UK). A spatial resolution of 150 µm x 150 µm was employed with the instruments Nd:YAG laser being fired at $1kH_z$. A full description of the MALDI SYNAPT^{TM} HDMS instrument has been reported (Pringle *et al.*, 2007). Analysis was performed in positive ion mode and mass spectra were collected over the range of 200 to 1200 *m/z* following initial calibration with a standard solution of polyethylene glycol (PEG). All images were processed using HDI imaging software (Waters Corporation, Manchester, UK). After acquisition, the data were recalibrated using the polyethylene glycol (PEG) signal at 701.3935 *m/z* as a lock mass and centroided prior to the generation of accurate mass peak lists. Assignment of structure was then made by searching the accurate centroided *m/z* values against the lipid map database (http://www.lipidmaps.org) and comparing the mass of the observed product ions to the matched mass in the database with mass tolerance of 0.05 Th to confirm the structure of the lipids. All TLC-MALDI-MS experiments were carried out in triplicate.

4.1.7 Quantitative Analysis of the TLC/MALDI/MS Data

The region of interest (ROI) peak list data were exported from the spots assigned to LPC and *m/z* PC from the 3 replicate TLC/MALDI/MS analyses. The intensities were then imported into Prism software for data analysis.

4.1.8 MALDI-MS imaging of LPC in LS174T colorectal adenocarcinoma

12 µm sections of tumour were cut using a Leica CM 3050 cryostat (Leica Microsystems, Milton Keynes, UK) and stored at -80°C prior to analysis by MALDI–MSI. The sections were spray coated with α-CHCA matrix using a ''Suncollect'' (SunChrom, Friedrichsdorf, Germany) automatic pneumatic sprayer. The sections were coated with four layers of α-CHCA matrix at 5mg/ml with a flow rate of 5 µl/min using the "slow" spray pass setting of the instrument.

The high resolution MALDI-MS images of LPC in the control, 4h and 24h post-treatment xenograft tumours were acquired simultaneously, to allow direct comparison, using a MALDI high-definition MS (HDMS) SYNAPT G2-HDMS™ system (Waters, Manchester, UK). Data were acquired over the range of 200–1200 *m/z* at a spatial resolution of 150 μm ×150 μm.

4.1.9 Statistical Analysis of Imaging Data

Principal components analysis - Discriminate Analysis (PCA-DA) was carried out using the MarkerView™ statistical analysis package (Applied Biosystems/MDS Sciex, Concord, Ontario, Canada). Ten Spectra were randomly selected from the imaging data set collected for each of the time points. The spectra were imported into the MarkerView™ software with a mass tolerance of 0.1 amu (i.e. the bin size the data was grouped into), and a minimum signal count of 0.5. PCA-DA was carried out using Pareto scaling. Pareto scaling uses the square root of the standard deviation as a scaling factor to reduce the dominance of large scale intensity changes in high abundance ions (Eriksson & Johansson., 1999). These may mask the variation in lower abundance ions during PCA-DA. The overall outcome of PCA-DA is greatly affected by the masking of the underlying relevant information by high intensity ions. D1 verses D2 was chosen for display since these components resulted in the highest overall degree of separation of the spectra within the PCA-DA scores plots 50.2% and 49.8% respectively.

4.1.10 MS/MS Experiments

To form lithiated adducts of GPC species, LiCl (42mg) was dissolved in 10 mL 70:30 EtOH: H2O, 0.2% TFA v/v/v, with α-CHCA (100mg) being added to the solution to give a final matrix solution of 10 mg/ml α-CHCA (0.2% v/v TFA) in 100mM LiCl. 0.5 μl of this matrix solution was mixed with 0.5 μl of lipid extract and spotted onto the MALDI target plate. MALDI-MS/MS spectra were acquired directly from each spot of the precursor ions selected at 502,709 and 766 *m/z* using a modified MALDI quadrupole time-of-flight Q-Star Pulsar-iTM (Applied Biosystems / MDS Sciex, Concord, ON, Canada).

This instrument has been modified by incorporation of a variable repetition rate (up to 20 kHz) Nd: YVO4 laser. These modifications have been described elsewhere (Trim *et al.*, 2010). Data were acquired in positive ion mode with laser energy of 4.2 μJ and laser repetition rate of 5 kH_z. During acquisition the collision energy was increased from 30 to 40 eV. The chemical structures of lipids that have been previously identified using the Lipid Maps data base were compared with the chemical structures of product ions produced in individual MS/MS spectra to confirm identity.

4.2 Results and Discussion

The PCA-DA scores and loadings plots obtained from the analysis of the 30 (3x10) MALDI mass spectra recorded from the surface of control, 4 hours and 24 hours post DMXAA treatment LS174T colorectal adenocarcinoma xenografts samples are shown in Fig 4.1.a and Fig 4.1.b, respectively. As might be expected using PCA-DA the spectra from each of the time points group extremely well in the scores plot (Fig.1.a), examination of the loadings plot (Fig.1.b) indicates those signals that are associated with each time point. It can be clearly seen that signals at 782.57, 725.56, 756.56, 518.32 *m/z* and 616.17 *m/z* are associated with the 24 hour time point. These are therefore likely to be associated with the effects of DMXAA treatment. Tentative assignments based on a search of the LIPID MAPS database for the signals at *m/z* 782.57, 725.56, 756.56 and 518.32 were made assigning the signals to SM, PC and LPC signals respectively. The signal at *m/z* 616.17 was tentatively identified as arising from the haeme group (of haemoglobin) based on previous experience.

a)

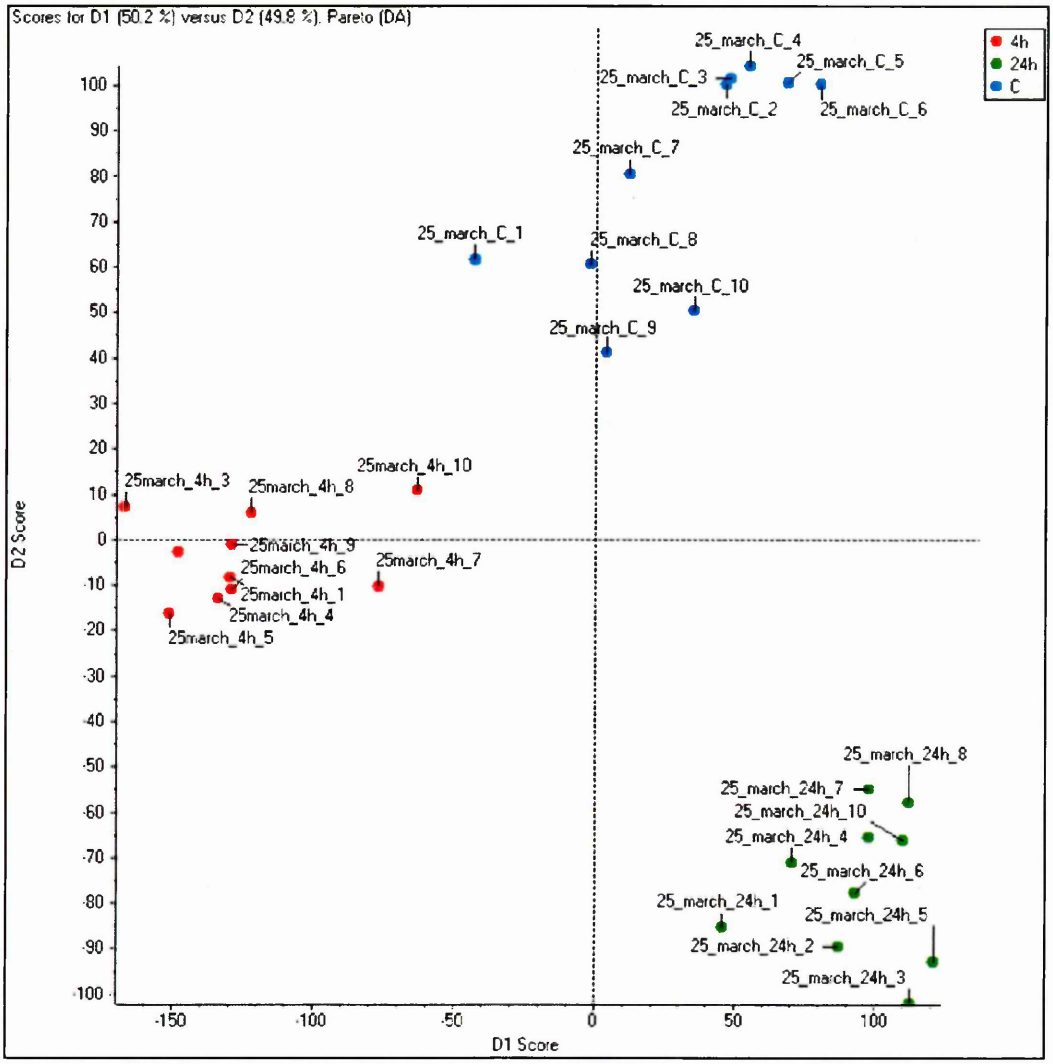
Scores for D1 (50.2 %) versus D2 (49.8 %), Pareto (DA)
4h
24h
C
25_march_C_4
25_march_C_5
25_march_C_3
25_march_C_2
25_march_C_6
25_march_C_7
25_march_C_1
25_march_C_8
25_march_C_10
25_march_C_9
25march_4h_10
25march_4h_3
25march_4h_8
25march_4h_9
25march_4h_6
25march_4h_7
25march_4h_1
25march_4h_4
25march_4h_5
25_march_24h_8
25_march_24h_7
25_march_24h_10
25_march_24h_4
25_march_24h_6
25_march_24h_1
25_march_24h_5
25_march_24h_2
25_march_24h_3
D2 Score
D1 Score
100
90
80
70
60
50
40
30
20
10
0
-10
-20
-30
-40
-50
-60
-70
-80
-90
-100
-150
-100
-50
0
50
100

b)

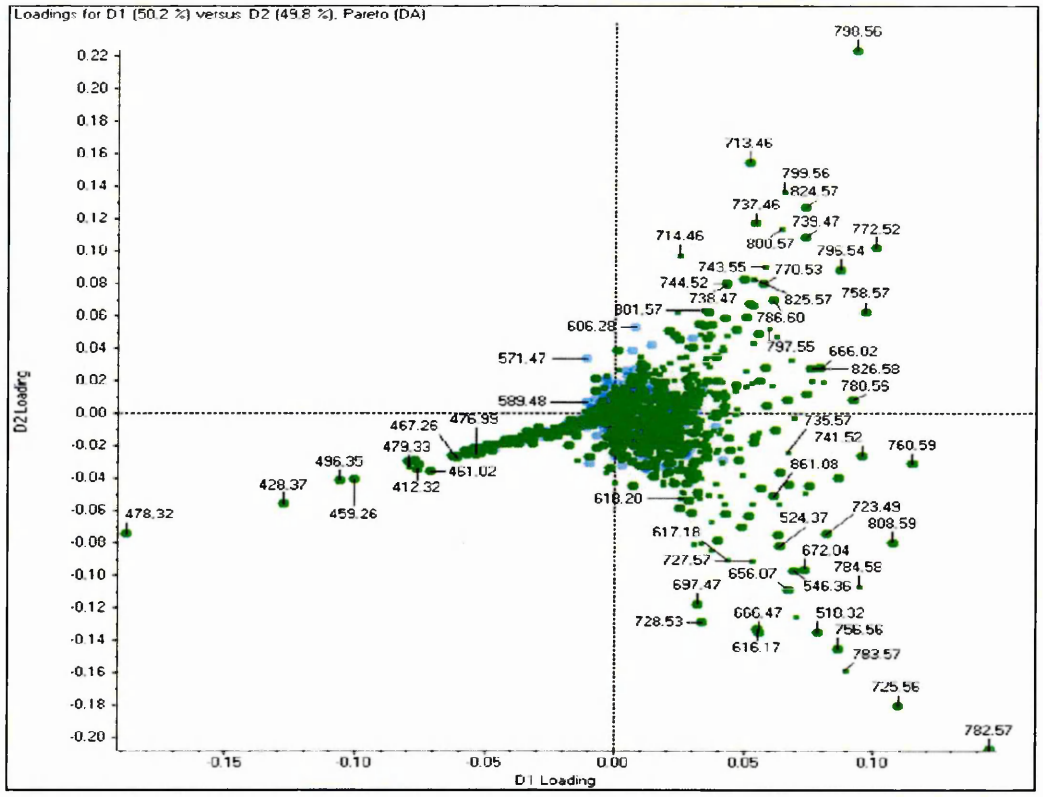

Figure 4.1 (a-b) *(a) PCA-DA Scores plot showing the grouping between the control (blue), 4h (Red) and 24h (green) xenografts tumour and (b) Loadings plots obtained from the analysis of 30 (3 x10) MALDI mass spectra recorded from the surface of control, 4hours and 24 hours post DMXAA treatment LS174T colorectal adenocarcinoma xenografts samples.*

The MALDI image of the TLC plate obtained from the separation of lipids extracted from control and LS174T colorectal adenocarcinoma xenografts treated with DMXAA 4 and 24 hours after treatment is shown in Fig 4.2. As can be seen the lipid extract was separated into 6 spots. The first 4 spots were tentatively identified, using the mass to charge (*m/z*) ratio of significant peaks within mass spectra obtained from each spot, as arising from LPC, SM, PC and PE respectively, whilst the other two spots were considered as unknown. For each class of lipid, the intensity of a representative signal was chosen to produce the coloured spots shown in Fig 4.2 as described below.

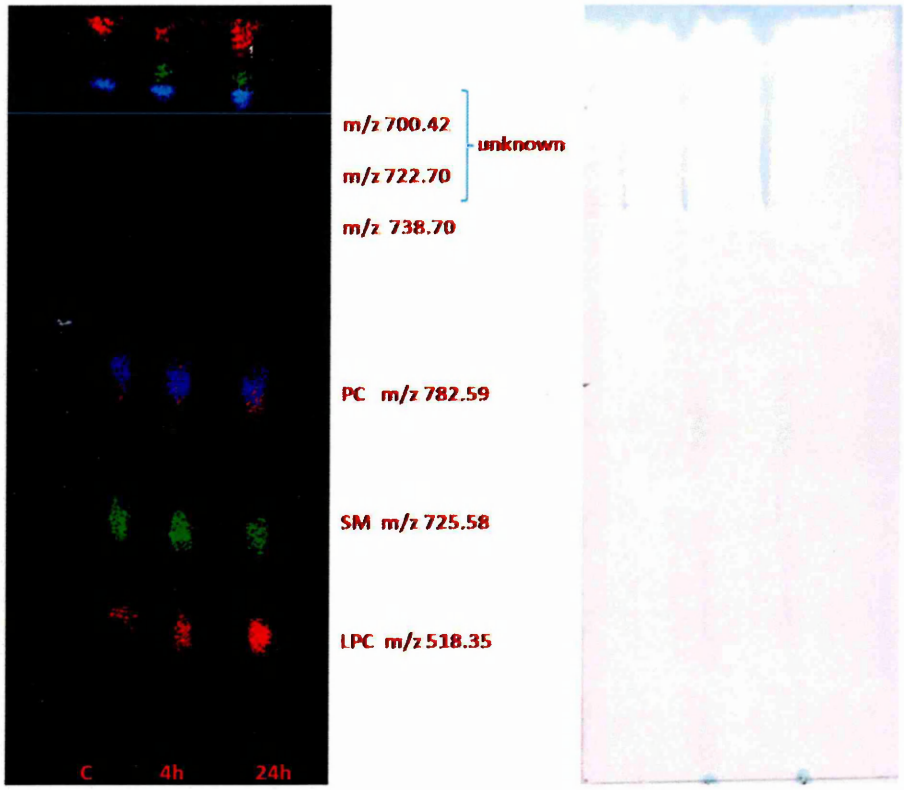

Figure 4.2 (a-b) *Images of phospholipids extracted from control, 4h and 24h post DMXAA treatment LS174T colorectal adenocarcinoma xenografts by TLC. (a) MALDI-MSI image showing phospholipids separated according to retention value (RF). LPC (red spot) represent signals arising from 518.35 m/z, Rf = 0.19. SM at 725.58 m/z (green spot), Rf = 0.28. PC at 782.59 m/z (purple spot), Rf = 0.47. Unknown 1 at 738.70 m/z (blue spot), Rf = 0.80. Unknown 2 at 722.7 m/z (green spot), Rf = 0.85 and unknown 3 at 700.42 m/z (red spot), Rf = 1.0. (b) Photograph of the TLC plate (stained with 0.5% amido black 10 B in 1M NaCl), and prior to matrix deposition for analysis by MALDI-MSI.*

Summed MALDI mass spectra were obtained from each spot by defining it as a region of interest (ROI) in the imaging software. The summed MALDI mass spectra recorded from the LPC spots of the control, 4h and 24h post-treated samples are shown in Fig. 4.3.

In Fig.4.3 it can be seen that the most abundant signals arising from the spots at Rf = 0.19 in the control, 4h and 24hr post-treatment samples were the peaks at 496.36 *m/z* and 518.34 *m/z*. These two peaks showed an increased signal in the 24h post-treatment sample compared to the 4h post-treatment and control tumour.

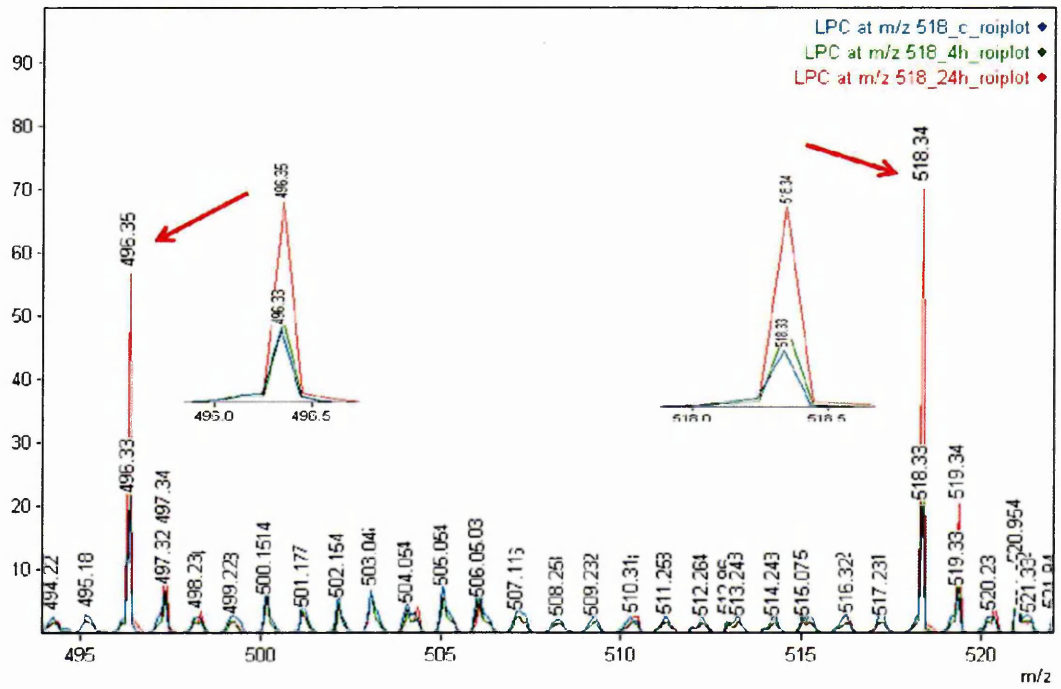

Figure 4.3 *MALDI mass spectra exported from the spots observed on the TLC plate shown in Figure 1. Each spot has been defined as a "region of interest" (ROI) in the instrument software and the summed mass spectrum from the region exported of spectrum from the spot at Rf = 0.19*

Fig. 4.4 shows the summed MALDI mass spectra recorded from the spots at Rf = 0.28 in the control, 4h and 24h post-treated samples. Clearly observable in these data are peaks at 703.59 *m/z* tentatively assignable (Table 4.1) to SM (d 18:1/16:0 $[M+H]^+$) and the corresponding $[M+Na]^+$ ion at 725.58 *m/z*. These two peaks were of higher relative abundance in the 4h post-treated sample compared to the control sample and 24h post-treated sample. The signal at 725.58 *m/z* identified as arising from the $[M+Na]^+$ adduct of SM 16:0/18:1 is shown as a green spot in Fig 4.2.

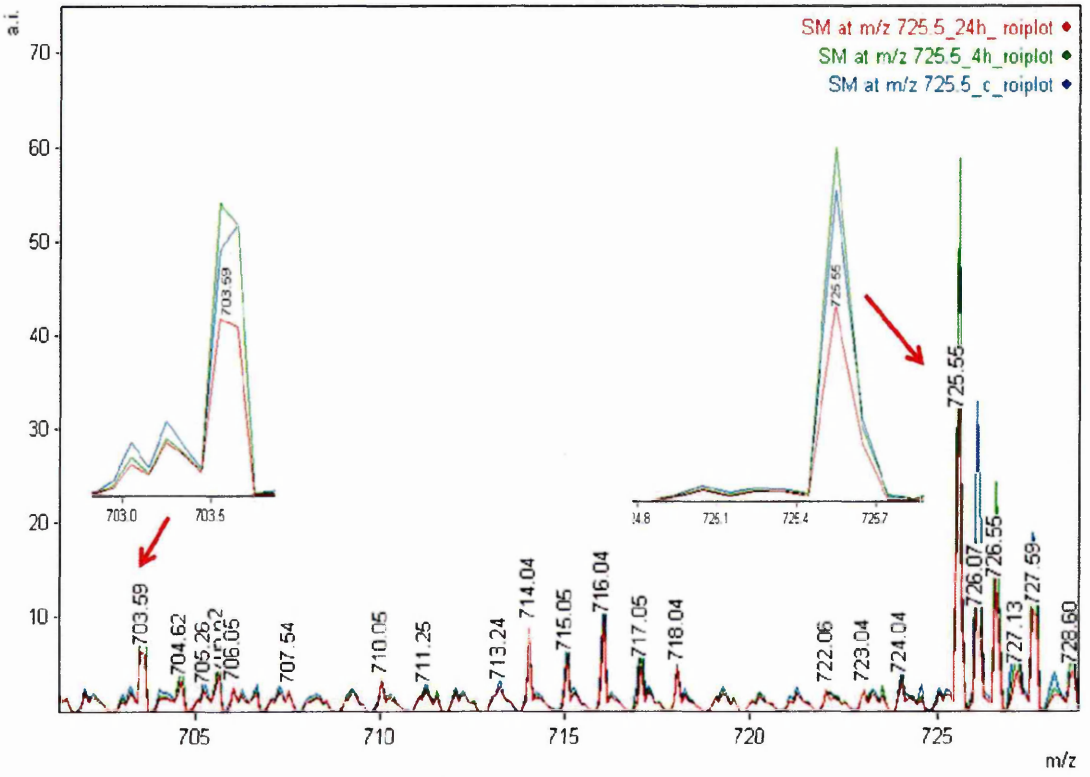

Figure 4.4 *MALDI mass spectra exported from the spots observed on the TLC plate shown in Figure 1. Each spot has been defined as a "region of interest" (ROI) in the instrument software and the summed mass spectrum from the region exported of spectrum from the spot at Rf = 0.28.*

Fig. 4.5 displays the summed MALDI mass spectra obtained from the PC spots at Rf = 0.47 of the control, 4h and 24h post-treated samples. In this data set, notable are signals observed at 756.55 *m/z* which can be assigned (Table 4.1) to PC (16:0/16:0 $[M+H]^+$), 760.63 *m/z* which can be assigned to PC (16:0/18:1) $[M+H]^+$ and 782.57 *m/z* which can be assigned to PC (16:0/18:1) $[M+Na]^+$. The signal at 782.57 *m/z* identified as arising from the $[M+Na]^+$ adduct of PC 16:0/18:1, is shown as a purple spot in Fig 4.2.

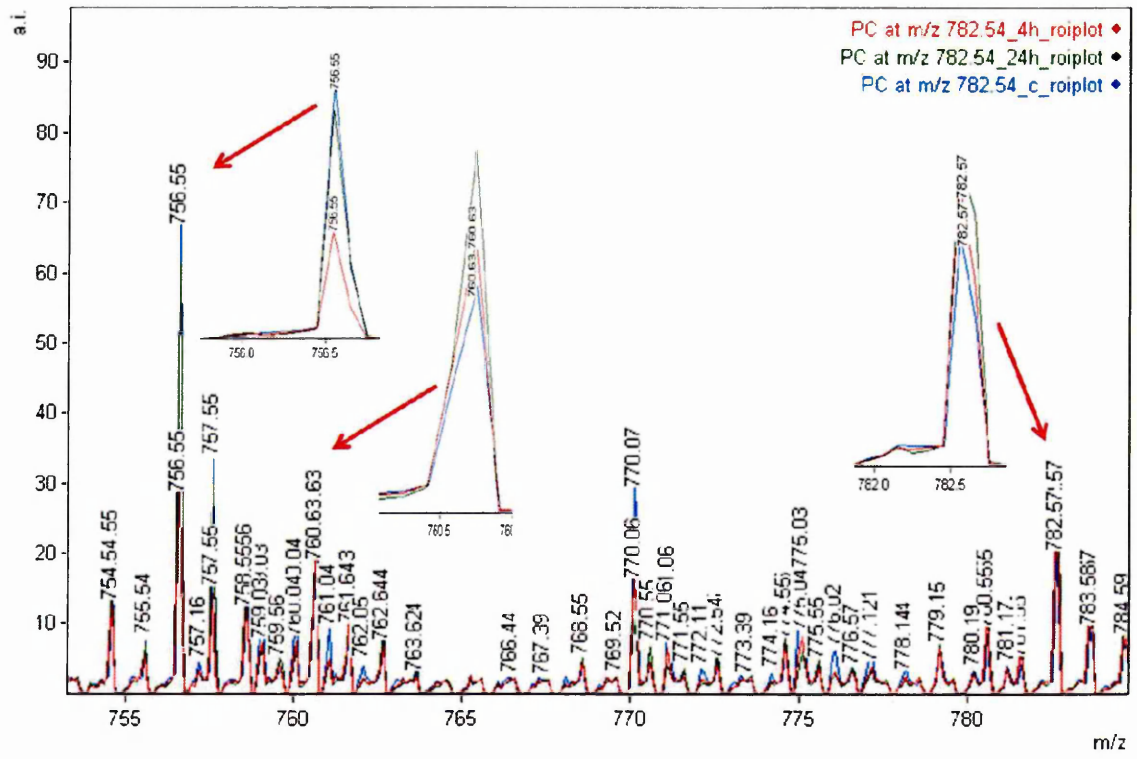

Figure 4.5 *MALDI mass spectra exported from the spots observed on the TLC plate shown in Fig.1. Each spot has been defined as a "region of interest" (ROI) in the instrument software and the summed mass spectrum from the region exported of spectrum from the spot at Rf = 0.47.*

The outputs obtained from the database searching of peak lists via lipid maps (www.lipidmaps.org) are shown in Table 4.1 The peak at 496.36 *m/z* was tentatively identified as arising from the $[M+H]^+$ ion of LPC (16:0/0:0) and the signal at 518.35 *m/z* was identified as arising from the corresponding $[M+Na]^+$ adduct. This is the signal shown as a red spot in Fig 4.2. This signal is also observable (as a faint red spot underlying the purple PC spot), in the PC region of the plate. However, here it probably arises via the fragmentation of PC lipids which contain a 16:0 side chain, as this produces a fragment ion isobaric with the LPC 16:0 signal.

This demonstrates the advantage of using TLC/MALDI/MS to separate the lipid classes as in the MS imaging data alone it would not be possible to distinguish the LPC signal from this fragment ion.

Input Mass	Matched Mass	Carbons	Double bonds	Abbreviation	Formula	Ion
496.35	496.34	16	0	LPC (16:0/0:0)	$C_{24}H_{51}NO_7P$	$[M+H]^+$
518.34	518.32	16	0	LPC (16:0/0:0)	$C_{24}H_{50}NO_7PNa$	[M+Na
703.59	703.57	16	0	SM (d18:1/16:0)	$C_{39}H_{80}N_2O_6P$	$[M+H]^+$
725.55	725.55	16	0	SM (d18:1/16:0)	$C_{39}H_{79}N_2O_6PNa$	[M+Na
756.55	756.55	32	0	PC (16:0/16:0)	$C_{40}H_{80}NO_8PNa$	[M+Na
760.63	760.58	34	1	PC (16:0/18:1)	$C_{42}H_{83}NO_8$	$[M+H]^+$
782.57	782.56	34	1	PC (16:0/18:1)	$C_{42}H_{82}NO_8PNa$	[M+Na

Table 4.1 *Some of the Major Phospholipids identified from TLC-MALDI-MS Analysis of extracts of LS174T colorectal adenocarcinoma xenografts by searching accurate mass centroided peak lists from each TLC spot against the lipid map database (http://www.lipidmaps.org) with 0.05 Th mass tolerance.*

The spot at Rf = 0.80 has been tentatively assigned to PE type lipids. This assignment is on the basis of the largest signal observed, 738.70 *m/z*, which has been assigned to the $[M+Na]^+$ adduct of PE (16:0/18:2).(This is the signal shown as a blue spot at Rf = 0.8 in Figure 4.2). The confident assignment of PE proved difficult, however, due to low intensity of the "PE" signals. This has been previously explained as an affect caused by the acidity of the PE head group compared to PC species (Fuchs *et al.*, 2007).

The effect of DMXAA treatment on the expression of LPC (16:0/0:0) (represented by *m/z* 518.35) and PC (16:0/18:1) (represented by *m/z* 782.59) in control, 4h and 24h post-treated sample was investigated, The intensities of these signals was extracted from three replicate TLC/MALDI/MS analyses and these data are shown in Fig 4.6.

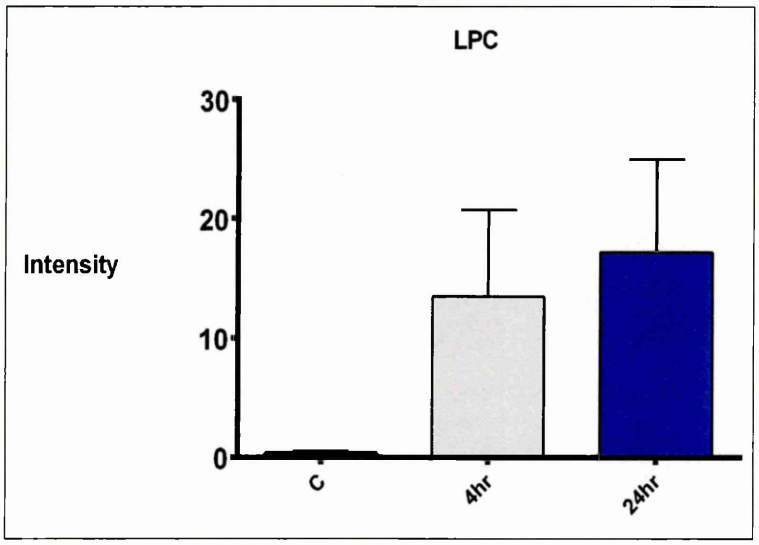

Figure 4.6 *Shows the comparison of (mean ± SD) of the intensities of signals arising from spot of LPC (16:0,0:0), 518.35 m/z from the control, 4h post-treated and 24h post-treated sample, extracted from TLC/MALD/MS analyses* ,n=3 *(technical replicates).*

As shown in Fig 4.6 an increased expression of LPC (16:0/0:0) was observed in 24h post-treated sample compared to 4h post-treated and control sample. In contrast it can be seen that the expression of PC (16:0/18:1) is decreased in 24h post-treated sample compared to 4h post-treated and control sample Fig. 4.7.

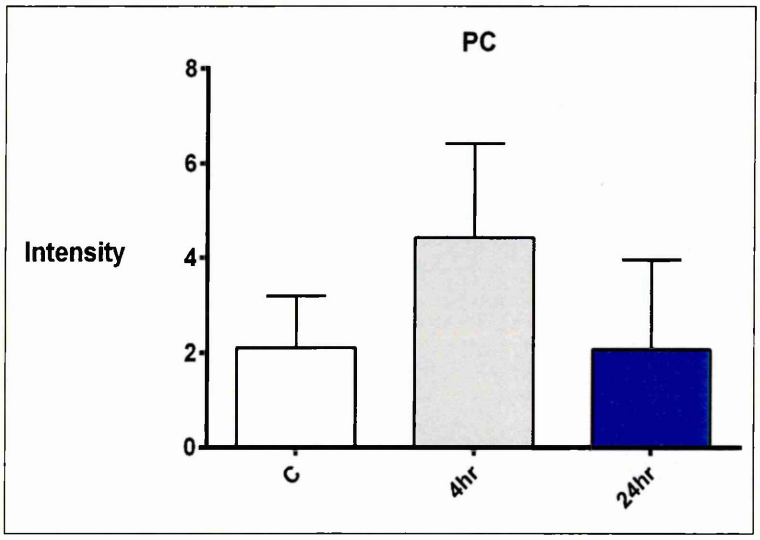

Figure 4.7 *Shows the comparison of (mean ± SD) of the intensities of signals arising from spot of PC (16:0,18:1), 782.59 m/z from the control, 4h post-treated and 24h post-treated sample, extracted from TLC/MALD/IMS analyses, n=3 (technical replicates).*

The reduction in the amount of PC in the 24h post-treated sample compared to 4h post-treated and control sample could also be as a result of the vascular-disrupting activity of DMXAA. It has been reported that a significant decrease in total choline occurs 24-hour post-treatment with 21 mg/kg DMXAA (McKeage *et al.*, 2006). The decrease of PC levels and increase of LPC levels following treatment has been related to a decline in mitochondrial function (Gao *et al.*, 2014).

In order to give further confirmation of the structural assignment, MS/MS experiments on selected species were undertaken. As described in the experimental section, LiCl was added to the MALDI matrix α-CHCA for MS/MS experiments. Performing MS/MS analyses on lithium adducts can provide more structural information in comparison to the MS/MS analysis of protonated adducts since the $[M+Li]^+$ ions are more susceptible to collisionally induced dissociation (Hsu *et al.*, 2004) . Fig 4.8 (a-c) shows representative MALDI MS/MS product ion spectra generated from lithiated adducts of lipid species. In Fig.4.8a, the MALDI MS/MS product ion spectrum of 502.51 *m/z*, tentatively identified as the $[M+Li]^+$ ion for LPC (16:0/0:0), the significant feature is the abundant peak at 443.33 *m/z* $[M+Li-59]^+$ which arises from loss of $N(CH_3)_3$. The high relative abundance of this signal compared to the $[M+Li-183]^+$ signal at 313.31 *m/z* is a characteristic feature of MS/MS spectra of LPC lipids compared to two acyl chain containing PC species (Hsu *et al.*, 2004). The identity of this species was therefore confirmed as LPC (16:0/0:0). Fig. 4.8b shows the MALDI MS/MS product ion spectrum of *m/z* 709, tentatively identified as the $[M+Li]^+$ ion for SM (18:1/16:0). Significant product ions are observed at 650.54 *m/z*, corresponding to the neutral loss of trimethylamine ($[M + Li]^+$-$N(CH_3)_3$), 526.54 *m/z* ($[M + Li]^+$-183) corresponding to loss of cholinephosphate and 520.53 *m/z* ($[M+Li]^+$ - 189) corresponding to loss of lithium cholinephosphate respectively. The product ion at 264.28 *m/z* can be identified as arising from a d18:1 side chain and that at 280.25 *m/z* as arising from a 16:0 side chain (Hart *et al.*, 2011, Hsu & Turk., 2000). The identity of this species was therefore confirmed as SM (18:1/16:0). Fig. 4.8c shows the MALDI MS/MS product ion spectrum of 766 *m/z*, tentatively identified as the $[M+Li]^+$ ion for PC(18:1/16:0). Significant product ions were observable at 707 *m/z*, corresponding to the loss of trimethylamine ($[M + Li]^+$-$N(CH_3)_3$), *m/z* 583 ($[M + Li]^+$ - 183) corresponding to the loss of cholinephosphate and 574 *m/z* ($[M+Li]^+$ - 189) corresponding to the loss of lithium cholinephosphate respectively. The product ions at 451 *m/z* and 425 *m/z* may reflect losses of trimethylamine plus the 16:0 (palmitic acid)

side chain and trimethylamine plus the 18:1 (oleic acid) side chain, respectively. The identity of this species was therefore confirmed as PC (16:0/18:1 (Hsu *et al.*, 1998).

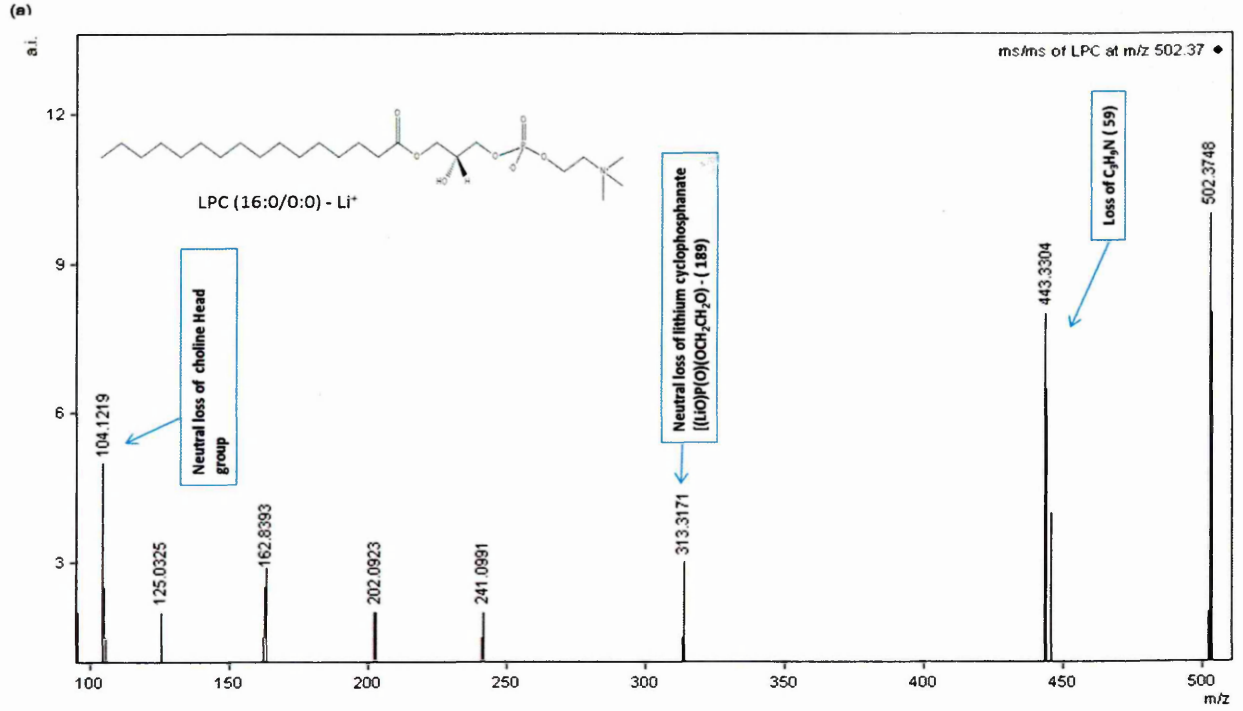

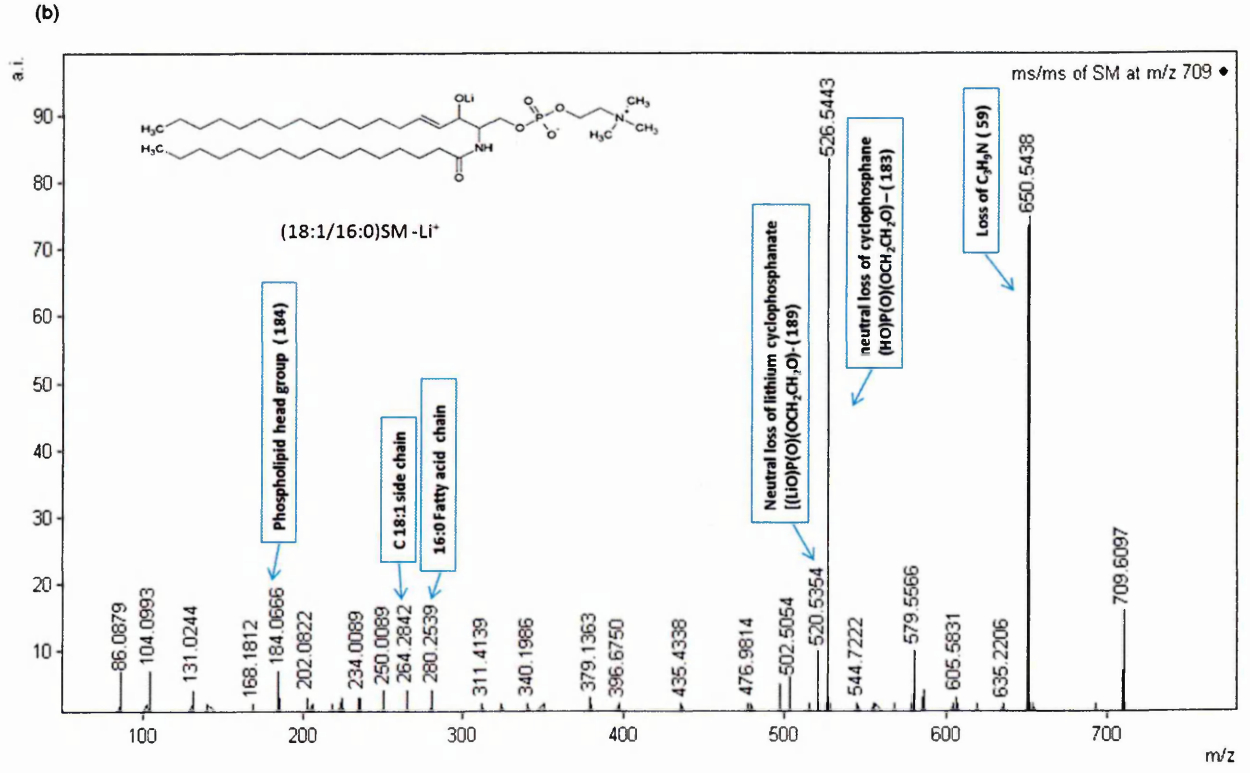

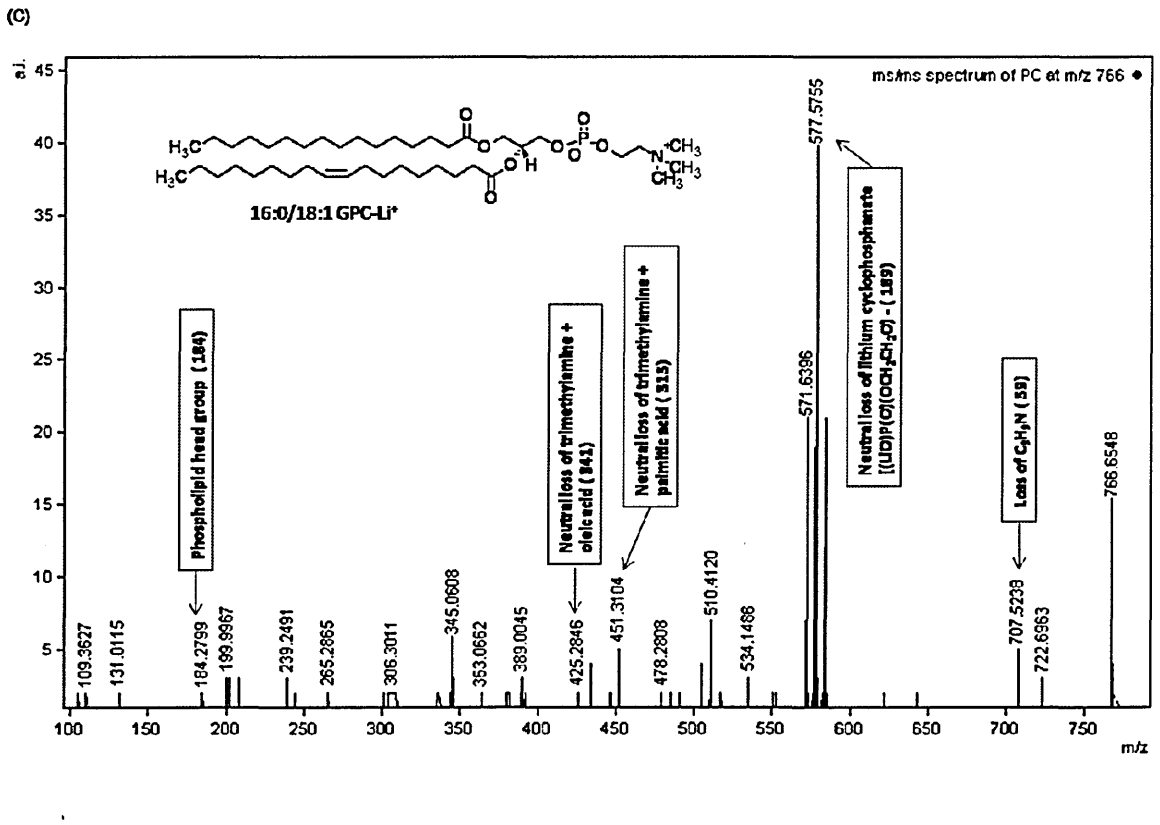

Figure 4.8 (a-c) *Positive ion MALDI product ion mass spectra of the lithium adducts of signals identified as arising from (a) LPC (16:0/0:0) $[M+Li]^+$ 502 m/z (b) SM (18:1/16:0) $[M+Li]^+$ 709 m/z (c) PC (16:0/18:1) $[M+Li]^+$ 766.8 m/z.*

Fig 4.9 (a-b) shows the MALDI-MSI images obtained from control, 4h and 24h post-treated DMXAA treated LS174T colorectal adenocarcinoma xenograft tumour samples. Fig. 4.9 a shows the distribution of LPC (16:0/0:0) $[M+H]^+$ at 496.34 m/z and Fig. 4.9b shows the distribution of LPC (16:0/0:0) $[M+Na]^+$ at 518.34 m/z. These images confirm the initial PCA-DA experiments, the TLC-MALDI-MS analysis and the extracted expression data shown in Fig.4.3. Taken together these demonstrate unambiguously that LPC levels were higher in the 24h post-treatment samples compared to 4hr post-treatment sample and control tumours.

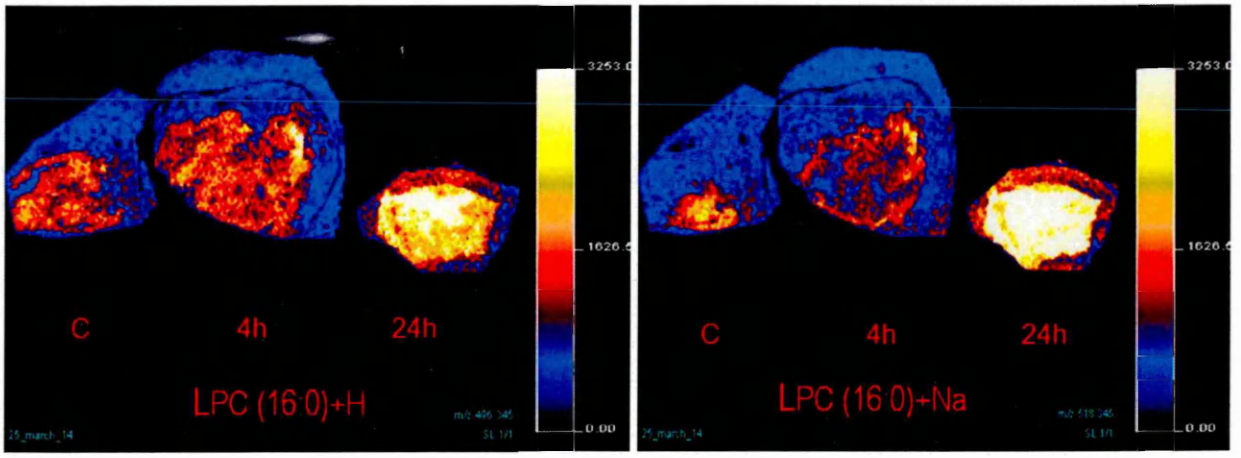

a) **b)**

Figure 4.9 *MALDI-MSI images of control (C), 4h and 24h post DMXAA treatment LS174T colorectal adenocarcinoma xenografts (a) the distribution of LPC (16:0/16:0) $[M+H]^+$,496.34 m/z and (b) the distribution of LPC (16:0/16:0) [M+Na]+, 518.34 m/z. Blue colour gives low intensity of signal while orange white colours indicates high intensity of signal as shown in scalebar.*

These findings are in agreement with the study carried out by Gao *et al.*, on HepG2 cells (Gao *et al.*, 2014). In that study, one pharmacodynamic response observed following treatment of HepG2 cells with a novel flavonoid agent was an increase in the amount of LPC type lipids. Gao *et al* proposed that such observations indicated increased oxidative stress, and hence mitochondrial dysfunction, within the cells. This affected cellular metabolism and they proposed that this would finally lead to cellular anti-proliferation *i.e.* an anti-cancer effect (Gao *et al.*, 2014).

In the study reported here, observation of increased LPC expression in the LS174T colorectal adenocarcinoma xenografts following treatment with DMXAA can be explained as a result of reactive oxygen species (ROS) release during DMXAA induced apoptosis and is hence a pharmacodynamic marker of DMXAA action.

These results demonstrate that the increase in the amount of LPC in the treated tumours provides a clinically diagnostic indicator of response to treatment with a vascular disrupting agent, such as DMXAA which could be exploitable by an *in vivo* imaging technique *i.e.* 31P MRSI (Glunde *et al* ., 2011).

4.3 Conclusions

This study investigated the expression of phospholipids in DMXAA treated LS174T colorectal adenocarcinoma xenografts. Different lipid classes with various fatty acid chains such as SM, PC ,LPC and PE were identified by MALDI-MS and MALDI-MS/MS analyses of TLC separated compounds. It could be seen clearly in the data that LPC were highly expressed in the 24h post-treatment sample compared to 4h post-treatment sample and the control. PC in contrast were decreased in 24h post treated sample compare to 4h and control samples. This increase of the amount of LPC is believed to be due to the anti-tumour effect of flavonoid drugs causing mitochondrial dysfunction and increased lipid peroxidation (Gao *et al.*, 2014). The increase in the amount of LPC therefore provides a clinically diagnostic biomarker of response to treatment with DMXAA which could be exploitable in the future by an *in vivo* imaging technique *i.e.* 31P MRSI.

4.4 References

Busch. KL. *Handbook of Thin-Layer Chromatography*, Marcel Dekker, New York, **1996.**

CATALÁ, A., 2009. Lipid peroxidation of membrane phospholipids generates hydroxy-alkenals and oxidized phospholipids active in physiological and/or pathological conditions. *Chemistry and physics of lipids,* **157**(1), pp. 1-11.

CRECELIUS, A., CLENCH, M.R., RICHARDS, D.S. and PARR, V., 2004. Quantitative determination of Piroxicam by TLC-MALDI TOF MS. *Journal of pharmaceutical and biomedical analysis,* **35**(1), pp. 31-39.

ERIKSSON, L. and JOHANSSON, E., 1999. kettaneh-Wold N, Wold S. *Introduction to Multi- and Megavariate Data Analysis using Projection Methods (PCA & PLS).UMETRICS, Sweden,* .

FOLCH, J., LEES, M. and SLOANE-STANLEY, G., 1957. A simple method for the isolation and purification of total lipids from animal tissues. *J.biol.Chem,* **226**(1), pp. 497-509.

FUCHS, B., SCHILLER, J., SÜß, R., SCHÜRENBERG, M. and SUCKAU, D., 2007. A direct and simple method of coupling matrix-assisted laser desorption and ionization time-of-flight mass spectrometry (MALDI-TOF MS) to thin-layer chromatography (TLC) for the analysis of phospholipids from egg yolk. *Analytical and bioanalytical chemistry,* **389**(3), pp. 827-834.

FUCHS, B., SÜß, R., TEUBER, K., EIBISCH, M. and SCHILLER, J., 2011. Lipid analysis by thin-layer chromatography- a review of the current state. *Journal of Chromatography A,* **1218**(19), pp. 2754-2774.

FUCHS, B., SCHILLER, J., Süß, R., ZSCHARNACK, M., BADER, A., Müller, P., Schürenberg , M., BECKER, M. and SUCKAU, D., 2008. Analysis of stem cell lipids by offline HPTLC-MALDI-TOF MS. *Analytical and bioanalytical chemistry,* **392**(5), pp. 849-860.

GAO, D., JIN, F., LIU, H., WANG, Y. and JIANG, Y., 2014. Metabonomic study on the antitumor effect of flavonoid derivative 3d in HepG2 cells and its action mechanism. *Talanta,* **118**, pp. 382-388.

GLUNDE, K., JIANG, L., MOESTUE, S.A. and GRIBBESTAD, I.S., 2011. MRS and MRSI guidance in molecular medicine: targeting and monitoring of choline and glucose metabolism in cancer. *NMR in biomedicine,* **24**(6), pp. 673-690.

HART, P.J., FRANCESE, S., CLAUDE, E., WOODROOFE, M.N. and CLENCH, M.R., 2011. MALDI-MS imaging of lipids in ex vivo human skin. *Analytical and bioanalytical chemistry,* **401**(1), pp. 115-125.

HSU, F. and TURK, J., 2000. Characterization of phosphatidylinositol, phosphatidylinositol-4-phosphate, and phosphatidylinositol-4, 5-bisphosphate by electrospray ionization tandem mass spectrometry: A mechanistic study. *Journal of the American Society for Mass Spectrometry,* **11**(11), pp. 986-999.

HSU,F.,TURK, J., SHI, Y. and GROISMAN, E.A., 2004. Characterization of acylphosphatidylglycerols from salmonella typhimurium by tandem mass spectrometry with electrospray ionization. *Journal of the American Society for Mass Spectrometry,* **15**(1), pp. 1-11.

HSU, F.F., BOHRER, A. and TURK, J., 1998. Formation of lithiated adducts of glycerophosphocholine lipids facilitates their identification by electrospray ionization tandem mass spectrometry. *Journal of the American Society for Mass Spectrometry,* **9**(5), pp. 516-526.

IVLEVA, V.B., SAPP, L.M., O'CONNOR, P.B. and COSTELLO, C.E., 2005. Ganglioside analysis by thin-layer chromatography matrix-assisted laser desorption/ionization orthogonal time-of-flight mass spectrometry. *Journal of the American Society for Mass Spectrometry,* **16**(9), pp. 1552-1560.

MCKEAGE, M.J., FONG, P., JEFFERY, M., BAGULEY, B.C., KESTELL, P., RAVIC, M. and JAMESON, M.B., 2006. 5,6-Dimethylxanthenone-4-acetic acid in the treatment of refractory tumors: a phase I safety study of a vascular disrupting agent. *Clinical Cancer Research,* **12**, pp. 1776.

NAKAMURA, K., SUZUKI, Y., GOTO-INOUE, N., YOSHIDA-NORO, C. and SUZUKI, A., 2006. Structural characterization of neutral glycosphingolipids by thin-layer chromatography coupled to matrix-assisted laser desorption/ionization quadrupole ion trap time-of-flight MS/MS. *Analytical Chemistry,* **78**(16), pp. 5736-5743.

PRINGLE, S.D., GILES, K., WILDGOOSE, J.L., WILLIAMS, J.P., SLADE, S.E., THALASSINOS, K., BATEMAN, R.H., BOWERS, M.T. and SCRIVENS, J.H., 2007. An investigation of the mobility separation of some peptide and protein ions using a new hybrid quadrupole/travelling wave IMS/oa-ToF instrument. *International Journal of Mass Spectrometry,* **261**(1), pp. 1-12.

ROHLFING, A., MÜTHING, J., POHLENTZ, G., DISTLER, U., PETER-KATALINIC, J., BERKENKAMP, S. and DREISEWERD, K., 2007. IR-MALDI-MS analysis of HPTLC-separated phospholipid mixtures directly from the TLC plate. *Analytical Chemistry,* **79**(15), pp. 5793-5808.

RUSTIN, G., BRADLEY, C., GALBRAITH, S., STRATFORD, M., LOADMAN, P., WALLER, S., BELLENGER, K., GUMBRELL, L., FOLKES, L. and HALBERT, G., 2003. 5, 6-dimethylxanthenone-4-acetic acid (DMXAA), a novel antivascular agent: phase I clinical and pharmacokinetic study. *British journal of cancer,* **88** (8), pp. 1160-1167.

TRIM, P.J., DJIDJA, M., ATKINSON, S.J., OAKES, K., COLE, L.M., ANDERSON, D.M., HART, P.J., FRANCESE, S. and CLENCH, M.R., 2010. Introduction of a 20 kHz Nd: YVO4 laser into a hybrid quadrupole time-of-flight mass spectrometer for MALDI-MS imaging. *Analytical and bioanalytical chemistry,* **397** (8), pp. 3409-3419.

Chapter 5

Analysis of Protein Induction in DMXAA treated LS 174T Xenograft Tumours

5 Introduction

An increased number of molecule-targeted anti-cancer therapies have been established and are in the process of clinical development (Reyzer *et al.*, 2004) and therefore the study of biomarkers that enable the prediction of therapeutic responses of tumours to anti-cancer therapies is of particular interest. The use of proteomics to study disease-related biomarkers by the over or under-expression of certain peptides can help to distinguish between healthy and diseased samples and thus aid the early diagnosis of disease (Rifai *et al.,* 2006).

Protein profiling using matrix-assisted laser desorption/ionization/imaging mass spectrometry (MALDI-IMS) provides a new technology which enables the generation of protein profiles and images directly from tissues from freshly frozen tissue sections (Caprioli *et al.*, 1997; Chaurand *et al.*, 2002). Around 400 distinctive signals from intact proteins, which are highly representative of the local proteome, are usually observable in the *m/z* range from 2000 to 100, 000 (Chaurand *et al.*, 2002).The generated data can be analysed to identify markers that are indicative of the biological processes which are occurring in the tissue (Yanagisawa *et al.*, 2003). *In situ* enzymatic digestion of proteins has also been demonstrated to be useful in proteomic analysis using MALDI-MSI. In contrast to the study of intact proteins this provides direct protein identification and localisation from the tissue section without the need for fractionation or the extraction of proteins from the tissue section (Djidja *et al.*, 2009).

Vascular disrupting agents (VDAs) are a promising class of anti-cancer drug (Kanthou & Tozer, 2008). 5,6-Dimethylxanthenone-4-acetic acid (DMXAA) is a small molecule vascular-disrupting agent that has recently completed phase 1 clinical trials (Kerr & Kaye, 1989). As described in Chapter 1 of this thesis, DMXAA induces tumour necrosis factor (TNFa) causing vascular collapse and the haemorrhage of a tumour's blood vessels (Watanabe *et al.*, 1988).

The overall anti-vascular effects of DMXAA lead to the occlusion and collapse of a tumour's blood vessels with the onset of haemorrhagic necrosis and tumour cell death triggered by prolonged ischemia. In addition, the cytostatic response provoked by DMXAA causes a large area of central necrosis and leaves a viable rim of cells at the tumour periphery (Siemann *et al.*, 2004). As a result of its demonstrated anti-tumour action, the clinical development of DMXAA would now be assisted by the identification of biomarkers that show response to treatment with the drug (Galbraith *et al.*, 2002).

Histone acetylation plays a vital role in controlling gene expression and influences the transcriptional control of many genes such as tumour suppressor genes. The deacetylated histones are usually associated with inactive non-transcribed DNA (Luo & Dean, 1999). It has been demonstrated that abnormal epigenetic transcriptional suppression is associated with a variety of tumour types (Brown & Strathdee., 2002). Drug induced protein changes, that indicate inhibition of cell proliferation or cell death, following vascular-targeted therapy would therefore characterise both the response to treatment and resistance mechanisms (Reyzer *et al.*, 2004).

In this Chapter the use of MALDI-MS profiling and MALDI-MSI imaging to observe the spatial distribution of peptides, as well as identifying protein biomarkers that are induced by DMXAA treatment such as histone, actin and haemoglobin. The aim of this work was to see if biomarkers of action/resistance could be observed by the using these techniques.

5.1 Materials and methods

5.1.1 Chemicals

∝-Cyano-4-hydroxycinnamic acid (CHCA), aniline (ANI), ethanol (EtOH), chloroform (CHCl3), acetonitrile (ACN), octyl-a/b-glucoside (OcGlc), tri-fluoroacetic acid (TFA), ammonium bicarbonate, haematoxylin, eosin, xylene and DPX mountant were purchased from Sigma–Aldrich (Gillingham, Dorset, UK). A modified sequence grade trypsin (20 µg lyophilised) was obtained from Promega (Southampton, UK).

5.1.2 Preparation of xenograft tumours

Male, immune-deficient, nude mice were subcutaneously implanted with a suspension of LS174T colorectal adenocarcinoma cell line in the right abdominal flank. Tumour was allowed to reach approximately 500 mm^3 before treatment with 27.5 mg/kg of DMXAA. The mice were killed and the tumours excised at various times after treatment.

5.1.3 Experimental groups

Tumour (4h after treatment), (n=3); tumour (24h after treatment), (n=3); and controls (no treatment, saline i.p), (n=3).

5.1.4 Tissue preparation

Frozen tumours were sliced into 12 µm thick tissue sections using a Lecia CM 1850 cryostat (Leica Microsystems, Milton Keynes, UK) set at -20°C. Then, tissue sections were mounted onto polylysine glass slides; these were stored at -80°C in a freezer prior to analysis.

5.1.5 In situ tissue digestion and trypsin deposition

The tissue samples were removed from the freezer and allowed to dry for 5 minutes at room temperature. Then, the tissues were initially washed with 70% and 90% ice cold ethanol for 1 min and left to dry completely. The slides were then immersed in chloroform for 10 seconds before the application of trypsin. *In situ* tissue digestion was performed using trypsin solution prepared (using lyophilised trypsin) at 20 µg/ml. The trypsin solution was made by the addition of 50 mM ammonium bicarbonate (NH_4HCO_3) pH 8, containing 0.5% octyl-a/b-glucoside (OcGlc); this was based on a protocol by Cole *et al.* (2011). The ''Suncollect'' (SunChrom, Friedrichsdorf, Germany) automatic pneumatic sprayer was used to deposit the trypsin in a series of layers (approximately 5 layers). Then, sections for MALDI-MS and MALDI MSI were incubated overnight in a sealed glass coplin jar containing 50% methanol: 50% water at 37°C and 5% CO_2.

5.1.6 Matrix application

The matrix ∝-CHCA was mixed with equimolar amounts of aniline: i.e. one ml of 5 mg/ml ∝-CHCA solution contained 2.4 µl of aniline. Matrix solutions were then dissolved in ACN: water: TFA (1:1:0.2 by volume) and sprayed onto the tissue sections using the Suncollect (SunChrom, Friedrichsdorf, Germany) in a series of layers (approximately 5 layers). The method parameters were based on those of Cole *et al.* (2011).

5.1.7 Direct protein analysis by MALDI-MSI

MALDI-MSI data were acquired directly from the digested tumour tissue sections in the positive ion mode using an HDMS SYNAPT™ G2 system (Waters Corporation, Manchester, UK) operating in imaging mode with laser repetition rate of 200 Hz and an m/z range between 600 to 2200 at 150 µm spatial resolution. Instrument calibration was performed using a mixture of polyethylene glycol (Sigma-Aldrich, Gillingham, UK) ranging between m/z 100 to 3000 Da (Djidja *et al.,* 2010). Images were generated and reconstructed using HDI imaging software. Peptide mass searches of histone, actin and haemoglobin were performed against the Swissprot database to identify tryptic sequences.

5.1.8 Data pre-processing and statistical analysis

In order to carry out a statistical analysis, data lists were exported as text files from the Analyst QS program (Applied Biosystems / MDS Sciex, Concorde, Ontario, Canada). Text files were then imported into SpecAlign software (Oxford, UK) and the resulting data were processed as follows: baseline subtraction, smooth, remove negative, denoise, normalise TIC, generate average spectrum, spectral alignment, and PAFFT correlation method (max. shift 20).

The resulting data were exported as text files and then re-imported into Marker View software 1.2 (Applied Biosystems / MDS Sciex , Concorde, Ontario, Canada) in order to perform Principle Component Analysis (PCA) and Partial Least Squares Discriminant Analysis (PLSDA).

In the Marker View software, a minimum requisition response of 0.1, a mass tolerance of 0.1 and a maximum number of peaks of 10,000 were selected (Cole *et al.,* 2011). PCA and PLSDA analyses were performed using MATLAB® (Matrix Laboratory) (Math Works, Inc., Natick, MA486USA).

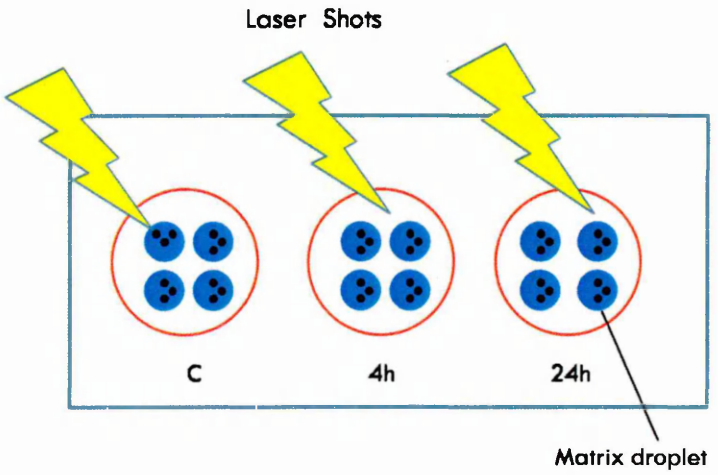

Figure 5.1: *Method of data collection for statistical analysis, showing four matrix droplets deposited on each tissue sections. Spectra were collected in triplicate from each matrix droplet using MALDI-MSI.*

Statistical data collection was performed by acquiring triplicate spectra from all droplets at each time point using MALDI-MSI (Fig. 5.1).

5.1.9 Haematoxylin and Eosin staining

Tissue sections were stained with H & E staining after MALDI imaging for a comparative study. The tissue sections were rehydrated using a series of graded alcohols, immersed in haematoxylin for 5 minutes, and then rinsed in tap water. The sections were then dipped three times in 0.1% HCl followed by water and also three times in 0.1% NaOH followed by water. The sections were stained with Eosin for three minutes and then dehydrated. Finally, the sections were placed in xylene until the cover slipped (this method is described in more detail in Chapter 2, Section 2.2.6.3).

5.2 Results and Discussion

5.2.1 MALDI/MS and MALDI/MSI imaging of the *in situ* tissue tryptic digest protein in the LS 174T xenograft tumour

MALDI/MS and MALDI/MSI profiling and imaging of the *in situ* tissue's tryptic digest protein in the LS 174T xenograft tumour were performed using HDMS SYNAPT™ G1/G2 system (Waters Corporation, Manchester, UK). Fig. 5.2 shows a mass spectrum of the peptide mass fingerprint acquired after *in situ* digestion of the control tumour. The peptide peak at 944.43 m/z was identified as histone H2A according to the UniprotKB / Swiss-port search, as seen in Fig. 5.2.

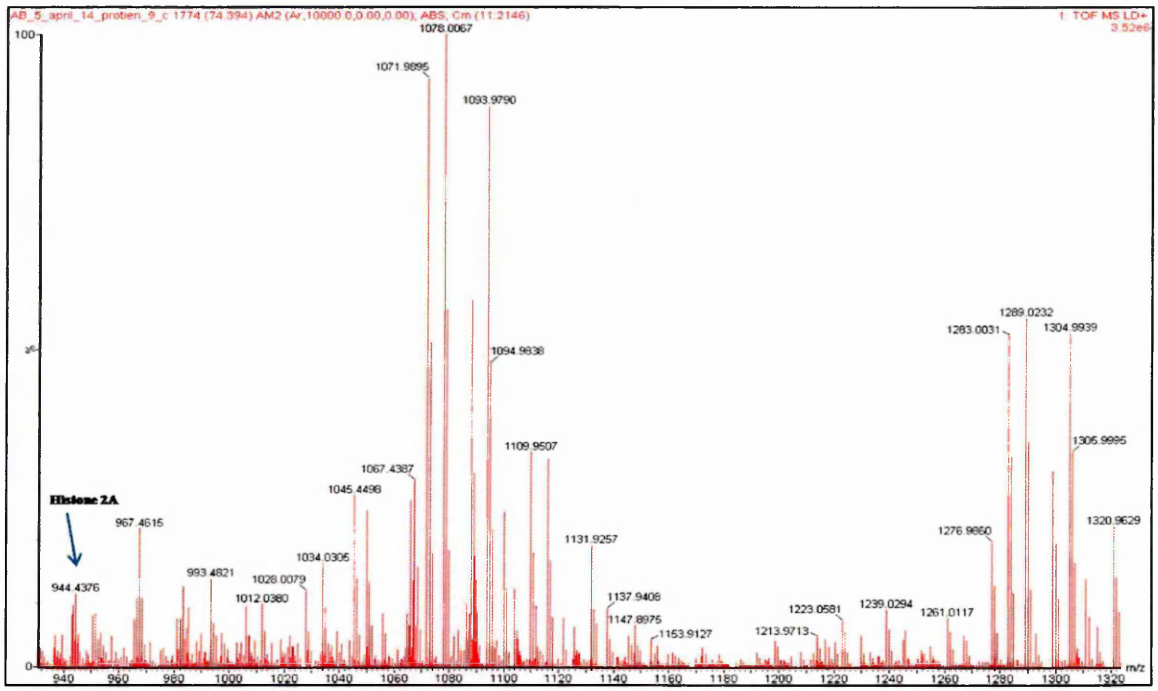

Figure 5.2: *Peptide mass fingerprint acquired from the control tumour. A number of peptide peaks were observed from an in situ tissue tryptic digest at an m/z range from 900 to 1320. The peak at 944.43 m/z was identified as Histone H2A.*

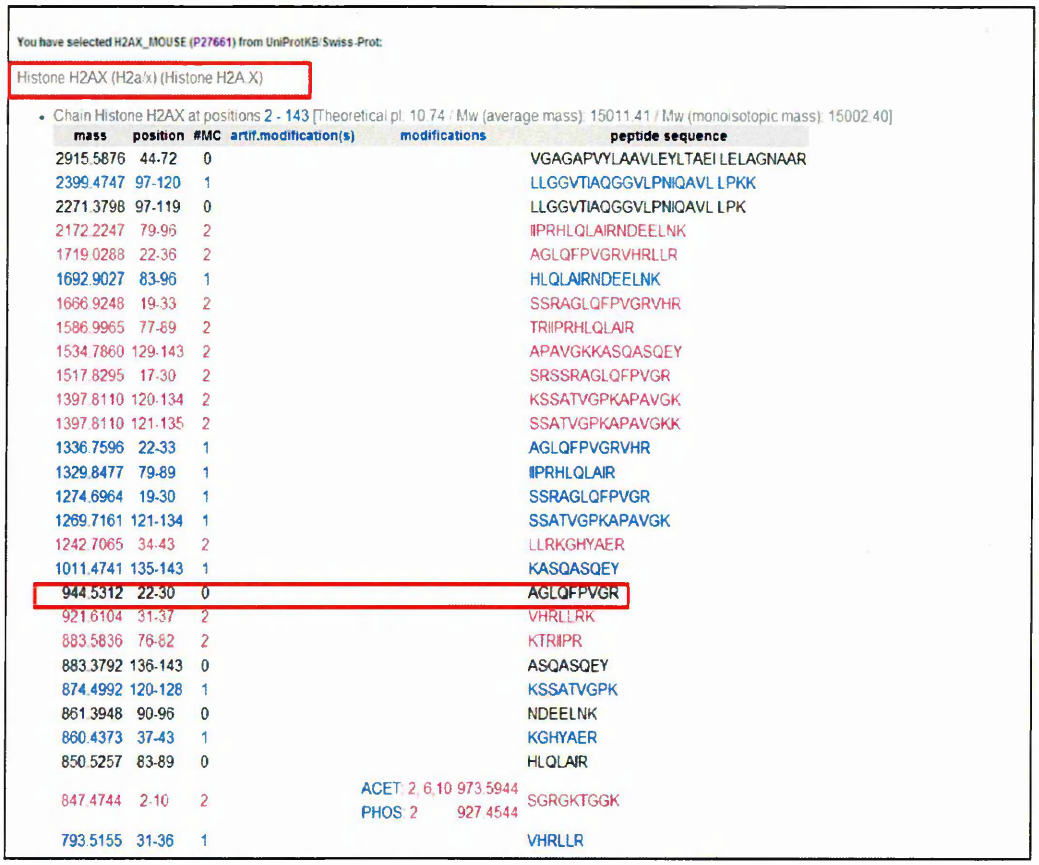

You have selected H2AX_MOUSE (P27661) from UniProtKB/Swiss-Prot:

Histone H2AX (H2a/x) (Histone H2A.X)

- Chain Histone H2AX at positions 2 - 143 [Theoretical pI: 10.74 / Mw (average mass): 15011.41 / Mw (monoisotopic mass): 15002.40]

mass	position	#MC	artif.modification(s)	modifications	peptide sequence
2915.5876	44-72	0			VGAGAPVYLAAVLEYLTAEI LELAGNAAR
2399.4747	97-120	1			LLGGVTIAQGGVLPNIQAVL LPKK
2271.3798	97-119	0			LLGGVTIAQGGVLPNIQAVL LPK
2172.2247	79-96	2			IIPRHLQLAIRNDEELNK
1719.0288	22-36	2			AGLQFPVGRVHRLLR
1692.9027	83-96	1			HLQLAIRNDEELNK
1666.9248	19-33	2			SSRAGLQFPVGRVHR
1586.9965	77-89	2			TRIIPRHLQLAIR
1534.7860	129-143	2			APAVGKKASQASQEY
1517.8295	17-30	2			SRSSRAGLQFPVGR
1397.8110	120-134	2			KSSATVGPKAPAVGK
1397.8110	121-135	2			SSATVGPKAPAVGKK
1336.7596	22-33	1			AGLQFPVGRVHR
1329.8477	79-89	1			IIPRHLQLAIR
1274.6964	19-30	1			SSRAGLQFPVGR
1269.7161	121-134	1			SSATVGPKAPAVGK
1242.7065	34-43	2			LLRKGHYAER
1011.4741	135-143	1			KASQASQEY
944.5312	22-30	0			AGLQFPVGR
921.6104	31-37	2			VHRLLRK
883.5836	76-82	2			KTRIIPR
883.3792	136-143	0			ASQASQEY
874.4992	120-128	1			KSSATVGPK
861.3948	90-96	0			NDEELNK
860.4373	37-43	1			KGHYAER
850.5257	83-89	0			HLQLAIR
847.4744	2-10	2	ACET: 2, 6, 10 973.5944 PHOS: 2 927.4544		SGRGKTGGK
793.5155	31-36	1			VHRLLR

Figure 5.3: *The peptide sequence obtained from Uniprot KB / Swiss-port search of Histone H2A at 944.53 m/z.*

Fig. 5.4 shows a spectrum of the peptide mass fingerprint obtained from the *in situ* tryptic digest of the 4h post-treated LS 174T xenograft tumour. The Histone H2A peak was observed at 944.45 m/z along with other peptide peaks.

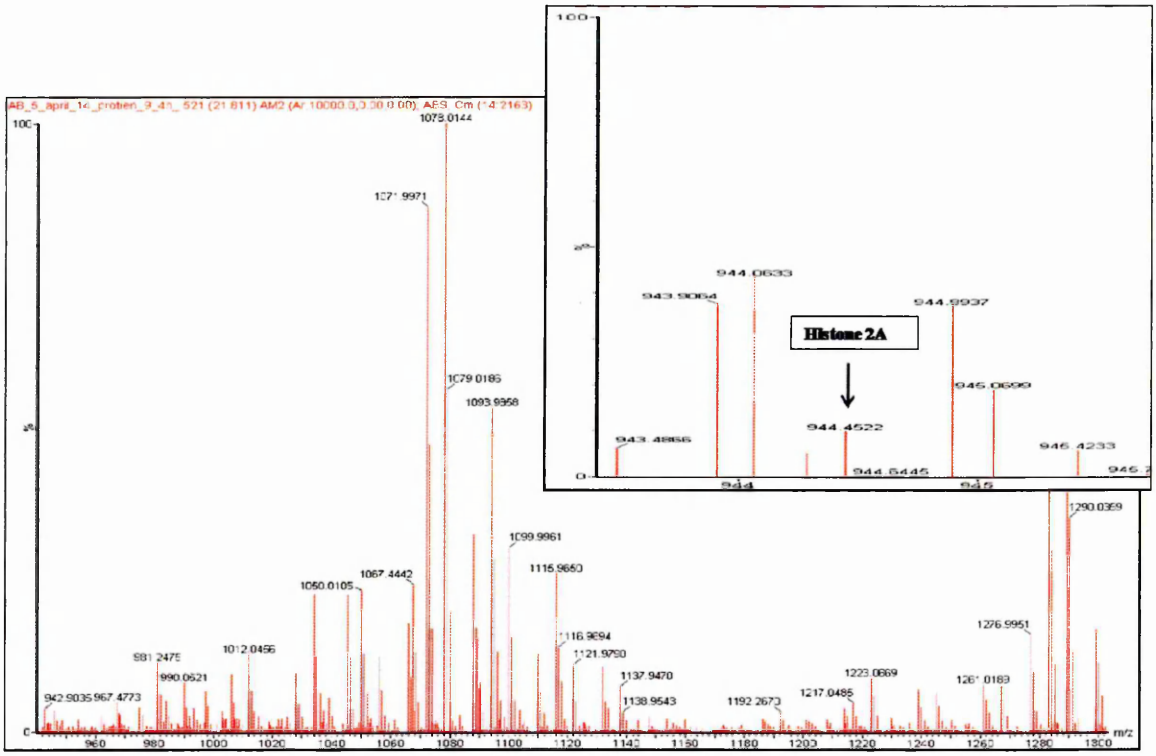

Figure 5.4: *Peptide mass fingerprint acquired from the in situ tryptic digest of the LS 174T xenograft tumour (4h after treatment with DMXAA). A number of peptide peaks were observed in an m/z range from 900 to 1300. The peak at 944.45 m/z was identified as Histone H2A.*

Fig. 5.5 shows a spectrum of the peptide mass fingerprint obtained from the *in situ* tryptic digest of a 24h post-treated LS 174T xenograft tumour. A Histone H2A peak was observed at 944.45 m/z and a Haemoglobin beta 1 chain (Hbβ) peak at 1274.62 m/z as identified by a UniprotKB / Swiss-port search (see Fig. 5.6). The increase in the intensity of the Hbβ peak is clearly seen in the 24h post-treated DMXAA spectrum.

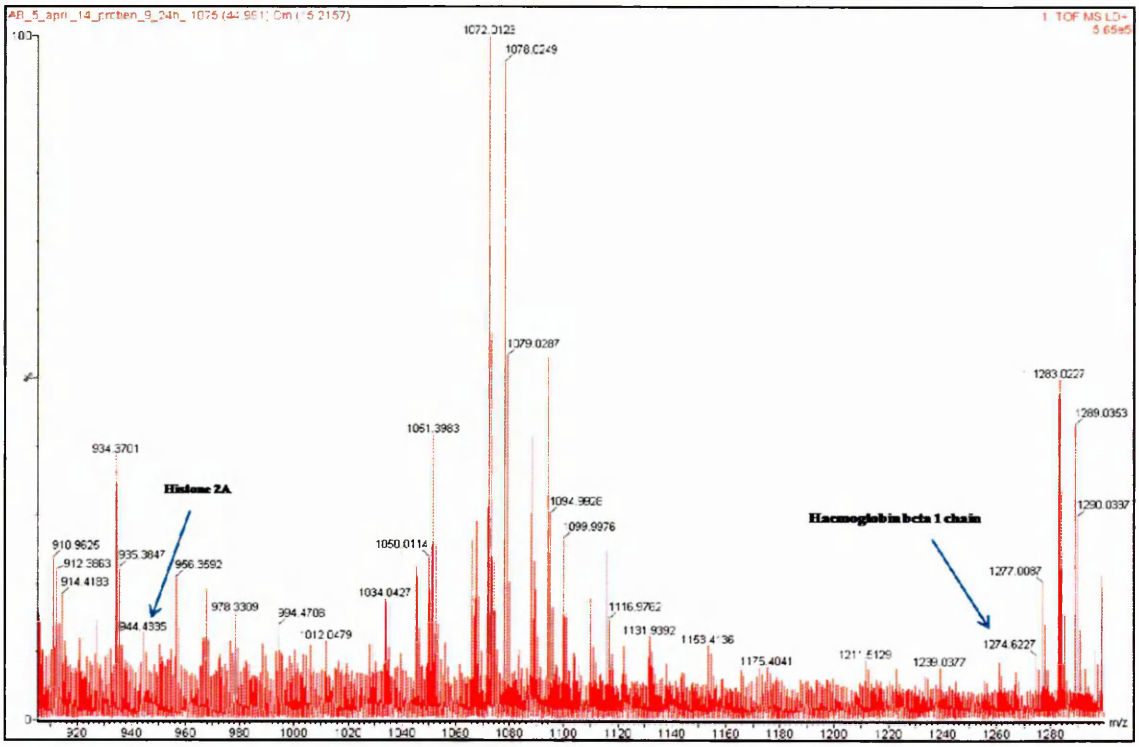

Figure 5.5: *Peptide mass fingerprint acquired from the in situ tryptic digest of the LS 174T xenograft tumour (24h after treatment with DMXAA). A number of peptide peaks were observed from 900 to 1280 m/z, such as a Histone H2A at 944.45 m/z and Hbβ1 at 1274.62 m/z.*

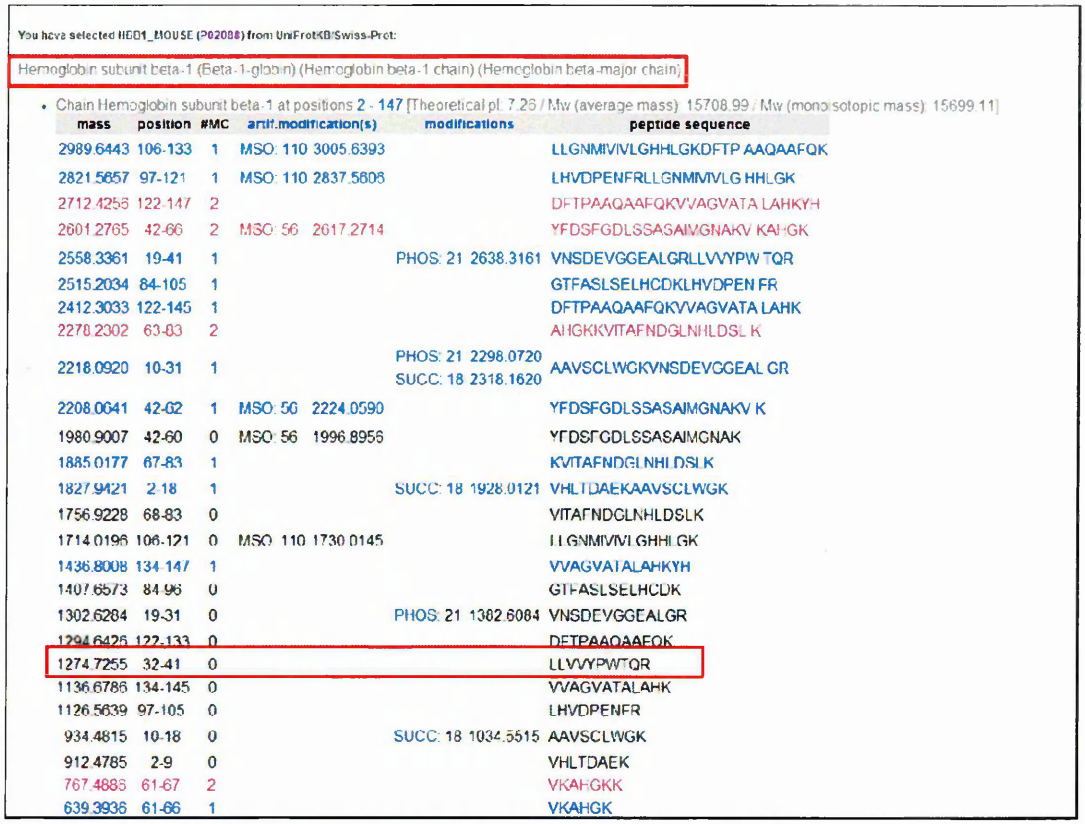

Figure 5.6: *The peptide sequence obtained from the Uniprot KB / Swiss-port search of Hbβ1 at 1274.72 m/z.*

MALDI-MSI images were acquired at a spatial resolution of 150 µm x 150 µm using a HDMS SYNAPT™ G1/G2 system (Waters Corporation, Manchester, UK). MALDI-MSI imaging was performed to investigate the peptide distribution within tissue sections of control, 4h and 24h post-treated tumours. The MALDI/ MSI images of the peptide distribution in the control tumour are shown in Fig. 5.7. The peaks at 944 m/z and 1032 m/z were identified based on a theoretical digest as Histone H2A and Histone H3. Also, the peaks at 1198 m/z and 1325 m/z were tentatively assigned to Actin and Histone H4.

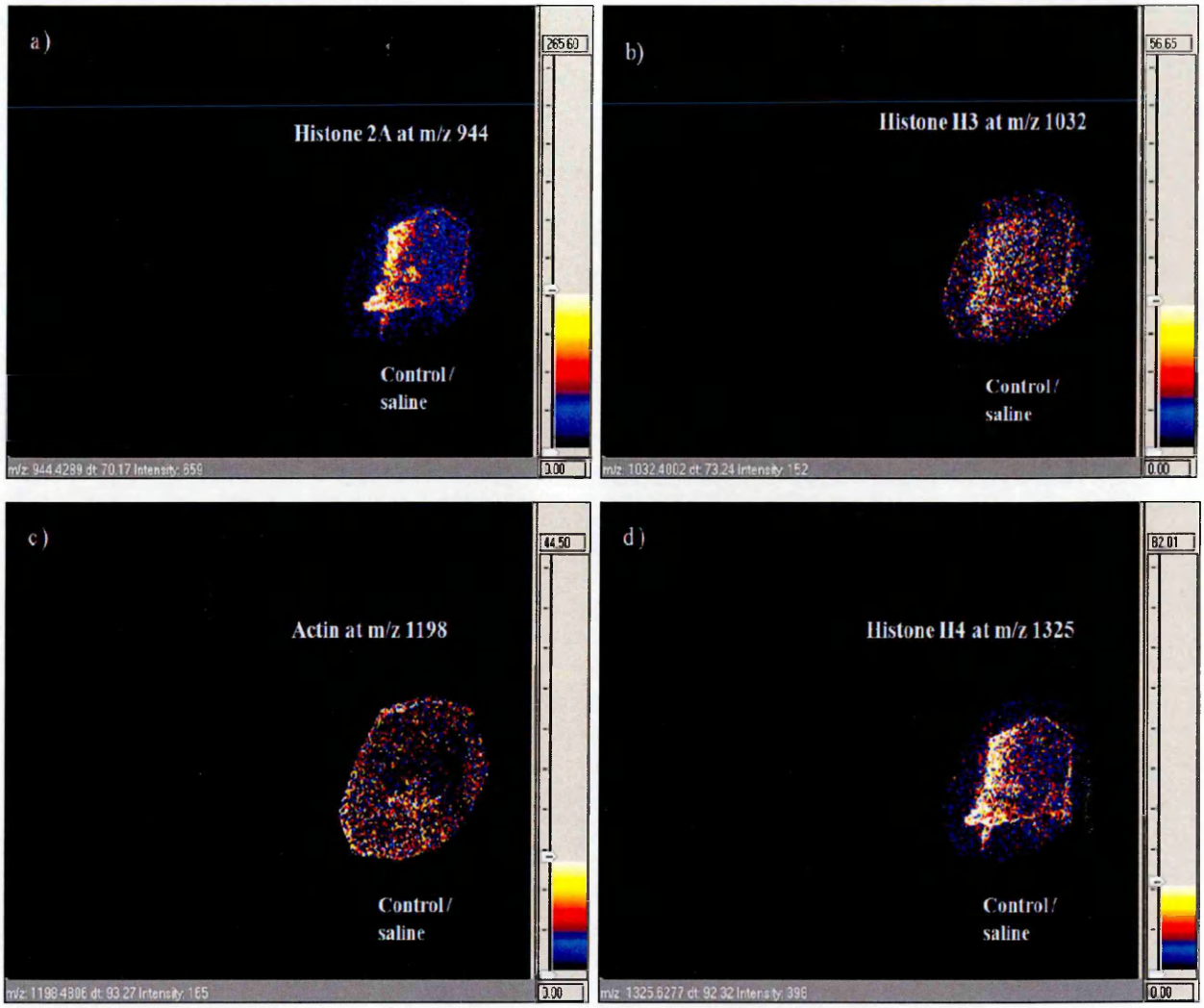

Figure 5.7: *The MALDI/MSI images showing the distribution of peptides in the control tumour: (a) Histone H2A at 944 m/z; (b) Histone H3 at 1032 m/z;(c) Actin at 1198 m/z; and (d) Histone H4 at 1325 m/z. Blue colour gives low intensity of signal while orange white colours indicates high intensity of signal as shown in scalebar.*

Fig. 5.8 shows the MALDI / MSI images of the peptides in the LS 174T xenograft tumour (4h post-treatment with DMXAA). Here, masses were identified according to the theoretical digest as follow: Histone H2A at 944 m/z; Actin at 1198 m/z; Hbβ1 at 1274 m/z; and Hbβ chain at 1302 m/z.

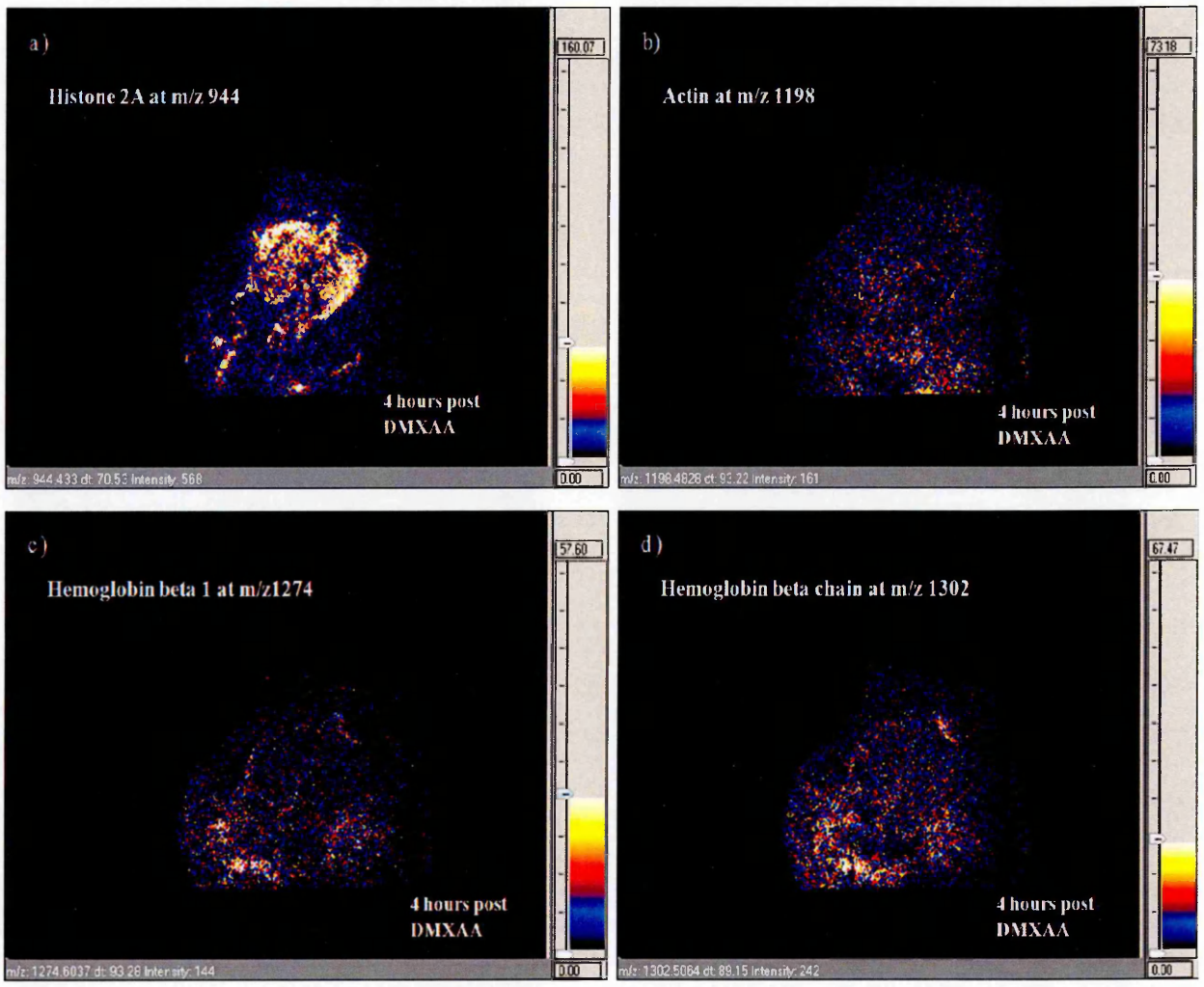

Figure 5.8: *The MALDI/MSI images showing the distribution of peptides in the LS 174T xenograft tumour 4h after treatment with DMXAA:(a) Histone H2A shows a strong signal at 944 m/z; (b) Actin at 1198 m/z; (c) Hbβ1chain at 1274 m/z; and (d) Hbβ chain at 1302 m/z. Blue colour gives low intensity of signal while orange white colours indicates high intensity of signal as shown in scalebar.*

From the images observed of the 4h post-treated DMXAA xenograft tumour (Fig 5.8), the image of Histone H2A (Fig 5.8a) showed an intense signal of histone the centre of the tumour tissue while other peptides, such as Actin (Fig 5.8b), Hbβ1 chains (Fig 5.8c) and Hbβ chains (Fig 5.8d) showed less intense signals in tumour.

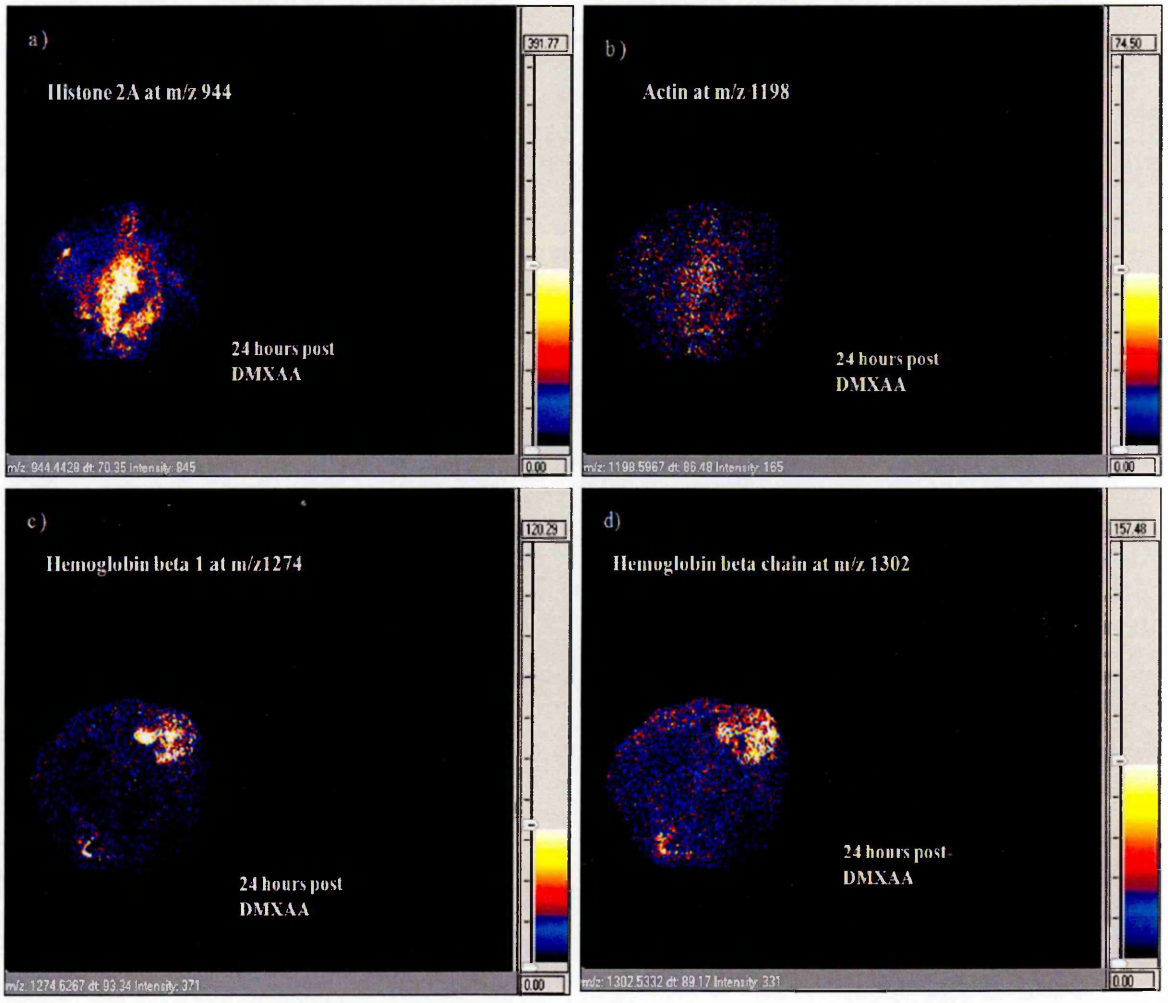

Figure 5.9: *The MALDI/MSI images showing the distribution of peptides in the LS 174T xenograft tumour 24h after treatment with DMXAA:(a) Histone H2A shows a strong signal at 944 m/z; (b) Actin at 1198 m/z; (c) Hbβ1 chain at 1274 m/z; and (d) Hbβ chain at 1302 m/z. Blue colour gives low intensity of signal while orange white colours indicates high intensity of signal as shown in scalebar.*

Fig. 5.9 shows the MALDI / MSI images of the peptides in the LS 174T xenograft tumour 24h post treatment with DMXAA. The masses were identified according to the theoretical digest as follow: Histone 2A at 944 m/z; Actin at 1198 m/z; Hbβ1 at 1274 m/z; and Hbβ chain at 1302 m/z.

The tumour shows a high level of expression of Histone H2A in the centre of the tissue following the 24h treatment with DMXAA. Also, Hbβ1 and Hbβ chains were highly expressed at the tumour's periphery.

On the whole, the MALDI-MSI images show an increase in the distribution of Histone H2A at 944 m/z in both the 4h and 24h post-treated xenograft tumours. This observation is in agreement with the previously reported study of Djidja *et al.* (2009) which stated that a signal of Histone H2A at 944 m/z was found in both the necrotic and tumour regions of an MCF7 breast tumour xenograft (Djidja *et al.*, 2009).

In addition, the increase in the relative intensity of haemoglobin peptides at 1274 m/z and 1302 m/z in the spectra and image of the 24h post-treated xenograft tumour could be a result of the vascular damage produced by DMXAA. The study of Cole *et al.* (2011) observed a similar effect but with a different kind of anti-vascular drug as their study related that the increase in tissue haemoglobin might be expected as a result of the vascular damaging properties of CA-4-P which causes disruption of the 3D capillaries, necrosis in endothelial cells, and a leakage of blood cells into tumour tissues (Cole *et al.*, 2011).

5.2.2 PCA and PLSDA statistical analysis of an LS 174T DMXAA treated xenograft tumour

PCA (Principal Component Analysis) data analysis of an LS1 74T xenograft tumour in the *in situ* tryptic digests was performed to detect intrinsic clustering and to identify protein signals characteristic of different regions of tumours.

PCA is an unsupervised method that describes the overall spread within a dataset by summarising sample variations as a series of 'latent variables' (LV) (Trygg *et al.*, 2007).

Fig. 5.10 shows the score plot resulting from the PCA analysis of an *in situ* tryptic digests of LS 174T xenograft tumour. The resulting score plot describes the grouping and variability of the spectra at each tumour time-point. The PCA loading plot is shown in Fig. 5.11 and shows the distribution and separation of the m/z peaks according to the groupings previously assigned by the score plot shown in Fig. 5.10. It is obvious from the data obtained from the loading plot that the Haemoglobin β chain (Hbβ) peak at 1274.74 m/z is characteristically assigned to the 24h post-DMXAA region; this finding confirms the previously acquired result from the spectra and image of the 24h time-point. In addition, several peaks of Histone H2A at 944 m/z and Actin at 1198 m/z were seen in the 24h region.

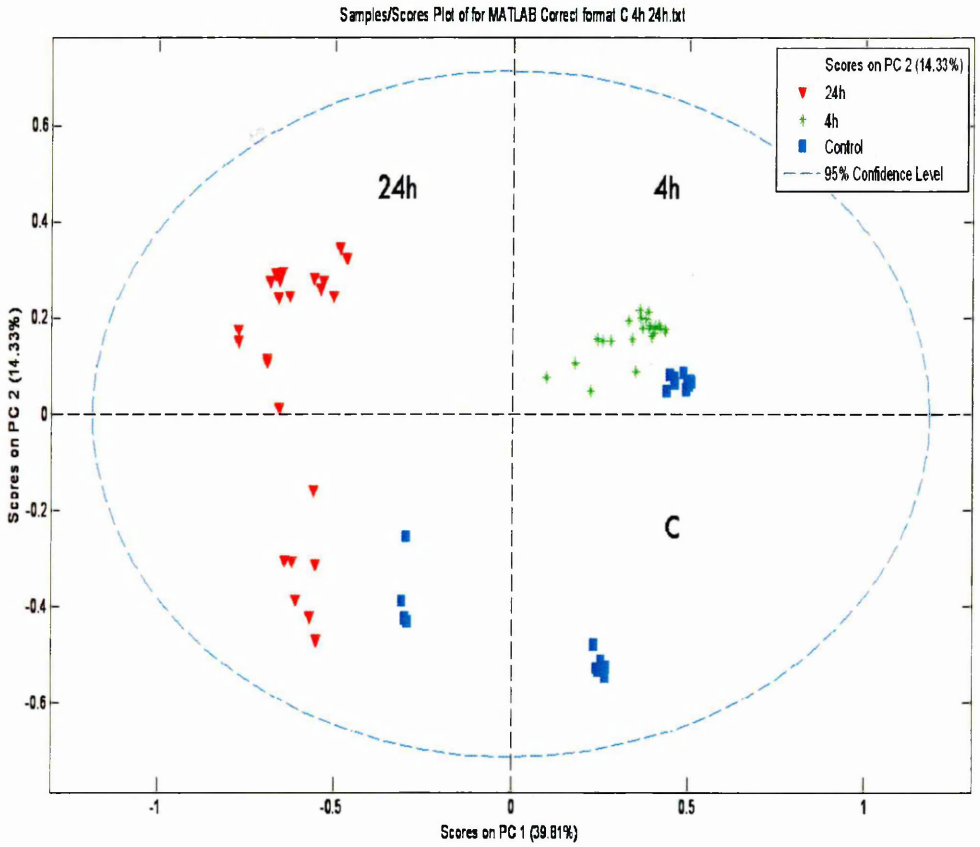

Figure 5.10: *The score plot produced by PCA showing the grouping and variability of the spectra of each tumour time-point. The control was allocated a blue colour, the 4h post-DMXAA a green and the 24h post-DMXAA a red colour.*

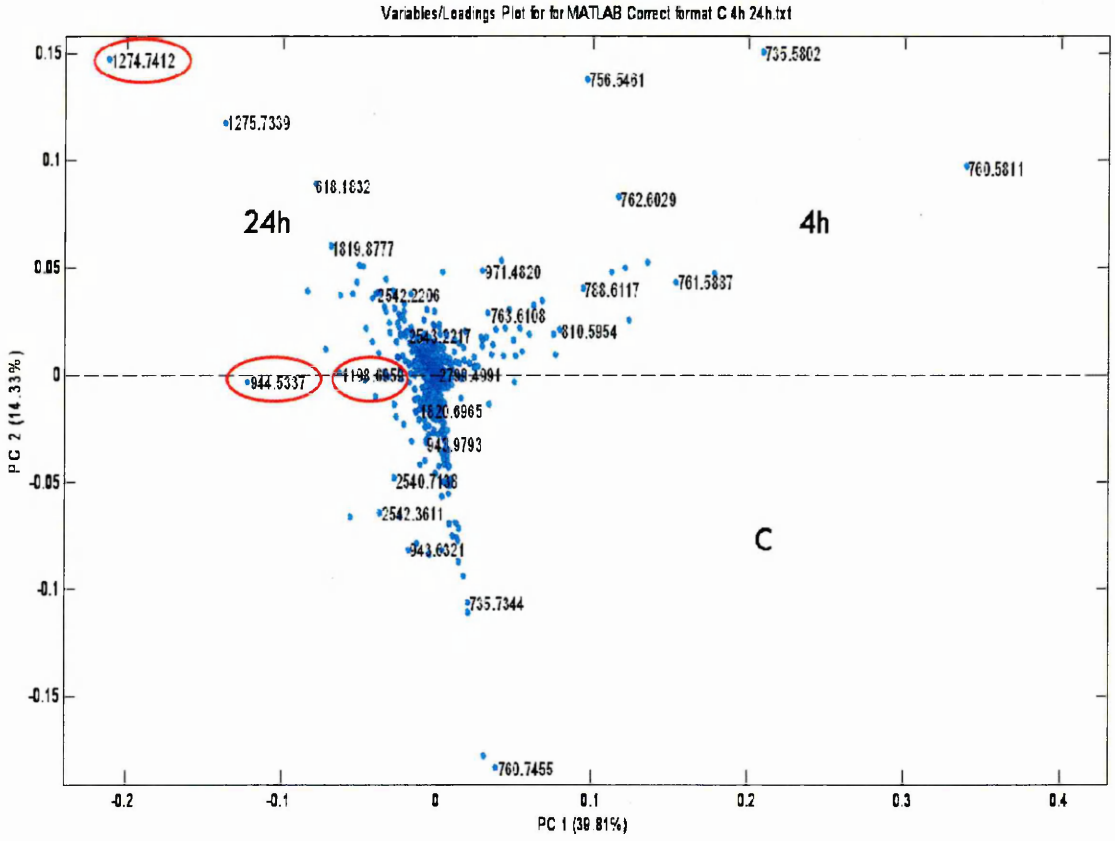

***Figure 5.11**: The loading plot with information on m/z peaks in relation to the grouping described in the PCA score plot. The peak at 1274.74 m/z is assigned to the 24h post-DMXAA time-point and it corresponds to the Haemoglobin β chain.*

For a more detailed analysis, Partial Least Squares Discriminate Analysis (PLS-DA) was carried out. PLS methods are an extension of PCA and are used to maximise the discrimination between the observed groups (Mirnezami *et al.*, 2014).

Fig. 5.12 shows the PLSDA regression vector plot between the control/saline and the 4h post-DMXAA treated group from an *in situ* tryptic digest of an LS1 74T xenograft tumour. A Histone H3 peak at 1032.57 m/z was seen in the 4h post-DMXAA treatment compared to the control group.

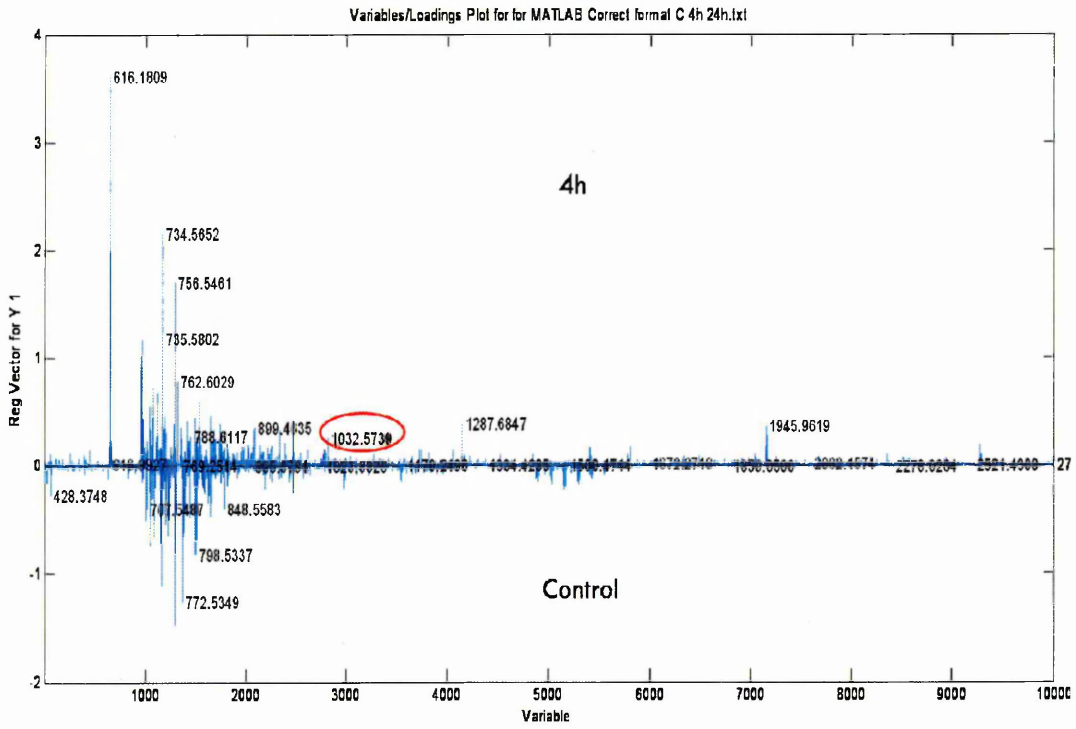

Figure 5.12: *The regression vector plot of the PLSDA analysis of the in situ digest of an LS1 74T xenograft tumour comparing the control/saline and 4h post-DMXAA treated groups. A Histone H3 peak is noticeable in the 4h post-DMXAA time-point.*

Fig. 5.13 shows the regression vector plot for the control/saline and 24h post-DMXAA treated group from the *in situ* tryptic digest of an LS1 74T xenograft tumour. A marked increase in Histone 2A at 944.53 m/z, Actin at 1198.84 m/z and the Haemoglobin β chain peak at m/z 1274.74 were seen in the 24h post-DMXAA time-point. The increase in the Hb β chain in the 24h post-DMXAA sample emphasised the data previously obtained from the MALDI-MS and MALDI-MSI profiling and imaging of a 24h post-DMXAA LS 174T xenograft tumour (Fig. 5.5 & Fig. 5.9).

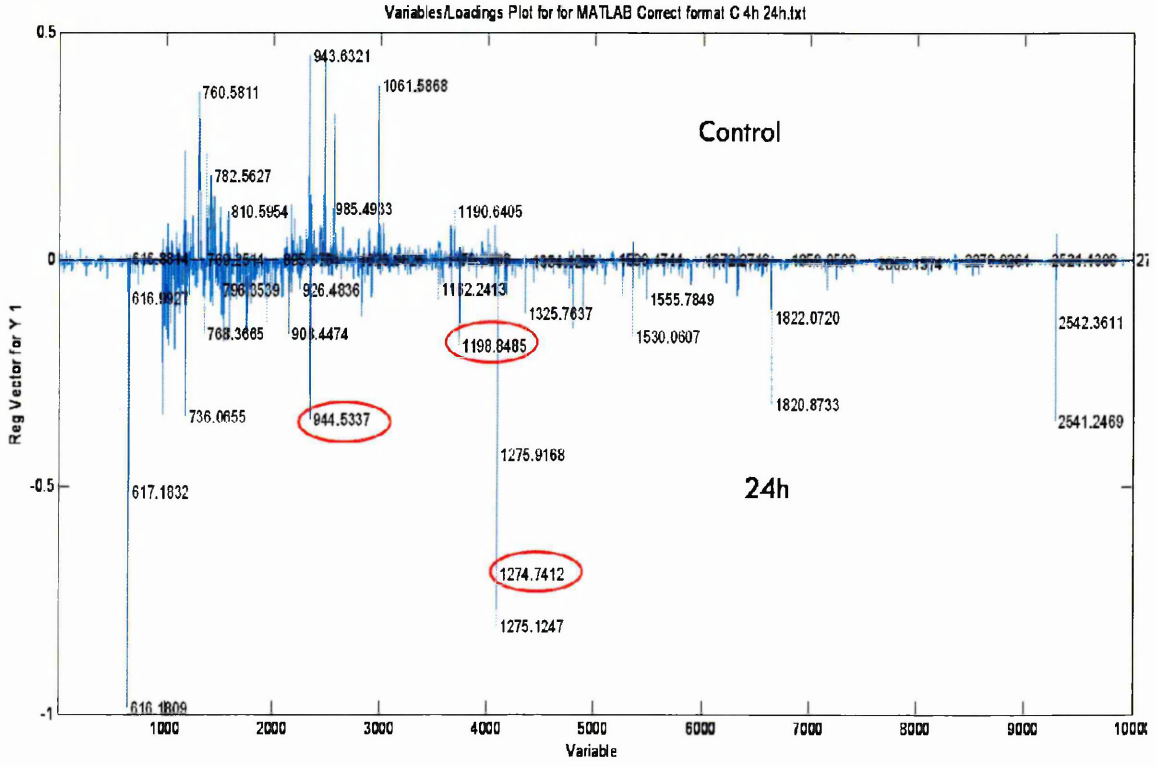

Figure 5.13: *The regression vector plot of PLSDA analysis of the in situ digest of an LS1 74T xenograft tumour comparing the control/saline and 24h post-DMXAA treated groups. The increase in Histone H2A at 944.53 m/z, Actin at 1198.84 m/z and some Haemoglobin peaks at 1274.74 m/z are visible in the 24h post-DMXAA time-point.*

Fig. 5.14 shows the regression vector plot of the 4h post-DMXAA and 24h post-DMXAA groups from the *in situ* tryptic digest of an LS1 74T xenograft tumour. This shows that the markers of necrosis / hemorrhaging (Histone 2A) at 944.53 m/z and the Haemoglobin β chain peak at 1274.74 m/z were relatively increased in the 24h post-DMXAA time-point compared to the 4h post-DMXAA time-point. Another marker of hemorrhaging the heme peak at 616.1 m/z is also clearly increased at the 24hr time point.

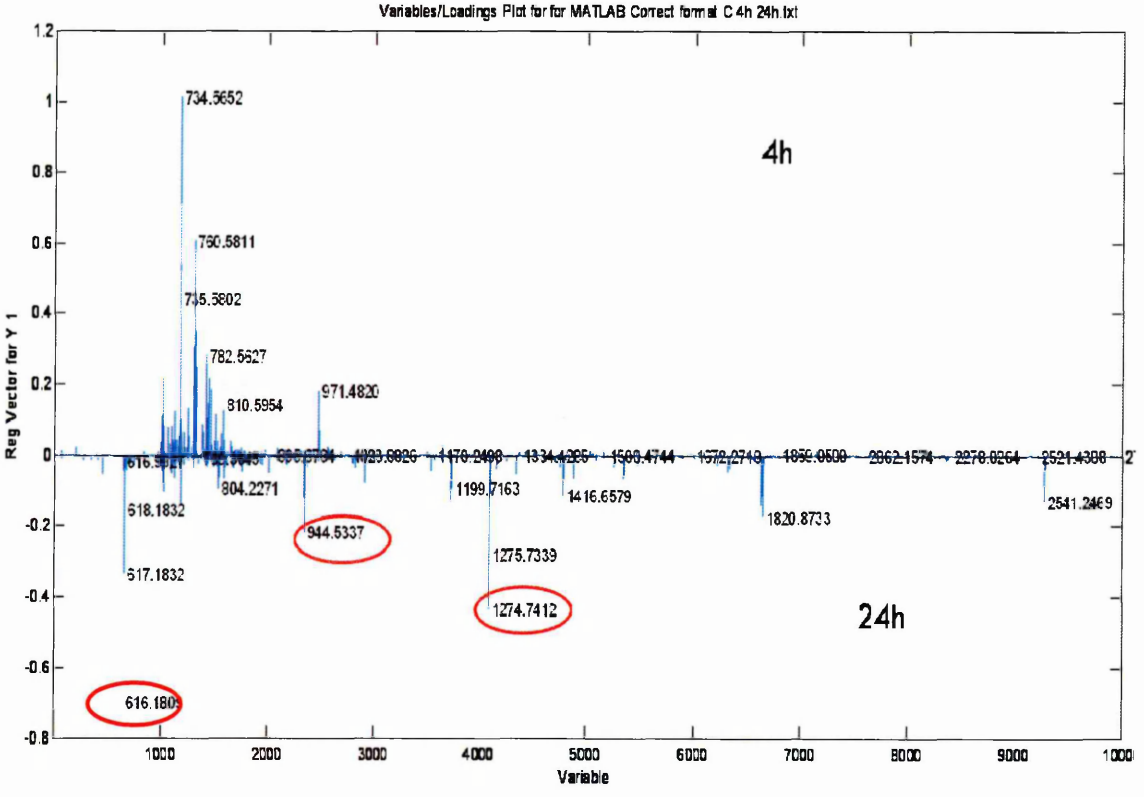

Figure 5.14: *The regression vector plot of the PLSDA analysis of the in situ digest of the LS1 74T xenograft tumour comparing the 4h post-DMXAA and 24h post-DMXAA treated groups. The increase in Histone H2A at 944.53 m/z and the Haemoglobin peak at 1274.74 m/z can be seen in the 24h post-DMXAA time-point compared to the 4h post-DMXAA.*

Finally, the characteristic increase of the Histone H2A peak at 944 m/z and the Haemoglobin peak at 1274.74 m/z in the PCA and PLSDA data of the 24h post-treated tumour might be as a result of the haemorrhagic necrosis occurring in the 24h xenograft tumour following DMXAA treatment. The same effect has been described in the study of McPhail *et al.* (2005).

5.2.3 Haematoxylin and Eosin staining

Haematoxylin and Eosin (H&E) staining of xenograft tumour tissue at each time-point was performed after MALDI-MSI protein imaging in order to carry out an optical observation and correlation study. Fig. 5.15 shows the H&E stained sections of xenograft tumour 4h post-DMXAA treatment. The effect of the vascular disrupting agent can be clearly seen as there are areas of necrotic and viable cells in the centre of the tumour tissue with a viable resistant rim at the tumour's periphery.

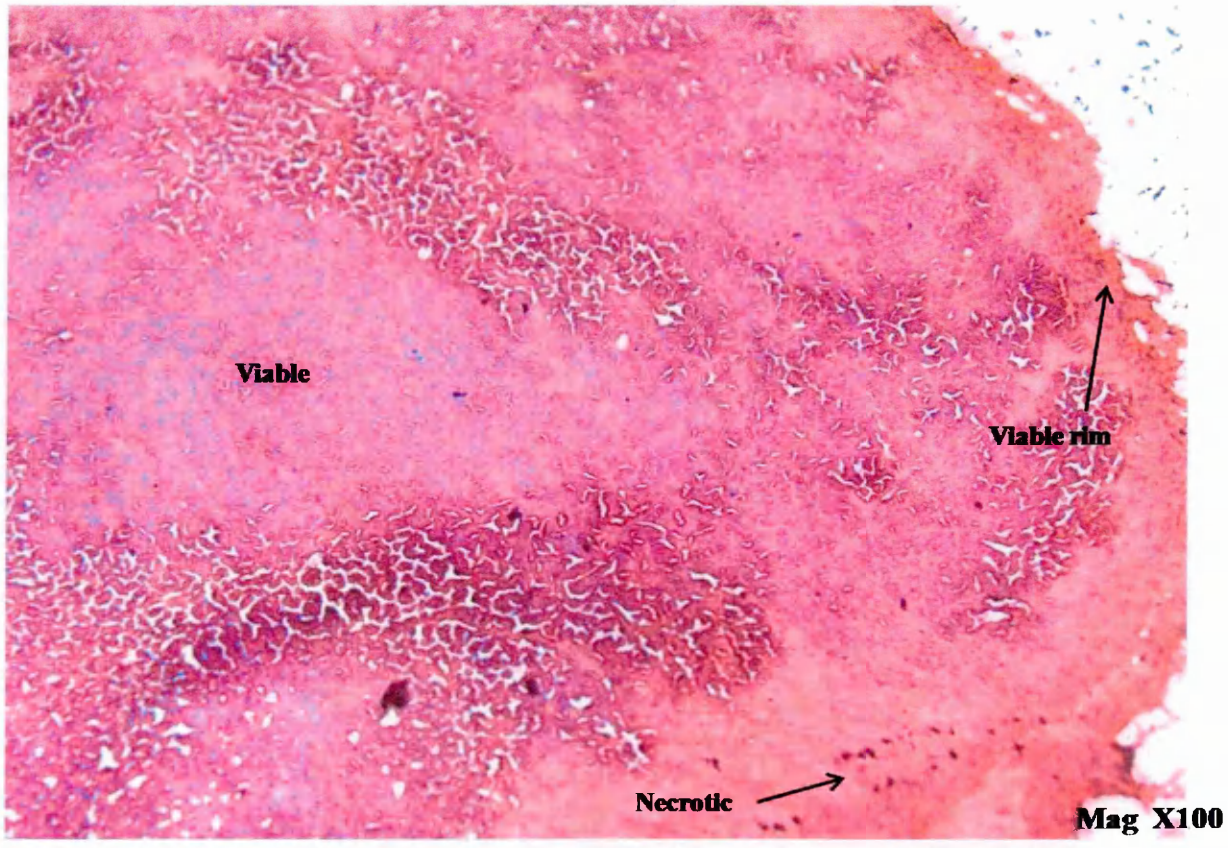

a)

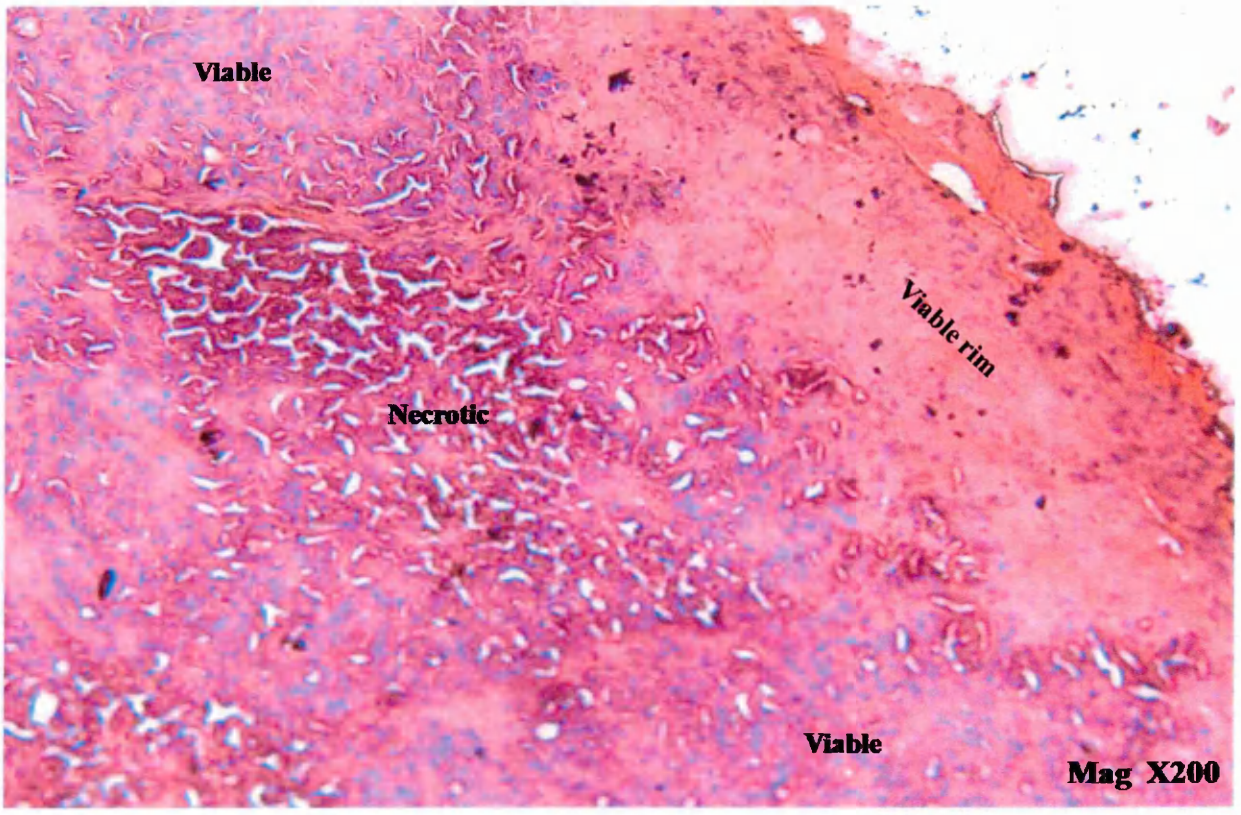

b)

Figure 5.15: *Haematoxylin and Eosin (H&E) stained sections of: a) Mag X100 and b) Mag X200 view of the xenograft tumour 4h post-DMXAA treatment. We can see the effect of drug following 4h post-treatment; there is a viable rim which shows some living cell, also there is an area of necrosis and viable cells in centre of tumour.*

Fig. 5.16 shows the H&E stained sections of xenograft tumour 24h post-DMXAA treatment. An increase in the area of total necrosis (nuclei stained blue) with some haemorrhaging (pink colour) can be seen following 24h DMXAA treatment.

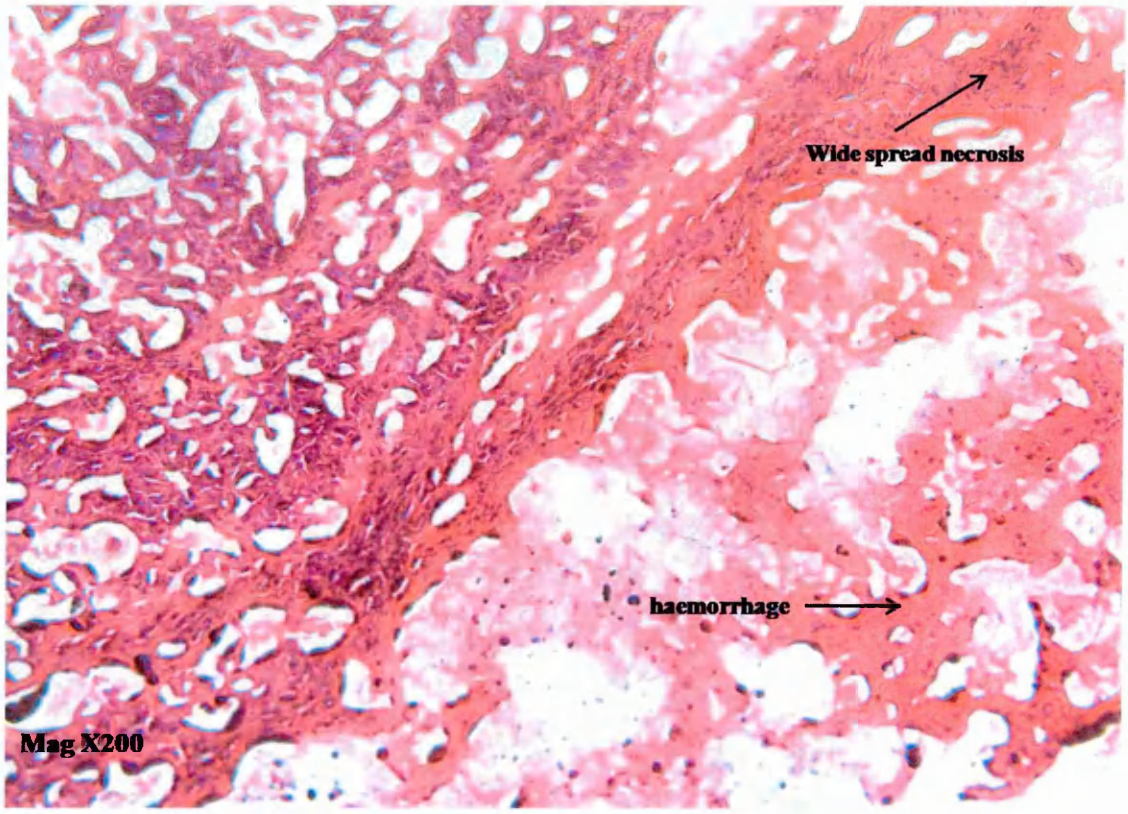

Figure 5.16: *Haematoxylin and Eosin (H&E) stained section of a 24h post DMXAA Xenograft tumour at Mag X200 showing an extensive area of wide spread necrosis(nuclei stained blue) and some hemorrhagic area (pink colour).*

Collectively, the data from the MALDI-MSI imaging and the PCA statistical study, combined with the histological analysis of tumours, support the action mechanism of DMXAA which causes necrosis in the centre of the tumour with a viable rim at the tumour's periphery.

5.3 Conclusion

MALDI/MS and MALDI /MSI profiling and imaging were used to investigate protein induction with DMXAA treatment of an LS 174T xenograft tumour. A method of *in situ* tryptic digest was used. The spectra and images of 4h and 24h post-DMXAA treatments showed some Histone H2A peaks at 944 m/z which were highly expressed in the region of the tumour. In addition, a characteristic increase in the Hb β chain at 1274.74 m/z in the 24h post-treated tumour was seen; this is indicative of haemorrhagic necrosis occurring due to the effect of DMXAA. The data obtained from the loading plots of PCA highlighted several peptide signals, including peptides at 944, 1198, 1274 m/z. These were identified as Histone H2A, Actin and Hb β chain respectively and were characteristically found in the 24h post-DMXAA region. The results of Haematoxylin and Eosin staining further confirmed the effect exerted by the anti-vascular drug.

5.4 References

BAGULEY, B.C., 2003. Antivascular therapy of cancer: DMXAA. *The lancet oncology,* **4**(3), pp. 141-148.

BROWN, Robert and STRATHDEE, Gordon (2002). Epigenomics and epigenetic therapy of cancer. *Trends in molecular medicine,* **8** (4), S43-S48.

CAPRIOLI, R.M., FARMER, T.B. and GILE, J., 1997. Molecular imaging of biological samples: localization of peptides and proteins using MALDI-TOF MS. *Analytical Chemistry,* **69**(23), pp. 4751-4760.

CHAURAND, P. and CAPRIOLI, R.M., 2002. Direct profiling and imaging of peptides and proteins from mammalian cells and tissue sections by mass spectrometry. *Electrophoresis,* **23**(18), pp. 3125-3135.

CHING, L., CAO, Z., KIEDA, C., ZWAIN, S., JAMESON, M. and BAGULEY, B., 2002. Induction of endothelial cell apoptosis by the antivascular agent 5, 6-dimethylxanthenone-4-acetic acid. *British journal of cancer,* **86**(12), pp. 1937-1942.

COLE, L., DJIDJA, M., BLUFF, J., CLAUDE, E., CAROLAN, V., PALEY, M., TOZER, G. and CLENCH, M., 2011. Investigation of protein induction in tumour vascular targeted strategies by MALDI MSI. *Methods,* **54**(4), pp. 442-453.

DJIDJA, M., FRANCESE, S., LOADMAN, P.M., SUTTON, C.W., SCRIVEN, P., CLAUDE, E., SNEL, M.F., FRANCK, J., SALZET, M. and CLENCH, M.R., 2009. Detergent addition to tryptic digests and ion mobility separation prior to MS/MS improves peptide yield and protein identification for in situ proteomic investigation of frozen and formalin-fixed paraffin-embedded adenocarcinoma tissue sections. *Proteomics,* **9**(10), pp. 2750-2763.

DJIDJA, M., CLAUDE, E., SNEL, M.F., FRANCESE, S., SCRIVEN, P., CAROLAN, V. and CLENCH, M.R., 2010. Novel molecular tumour classification using MALDI–mass spectrometry imaging of tissue micro-array. *Analytical and bioanalytical chemistry,* **397**(2), pp. 587-601.

GALBRAITH, S.M., RUSTIN, G.J., LODGE, M.A., TAYLOR, N.J., STIRLING, J.J., JAMESON, M., THOMPSON, P., HOUGH, D., GUMBRELL, L. and PADHANI, A.R., 2002. Effects of 5,6-dimethylxanthenone-4-acetic acid on human tumor microcirculation assessed by dynamic contrast-enhanced magnetic resonance imaging. *Journal of clinical oncology : official journal of the American Society of Clinical Oncology,* **20**(18), pp. 3826-3840.

JOSEPH, W.R., CAO, Z., MOUNTJOY, K.G., MARSHALL, E.S., BAGULEY, B.C. and CHING, L.M., 1999. Stimulation of tumors to synthesize tumor necrosis factor-alpha in situ using 5,6-dimethylxanthenone-4-acetic acid: a novel approach to cancer therapy. *Cancer research,* **59**(3), pp. 633-638.

KANTHOU, C. and TOZER, G.M., 2008. Selective destruction of the tumour vasculature by targeting the endothelial cytoskeleton. *Drug Discovery Today: Therapeutic Strategies,* **4**(4), pp. 237-243.

KERR, D. and KAYE, S., 1989. Flavone acetic acid—preclinical and clinical activity. *European Journal of Cancer and Clinical Oncology,* **25**(9), pp. 1271-1272.

LUO, R. X. and DEAN, D. C. (1999). Chromatin remodeling and transcriptional regulation. *Journal of the national cancer institute,* **91** (15), 1288-1294.

MCPHAIL, L.D., CHUNG, Y.L., MADHU, B., CLARK, S., GRIFFITHS, J.R., KELLAND, L.R. and ROBINSON, S.P., 2005. Tumor dose response to the vascular disrupting agent, 5,6-dimethylxanthenone-4-acetic acid, using in vivo magnetic resonance spectroscopy. *Clinical cancer research: an official journal of the American Association for Cancer Research,* **11**(10), pp. 3705-3713.

MIRNEZAMI, R., SPAGOU, K., VORKAS, P., LEWIS, M., KINROSS, J., WANT, E., SHION, H., GOLDIN, R., DARZI, A. and TAKATS, Z., 2014. Chemical mapping of the colorectal cancer microenvironment via MALDI imaging mass spectrometry (MALDI-MSI) reveals novel cancer-associated field effects. *Molecular oncology,* **8**(1), pp. 39-49.

REWCASTLE, G.W., ATWELL, G.J., ZHUANG, L., BAGULEY, B.C. and DENNY, W.A., 1991. Potential antitumor agents. 61. Structure-activity relationships for in vivo colon 38 activity among disubstituted 9-oxo-9H-xanthene-4-acetic acids. *Journal of medicinal chemistry,* **34**(1), pp. 217-222.

REYZER, M.L., CALDWELL, R.L., DUGGER, T.C., FORBES, J.T., RITTER, C.A., GUIX, M., ARTEAGA, C.L. and CAPRIOLI, R.M., 2004. Early changes in protein expression detected by mass spectrometry predict tumor response to molecular therapeutics. *Cancer research,* **64**(24), pp. 9093-9100.

RIFAI, N., GILLETTE, M.A. and CARR, S.A., 2006. Protein biomarker discovery and validation: the long and uncertain path to clinical utility. *Nature biotechnology,* **24**(8), pp. 971-983.

SIEMANN, D.W., CHAPLIN, D.J. and HORSMAN, M.R., 2004. Vascular-targeting therapies for treatment of malignant disease. *Cancer,* **100**(12), pp. 2491-2499.

TRYGG, J., HOLMES, E. and LUNDSTEDT, T., 2007. Chemometrics in metabonomics. *Journal of proteome research,* **6**(2), pp. 469-479.

WATANABE, N., NIITSU, Y., UMENO, H., KURIYAMA, H., NEDA, H., YAMAUCHI, N., MAEDA, M. and URUSHIZAKI, I., 1988. Toxic effect of tumor necrosis factor on tumor vasculature in mice. *Cancer research,* **48**(8), pp. 2179-2183.

YANAGISAWA, K., SHYR, Y., XU, B.J., MASSION, P.P., LARSEN, P.H., WHITE, B.C., ROBERTS, J.R., EDGERTON, M., GONZALEZ, A. and NADAF, S., 2003. Proteomic patterns of tumour subsets in non-small-cell lung cancer. *The Lancet,* **362**(9382), pp. 433-439.

Chapter 6

Conclusions and suggestions for future work

6 Conclusions

This study demonstrates the ability of Matrix Assisted Laser Desorption Ionisation-Mass Spectrometry Imaging (MALDI-MSI) to study the distribution of anti-cancer drugs, 5, 6 dimethylxanthenone-4-acetic acid (DMXAA) in LS1 74T xenograft tumours. The thesis also focuses on the response of tumours to drug therapy by studying phospholipids and protein levels in DMXAA treated xenograft tumours. In addition, the methodology of TLC-MALDI coupling has been developed for the analysis of phospholipids extracted from DMXAA treated xenograft tumours.

The ability to map drug distribution in tissues whilst retaining compound specificity is a major challenge. MALDI-MSI not only has the potential to allow rapid direct analysis of compounds from tissue surfaces without the need for radiolabelling, but it also allows greater compound specificity than may be achieved with conventional tissue imaging approaches.

The work presented in **Chapter 2** relates to the main objective of this thesis: i.e., to study the distribution and fate of anti-cancer drugs, in particular DMXAA, in dosed LS 174T xenograft tumours using MALDI-MSI. It was shown in this work that the use of matrix solvent containing 70% EtOH / H_2O + 0.1 TFA improves the sensitivity and detection of DMXAA by MALDI-MSI; this was therefore selected as the matrix solvent of choice for this study. MALDI-MSI was used to determine the limit of detection / quantitation of DMXAA in tissue and it was detected in a range of 10 ng/ml to 250 ng/ml. The drug limit of detection (LoD) is determined as 10 ng/ml and the drug lower limit of quantitation (LLoQ) is 45 ng/ml.

MALDI images were recorded from LS174T colorectal adenocarcinoma xenografts removed from immunodeficient mice following treatment with with 27.5 mg/kg DMXAA. These indicated that the drug was distributed mainly in the centre of tumour 4h post-treatment, whilst it was distributed around the periphery 24h post-treatment following vascular damage.

Finally, the characteristic feature of VDA treatment was revealed in the H&E stained sections of a 4h post-treated tumour where a necrotic area could be seen in the center of the tumour with viable cells at the tumour's periphery. Also, the H&E stained sections of a 24h post-treated tumour showed an area of haemorrhage with widespread necrosis at the tumour's periphery, demonstrating the vascular damage occurred by DMXAA.

Profiling biological molecules on tissues using MALDI-MSI can identify subtypes of phospholipids. This area of study was extended to visualise the distribution of phospholipid subtypes in a tissue section using mass spectrometry imaging (MSI). The analysis of phospholipids using MALDI-MSI in both positive and negative ion modes was described in **Chapter 3**. The addition of a 150 mM NH_4Ac wash step into the sample preparation procedure resulted in better images of lipids and it also enhanced the abundance of signals. In positive ion mode, the phospholipids at 703.38 m/z $[M+H]^+$ and 725.30 m/z $[M+Na]^+$ were identified as SM (16:0). These molecules were found to be highly expressed in tumour tissue compared to the control. In addition, spectra and images of phospholipids in negative ion mode showed a significant decrease in PC and PE in the 24h post-treated tumour. Finally, the MALDI images of phospholipids were correlated with H&E stained tissue sections.

An increasing number of diseases are recognised to be accompanied by alterations in the lipid composition. TLC has been classically used for routine separations and for identifying the individual lipids. However, if an unknown spot appears, the only qualitative information that can be obtained from it is the retention factor (Rf) value. In **Chapter 4,** a methodology employing TLC-MALDI-MS coupling was developed for the analysis of phospholipids extracted from DMXAA treated xenograft tumours.

This method has demonstrated the ability to obtain spectral information and to identify lipids with different acyl compositions from a single spot on the TLC plate without the need for staining, thus illustrating the potential applications of TLC - MALDI in lipid analysis. Different lipid classes with various fatty acid chains, such as SM, PC and LPC, were identified using MALDI-TOF MS analysis of TLC separated compounds. An increase in the expression of LPC in solid tumours treated with DMXAA was demonstrated and shown to be localised in the central area of the tumour. The conversion of phospholipids species to their lithiated adducts to facilitate their identification by MALDI MS/MS analysis was demonstrated. Finally, PCA and PCA-DA of MALDI-MSI data sets were used to confirm the results obtained using TLC-MALDI-MSI.

Characterising proteins will help to determine both the treatment responses and resistance mechanisms in tumours. In the work reported in **Chapter 5**, mass spectrometry imaging was used for this purpose. Protein analysis using MALDI-MSI was carried out after *in situ* tissue tryptic digestion. MALDI-MSI spectra and images revealed some proteins connected with necrosis, such as Histone H2A; this was found in both 4h and 24h post-treated tumours. The gross haemmoragic response elicited by the anti-vascular drug, DMXAA, was demonstrated by the significant increase in the Hb β chain peptide peaks at 1274.74 m/z in the 24h post-treated tumour. Furthermore, the use of PCA, PCA-DA and PLSDA has been used to classify each protein type to a different tumour time courses. H&E stained sections of the tumour samples has been correlated with the MALDI images and the statistical data.

6.1 Suggestions for future work

For the drug distribution study, complementary staining, such as immunohistochemical staining might be required in order to identify biomarkers of vascular collapse and any signs of necrosis.

Also, information on microscopic structures in tissues, such as the cell density and necrotic fraction of tumours, would be useful to determine tumor aggressiveness. Moreover, changes in cell density and necrotic fraction during and after treatment may reflect tumour response (Hendry & West., 1997). Methods for measurement of cell density and necrosis in tumors are used to monitor tumor response to therapy (Zhao *et al.,* 1996-Poptani *et al.,* 1998).

Apoptosis which is a type of cell death is usually evaluated by electrophoretic or colorimetric methods that measure DNA fragmentation in the nuclear extracts (Nicoletti *et al.,* 1991). Many methods are available for the measurement of apoptosis however the 'gold standard' method to identify apoptotic cells based on their morphological features using microscopy by using immunohistochemistry with an antibody against the active form of caspase 3. Caspase 3 is a cytosolic enzyme that is activated only in cells that undergo apoptosis (Hadjiloucas et al ., 2001).

A study on pharmacological mechanism of flavonid derivate has been focused on cell and gene levels and there is little information about its metabolomics study (Gao *et al.*, 2014). Therefore, further biological experiments which measure reactive oxygen species (ROS) can confirm the mitochondrial dysfunction occurred by the anti-tumour effect of flavonid derivate.

Despite the major advances in the field of tumour angiogenesis, little attention has been considered to the permeability of blood vessels in tumours (McDonald and Baluk., 2002). The leakiness of tumour vessels is well documented in experimental tumour models and in human cancer, but the exact mechanism is poorly understood. The cellular basis of tumor vessel leakiness, endothelial barrier function of blood vessels, monitoring tumour vessel leakiness, mediators of endothelial leakiness, consequences of tumour vessel leakiness, genomic analysis of vascular targets, targeting drugs to tumour vessels, and therapeutic manipulation of tumour vessels need more understanding (McDonald and Baluk., 2002). Therefore, method such as intravital measurements of tumour blood flow and vessel leakiness, *in vivo* phage display and magnetic resonance imaging could contribute to this understanding.

Also, the number of xenografts tumours need to be increase in order to do some statistical work.

The further employment of a high resolution MALDI-MSI technique, such as ion mobility spectrometry (IMS) especially for lipid analysis in both positive and negative ion modes, could allow more lipid species to be identified; it might also improve the sensitivity of lipid detection and remove any matrix interference by using the drift time technology.

Further consideration might be given is to use LC/MS techniques to obtain some quantitative information about drugs and lipids in tumours.

Further phospholipid analysis using 31P PNMR, in addition to TLC-MALDI techniques, are recommended to allow the differentiation of phospholipids based on their head groups, and to locate the position of double bonds within a given lipid in a single spectrum.

For protein analysis, a further optimisation of sample preparation and method for in *situ* tissue digestion might be required to identify more protein biomarkers.

6.2 References

GAO, D., JIN, F., LIU, H., WANG, Y. and JIANG, Y., 2014. Metabonomic study on the antitumor effect of flavonoid derivative 3d in HepG2 cells and its action mechanism. *Talanta,* **118**, pp. 382-388.

H. HENDRY AND CML WEST, J, 1997. Apoptosis and mitotic cell death: their relative contributions to normal-tissue and tumour radiation response. *International journal of radiation biology,* **71**(6), pp. 709-719.

MCDONALD, D.M. and BALUK, P., 2002. Significance of blood vessel leakiness in cancer. *Cancer research,* **62**(18), pp. 5381-5385.

NICOLETTI, I., MIGLIORATI, G., PAGLIACCI, M., GRIGNANI, F. and RICCARDI, C., 1991. A rapid and simple method for measuring thymocyte apoptosis by propidium iodide staining and flow cytometry. *Journal of immunological methods,* **139**(2), pp. 271-279.

POPTANI, H., PUUMALAINEN, A.M., GROHN, O.H., LOIMAS, S., KAINULAINEN, R., YLA-HERTTUALA, S. and KAUPPINEN, R.A., 1998. Monitoring thymidine kinase and ganciclovir-induced changes in rat malignant glioma in vivo by nuclear magnetic resonance imaging. *Cancer gene therapy,* **5**(2), pp. 101-109.

ZHAO, M., PIPE, J.G., BONNETT, J. and EVELHOCH, J.L., 1996. Early detection of treatment response by diffusion-weighted 1H-NMR spectroscopy in a murine tumour in vivo. *British journal of cancer,* **73**(1), pp. 61-64.

HADJILOUCAS, I., GILMORE, A.P., BUNDRED, N.J. and STREULI, C.H., 2001. Assessment of apoptosis in human breast tissue using an antibody against the active form of caspase 3: relation to tumour histopathological characteristics. *British journal of cancer,* **85**(10), pp. 1522-1526.

Appendices

Appendix 1: Publications

PATEL, E., COLE, L.M., BRADSHAW, R., BATUBARA, A., MITCHELL, C.A., FRANCESE, S. and CLENCH, M.R., 2015. MALDI-MS imaging for the study of tissue pharmacodynamics and toxicodynamics. *Bioanalysis*, **7**(1), 91-101.

BATUBARA, A., CAROLAN, V.A., LOADMAN, P., SUTTON, C., SHNYDER, S and CLENCH, M.R., 2015. TLC-MALDI-MS and MALDI-MS Imaging for the Analysis of Phospholipids in LS174T Colorectal Adenocarcinoma Xenografts Treated with the Vascular Disrupting Agent DMXAA (Manuscript submitted to journal of Rapid Communications in Mass Spectrometry).

Appendix 2: Oral presentations

BATUBARA, A., CAROLAN, V.A., LOADMAN, P., SUTTON, C., SHNYDER, S and CLENCH, M.R. TLC-MALDI-MS and MALDI-MS Imaging for the Analysis of Phospholipids in LS174T Colorectal Adenocarcinoma Xenografts Treated with the Vascular Disrupting Agent DMXAA. *7th Saudi Students Conference*, Edinburgh, UK, 1st-2nd February 2014.

Appendix 3: Poster presentations

BATUBARA, A., LOADMAN, P., SUTTON, C. and CLENCH, M.R., 2012. The distribution of Anti-Cancer drug in solid tumours studied by MALDI-MSI. *60 ASMS Conference on Mass Spectrometry and Allied Topics,* Vancouver, BC, Canada, 20-24 May 2012.

BATUBARA, A ., LOADMAN, P., SUTTON, C. and CLENCH, M.R., 2012. The distribution of Anti-Cancer drug in solid tumours studied by MALDI-MSI. *Ourense Conference on Imaging Mass Spectrometry,* Ourense, Spain, 3rd-5th September 2012.

BATUBARA, A., LOADMAN, P., SUTTON, C. and CLENCH, M.R., 2013. Direct coupling of TLC with MALDI-TOF Mass spectrometry for Analysis of extracted phospholipids from DMXAA treated xenograft tumor. *61 ASMS Conference on Mass Spectrometry and Allied Topics,* Minneapolis, USA, 6-9 June 2013.

BATUBARA, A., LOADMAN, P., SUTTON, C. and CLENCH, M.R., 2014. Direct coupling of TLC with MALDI-TOF Mass spectrometry for Analysis of extracted phospholipids from DMXAA treated xenograft tumor. NCRI Cancer conference, Liverpool, Uk, 2-5 November 2014.

Appendix 4: Conference attended

- 59th American Society for Mass Spectrometry Conference on Mass Spectrometry and Allied Topics, Denver, Clorado, USA,5^{th}-9^{th} June 2011.
- 60th American Society for Mass Spectrometry Conference on Mass Spectrometry and Allied Topics, Vancouver, Canada, 20-24 May 2012.
- Ourense Conference on Imaging Mass Spectrometry, Spain, 3rd - 5th September 2012.
- 61 th American Society for Mass Spectrometry Conference on Mass Spectrometry and Allied Topics , Minneapolis, MN, USA, 9–13 June 2013.
- The 7th Saudi Students Conference, Edinburgh, UK, 1st-2nd February 2014.
- The 10^{th} National Cancer Research Institute (NCRI) Cancer Conference, Liverpool, UK, 2-5 Nov 2014.